NASA/TM-20230012171



# Goddard Institute for Space Studies Research Publications 2022

*Priscilla De Leon, Josefina Mora, and Robert B Schmunk*

**August 2023**

# NASA STI Program ... in Profile

Since its founding, NASA has been dedicated to the advancement of aeronautics and space science. The NASA scientific and technical information (STI) program plays a key part in helping NASA maintain this important role.

The NASA STI program operates under the auspices of the Agency Chief Information Officer. It collects, organizes, provides for archiving, and disseminates NASA's STI. The NASA STI program provides access to the NTRS Registered and its public interface, the NASA Technical Reports Server, thus providing one of the largest collections of aeronautical and space science STI in the world. Results are published in both non-NASA channels and by NASA in the NASA STI Report Series, which includes the following report types:

- TECHNICAL PUBLICATION. Reports of completed research or a major significant phase of research that present the results of NASA Programs and include extensive data or theoretical analysis. Includes compilations of significant scientific and technical data and information deemed to be of continuing reference value. NASA counterpart of peer-reviewed formal professional papers but has less stringent limitations on manuscript length and extent of graphic presentations.

- TECHNICAL MEMORANDUM. Scientific and technical findings that are preliminary or of specialized interest, e.g., quick release reports, working papers, and bibliographies that contain minimal annotation. Does not contain extensive analysis.

- CONTRACTOR REPORT. Scientific and technical findings by NASA-sponsored contractors and grantees.

- CONFERENCE PUBLICATION. Collected papers from scientific and technical conferences, symposia, seminars, or other meetings sponsored or co-sponsored by NASA.

- SPECIAL PUBLICATION. Scientific, technical, or historical information from NASA programs, projects, and missions, often concerned with subjects having substantial public interest.

- TECHNICAL TRANSLATION. English-language translations of foreign scientific and technical material pertinent to NASA's mission.

Specialized services also include organizing and publishing research results, distributing specialized research announcements and feeds, providing information desk and personal search support, and enabling data exchange services.

For more information about the NASA STI program, see the following:

- Access the NASA STI program home page at http://www.sti.nasa.gov

- E-mail your question to help@sti.nasa.gov

- Phone the NASA STI Information Desk at 757-864-9658

- Write to:
  NASA STI Information Desk
  Mail Stop 148
  NASA Langley Research Center
  Hampton, VA 23681-2199

NASA/TM-20230012171



# Goddard Institute for Space Studies Research Publications 2022

*Priscilla De Leon, Josefina Mora, and Robert B Schmunk*
*Autonomic Integra, LLC, New York, NY*

National Aeronautics and
Space Administration

Goddard Space Flight Center
Greenbelt, Maryland 20771

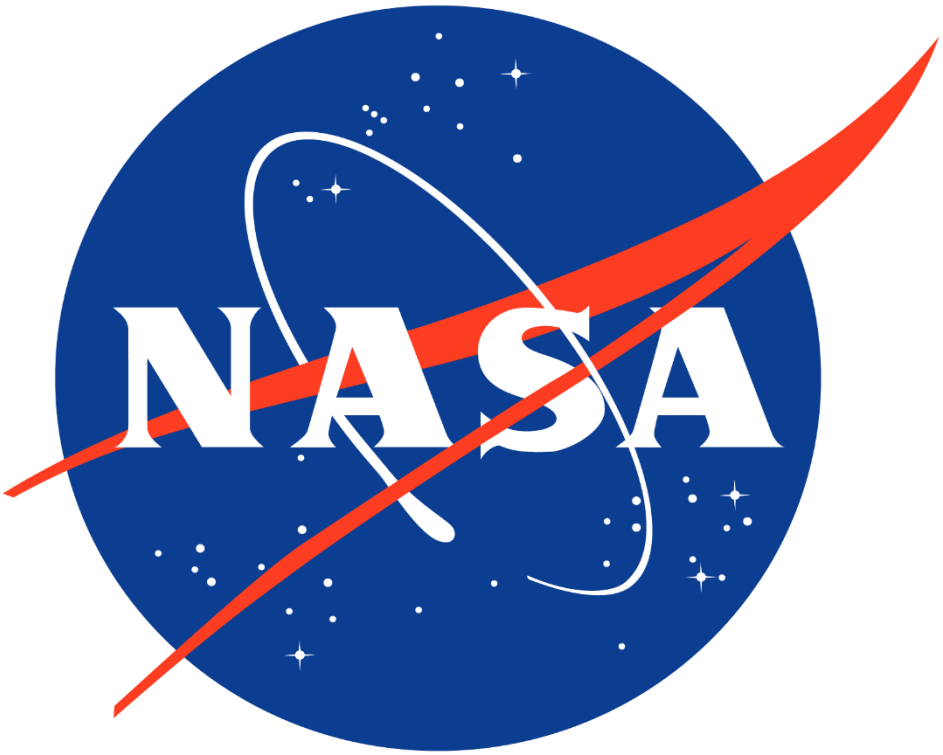
**August 2023**

Trade names and trademarks are used in this report for identification only. Their usage does not constitute an official endorsement, either expressed or implied, by the National Aeronautics and Space Administration.

*Level of Review: This material has been technically reviewed by technical management.*

This report is available in electronic form at https://www.sti.nasa.gov/ and https://ntrs.nasa.gov/

# GODDARD INSTITUTE FOR SPACE STUDIES




# Research Publications 2022

**National Aeronautics and Space Administration**
**Goddard Space Flight Center**

**2880 Broadway**
**New York, NY 10025**
**(212) 678-5500**

# GISS Research Publications 2022

The GISS Research Publications document was initiated in 1992 as an annual summary of our research based on quick inexpensive reproduction of excerpts of published papers. Its aim is twofold: to communicate in and outside the GISS community what we do and how we got about it, as well as to record annual accomplishments, providing a continual basis for measuring progress.

## Background

Pictured below, GISS is a laboratory of NASA's Goddard Space Flight Center (GSFC) in Goddard's Earth Sciences Division and is located at Columbia University's Armstrong Hall in New York City. GISS was established in 1961 by Dr. Robert Jastrow. Our mission is to conduct basic research in support of NASA programs. Led by Dr. James E. Hansen from 1981 to 2013, the prime objective has been improved understanding of global change. Research areas include global climate, biogeochemical cycles, planetary atmospheres, earth observations and related interdisciplinary studies. In 2014, Dr. Gavin A. Schmidt was named Chief of GISS.

Research is carried out in cooperation with the academic community, especially Columbia University, near whose campus GISS is housed, City University of New York (CUNY) and the Massachusetts Institute of Technology (MIT). Typically, about six graduate students carry out their Ph.D. thesis research under the supervision of GISS staff members at any given time. GISS is made up of approximately 150 employees including high school, undergraduate, graduate students, post-doctoral scientists, university research associates and visiting faculty, all of whom contribute to collaborative research projects.




*Image Credit: John Barbara, NASA Goddard Institute for Space Studies (GISS), New York, NY.*

## Table of Contents


**1. OUTREACH**

A. World Wide Web: GISS Home Page .....1

B. Global Data and Model Simulations .....5

C. Research News and Features, Science Briefs, and Science Nuggets.....8

D.Science Education at GISS .....29

**2. PUBLICATIONS**

A. GISS Best Publication Award .....31

B. Journal Papers ….....33

C.Chapters, Conferences, Workshops, and Other Publications…….....….187

D. Theses .....210

**3. AUTHOR INDEX** .....212

## 1. OUTREACH

### A. WORLD WIDE WEB: GISS HOME PAGE

The GISS homepage on the Word Wide Web is located at the URL:

https://www.giss.nasa.gov/

All of the GISS website can be reached via the GISS homepage. These sites host a growing body of datasets, journal papers, preprints, software, and educational material. Sample GISS websites are depicted on the following pages including the GISS Publications main page.

The extensive GISS publications database is located at the URL:

https://pubs.giss.nasa.gov/

The publications website presently includes abstracts for more than 5700 GISS papers published since the institution's creation in 1961, with near complete coverage of papers published since 1990. Additionally, the publications site includes downloadable copies of about half of these papers, almost all of them in the widely used Acrobat/PDF format.

Information about GISS Research Projects and Groups can be found at:

https://www.giss.nasa.gov/projects/

Research at GISS emphasizes a broad study of global change, an interdisciplinary research initiative addressing natural and man-made changes in our environment which occur on various time scales from decades to millennia and which affect the habitability of our planet. The research combines analysis of comprehensive global datasets with global models of atmospheric, land surface, and oceanic processes and includes safety of past events on Earth such as paleoclimate surface, and oceanic processes includes study of past events on Earth such paleoclimate change and the study of to their planets as an aid to production of future evolution of Earth on a planetary scale.

Individual GISS projects can be accessed from the "Projects & Groups" tab on the GISS homepage. Some of these websites include:

Astrobiology — ROCKE-3D,

https://www.giss.nasa.gov/projects/astrobio/

Climate Impacts,

https://www.giss.nasa.gov/projects/impacts/

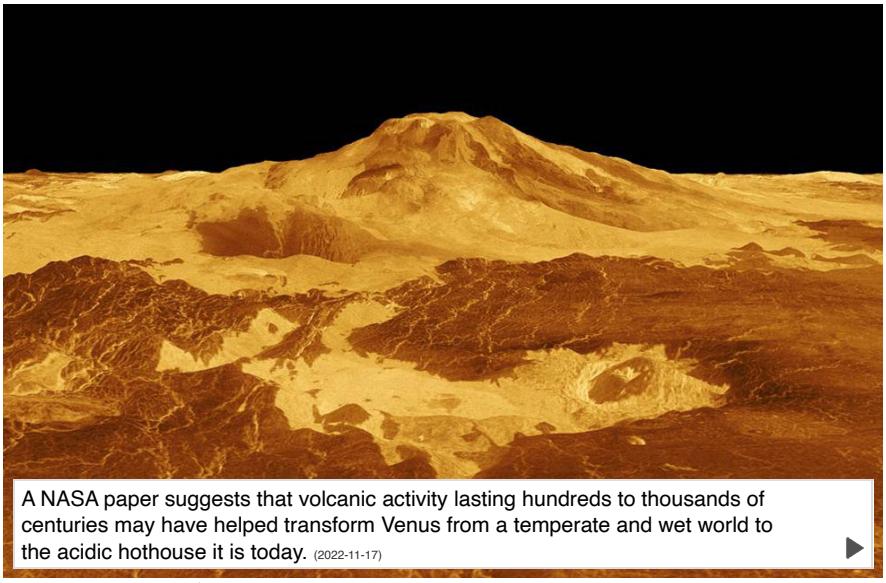
Goddard Institute Surface Temperature Analysis (GISTEMP),

https://data.giss.nasa.gov/gistemp/

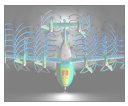


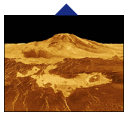



## Massive Volcanism May Have Altered Ancient Venus' Climate

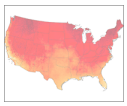


A NASA paper suggests that volcanic activity lasting hundreds to thousands of centuries may have helped transform Venus from a temperate and wet world to the acidic hothouse it is today. (2022-11-17)


Supercomputing


Venus Volcanism


Hispanic Month

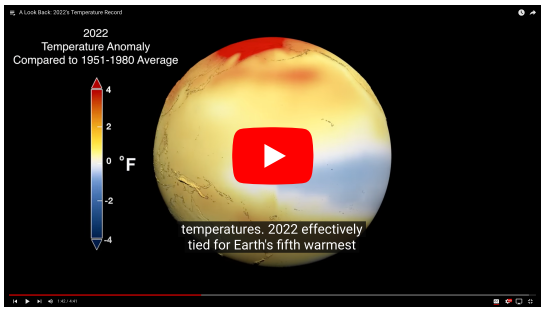

Extreme Heat


Food Prize


Best Paper 2021

More News & Features

### Featured Video




### Recent Publications

Casas, M.C., G.A. Schmidt, R.L. Miller, C. Orbe, K. Tsigaridis, L.S. Nazarenko, S.E. Bauer, and D.T. Shindell, 2023: Understanding model-observation discrepancies in satellite retrievals of atmospheric temperature using GISS ModelE. *J. Geophys. Res. Atmos.*, **128**, no. 1, e2022JD037523, doi:10.1029/2022JD037523.

Bauer, S.E., K. Tsigaridis, G. Faluvegi, L. Nazarenko, R.L. Miller, M. Kelley, and G. Schmidt, 2022: The turning point of the aerosol era. *J. Adv. Model. Earth Syst.*, **14**, no. 12, e2022MS003070, doi:10.1029/2022MS003070.

Mogul, R., S.S. Limaye, and M.J. Way, 2023: The $CO_2$ profile and analytical model for the Pioneer Venus Large Probe neutral mass spectrometer. *Icarus*, **392**, 115374, doi:10.1016/j.icarus.2022.115374.

Alexandrov, M.D., A. Marshak, B. Cairns, and A.S. Ackerman, 2022: Markovian statistical model of cloud optical thickness. Part I: Theory and examples. *J. Atmos. Sci.*, **79**, no. 12, 3315-3332, doi:10.1175/JAS-D-22-0125.1.

+ More Publications

### @NASAGISS Tweets

NASA GISS
@NASAGISS · Jan 12

2022 effectively tied for the 5th warmest year on @NASA's record, continuing a trend of warming temperatures. The last nine years were the warmest nine years on record, the result of human activities.
go.nasa.gov/3GEDYNA




Follow @nasagiss

### About GISS

Research at the NASA Goddard Institute for Space Studies (GISS) emphasizes a broad study of global change, which is an interdisciplinary initiative addressing natural and man-made changes in our environment that occur on various time scales — from one-time forcings such as volcanic explosions, to seasonal and annual effects such as El Niño, and on up to the millennia of ice ages — and that affect the habitability of our planet.

+ More About GISS




These database pages index more than 5700 publications authored or co-authored by NASA Goddard Institute for Space Studies scientists and colleagues since the institute was founded in 1961. Most entries are refereed journal articles, but the database also includes tech reports and tech notes, book chapters, conference proceedings papers, doctoral dissertations, and other research publications. The database is not complete but is nearly so for the years after 1990.

Copies of some listed publications are also available here in PDF form. Otherwise, entries are citation and abstract only. Most listings also include a link to the appropriate journal website. Some include links to related news releases or non-technical science briefs describing the research.

Some complete papers provided here differ from the published form, most likely because they are post-publication versions that include typographical or other corrections. Unless otherwise indicated, the published version is the version intended by the author(s).

## Recent Publications

Casas, M.C., G.A. Schmidt, R.L. Miller, C. Orbe, K. Tsigaridis, L.S. Nazarenko, S.E. Bauer, and D.T. Shindell, 2023: Understanding model-observation discrepancies in satellite retrievals of atmospheric temperature using GISS ModelE. *J. Geophys. Res. Atmos.*, **128**, no. 1, e2022JD037523, doi:10.1029/2022JD037523.

Bauer, S.E., K. Tsigaridis, G. Faluvegi, L. Nazarenko, R.L. Miller, M. Kelley, and G. Schmidt, 2022: The turning point of the aerosol era. *J. Adv. Model. Earth Syst.*, **14**, no. 12, e2022MS003070, doi:10.1029/2022MS003070.

Mogul, R., S.S. Limaye, and M.J. Way, 2023: The $CO_2$ profile and analytical model for the Pioneer Venus Large Probe neutral mass spectrometer. *Icarus*, **392**, 115374, doi:10.1016/j.icarus.2022.115374.

Alexandrov, M.D., A. Marshak, B. Cairns, and A.S. Ackerman, 2022: Markovian statistical model of cloud optical thickness. Part I: Theory and examples. *J. Atmos. Sci.*, **79**, no. 12, 3315-3332, doi:10.1175/JAS-D-22-0125.1.

Van Diedenhoven, B., O.P. Hasekamp, B. Cairns, G.L. Schuster, S. Stammes, M.A. Shook, and L.D. Ziemba, 2022: Remote sensing of aerosol water fraction, dry size distribution and soluble fraction using multi-angle, multi-spectral polarimetry. *Atmos. Meas. Tech.*, **15**, no. 24, 7411-7434, doi:10.5194/amt-15-7411-2022.

Roach, L.A., E. Blanchard-Wrigglesworth, S. Ragen, W. Cheng, K.C. Armour, and C.M. Bitz, 2022: The impact of winds on AMOC in a fully-coupled climate model. *Geophys. Res. Lett.*, **49**, no. 24, e2022GL101203, doi:10.1029/2022GL101203.

Luo, Z.J., G. Tselioudis, and W.B. Rossow (Eds.), 2022: *Studies of Cloud, Convection and Precipitation Processes Using Satellite Observations*. Lectures in Climate Change, Vol. 3. World Scientific, doi:10.1142/12862.

Cesana, G., T. Khadir, H. Chepfer, and M. Chiriaco, 2022: Southern Ocean solar reflection biases in CMIP6 models linked to cloud phase and vertical structure representations. *Geophys. Res. Lett.*, **49**, no. 22, e2022GL099777, doi:10.1029/2022GL099777.

## Annual Lists

Publications in
2023, 2022, 2021,
2020, 2019, 2018, 2017, 2016,
2015, 2014, 2013, 2012, 2011,
2010, 2009, 2008, 2007, 2006,
2005, 2004, 2003, 2002, 2001,
2000, 1999, 1998, 1997, 1996,
1995, 1994, 1993, 1992, 1991,
1990, 1989, 1988, 1987, 1986,
1985, 1984, 1983, 1982, 1981,
1980, 1979, 1978, 1977, 1976,
1975, 1974, 1973, 1972, 1971,
1970, 1969, 1968, 1967, 1966,
1965, 1964, 1963, 1962, 1961.

Papers in press or accepted for publication.

## Other Lists

+ Author Bibliographies
+ Best Paper of the Year
+ Most Cited Papers
+ Doctoral Dissertations

## Publication Links

+ GSFC Earth Sciences Publications
+ GSFC Library Authors & Publications
+ SAO/NASA Astrophysics Data System
+ NASA Technical Reports Server
+ AGU Journals
+ AIP Scitation
+ AMS Journals
+ DOI Resolver
+ EGU Journals
+ Google Scholar
+ IPCC Assessment Reports
+ ISI Web of Science
+ Optics Infobase

National Aeronautics and Space Administration
Goddard Institute for Space Studies

# Research Projects & Groups

Following are links to some research project and group homepages located on the NASA Goddard Institute for Space Studies websites.

A B C D E F G H I J K L M N O P Q R S T U V W X Y Z

**ACCMIP - Atmospheric Chemistry and Climate Model Intercomparison Project**




ACCMIP aims to better evaluate the role of atmospheric chemistry, both gases and aerosols, in driving climate change. In particular, the intercomparison is designed to facilitate analyses of the driving forces of climate change in simulations being performed in the Climate Model Intercomparison Project phase 5 (CMIP5) in support of the IPCC AR5. ACCMIP consists of a set of experiments designed to provide insight into the CMIP5 simulations of historical and future climate change, along with additional simulations to better understand the role of particular processes and constrain uncertainties.
+ Read More

**Astrobiology — Nexus for Exoplanet System Science**




The GISS Astrobiology group is an interdisciplinary team of scientists interested in understanding our solar system through time — from the early configuration of the planets nearly 4 billion years ago to their modern state. Our focus is on characterizing the habitability of rocky planets, extending that understanding to the climates of extrasolar planets, but also includes understanding environments as diverse as Titan and Archean Earth.
+ Read More

**Climate Impacts**



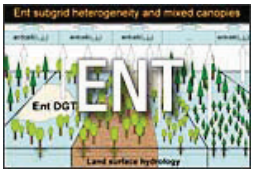

The Climate Impacts group at NASA GISS seeks to improve understanding of how climate affects human society through assessment of the effect of current climate variability and of potential climate change impacts caused by anthropogenic emissions of greenhouse gases and aerosols. Impacts research includes development of a framework to analyze complex interactions among biophysical and socio-economic processes.
+ Read More

**EdGCM - Education Global Climate Model**



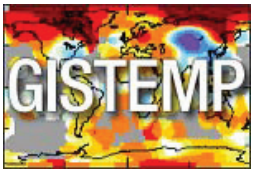

The Education GCM project at the Columbia University Center for Climate Systems Research couples the GISS Model II with a user-friendly interface that runs on desktop Macintosh and Windows PCs. EdGCM allows students to experience the full scientific process, from designing experiments to setting up and running climate simulations, processing output, displaying results, and creating scientific reports.
+ Read More

**Ent Dynamic Global Terrestrial Ecosystem Model**




The Ent model is a dynamic global terrestrial ecosystem model (DGTEM) developed specifically for coupling with atmospheric general circulation models (GCMs). Ent will be capable of predicting the fast time scale fluxes of water, carbon, nitrogen and energy between the land-surface and the atmosphere and the resulting diurnal surface fluxes, seasonal and inter-annual vegetation growth, and decadal to century-scale alterations in vegetation structure and soil carbon and nitrogen.
+ Read More

**GISTEMP - Goddard Institute Surface Temperature Analysis**




Surface air temperature change is a primary measure of global climate change. The GISTEMP project started in the late 1970s to provide an estimate of the changing global surface air temperature which could be compared with the estimates obtained from climate models simulating the effect of changes in atmospheric carbon dioxide, volcanic aerosols, and solar irradiance. The continuing analysis updates global temperature change from the late 1800s to the present.
+ Read More

For more, see https://www.giss.nasa.gov/projects/

## B. Global Data and Model Simulations

GISS datasets are accessible from our main datasets index at:

https://data.giss.nasa.gov/

This page links to introductory pages for each available dataset, which in turn link to the actual data and to sample code snippets and images. In many cases, such as model simulation datasets and the GISS global temperature analysis, the user can interactively create graphics from the data.

Ready access to our global data sets and the results of our model simulations facilitates interactions with the outside community. It is with this in mind that we are giving priority to putting these data in convenient forms. This includes data that can be downloaded directly from our web pages, larger data sets that are available via ftp, climate model simulations, and downloadable software.

This section also includes the GISS "Software Tools" homepage, which can be found at:

https://www.giss.nasa.gov/tools/

This page provides an index of downloadable GISS-created software applications, including three versions of the GISS climate model and other research tools. Among these are the FORTRAN source code for the new GISS ModelE coupled atmosphere-ocean model and the cross-platform Panoply netCDF data viewer.

National Aeronautics and Space Administration
Goddard Institute for Space Studies




Datasets and derived material are available from the NASA GISS websites for the following research projects:

## Climate Simulations

### GISS ModelE

- Earth's Energy Imbalance
- Efficacy of Climate Forcings
- Climate Simulations for 1880-2003
- Dangerous Human-Made Interference
- Transient Simulations with Beryllium-10
- Simulated Greenland Surface Mass Balance
- Desert Dust, Industrialization and Agricultural Fires

### SWING2 Stable Water Isotope Intercomparisons

## Climate Forcings

- Forcings in GISS Climate Model
- Dust Mineral Fractions at Emission
- Globally Uniform Mineral Dust Aerosols
- Global Land Cover Datasets
- Surface Exchange of Carbon Dioxide
- Surface Exchange of Methane

## Climate Impacts

- AgMIP Climate Forcing Datasets for Agricultural Modeling
- Evolving Fragility of the Global Food System
- Global Fire Weather Database (GFWED)

## Planets, Exoplanets and Astrobiology

- Simulations of Planetary Climates with ROCKE-3D
- Saturn Mean Zonal Winds and Eddy Momentum Fluxes
- Objective Classification of Saturn Cloud Features

## Astrophysics

- Molecular Collision Rates Relevant to Microwave and IR Astronomy

## Earth Observations

### Temperature

- GISS Surface Temperature Analysis (GISTEMP)
- GISTEMP Uncertainty Quantification
- Common Sense Climate Index (CSCI)

### Aerosols

- Photopolarimetry Measurements of Aerosols (RSP-Air)
- Global Aerosol Climatology Project (GACP)
- Stratospheric Aerosol and Gas Experiment II (SAGE II) V6.20

### Clouds

- International Satellite Cloud Climatology Project (ISCCP)
- GEWEX Cloud System Study Data Integration for Model Evaluation (GCSS-DIME)
- Cumulus And Stratocumulus Cloudsat-CAlipso Dataset (CASCCAD)

### Oceans

- Global Seawater Oxygen-18 Database
- Ocean Carbon States — Database and Toolbox

### Precipitation

- Observed Land Surface Precipitation Data: 1850-1995 (GISS/Dai)
- Observed Land Surface Precipitation Data: 1901-2000 (CRU TS 2.0)

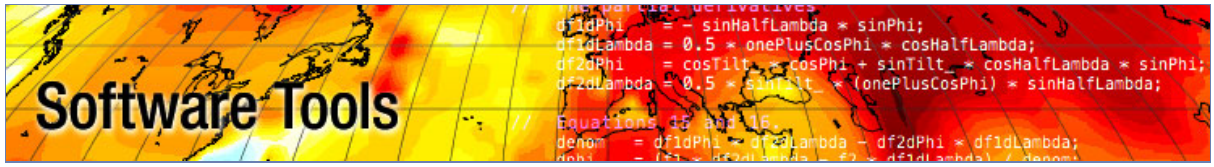
### Radiative Flux

- ISCCP Global Surface and Atmospheric Radiative Fluxes
- Surface Solar Irradiance: Datasets Produced for SeaWiFS

### Storms

- Atlas of Extratropical Storm Tracks
- Observations of Extratropical Cyclones — Databases

National Aeronautics and Space Administration
Goddard Institute for Space Studies




This page provides links to several self-contained, downloadable software products that have been developed by GISS personnel, either for specific research purposes or for more general analytic use.

## Climate Modeling

### GISS GCM - Model E

Fortran 90 source and documentation for the GISS ModelE series of coupled atmosphere-ocean models. These models have been used for our contribution to the CMIP3 and CMIP5 archives of model simulation results.
+ Read More

## Exoplanets & Planetary Science

### GISS GCM - ROCKE-3D

Fortran 90 source and documentation for a version of GISS modelE GCM specially adapted for planetary (non-modern-Earth) simulations.
+ Read More

### Mars24

Desktop application that calculates the solar and mean time for any location on the planet Mars, presenting the data as digital readouts and in "sunclock" format. (Requires Java)
+ Read More

## Radiation

### T-Matrix Codes

Fortran source code for computing electromagnetic scattering by nonspherical and aggregated particles.
+ Read More

### Bidirectional Reflection Codes

Fortran source code for computing bidirectional reflection function for a semi-infinite homogeneous slab composed of arbitrarily shaped, randomly oriented particles.
+ Read More

## Data Visualization

### Panoply

Desktop application that interactively plots georeferenced and other data encoded in netCDF, HDF and GRIB file formats. (Requires Java)
+ Read More

### G.Projector

Desktop application that explores over 200 map projections, including transformation of input equirectangular map images. (Requires Java)
+ Read More

## Numerical Tools

### JIGSAW(GEO)

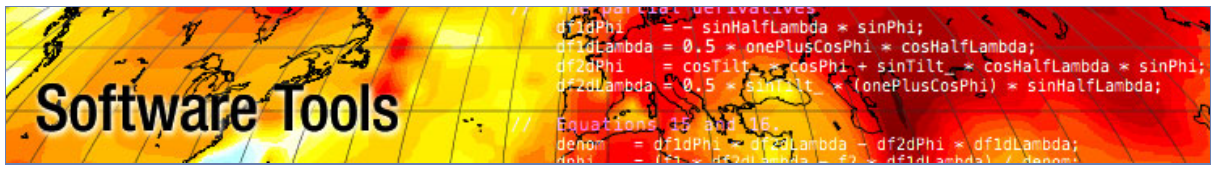
C++ package that generates variable resolution unstructured mesh grids in complex domains. It is useful for multi-resolution GCMs and climate process modeling.
+ Read More

## Astrophysics

### MOLSCAT

Fortran source for quantum mechanical solution of nonreactive molecular scattering, useful in astrophysical studies.
+ Read More

National Aeronautics and Space Administration
Goddard Institute for Space Studies




This page provides links to several self-contained, downloadable software products that have been developed by GISS personnel, either for specific research purposes or for more general analytic use.

## Climate Modeling

### GISS GCM - Model E

Fortran 90 source and documentation for the GISS ModelE series of coupled atmosphere-ocean models. These models have been used for our contribution to the CMIP3 and CMIP5 archives of model simulation results.
+ Read More

## Exoplanets & Planetary Science

### GISS GCM - ROCKE-3D

Fortran 90 source and documentation for a version of GISS modelE GCM specially adapted for planetary (non-modern-Earth) simulations.
+ Read More

### Mars24

Desktop application that calculates the solar and mean time for any location on the planet Mars, presenting the data as digital readouts and in "sunclock" format. (Requires Java)
+ Read More

## Radiation

### T-Matrix Codes

Fortran source code for computing electromagnetic scattering by nonspherical and aggregated particles.
+ Read More

### Bidirectional Reflection Codes

Fortran source code for computing bidirectional reflection function for a semi-infinite homogeneous slab composed of arbitrarily shaped, randomly oriented particles.
+ Read More

## Data Visualization

### Panoply

Desktop application that interactively plots georeferenced and other data encoded in netCDF, HDF and GRIB file formats. (Requires Java)
+ Read More

### G.Projector

Desktop application that explores over 200 map projections, including transformation of input equirectangular map images. (Requires Java)
+ Read More

## Numerical Tools

### JIGSAW(GEO)

C++ package that generates variable resolution unstructured mesh grids in complex domains. It is useful for multi-resolution GCMs and climate process modeling.
+ Read More

## Astrophysics

### MOLSCAT

Fortran source for quantum mechanical solution of nonreactive molecular scattering, useful in astrophysical studies.
+ Read More

## C. Research News and Features, Science Briefs, and Science Nuggets

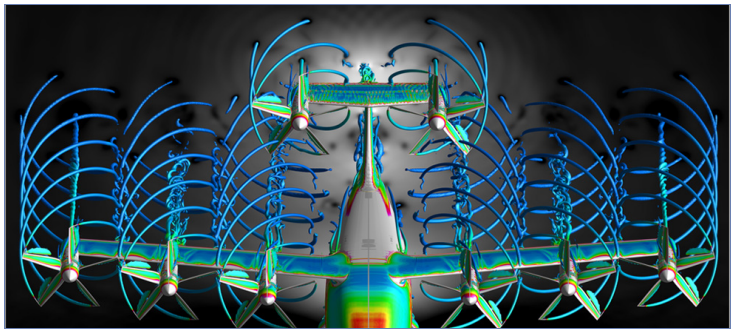
The communication of research goals and results with the public is one important aspect of our research program. GISS researchers are encouraged to prepare one-page summaries of their principal publications, in language meaningful to the educated laity.

To further our communication of GISS research, this publications document also includes "News & Features," NASA media releases about notable GISS research accomplishments. Following are copies of this year's "NASA News and Feature Releases," popular science papers ("Science Briefs"), and "Science Nuggets." All belong to a larger collection of articles which are available at the GISS homepage.




Following are news releases, features and updates about GISS research posted during 2022

## 5 Ways Supercomputing is Key to NASA Mission Success

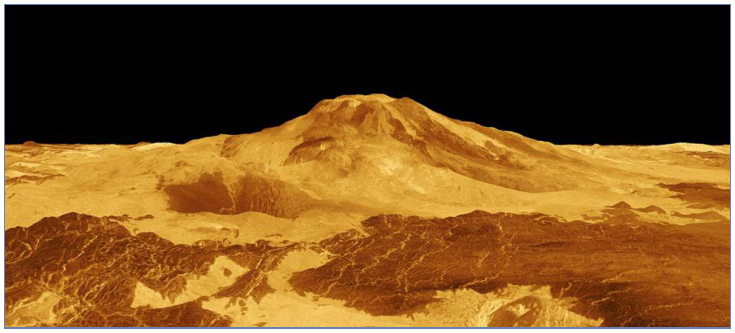


Whether developing new technologies for landing on other planets, improving air travel here at home, or more realistically simulating global weather and climate, supercomputing is key to the success of NASA missions.

(2022-11-22)

+ Read NASA Release

## Massive Volcanism May Have Altered Ancient Venus' Climate

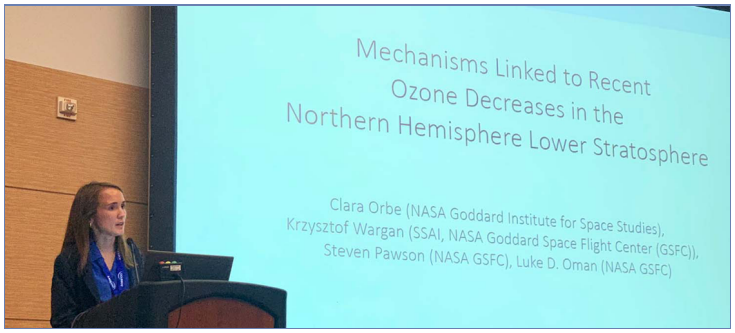


A NASA paper suggests that volcanic activity lasting hundreds to thousands of centuries may have helped transform Venus from a temperate and wet world to the acidic hothouse it is today.

(2022-11-17)

+ Read NASA Release

## Celebrating Nat'l Hispanic American Heritage Month: Dr. Clara Orbe

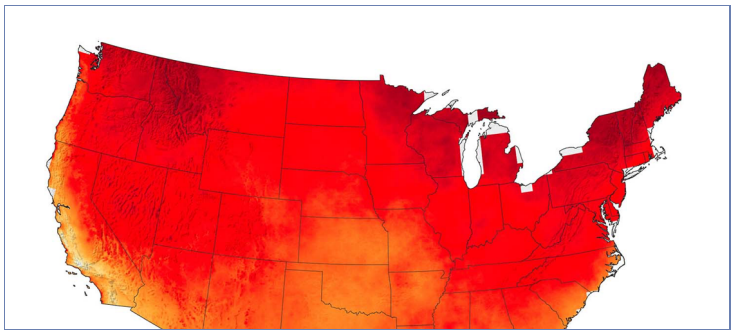



NCCS highlights GISS scientist Dr. Clara Orbe of Argentine heritage, from her early schooling to college career and eventually becoming a leading scientist at GISS.

(2022-10-12)

+ Read Feature

## Feeling the Heat in the Extremes



If trends continue, oppressively hot and humid summers like the record-breaking heat waves in California will continue.

(2022-09-16)

+ Read Feature

**For more GISS Research News & Features, see https://www.giss.nasa.gov/research/**

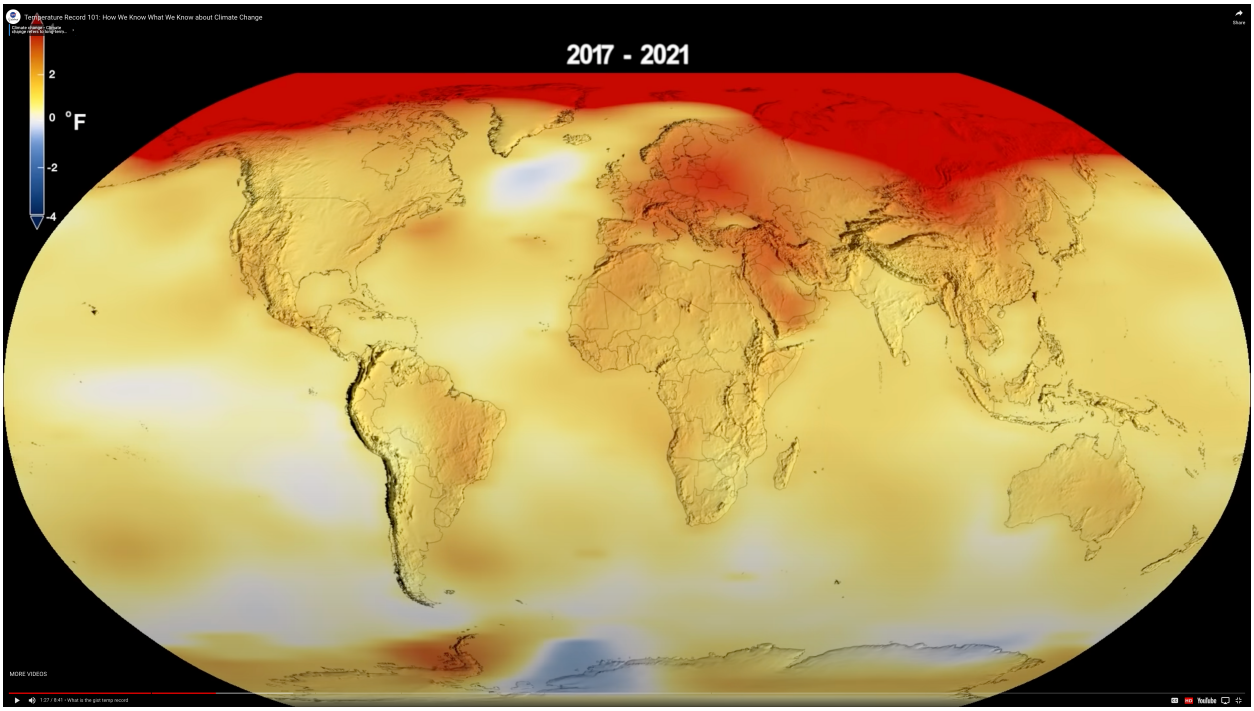
## NASA News & Feature Releases

### 2021 Tied for 6th Warmest Year in Continued Trend, NASA Analysis Shows

*Posted Jan. 13, 2022*

*Lee esta nota de prensa en español aquí.*

Earth's global average surface temperature in 2021 tied with 2018 as the sixth warmest on record, according to independent analyses done by NASA and the National Oceanic and Atmospheric Administration (NOAA).




2021 was tied for the sixth warmest year on NASA's record, stretching more than a century. Because the record is global, not every place on Earth experienced the sixth warmest year on record. Some places had record-high temperatures, and we saw record droughts, floods and fires around the globe. (Credit: NASA/GSFC/SVS/Kathryn Mersmann)

Continuing the planet's long-term warming trend, global temperatures in 2021 were 1.5 degrees Fahrenheit (0.85 degrees Celsius) above the average for NASA's baseline period, according to scientists at NASA's Goddard Institute for Space Studies (GISS) in New York. NASA uses the period from 1951-1980 as a baseline to see how global temperature changes over time.

Collectively, the past eight years are the warmest years since modern recordkeeping began in 1880. This annual temperature data makes up the global temperature record — which tells scientists the planet is warming.

According to NASA's temperature record, Earth in 2021 was about 1.9 degrees Fahrenheit (or about 1.1 degrees Celsius) warmer than the late 19th century average, the start of the industrial revolution.

“Science leaves no room for doubt: Climate change is the existential threat of our time,” said NASA Administrator Bill Nelson. “Eight of the top 10 warmest years on our planet occurred in the last decade, an indisputable fact that underscores the need for bold action to safeguard the future of our country — and all of humanity. NASA's scientific research about how Earth is changing and getting warmer will guide communities throughout the world, helping humanity confront climate and mitigate its devastating effects.”

This warming trend around the globe is due to human activities that have increased emissions of carbon dioxide and other greenhouse gases into the atmosphere. The planet is already seeing the effects of global warming: Arctic sea ice is declining, sea levels are rising, wildfires are becoming more severe and ianimal migration patterns are shifting. Understanding how the planet is changing — and how rapidly that change occurs — is crucial for humanity to prepare for and adapt to a warmer world.

Weather stations, ships, and ocean buoys around the globe record the temperature at Earth's surface throughout the year. These ground-based measurements of surface temperature are validated with satellite data from the Atmospheric Infrared Sounder (AIRS) on NASA's Aqua satellite. Scientists analyze these measurements using computer algorithms to deal with uncertainties in the data and quality control to calculate the global average surface temperature difference for every year. NASA compares that global mean temperature to its baseline period of 1951-1980. That baseline includes climate patterns and unusually hot or cold years due to other factors, ensuring that it encompasses natural variations in Earth's temperature.

Many factors affect the average temperature any given year, such as La Nina and El Nino climate patterns in the tropical Pacific. For example, 2021 was a La Nina year and NASA scientists estimate that it may have cooled global temperatures by about 0.06 degrees Fahrenheit (0.03 degrees Celsius) from what the average would have been.

A separate, independent analysis by NOAA also concluded that the global surface temperature for 2021 was the sixth highest since record keeping began in 1880. NOAA scientists use much of the same raw temperature data in their analysis and have a different baseline period (1901-2000) and methodology.

“The complexity of the various analyses doesn't matter because the signals are so strong,” said Gavin Schmidt, director of GISS, NASA's leading center for climate modeling and climate change research. “The trends are all the same because the trends are so large.”

NASA's full dataset of global surface temperatures for 2021, as well as details of how NASA scientists conducted the analysis, are publicly available from GISS.

GISS is a NASA laboratory managed by the Earth Sciences Division of the agency's Goddard Space Flight Center in Greenbelt, Maryland. The laboratory is affiliated with Columbia University's Earth Institute and School of Engineering and Applied Science in New York.

For more information about NASA's Earth science programs, visit: https://www.nasa.gov/earth

**Media Contacts**
Tylar Greene, NASA Headquarters, Washington, D.C., 202-358-0030, tylar.j.greene@nasa.gov

Peter Jacobs, NASA Goddard Space Flight Center, Greenbelt, Md., 301-286-0535, peter.jacobs@nasa.gov

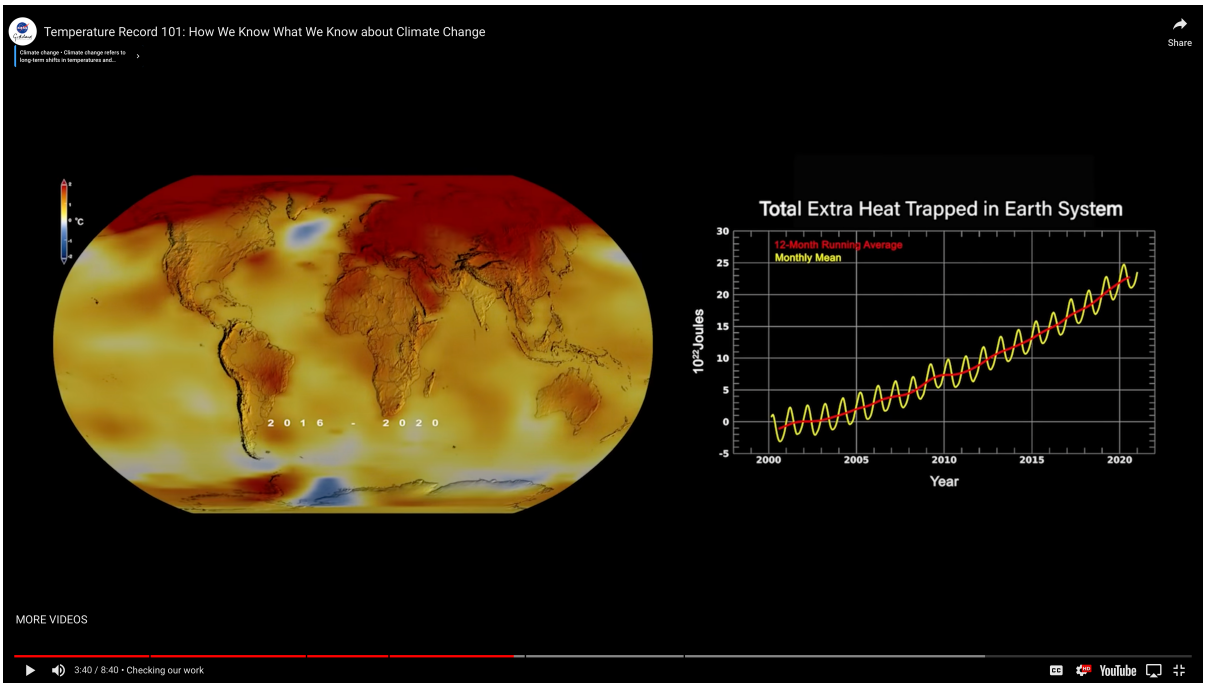
*This article was originally prepared as NASA Release 22-006.*

## NASA News & Feature Releases

### Six Questions to Help You Understand the 6th Warmest Year on Record

*Posted Jan. 13, 2022*

2021 tied with 2018 as the sixth warmest year on a record that extends back to 1880, according to NASA's annual analysis of global average temperatures. The year contributed to an unprecedented, but well-understood trend in which the last eight years have been the warmest ever recorded.




2021 was tied for the sixth warmest year on NASA's record, stretching more than a century. Because the record is global, not every place on Earth experienced the sixth warmest year on record. Some places had record-high temperatures, and we saw record droughts, floods and fires around the globe. (Credit: NASA/GSFC/SVS/Katie Jepson, Kathryn Mersmann, Kathleen Gaeta)

Scientists at NASA's Goddard Institute for Space Studies (GISS) in New York City produce this record using data from instruments all over the world, which is validated by satellite data. Scientists update the record every year, maintaining one of the world's most important datasets to study the extent, pace and causes of warming on our home planet.

Here, we answer six questions to help you understand the GISS global surface temperature analysis, what it shows about 2021 and how NASA makes sense of the data.

**1. What is the GISS Global Surface Temperature Analysis?**

Also known as GISTEMP, this product is one of several independent datasets by major scientific organizations that track Earth's temperatures. Its publicly available raw data come from tens of thousands of instruments on weather stations, ships and ocean buoys, and Antarctic research stations.

The NASA analysis takes into account the seasonal cycle and average climate in each of these locations to determine how much warmer or cooler it is on average. Temperatures at different locations on Earth can vary by as much as 100 degrees Fahrenheit (55 degrees Celsius), but the average global temperature over the course of the year changes much more subtly. In other words, when scientists pull all that data together to estimate global average temperatures, the analysis serves as a massive, planetary thermometer.

**2. If the record shows unprecedented warming, why isn't every year the warmest year ever?**

Earth's temperature varies every year because of the many interactions among the land, air and ocean. These complex connections influence weather and temperatures regionally and globally.

One of these interactions is the El Niño-Southern Oscillation, a natural phenomenon in which heat transfers for several months between the Pacific and the atmosphere lead to temperature and rainfall fluctuations all over the world. La Niña, the cooler phase of this phenomenon, generally leads to weather patterns that lower Earth's average temperature with a slight lag of several months. That's how a La Niña event in early 2021 led to a cooler year than it would have been otherwise, in particular cooler than 2020 or 2016 — the warmest years on record.

Scientists are predicting that because La Niña reappeared in late 2021, its cooling influence will likely affect temperatures in 2022. Still, even with these phenomena, 2021 contributes to, and is consistent with, the observed long-term warming trend.

Global temperatures are rising at a pace that the planet has not experienced in millennia, according to NASA. That is, even though short-term weather cycles can affect any single year, the warming trends are still very clear and growing.

**3. How does NASA crunch the numbers to analyze global temperatures?**

NASA's analysis averages temperature estimates made over many decades. That produces a trend, or pattern, of how fast Earth's surface temperatures have changed in recent times. The analysis uses a fixed period of 1951 to 1980 that serves as a baseline to compare how global temperatures today are deviating from what was normal then.

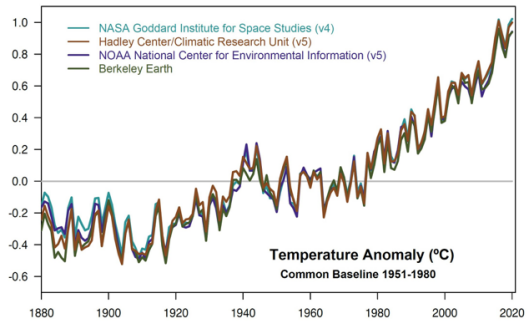
The baseline period included the best available data when scientists designed the basic methods for NASA's analysis in the 1980s. These data also included comprehensive global coverage, since datasets from pre-1950 generally excluded input from the Southern Hemisphere.

The steps to calculate temperature anomalies today remain fundamentally the same as they did in the 1980s. A key exception is that refined algorithms now minimize errors resulting from data in urban areas, which tend to warm more than rural areas. The amount and quality of data available also has increased substantially over time, improving how much of Earth's surface the dataset covers.

**4. How reliable is NASA's temperature analysis?**

Scientists always try to confirm the accuracy of the record with independent studies and, in recent decades, satellites. Recent assessments revealed the agency's estimates of the annual average are accurate to within a tenth of a degree Fahrenheit.

The record uses raw data stretching back to 1880, when methods to measure temperature were less developed. But these historic data still provide a very useful window into the past. The recent assessments show that even when factoring in greater uncertainties in data from before 1950, they still provide the basis for a good estimate of past global annual temperatures. In other words, the pre-1950 data are like a blurry photo compared to the sharpness of today's datasets: Scientists are a little more uncertain about some of its details but can still be certain about the overall picture the data show.




This plot shows yearly temperature anomalies from 1880 to 2019, as analyzed by NASA and other scientific institutions. Though there are minor variations from year to year, all five temperature records show peaks and valleys in sync with each other. (Credits: NASA GISS/Gavin Schmidt)

NASA also checks for irregularities in the quality and distribution of data, as faulty instruments, human errors in recording and processing data and other non-climatic factors can yield unrealistic readings. When raw data from individual stations seems inaccurate, scientists double-check them manually by comparing these data against neighboring areas with similar climatic conditions. These adjustments can influence records at individual stations and small regions, but they barely change global averages.

Other organizations also process the same data with slightly different methods. Their records all show trends remarkably similar to NASA's analysis.

**5. What are some indicators and consequences of warming?**

Satellite data confirm how warming on the land, air and ocean is affecting different parts of the planet. The rising temperatures are causing ice sheets and glaciers worldwide to melt, heatwaves to be longer and more intense, and plants and animal habitats to shift as they respond to warming.

As NASA's temperature analysis shows the Arctic is warming four times faster than the rest of the planet, satellites show a decline in the region's sea ice extent of about 13% per decade. Satellites also show the ocean is warming at an unprecedented rate, with 2021 marking the hottest ocean temperatures and the highest global sea levels ever recorded.

In 2021, Earth saw several extreme examples of how excess heat in the ocean and atmosphere can influence often devastating, sometimes unexpected, disasters in different parts of the world. Australia, Europe and Asia experienced historic floods driven by record-breaking levels of intense rainfall. In the United States, the record-setting Dixie Fire burned in California, massive heat-waves were seen in the Pacific Northwest and Hurricane Ida caused damages from Louisiana to New York.

**6. Why does NASA estimate global surface temperature change?**

In the early 1970s, research into Venus' atmosphere provided a stark example of how extremely high amounts of greenhouse gasses, which trap heat in the atmosphere, turned Earth's so-called twin into an uninhabitable world with blistering surface temperatures that would melt lead.

Scientists then became increasingly concerned about the influence of carbon dioxide and other greenhouse gasses on Earth. In 1981, NASA scientists were the first to estimate global temperature averages using the techniques that eventually evolved into the current analysis. The idea was to provide context for predictions of future climate change.

Today, the analysis has helped explain how carbon dioxide emissions, deforestation and other human activities are driving global warming — and why volcanic eruptions, fluctuations in the Sun's energy output and other natural factors are not the primary drivers of the observed warming trend.

## NASA News & Feature Releases



### NASA Researcher Finding Ways to Turn Down the Heat in Cities

*Posted Mar. 21, 2022*

Rooftop gardens and greenery can help ease some of the severe heat in cities, according to research from climate scientists at NASA's Goddard Institute for Space Studies (GISS) in New York. For several decades, researchers have promoted replacing black tar and other dark-colored roofing materials with bright, Sun-reflecting surfaces or "green roofs" full of plant cover. Now they have used freely available satellite data to measure how effective these changes are.

Heat is often intensified or amplified in cities, a phenomenon known as the urban heat island effect. Asphalt, concrete, and similar materials absorb and retain significantly more heat than vegetation, so temperatures in urban areas are often 10 degrees Fahrenheit hotter than surrounding suburbs or rural regions. In neighborhoods with fewer trees and green spaces, this heat often disproporptionately affects older adults, low-income communities and some communities of color.

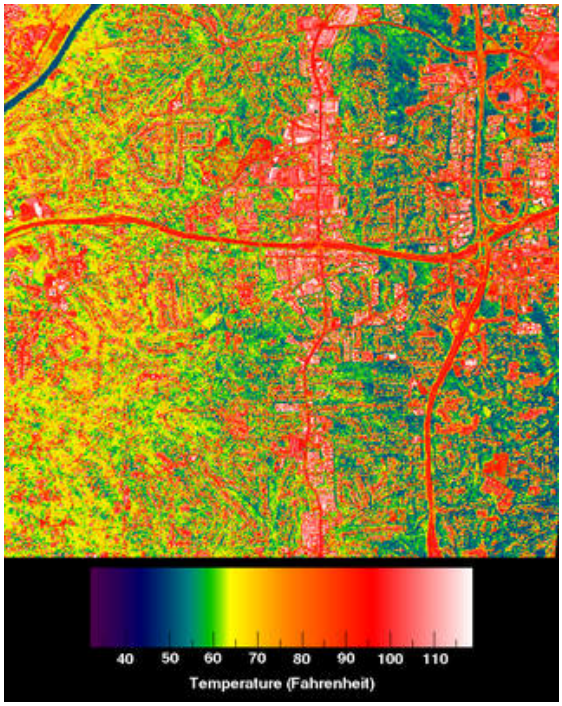
Green roofs are designed to harness the cooling power of plants to lower the temperature in city spaces. The greenery may be extensive (shallow soil, low-maintenance plants) or intensive (deeper soil, more diverse plants and trees).

The GISS team studied three sites in Chicago to see how green roofs affected surface temperatures around those buildings, and whether there was a difference between those sites and others nearby without green roofs. Two of three green roofs in the study reduced temperatures, but results indicated that effectiveness may depend on location and plant diversity, among other factors. The results were recently published in the journal *Sustainable Cities and Society*.

**Studying green roofs in urban jungles**

“As cities grow and develop, they need to make good decisions about their infrastructure, because these decisions often last for 30 or 50 years or longer,” said Christian Braneon, a climate scientist and civil engineer at Columbia University and GISS. “In the context of more frequent heat waves and more extreme heat, it's important to understand how these urban design interventions can be effective.”

Braneon and the GISS team partnered with Chicago's Public Health and Planning and Development departments to study three sites that had installed green roofs in the early 2000s: Millennium Park, City Hall, and a Walmart shopping center. Using imagery captured by the Landsat 5 satellite between 1990 and 2011, the researchers compared changes in land surface temperatures and vegetation abundance at the study sites as well as nearby control sites without green roofs.




Urban heat is a growing issue in other cities besides Chicago, too. This satellite imagery of suburban Atlanta, captured by Landsat 5 in an older study, shows the differences in daytime heating, as caused by the urban heat island effect. These data were collected May 11 and 12, 1997 (using the same instrument as the Chicago study data). While daytime air temperatures on that date were only about 80 °F, surface temperatures reached as much as 118 °F; nighttime air temperatures hovered between 50 °F and 55 °F, but due to the heat sink, surface temperatures hung on as high as 75 °F. (Credits: NASA's Scientific Visualization Studio / Greg Shirah)

Results from the three sites were mixed. Millennium Park, which has an intensive mix of plants and is located near Lake Michigan, showed significantly lower average temperatures after its green roof was installed in 2004. It was the only site where the roof fully mitigated climate warming over the study period.

City Hall, also an intensive site, had a green roof installed in 2002. Its temperatures after green roof installation were lower than those at the control site, but they were rising toward the end of the study period.

The Walmart site told a different story. While the green roofs at Millennium Park and City Hall were added onto existing buildings, the supermarket was newly built during the study period. Even though the Walmart installed an extensive green roof, the conversion of the land from a vacant, grassy lot to a store meant the vegetation index for the landscape decreased.

“In a lot of places, you might be developing an area that didn't have something there before; it just had overgrown vegetation,” said Braneon, who co-leads urban research for the Climate Impacts Group at GISS. “You might think that putting a green roof on your new building would make a significant impact. But what we see is that a lot of impervious material may also be added there — such as a parking lot around the building. As a result, you might reduce the impact of the parking lot, but you certainly haven't created the cooling effect that the overgrown vegetation had.”

The benefits of green roofs depend on a variety of factors — from geographic region and plant diversity to rooftop structure and the cooling efficiency of the building itself, the scientists said.

Studies with larger sample sizes are needed to tease apart these details, but this study represents a promising start. With urban heat island effects expected to intensify as Earth's climate warms, it will become more important to understand these variables.

The study method is designed to be used by other cities for further research, said lead author Kathryn McConnell, a doctoral candidate at Yale University's School of the Environment. The simple analysis, publicly available data, and model for working directly with cities could help urban planners assess the viability of green roofs in their own areas.

“My hope would be that the methods we proposed show a low-cost way for folks working in less-resourced cities — who maybe don't have access to a university or government researcher — to study their own communities,” McConnell said.

“Traditionally, civil engineers and urban planners assumed a stationary climate,” Braneon added. “The whole practice is built on the premise that we can look at the past to assess risk in the future. Everything is being flipped on its head due to climate change, so I'm hoping to do more work that changes how civil engineers and urban planners practice.”

**References**

McConnell, K., C. Braneon, E. Glenn, N. Stamler, E. Mallen, D.P. John, R. Pandya, J. Abramowitz, G. Fernandez, and C. Rosenzweig, 2022: A quasi-experimental approach for evaluating the heat mitigation effects of green roofs in Chicago, Illinois. Sustain. Cities Soc., 76, 103376, doi:10.1016/j.scs.2021.103376.

***Banner Image:*** *Chicago's O'Hare International Airport is centered in this photograph, taken by astronauts aboard the International Space Station. The station was orbiting 259 miles above the state of Illinois when this picture was taken. (Credit: NASA)*

*This article was originally prepared by Jordan Hickey and Jessica Evans as a NASA webportal Earth Climate feature.*

## NASA News & Feature Releases

### NASA-Funded Study Extends Period When Mars Could Have Supported Life

*Posted Feb. 2, 2022*

The surface of Mars is barren and inhospitable, but perhaps it wasn't always that way. Billions of years ago, when life emerged on Earth, the climate of Mars could have been Earth-like as well, with a thicker atmosphere than today and oceans of liquid water. A study funded by NASA and international partners indicates this period could have lasted longer than originally thought.




“Our simulation revealed that three billion years ago, the climate in much of the northern hemisphere of Mars was very similar to present-day Earth, with a stable ocean,’ said Frédéric Schmidt of the University Paris-Saclay, France, co-lead author of a paper on the research published in the *Proceedings of the National Academy of Sciences* Jan. 17. “Our result contradicts theories claiming that such a northern ocean could not be stable. It also increases the time period for an Earth-like climate on Mars.’

The late Noachian period (from 4.1 billion to 3.5 billion years ago) is the period usually thought to be habitable on Mars, with significant rain near the equator, as demonstrated by the presence of valley networks — features formed by erosion from flowing water — at this age.

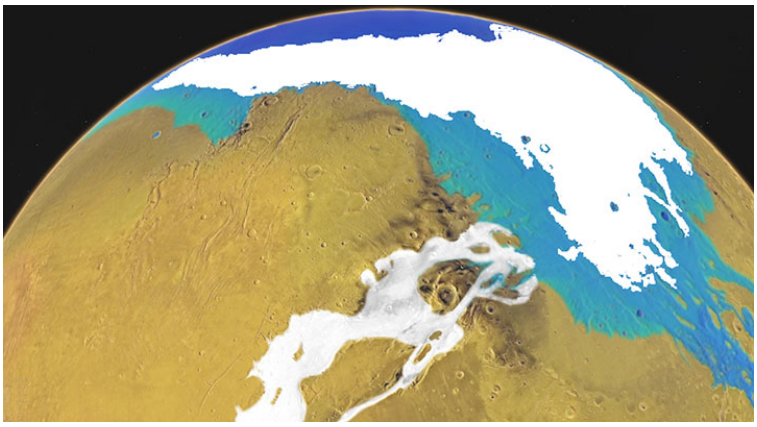
However, this clement period was not to last, and as the eons passed Mars gradually transitioned to its present-day climate, with an atmosphere too cold and thin to support liquid water, a necessary ingredient for life, on the surface. Scientists want to know the duration of the habitable period; the longer it was, the more time there would have been for any potential Martian life to form. The new work extends the potentially habitable period on Mars by about 500 million years, into the late Hesperian age.

“Discerning the climate of Mars approximately three billion years ago is challenging because the Martian surface features do not seem to fully support either a warm and wet or cold and dry climate during that time,’ said Michael Way, co-lead author of the paper at NASA's Goddard Institute for Space Studies, New York. “A warm and wet climate would have produced extensive erosion from flowing water, but few valley networks have been observed from this age. A too-cold climate would have kept any northern ocean frozen most of the time. A moderate cold climate would have transferred the water from the ocean to the land in the form of snow and ice. But this would prevent tsunami formation, for which there is some evidence.’

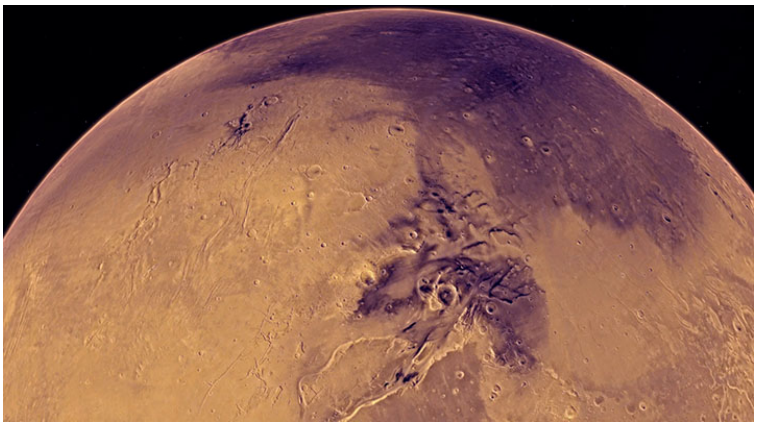
The new simulation revealed that the Martian climate at this time could have been cold and wet instead. An ocean would have formed in the northern lowland basin where the atmosphere was denser and warmer. Water would evaporate from this ocean and return to the surface as rain or snow. In and near the ocean, it would be mainly rain, but in the southern highlands where the air was cold, it would be mostly snow. The snow would accumulate into extensive glaciers which would flow down to the lowland basin, returning the water to the ocean.

The model shows that the northern ocean could remain liquid even with global mean surface temperatures below the freezing point of water because ocean circulation can bring warm water from mid-latitudes to the pole, regionally warming the surface up to 4.5° Celsius (40 degrees Fahrenheit). Also, just as a dark asphalt parking lot is hotter than a white concrete sidewalk on a sunny day, liquid water is darker than snow and ice, allowing the ocean to absorb more heat from sunlight.

Mars's current atmosphere is mostly carbon dioxide and extremely thin, around one percent of Earth's atmospheric pressure at sea level, but there is evidence it was thicker in the past. The model predicted a stable northern ocean if Mars had an ancient atmosphere as thick as present-day Earth's, made primarily of carbon dioxide with 10 percent hydrogen (H2). Just as a heavy coat traps more heat than a light jacket, a thick atmosphere would have helped warm a young Mars by retaining more heat from sunlight. Also, hydrogen helps the atmosphere trap even more heat since it's an efficient greenhouse gas, and it could have been released by extensive volcanic eruptions or meteorite impacts on early Mars.



This conceptual image reveals what the Kasei Valles region on Mars may have looked like three billion years ago. White areas are glaciers and blue represents ocean. Credits: F. Schmidt/NASA/USGS/ESA/ DLR/FU Berlin (G. Neukum)



Orbital imagery of the Kasei Valles region today.

Mars's ancient climate was simulated using the ROCKE-3D Global Climate Model (GCM) developed at the NASA Goddard Institute for Space Studies. The team used the current Martian landscape and surface elevations, removed all present-day ice sheets, and included a small northern ocean whose boundaries were set to where the geological evidence points.

The simulation was one of the first fully coupled GCMs used for Mars. This means that the 3D atmospheric and oceanic components are calculated at the same time, making it more realistic. “Since incorporating the full 3D ocean circulation is computationally expensive and takes longer to complete, most Mars global climate models couple the 3D atmosphere to a simple, thin, single-layer ocean that has no horizontal or vertical heat transport unlike the full 3D ocean used in our study,’ said Way.

The cold and wet climate predicted by the team's model is consistent with geologic evidence on Mars from this period. Glaciers carve wide U-shaped valleys as they flow, and compatible valley structures are found in the southern highlands, where the model indicates glaciers formed because these areas had the coldest temperatures. Rain forms many small, V-shaped valley networks that resemble tree branches as water flows downhill and streams merge into larger rivers. Valley networks of this age only appear at low altitudes near the ancient shoreline, which would have had the warmer temperatures required to form rain, as the model predicts.

The team members plan to continue studying the Red Planet to see whether there is more evidence to support their model. They will examine more images of Martian surface features, such as the glacial valleys, from recent missions. Also, the Mars Ice Mapper, a proposed mission by NASA and international partners, will have an unprecedented radar sounder that will be able to study the structure of the shallow subsurface to look for evidence of an ancient ocean. Finally, China's Zhurong rover landed in the region where the ocean may have formed, and rocks examined by the mission could provide evidence that an ocean once existed there.

**More about the research program and partners:**
The research was funded by NASA and international partners: the Goddard Sellers Exoplanet Environments Collaboration, which is funded by the NASA Planetary Science Division's Internal Scientist Funding Model, the NASA Astrobiology Program through collaborations arising from participation in the Nexus for Exoplanet System Science and the NASA Habitable Worlds Program, the University Paris-Saclay, France, the National Institute for Earth Sciences and Astronomy (Institut National des Sciences de l'Univers or INSU), Paris, France, the National Centre for Scientific Research (Centre National de la Recherche Scientifique or CNRS), Paris, France, and the French Space Agency (Centre National d'Etudes Spatiales or CNES), Paris, France, through the National Planetology Program (Programme National Planétologie). Resources supporting this work were provided by the NASA High-End Computing Program through the NASA Center for Climate Simulation at Goddard Space Flight Center.

**References**

Schmidt, F., M.J. Way, S. Bouley, A. Séjourné, and I. Aleinov, 2022: Circumpolar ocean stability on Mars 3 Gy ago. *Proc. Natl. Acad. Sci.*, **119**, no. 4, e2112930118, doi:10.1073/pnas.2112930118.

## NASA News & Feature Releases



### NASA's Cynthia Rosenzweig Receives 2022 World Food Prize

*Posted May 5, 2022*

Cynthia Rosenzweig, a senior research scientist and head of the Climate Impacts Group at NASA's Goddard Institute for Space Studies (GISS) in New York City, received the 2022 World Food Prize from the World Food Prize Foundation on May 5. According to the World Food Prize Foundation, the World Food Prize is a prestigious international award conceived as the "Nobel Prize for Food and Agriculture" with a mission to elevate innovations and inspire action to sustainably increase the quality, quantity and availability of food for all.

Rosenzweig was selected for the award for her research to understand the relationship between climate and food systems and forecast how both will change in the future. Her modeling work has provided a foundation for decision-makers around the world to create strategies to mitigate climate change and adapt our food systems to a changing planet, which has helped communities worldwide address the consequences of Earth's changing climate.



Cynthia Rosenzweig, winner of the 2022 World Food Prize and senior research scientist and head of the Climate Impacts Group at NASA GISS. (Credit: Courtesy of Kisha Bari)

"I am thrilled and honored to receive the World Food Prize this year because food systems are now emerging as a key component of climate change," said Rosenzweig.

Rosenzweig has been a research scientist at NASA GISS and head of the Climate Impacts Group since 1994. Her research focuses on improving models and assessments of how climate change will affect agriculture and the food supply in the future. In addition, she uses data from NASA satellites and models to study agricultural regions around the world and how they are changing. Rosenzweig has previously served as coordinating lead author for the Intergovernmental Panel on Climate Change (IPCC) Working Group II Fourth Assessment Report in 2007 and the IPCC Special Report on Climate Change and Land in 2019.

She is also a co-founder of the Agricultural Model Intercomparison and Improvement Project (AgMIP), an international project using climate science, crop modeling and economic modeling to understand crop yield and food security in a changing climate. Over 1,000 researchers from developed and developing nations have partnered with AgMIP to improve agricultural models and techniques to assess the future impacts of climate change on agriculture and food systems both regionally and globally. Through AgMIP, Rosenzweig has worked on research projects studying the effects of rising atmospheric carbon dioxide on crops as well as quantifying greenhouse gas emissions released through food production.

"I'm proud of Dr. Rosenzweig's dedication to improving agricultural models and capabilities that improve life around the globe," said NASA Administrator Bill Nelson. "On behalf of the entire NASA community, I want to congratulate her on this accomplishment. As our climate changes, NASA will continue working to understand the impact of more intense weather events that increasingly strain the worldwide food supply. We'll continue to support scientists like Dr. Rosenzweig as we plan for the future in a changing climate."

Scientists like Rosenzweig are already using agricultural data from NASA's fleet of Earth-observing satellites to understand food production and security in a changing climate. Modeling drought, water availability, changing surface temperature and other factors helps scientists like Rosenzweig understand crop yields and how they are changing. In the future, NASA's upcoming Earth System Observatory will provide more key information to guide understanding of how climate change impacts food and agriculture.

"Congratulations to Dr. Rosenzweig on this accomplishment," said Gavin Schmidt, director of NASA GISS. "This award and Dr. Rosenzweig's work is a great example of the value of NASA's research to help people around the world and in meeting our mission to innovate for the benefit of humanity."

For more information about the World Food Prize see: https://www.worldfoodprize.org/

For more information about Cynthia Rosenzweig see: https://www.giss.nasa.gov/staff/crosenzweig.html

*Banner image: Cynthia Rosenzweig explaining AgMIPs Farm System approach. Credit: Shari Lifson*

*This article was originally prepared by Sofie Bates as a NASA webportal Goddard feature.*

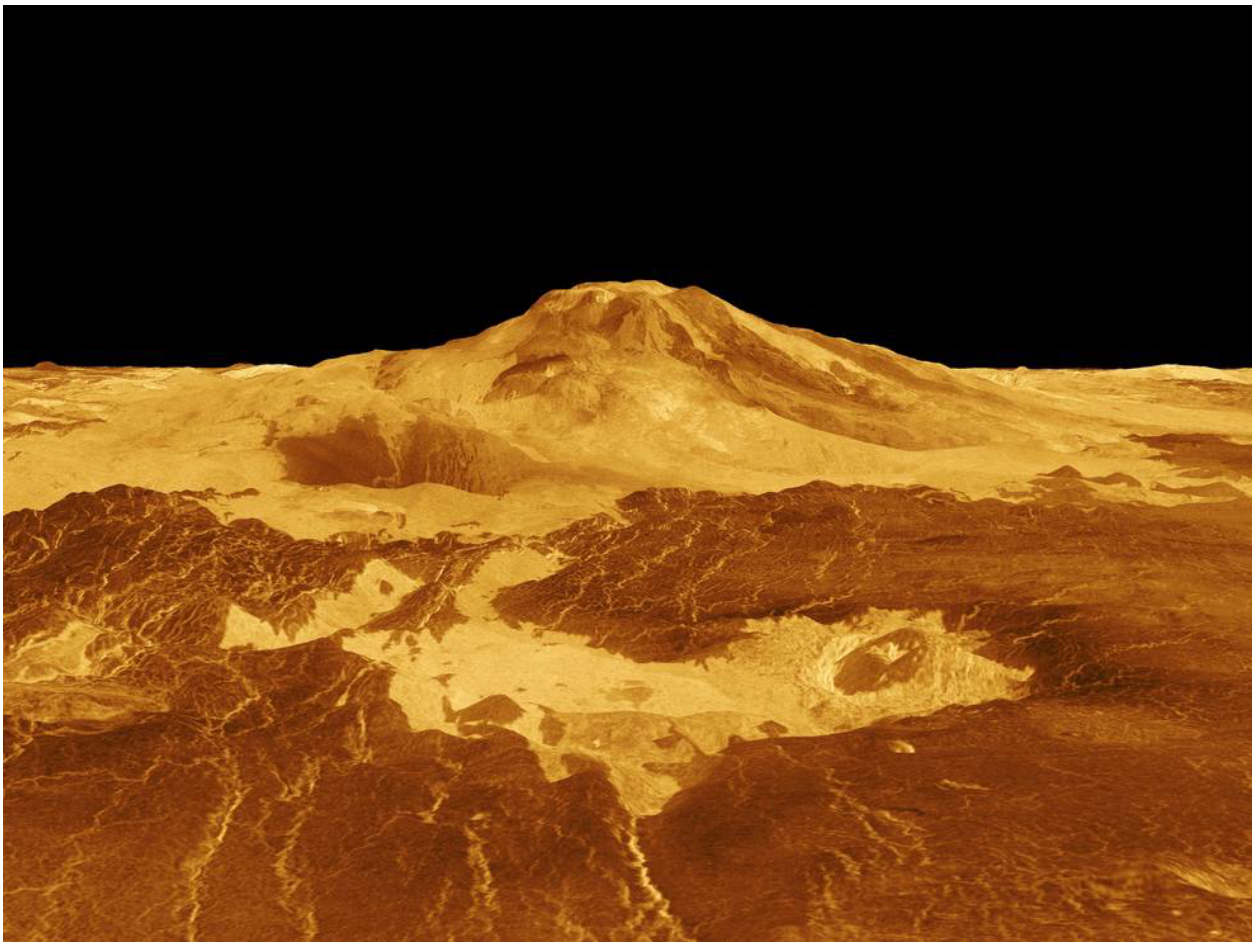
## NASA News & Feature Releases

### NASA Study: Massive Volcanism May Have Altered Ancient Venus' Climate

*Posted Nov. 17, 2022*

Volcanic activity lasting hundreds to thousands of centuries and erupting massive amounts of material may have helped transform Venus from a temperate and wet world to the acidic hothouse it is today, a NASA paper suggests.

The paper also discusses these “large igneous provinces” in Earth's history which caused several mass extinctions on our own planet millions of years ago.



Maat Mons is displayed in this computer-generated, three-dimensional perspective of the surface of Venus. The viewpoint is located 634 kilometers (393 miles) north of Maat Mons at an elevation of 3 kilometers (2 miles) above the terrain. Lava flows extend for hundreds of kilometers across the fractured plains shown in the foreground, to the base of Maat Mons. NASA Magellan mission synthetic aperture radar data is combined with radar altimetry to develop a three-dimensional map of the surface. The vertical scale in this perspective has been exaggerated 10 times. (Credit: NASA/JPL)

“By understanding the record of large igneous provinces on Earth and Venus, we can determine if these events may have caused Venus' present condition,” said Dr. Michael J. Way, of NASA's Goddard Institute for Space Studies in New York. Way is lead author on the paper, published April 22 in *The Planetary Science Journal*.

Large igneous provinces are the products of periods of large-scale volcanism lasting tens of thousands or even hundreds of thousands of years. They can deposit more than 100,000 cubic miles of volcanic rock onto the surface. At the upper end, this could be enough molten rock to bury the entire state of Texas half a mile deep.

Venus today boasts surface temperatures of around 864 F on average, and an atmosphere 90 times the surface pressure of Earth's. According to the study, these massive volcanic outpourings may have initiated these conditions sometime in Venus'

ancient history. In particular, the occurrence of several such eruptions in a short span of geologic time (within a million years) could have led to a runaway greenhouse effect which kicked off the planet's transition from wet and temperate to hot and dry.

Large fields of solidified volcanic rock cover 80% of Venus' surface in total, Way said. “While we're not yet sure how often the events which created these fields occurred, we should be able to narrow it down by studying Earth's own history.”

Life on Earth has endured at least five major mass extinction events since the origin of multicellular life about 540 million years ago, each of which wiped out more than 50% of animal life across the planet. According to this study and others before it, the majority of these extinction events were caused or exacerbated by the kinds of eruptions that produce large igneous provinces. In Earth's case, the climate disruptions from these events were not sufficient to cause a runaway greenhouse effect as they were on Venus, for reasons that Way and other scientists are still working to determine.

NASA's next missions to Venus, scheduled for launch in the late 2020s — the Deep Atmosphere Venus Investigation of Noble gases, Chemistry, and Imaging (DAVINCI) mission and the Venus Emissivity, Radio science, InSAR, Topography, And Spectroscopy (VERITAS) mission — aim to study the origin, history, and present state of Venus in unprecedented detail.

“A primary goal of DAVINCI is to narrow down the history of water on Venus and when it may have disappeared, providing more insight into how Venus' climate has changed over time,” Way said.

The DAVINCI mission will precede VERITAS, an orbiter designed to investigate the surface and interior of Venus from high above, to better understand its volcanic and volatile history and thus Venus' path to its current state. The data from both missions could help scientists to narrow down the exact record of how Venus may have transitioned from wet and temperate to dry and sweltering. It may also help us to better understand how volcanism here on Earth has affected life in the past, and how it may continue to do so in the future.

This study was supported by Goddard Space Flight Center's Sellers Exoplanet Environments Collaboration (SEEC) and was part of NASA's Nexus for Exoplanet System Science (NExSS) RCN.

**Reference**

Way, M.J., R.E. Ernst, and J.D. Scargle, 2022: Large scale volcanism and the heat-death of terrestrial worlds. *Planet. Sci. J.*, **3**, no. 4, 92, doi:10.3847/PSJ/ac6033.

*This article was originally prepared by Nick Oates as NASA webportal Venus feature.*

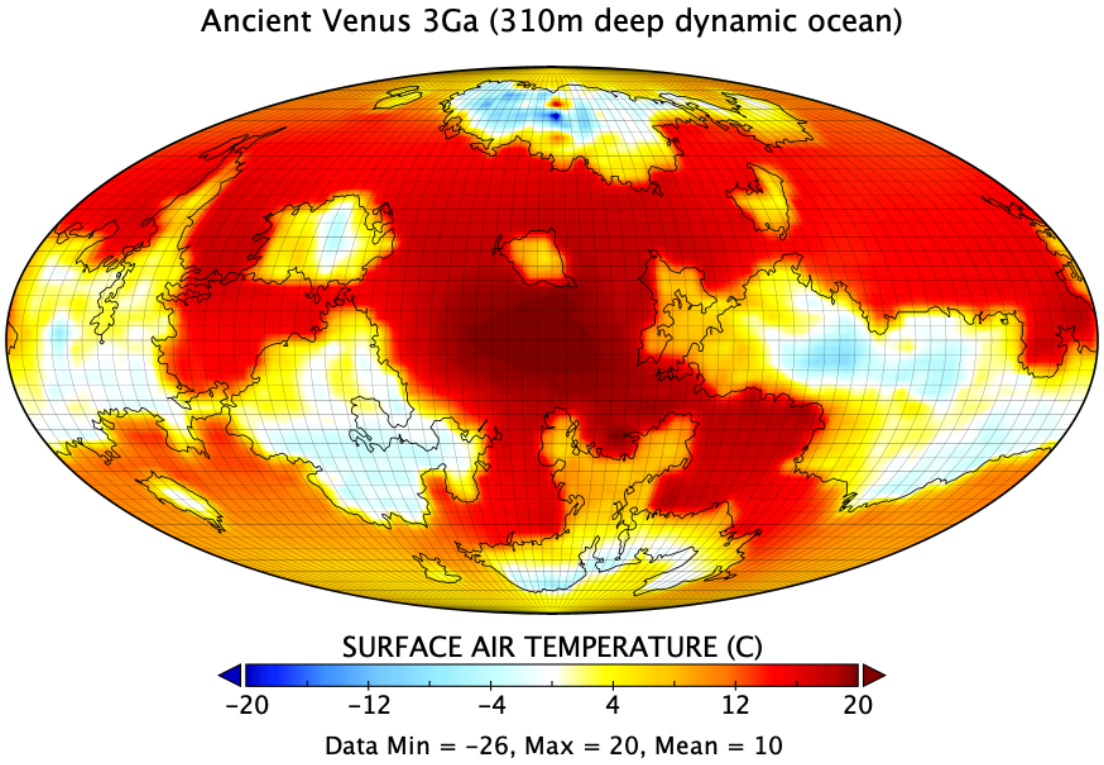
## NASA News & Feature Releases

### 5 Ways Supercomputing is Key to NASA Mission Success

*Posted Nov. 22, 2022*

Whether developing new technologies for landing on other planets, improving air travel here at home, or more realistically simulating global weather and climate, supercomputing is key to the success of NASA missions. These advances and more were on display in the agency's hybrid exhibit during SC22, the International Conference for High Performance Computing, Networking, Storage and Analysis:

**Exploring the past, present, and future of planets inside and outside our solar system.**




A map of the simulated surface temperature of Venus three billion years ago, with a 310 meter-deep dynamic ocean. Temperatures on the continents are around or below the freezing point of water. This is because the planet rotates very slowly, and the continents get quite cold during Venus' night. Credits: NASA/Michael Way

Supercomputers are like computational “time machines,” and scientists use them to explore the past, present, and future universe. Using the NASA Center for Climate Simulation's Discover supercomputer and the ROCKE-3D computer model, scientists from NASA's Goddard Institute for Space Studies in New York are simulating the climates of planets inside and outside our solar system. These simulations show that three billion years ago, Venus, Earth's closest planetary neighbor, may have been temperate long enough to have an ocean — making Venus possibly the first habitable world in our solar system.

Farther from Earth, running ROCKE-3D with ocean characteristics more realistic than in previous models, scientists found that extrasolar world Proxima Centauri b is more habitable than previously believed.

Closer to home, simulations of the Moon reveal that water released by ancient volcanoes closer to the lunar equator can find its way to permanently shadowed polar regions, where we could potentially use it for future exploration.

Learn more about other NASA supercomputing research at SC22 at www.giss.nasa.gov/research/news/20221122/, including:

1. **Designing safe, efficient air taxis.**
2. **Keeping planetary rovers safe during risky landings.**
3. **Modeling spacecraft heat shield materials at the microscale.**
4. **Predicting weather and climate to keep humans safe.**

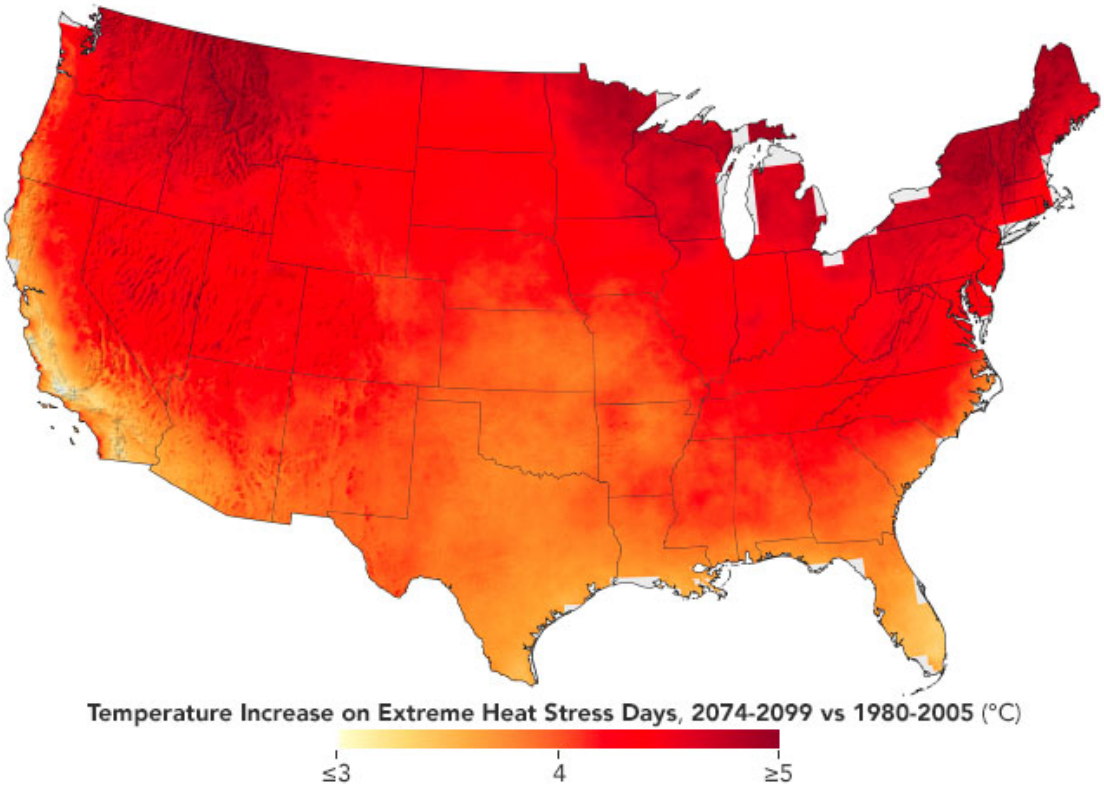
For more information about NASA's virtual exhibit at the International Conference for High Performance Computing, Networking, Storage and Analysis, visit: https://www.nas.nasa.gov/sc22

For more information about supercomputers run by NASA's High-End Computing Program, visit: https://hec.nasa.gov/

## Research Features

### Feeling the Heat in the Extremes

*By Adam Voiland, NASA Earth Observatory — Sep. 16, 2022*




2020

In summer 2022, record-breaking heat waves in California and elsewhere have triggered a stream of health alerts and warnings, strained power grids, and left millions of the most vulnerable Americans sweating through uncomfortable and sometimes deadly conditions.

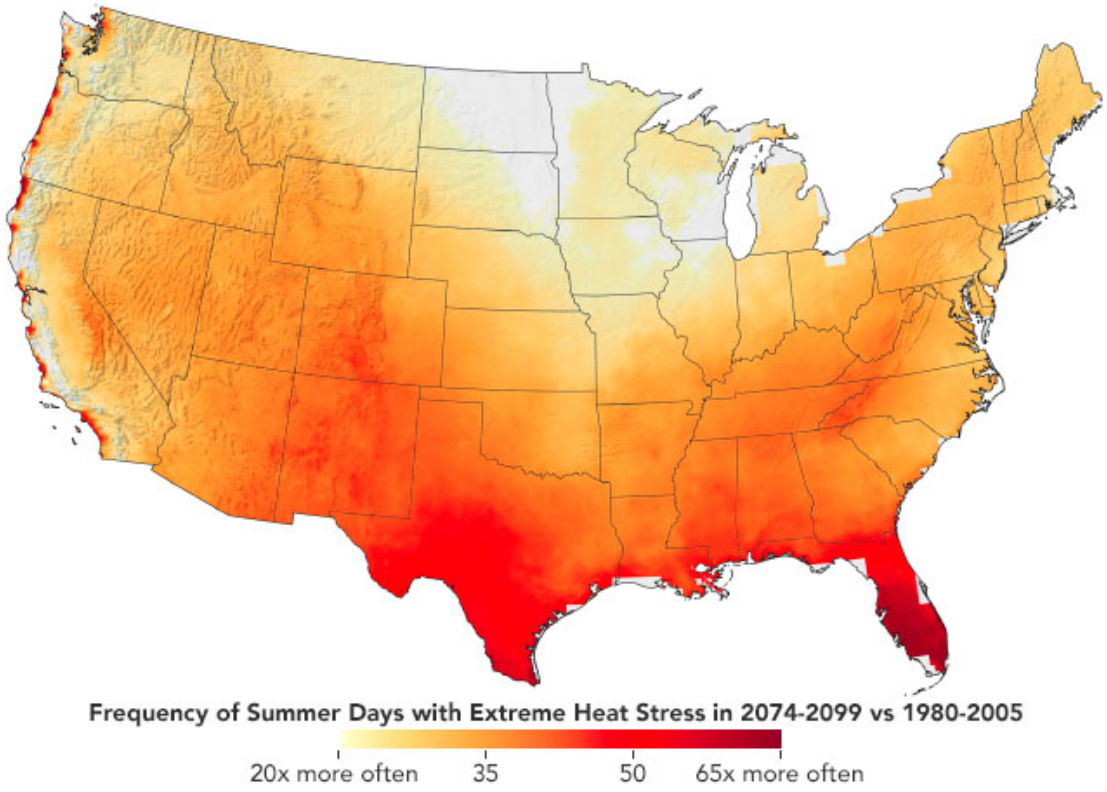
If trends continue, oppressively hot and humid summers like this one are going to become much more common. That is the key finding from a set of new climate projections conducted by a team of researchers from NASA's Jet Propulsion Laboratory (JPL) and several universities. Colin Raymond, a researcher at JPL, and colleagues used projections from 20 climate models to analyze how much heat stress people across the United States might face between 2075-2099 on the hottest summer days compared to observed norms between 1980 and 2005.

"If we assume a high-end emissions scenario and we end up with a 3°C to 5°C increase in global temperatures by 2075, what has been the top 1 percent of summer days for heat stress will be happening for a quarter to half of the summer. That's a huge difference," said Raymond. "That one oppressively hot day you remember as summer's worst could well be happening on 30 or even 50 days each summer by 2075."

Using downscaled output from the Coupled Model Intercomparison Project 5 (CMIP5), the researchers went beyond simple modeling of future air temperatures. They combined heat, humidity, and exposure to sunlight to project future heat stress by calculating a metric known as an environmental stress index (ESI). Their full results, published in Environmental Research Letters, indicate serious changes ahead.

Raymond considers the incorporation of humidity changes into the analysis to be critical. The human body has more difficulty cooling itself in humid heat compared to dry heat because humid conditions make sweating and evaporation less efficient. That's why humid conditions are not only less comfortable, but perhaps also more likely to contribute to heat-related illnesses and deaths. In the United States, heat waves are the deadliest type of natural disaster, leading to an average of at least 100 deaths per year and likely contributing to many more, according to data from the Centers for Disease Control and Prevention.

The researchers first calculated the top 1 percent of days on the ESI, a proxy for extreme heat stress, averaged for May-September for 1980-2005 as a baseline. They then computed the same for 2074-2099, assuming higher levels of




2020

greenhouse gases in the atmosphere and changes to air temperatures, humidity, and sunlight reaching the surface due to changes in cloudiness. As seen in the map above, some of the largest changes in extreme heat stress will likely occur in the high latitudes, inland, and in mountainous areas—particularly in the Upper Midwest, Northeast, and the Pacific Northwest. In these areas, the top 1 percent of days for heat stress could have temperatures that are roughly 5°C (9°F) higher than during the 1980-2005 baseline.

Increases in extreme heat stress in coastal areas, especially in California, would be more moderate than other areas because climate change is causing the land to warm up more quickly than oceans, and upwelling ocean water fuels sea breezes that help disperse stagnant heat and air. Higher elevation areas show amplified heat stress because they are expected to warm up more quickly than lower elevation areas due to a shift toward drier air, drier soil, and less cloud cover.

The Gulf Coast states will likely experience less pronounced changes on the hottest days. But since they have less variability between highs and lows to begin with compared to more northerly states, they will see the greatest relative increases in the frequency of extreme heat stress days (as seen in the second map). Southern Florida and Texas could see extreme heat stress days up to 50 times more often compared to the historical (1980-2005) norms. The increase in the frequency of extreme heat stress days in the Pacific Northwest or Upper Midwest would be closer to 20 times. Rising temperatures were the primary driver of the changes in heat stress throughout the United States, but humidity increases were nearly as important in the southern and eastern U.S. Elevation was also an important factor in which areas will see increases in heat stress.

Dangerous heat wasn't only a problem in the United States in summer 2022. Parts of Europe, Asia, and the Middle East broiled along with the United States. At times, runways melted and train tracks buckled in the United Kingdom. In Shanghai, authorities started dimming lights in the Bund and factories due to power shortages.

None of this was a coincidence. "We're seeing more heat waves, and they're becoming more intense—and that's because of climate change," explained Gavin Schmidt, the director of NASA's Goddard Institute for Space Studies. "We have warmed up the planet by about two degrees Fahrenheit in the last century or so. That is juicing the extremes, so the number of times places are exceeding 90 or 100 degrees Fahrenheit (32 or 37 degrees Celsius) is going up—and not just by a little bit. It's gone up four, five, seven times more than before."

*NASA Earth Observatory images by Joshua Stevens, using data courtesy of Raymond, C., et al. (2022). Story by Adam Voiland.*

*This article was originally prepared as an Earth Image of the Day for the NASA Earth Observatory.*

## Research Features

### Celebrating National Hispanic American Heritage Month NCCS User Spotlight: Clara Orbe

*By Jarrett Cohen, NASA Center for Climate Simulations — Oct. 13, 2022*

As part of NASA's National Hispanic American Heritage Month celebration, this spotlight shines on NASA Center for Climate Simulation (NCCS) user Dr. Clara Orbe. We follow Orbe from her childhood living in several East Coast states to her current role leading the atmospheric dynamics group at the NASA Goddard Institute for Space Studies (GISS) in New York City.



*(Photo courtesy of Clara Orbe)*

What is your family ancestry/country of origin? While I was born in the United States, my parents (and all other family members) are from a small province outside of Buenos Aires in Argentina. I have dual citizenship with Argentina.

**Where is your hometown?**
I grew up moving around a lot, as my father tried to secure stable work. I was born in Carlisle, Pennsylvania; moved to Winston-Salem, North Carolina, until I was 11 years old; and then settled down in Shrewsbury, Massachusetts, during high school. My new hometown is Brooklyn, New York, where I've been since 2008, with a five-year stint in Washington, DC, in the middle.

**What was your career path to NASA?**
I majored in math at Brown University (Bachelor of Science, 2007), received a Ph.D. in applied math at Columbia University (2013), and then served as a NASA Postdoctoral Program fellow at NASA Goddard Space Flight Center (GSFC) in the Atmospheric Chemistry and Dynamics Laboratory. I then transitioned to working as an Associate Research Scientist in the Global Modeling Assimilation Office (GMAO) at GSFC until I was hired as a civil servant Research Physical Scientist at the NASA Goddard Institute for Space Studies (GISS) in 2018.

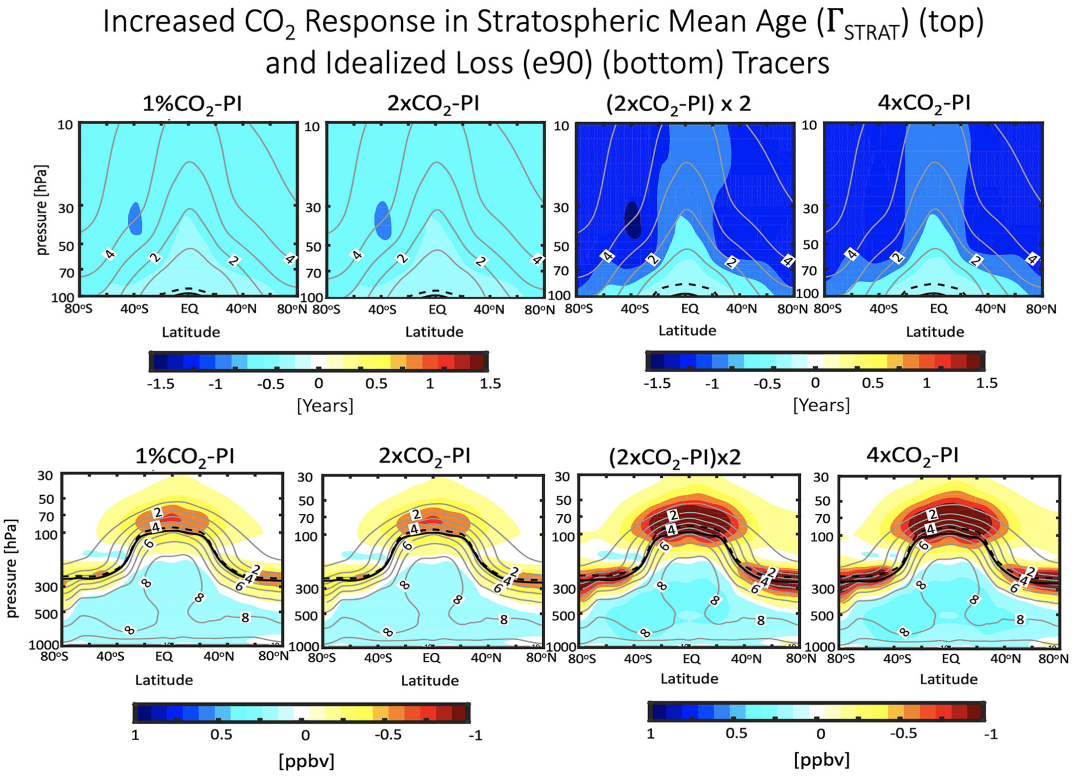
**What is your current role at NASA?**
At GISS, I lead the atmospheric dynamics group and the development of the high-top stratosphere-resolving configuration of the GISS climate model (ModelE2.2). I also maintain an active relationship with the GMAO in support of evaluating large-scale atmospheric transport processes in NASA's Goddard Earth Observing System (GEOS) model developed at GSFC. I also serve as an associate adjunct faculty member in the Department of Applied Physics and Applied Mathematics at Columbia University, where I advise doctoral students and postdoctoral fellows in various problems related to stratospheric dynamics and understanding Earth's climate sensitivity.

**How has NCCS supported your research/career?**
As a researcher whose primary tool is numerical modeling, my entire research career is indebted to the services provided by NCCS. My research portfolio is centered around the development and analysis of climate- and decadal-scale projections using NASA's premier Earth system models (GEOS and ModelE). So, basically, without NCCS, I would be a lot less productive!

**What is your current research focus?**
My current research interests are oriented toward an improved understanding of large-scale atmospheric dynamics and transport. Specifically, I am interested in using models to project and understand future changes in how the stratosphere potentially couples to Earth's surface climate. I am also interested in developing observational constraints of large-scale transport processes that control how air pollution travels around in the Earth system.

**What or who especially inspires you?**
I am inspired by several fellow scientists and how they think about science, ranging from how they formulate questions to how they propose tackling problems. Among others, these include several mentors with whom I've been fortunate to have had really intellectually rewarding relationships, including Dr. Steven Pawson (GSFC), Professor Darryn Waugh (Johns Hopkins University), and Dr. Paul Newman (GSFC).

**Are there any people of Hispanic heritage in history/in your field who have influenced you?**
As an undergraduate I was strongly influenced by Dr. Carlos Castillo-Chavez. He founded and led a mathematical epidemiology program based at Los Alamos National Laboratory, where I interned the summer between my sophomore and




GISS ModelE2.2-Altered-Physics simulations submitted to the Coupled Model Intercomparison Project Phase 6 (CMIP6) show how increases in global carbon dioxide ($CO_2$) — following a 1%-per-year transient scenario as well as both doubling and abrupt quadrupling of $CO_2$ scenarios — might affect the stratosphere, the second layer of Earth's atmosphere.

**Top row:** Effects on the stratospheric mean age of air ($\Gamma_{STRAT}$), that is how long air parcels have been in the stratosphere since leaving the troposphere underneath, shown in years.

**Bottom row:** Effects on e90, an idealized tracer that quantifies how air gets transported in the upper troposphere/lower stratosphere, shown in parts per billion by volume (ppbv).

The black dashed and solid thick lines show the climatological annually averaged tropopause (the boundary between the troposphere and stratosphere) for the increased $CO_2$ and PI control experiments, respectively. Gray contours show climatological values for the PI control experiments. (*Image credit, Orbe et al., 2020*)

junior years at Brown. That was a very transformational period for me, in terms of deciding to pursue graduate studies in applied math.

*[Editor's note: Dr. Castillo-Chavez is a Mexican-American mathematician who retired from Arizona State University in 2020.]*

**What challenges have you had to overcome?**

One recent challenge has been task delegation and management. I am a rather reserved person, and I really enjoy doing scientific analysis. So, leading a group and assigning tasks that I was otherwise okay performing myself were initially a real challenge when I joined NASA GISS, especially given issues related to large age gaps and gender role dynamics with those I supervise. But now, with practice, I am much more comfortable delegating work.

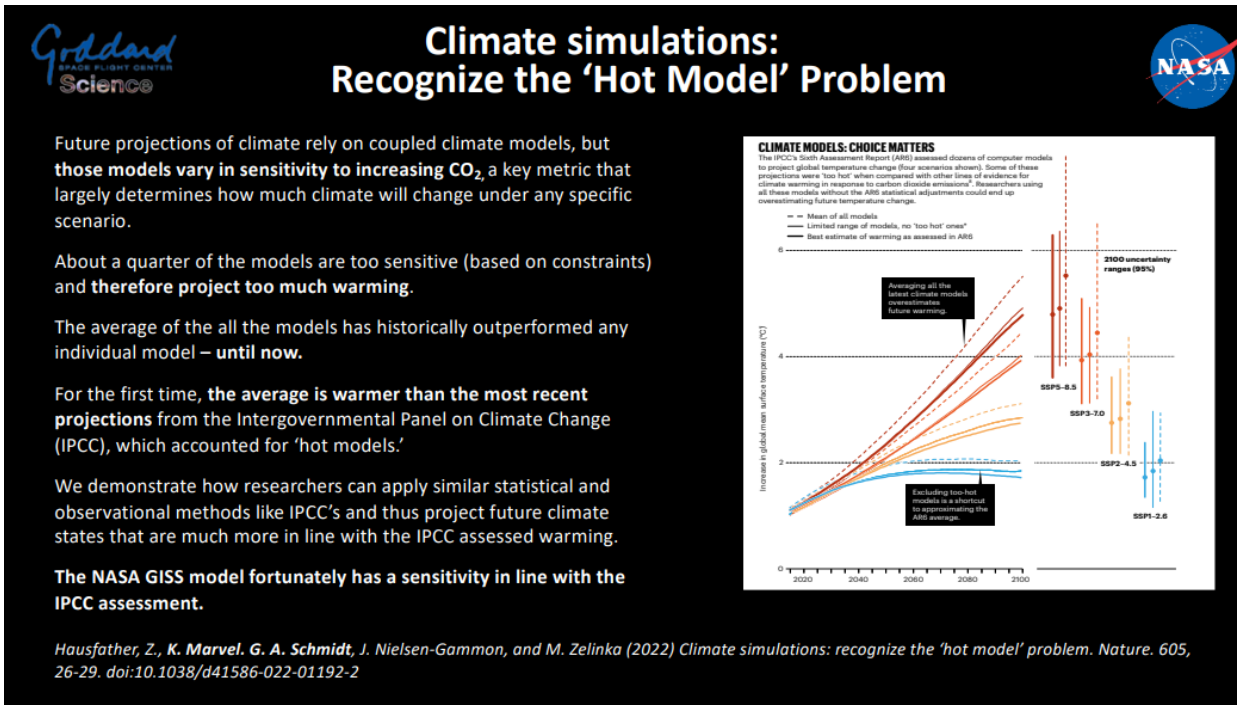
**How can the science and technology sector better encourage and support people of Hispanic heritage?**

I think that Latino students (especially women) need to be explicitly told early on that they are completely capable of carving out a career in math and science. The Latino community may not even think that STEM-related fields are an option, especially if they're cast as too academic or elitist. To this end, this message needs to be instilled at the beginning of elementary school and consistently communicated during all levels of secondary education. Attempts to diversify applicant pools post-undergraduate are well intentioned but ultimately too late.

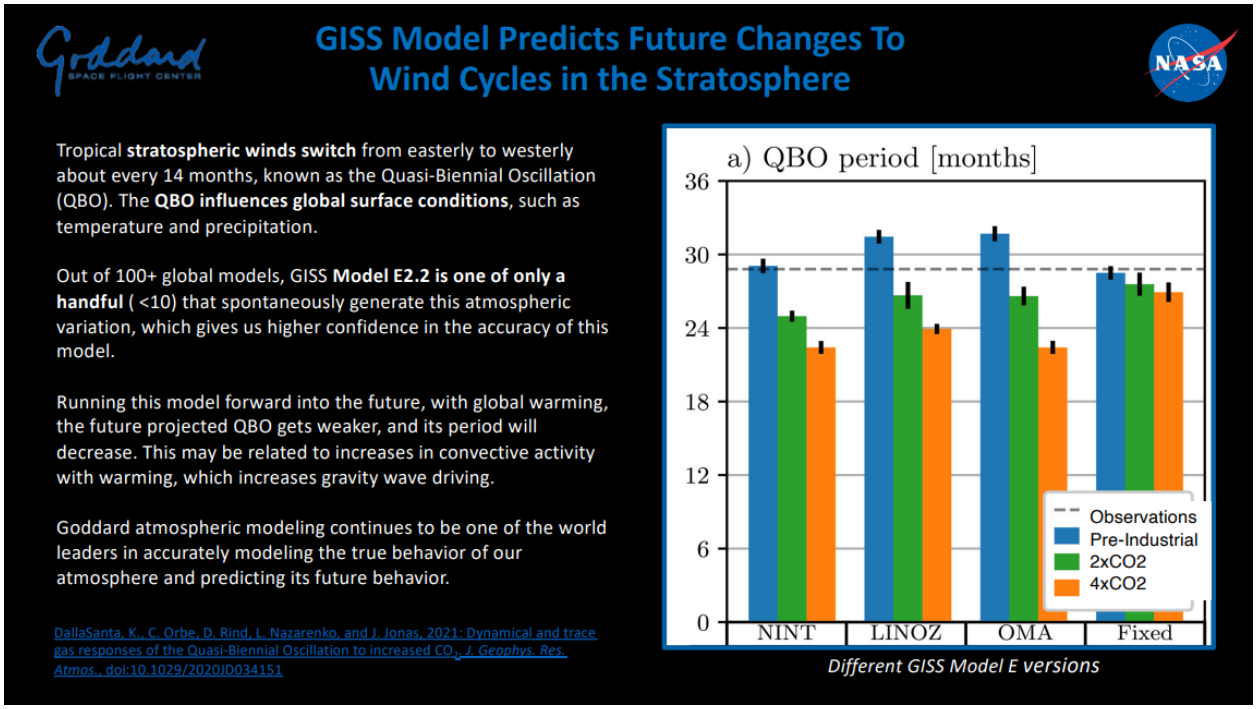
**Reference**

Orbe, C., D. Rind, J. Jonas, L. Nazarenko, G. Faluvegi, L.T. Murray, D.T. Shindell, K. Tsigaridis, T. Zhou, M. Kelley, and G. Schmidt, 2020: GISS Model E2.2: A climate model optimized for the middle atmosphere. Part 2: Validation of large-scale transport and evaluation of climate response. *J. Geophys. Res. Atmos.*, **125**, no. 24, e2020JD033151, doi:10.1029/2020JD033151.

*This article was originally prepared as an NCCS Highlight for the NASA Center for Climate Simulations.*




Hausfather, Z., **K. Marvel**, **G. A. Schmidt**, J. Nielsen-Gammon, and M. Zelinka (2022) Climate simulations: recognize the 'hot model' problem. Nature. 605, 26-29. doi:10.1038/d41586-022-01192-2.




**K. DallaSanta**, **C. Orbe**, **D. Rind**, **L. Nazarenko**, **J. Jonas**, 2021. Dynamical and Trace Gas Responses of the Quasi-Biennial Oscillation to Increased CO2. J. Geophys. Res Atmos. Doi: 10.1029/2020JDO34151.

## D. Science Education at GISS

Information about the GISS educational programs are available at:
https://www.giss.nasa.gov/edu/

GISS personnel include students and educations who participate as partners with the Institute's scientists in their research. Typically, six graduate students carry out their Ph.D. thesis research under the supervision of GISS staff members at any given time. Other participants include students and teachers from junior and senior high schools and senior colleges.

The Climate Change Research Initiative (CCRI) is a year-long STEM engagement program for educators and graduate students to work directly with NASA scientists and lead research teams in a NASA research project. Participating educators become associate researchers at NASA GISS and integrate NASA education resources and content into their classrooms while improving STEM education within their communities. During the summer session, CCRI teams add undergraduate and high school interns.

Further information about CCRI and other GISS student internship programs is available at: https://www.giss.nasa.gov/edu/intern/

National Aeronautics and Space Administration
Goddard Institute for Space Studies

# Education @ GISS

## Advanced Study Programs

**Columbia University Graduate Study**
Study toward an advanced degree in the atmospheric sciences may be conducted at GISS through enrollment in departments at Columbia University.
+ Read More

**Postdoctoral Research Programs**
Advanced programs through which new scientists may participate in GISS research, including NASA and Columbia University postdoctoral appointments, are announced in the GISS employment pages.
+ Read More

## Resource Materials

**CCRI STEM Curriculum Modules**
Instructional modules developed during the GISS Climate Change Research Initiative and NASA/SMD approved.
+ Read More

**Education GCM**
The EdGCM project at the Columbia University Center for Climate Systems Research couples GISS Model II with a user-friendly interface that runs on macOS and Windows desktop computers.
+ Go to Website

**ICP Educational Materials Archive**
Curriculum modules and learning tools developed during the Institute for Climate and Planets program (1994-2004) for use in classroom learning about climate and environmental research.
+ Read More

## Educator and Internship Opportunities



**Climate Change Research Initiative**
CCRI is a year-round STEM engagement program allowing educators and students to work directly with NASA GISS scientists, with a summer program for high school and undergraduate interns.
+ Read More



**Internships**
General information about student internships at NASA/GISS and its NYC-area partners, as well as links to useful related resources.
+ Read More

## Past Programs



**New York City Research Initiative**
Educator and internship program in which teams of students worked with GISS scientists and affiliated university researchers. NYCRI concluded in 2014.
+ Read More

**GISS Institute on Climate and Planets**
A collaborative program between GISS, Columbia University, and the City University of New York. ICP concluded in 2004
+ Go to Website

## NASA Education Links

+ NASA STEM Engagement
+ NASA Interns, Fellows & Scholars

## GISS Best Publication Award

Each spring/summer, scientists at the NASA Goddard Institute for Space Studies vote on the "best" paper published during the previous calendar year by a member or members of the institute. We consider this peer award to be the highest scientific honor that we bestow. Since 1993, the winners have been:

**2022**

Bauer, S.E., K. Tsigaridis, G. Faluvegi, L. Nazarenko, R.L. Miller, M. Kelley, and G. Schmidt, 2022: The turning point of the aerosol era. *J. Adv. Model. Earth Syst.*, **14**, no. 12, e2022MS003070, doi:10.1029/2022MS003070.

**2021**

Miller, R.L., G.A. Schmidt, L. Nazarenko, S.E. Bauer, M. Kelley, R. Ruedy, G.L. Russell, A. Ackerman, I. Aleinov, M. Bauer, R. Bleck, V. Canuto, G. Cesana, Y. Cheng, T.L. Clune, B. Cook, C.A. Cruz, A.D. Del Genio, G.S. Elsaesser, G. Faluvegi, N.Y. Kiang, D. Kim, A.A. Lacis, A. Leboissetier, A.N. LeGrande, K.K. Lo, J. Marshall, E.E. Matthews, S. McDermid, K. Mezuman, L.T. Murray, V. Oinas, C. Orbe, C. Pérez García-Pando, J.P. Perlwitz, M.J. Puma, D. Rind, A. Romanou, D.T. Shindell, S. Sun, N. Tausnev, K. Tsigaridis, G. Tselioudis, E. Weng, J. Wu, and M.-S. Yao, 2021: CMIP6 historical simulations (1850-2014) with GISS-E2.1. *J. Adv. Model. Earth Syst.*, **13**, no. 1, e2019MS002034, doi:10.1029/2019MS002034.

**2020**

Kelley, M., G.A. Schmidt, L. Nazarenko, S.E. Bauer, R. Ruedy, G.L. Russell, A.S. Ackerman, I. Aleinov, M. Bauer, R. Bleck, V. Canuto, G. Cesana, Y. Cheng, T.L. Clune, B.I. Cook, C.A. Cruz, A.D. Del Genio, G.S. Elsaesser, G. Faluvegi, N.Y. Kiang, D. Kim, A.A. Lacis, A. Leboissetier, A.N. LeGrande, K.K. Lo, J. Marshall, E.E. Matthews, S. McDermid, K. Mezuman, R.L. Miller, L.T. Murray, V. Oinas, C. Orbe, C. Pérez García-Pando, J.P. Perlwitz, M.J. Puma, D. Rind, A. Romanou, D.T. Shindell, S. Sun, N. Tausnev, K. Tsigaridis, G. Tselioudis, E. Weng, J. Wu, and M.-S. Yao, 2020: GISS-E2.1: Configurations and climatology. *J. Adv. Model. Earth Syst.*, **12**, no. 8, e2019MS002025, doi:10.1029/2019MS002025.

**2019**

Carlson, B., A. Lacis, C. Colose, A. Marshak, W. Su, and S. Lorentz, 2019: Spectral signature of the biosphere: NISTAR finds it in our solar system from the Lagrangian L-1 point. *Geophys. Res. Lett.*, **46**, no. 17-18, 10679-10686, doi:10.1029/2019GL083736.

**2018**

Marvel, K.D., R. Pincus, G.A. Schmidt, and R.L. Miller, 2018: Internal variability and disequilibrium confound estimates of climate sensitivity from observations. *Geophys. Res. Lett.*, **45**, no. 3, 1595-1601, doi:10.1002/2017GL076468.

**2017**

Elsaesser, G.S., A.D. Del Genio, J. Jiang, and M. van Lier-Walqui, 2017: An improved convective ice parameterization for the NASA GISS Global Climate Model and impacts on cloud ice simulation. *J. Climate*, **30**, no. 1, 317-336, doi:10.1175/JCLI-D-16-0346.1.

**2016**

Way, M.J., A.D. Del Genio, N.Y. Kiang, L.E. Sohl, D.H. Grinspoon, I. Aleinov, M. Kelley, and T. Clune, 2016: Was Venus the first habitable world of our solar system? *Geophys. Res. Lett.*, **43**, no. 16, 8376-8383, doi:10.1002/2016GL069790.

**2015**

Hall, T.M., and K. Hereid, 2015: The frequency and duration of U.S. hurricane droughts. *Geophys. Res. Lett.*, **42**, no. 9, 3482-3485, doi:10.1002/2015GL063652.

**2014**

Miller, R.L., G.A. Schmidt, L.S. Nazarenko, N. Tausnev, S.E. Bauer, A.D. Del Genio, M. Kelley, K.K. Lo, R. Ruedy, D.T. Shindell, I. Aleinov, M. Bauer, R. Bleck, V. Canuto, Y.-H. Chen, Y. Cheng, T.L. Clune, G. Faluvegi, J.E. Hansen, R.J. Healy, N.Y. Kiang, D. Koch, A.A. Lacis, A.N. LeGrande, J. Lerner, S. Menon, V. Oinas, C. Pérez García-Pando, J.P. Perlwitz, M.J. Puma, D. Rind, A. Romanou, G.L. Russell, M. Sato, S. Sun, K. Tsigaridis, N. Unger, A. Voulgarakis, M.-S. Yao, and J. Zhang, 2014: CMIP5 historical simulations (1850-2012) with GISS ModelE2. *J. Adv. Model. Earth Syst.*, **6**, no. 2, 441-477, doi:10.1002/2013MS000266.

**2013**

Lacis, A.A., J.E. Hansen, G.L. Russell, V. Oinas, and J. Jonas, 2013: The role of long-lived greenhouse gases as principal LW control knob that governs the global surface temperature for past and future climate change. *Tellus B*, **65**, 19734, doi:10.3402/tellusb.v65i0.19734.

**2012**

Shindell, D., J.C.I. Kuylenstierna, E. Vignati, R. van Dingenen, M. Amann, Z. Klimont, S.C. Anenberg, N. Muller, G. Janssens-Maenhout, F. Raes, J. Schwartz, G. Faluvegi, L. Pozzoli, K. Kupiainen, L. Höglund-Isaksson, L. Emberson, D. Streets, V. Ramanathan, K. Hicks, N.T.K. Oanh, G. Milly, M. Williams, V. Demkine, and D. Fowler, 2012: Simultaneously mitigating near-term climate change and improving human health and food security. *Science*, **335**, 183-189, doi:10.1126/science.1210026.

**2011**

Hansen, J., M. Sato, P. Kharecha, and K. von Schuckmann, 2011: Earth's energy imbalance and implications. *Atmos. Chem. Phys.*, **11**, 13421-13449, doi:10.5194/acp-11-13421-2011.

**2010**

Lacis, A.A, G.A. Schmidt, D. Rind, and R.A. Ruedy, 2010: Atmospheric $CO_2$: Principal control knob governing Earth's temperature. *Science*, **330**, 356-359, doi:10.1126/science.1190653.

**2009**

Del Genio, A.D., R.K. Achterberg, K.H. Baines, F.M. Flasar, P.L. Read, A. Sánchez-Lavega, and A.P. Showman, 2009: Saturn atmospheric structure and dynamics. In *Saturn from Cassini-Huygens*. M.K. Dougherty, L.W. Esposito, and S.M. Krimigis, Eds. Springer-Verlag, pp. 113-159, doi:10.1007/978-1-4020-9217-6_6.

**2008**

Rosenzweig, C., D. Karoly, M. Vicarelli, P. Neofotis, Q. Wu, G. Casassa, A. Menzel, T.L. Root, N. Estrella, B. Seguin, P. Tryjanowski, C. Liu, S. Rawlins, and A. Imeson, 2008: Attributing physical and biological impacts to anthropogenic climate change. *Nature*, **453**, 353-357, doi:10.1038/nature06937.

**2007**

Del Genio, A.D., M.-S. Yao, and J. Jonas, 2007: Will moist convection be stronger in a warmer climate? *Geophys. Res. Lett.*, **34**, L16703, doi:10.1029/2007GL030525.

**2006**

Hansen, J., M. Sato, R. Ruedy, K. Lo, D.W. Lea, and M. Medina-Elizade, 2006: Global temperature change. *Proc. Natl. Acad. Sci.*, **103**, 14288-14293, doi:10.1073/pnas.0606291103.

**2005**

Hansen, J., L. Nazarenko, R. Ruedy, M. Sato, J. Willis, A. Del Genio, D. Koch, A. Lacis, K. Lo, S. Menon, T. Novakov, J. Perlwitz, G. Russell, G.A. Schmidt, and N. Tausnev, 2005: Earth's energy imbalance: Confirmation and implications. *Science*, **308**, 1431-1435, doi:10.1126/science.1110252.

**2004**

Hansen, J., and L. Nazarenko, 2004: Soot climate forcing via snow and ice albedos. *Proc. Natl. Acad. Sci.*, **101**, 423-428, doi:10.1073/pnas.2237157100.

**2003**

Koch, D., J. Park, and A. Del Genio, 2003: Clouds and sulfate are anticorrelated: A new diagnostic for global sulfur models. *J. Geophys. Res.*, **108**, no. D24, 4781, doi:10.1029/2003JD003621.

**2002**

Chen, J., B.E. Carlson, and A.D. Del Genio, 2002: Evidence for strengthening of the tropical general circulation in the 1990s. *Science*, **295**, 838-841, doi:10.1126/science.1065835.

**2001**

Allison, M., and D.H. Atkinson, 2001: Galileo Probe Doppler residuals as the wave-dynamical signature of weakly stable, downward-increasing stratification in Jupiter's deep wind layer. *Geophys. Res. Lett.*, **28**, 2747-2750, doi:10.1029/2001GL012927.

**2000**

Del Genio, A.D., and A.B. Wolf, 2000: The temperature dependence of the liquid water path of low clouds in the southern Great Plains. *J. Climate*, **13**, 3465-3486, doi:10.1175/1520-0442(2000)013<3465:TTDOTL>2.0.CO;2.

Hansen, J., M. Sato, R. Ruedy, A. Lacis, and V. Oinas, 2000: Global warming in the twenty-first century: An alternative scenario. *Proc. Natl. Acad. Sci.*, **97**, 9875-9880, doi:10.1073/pnas.170278997.

**1999**

Shindell, D.T., R.L. Miller, G.A. Schmidt, and L. Pandolfo, 1999: Simulation of recent northern winter climate trends by greenhouse-gas forcing. *Nature*, **399**, 452-455, doi:10.1038/20905.

**1998**

Shindell, D.T., D. Rind, and P. Lonergan, 1998: Increased polar stratospheric ozone losses and delayed eventual recovery owing to increasing greenhouse-gas concentrations. *Nature*, **392**, 589-592, doi:10.1038/33385.

**1997**

Miller, R.L., 1997: Tropical thermostats and low cloud cover. *J. Climate*, **10**, 409-440, doi:10.1175/1520-0442(1997)010<0409:TTALCC>2.0.CO;2.

**1996**

Tegen, I., A.A. Lacis, and I. Fung, 1996: The influence of mineral aerosols from disturbed soils on the global radiation budget. *Nature*, **380**, 419-422, doi:10.1038/380419a0.

**1995**

Russell, G.L., J.R. Miller, and D. Rind, 1995: A coupled atmosphere-ocean model for transient climate change studies. *Atmos.-Ocean*, **33**, 683-730.

**1994**

Del Genio, A.D., W. Kovari, Jr., and M.-S. Yao, 1994: Climatic implications of the seasonal variation of upper troposphere water vapor. *Geophys. Res. Lett.*, **21**, 2701-2704, doi:10.1029/94GL02658.

**1993**

Tselioudis, G., A.A. Lacis, D. Rind, and W.B. Rossow, 1993: Potential effects of cloud optical thickness on climate warming. *Nature*, **366**, 670-672, doi:10.1038/366670a0.

## B. Journal Papers

1. **Alexandrov, M.D.**, A. Marshak, **B. Cairns**, and **A.S. Ackerman**, 2022: Markovian statistical model of cloud optical thickness. Part I: Theory and examples. *J. Atmos. Sci.*, **79**, no. 12, 3315-3332, doi:10.1175/JAS-D-22-0125.1…….50

2. Antwerpen, R., **M. Tedesco**, X. Fettweis, **P.M. Alexander**, and W.J. van de Berg, 2022: Assessing bare ice albedo simulated by MAR over the Greenland ice sheet (2000-2021) and implications for meltwater production estimates. *The Cryosphere*, **16**, no. 10, 4185-4199, doi:10.5194/tc-16-4185-2022…….51

3. Bah, A.R., H. Norouzi, S. Prakash, **R. Blake**, R. Khanbilvardi, and **C. Rosenzweig**, 2022: Spatial downscaling of GOES-R land surface temperature over urban regions: A case study for New York City. *Atmosphere*, **13**, 332, doi:10.3390/atmos13020332...… .52

4. Banerjee, A., L.Y. Yeung, L.T. Murray, X. Tie, J.E. Tierney, and **A.N. LeGrande**, 2022: Clumped-isotope constraint on upper-tropospheric cooling during the Last Glacial Maximum. *AGU Adv.*, **3**, no. 4, e2022AV000688, doi:10.1029/2022AV000688…….....53

5. **Bauer**, **S.E.**, **K. Tsigaridis**, **G.S. Faluvegi**, **L.S. Nazarenko**, **R.L. Miller**, **M.A. Kelley**, and **G.A. Schmidt**, 2022: The turning point of the aerosol era. *J. Adv. Model. Earth Syst.*, **14**, no. 12, e2022MS003070, doi:10.1029/2022MS003070……...…….54

6. Bennington, V., **L. Gloege**, and G.A. McKinley, 2022: Observation-based variability in the global ocean carbon sink from 1959-2020. *Geophys. Res. Lett.*, **49**, no. 14, e2022GL098632, doi:10.1029/2022GL098632…….....55

7. Bo, Y., **J. Jägermeyr**, Z. Yin, Y. Jiang, J. Xu, H. Liang, and F. Zhou, 2022: Global benefits of non-continuous flooding to reduce greenhouse gases and irrigation water use without rice yield penalty. *Glob. Change Biol.*, **28**, no. 11, 3636-3650, doi:10.1111/gcb.16132…….…56

8. Boulet, C., and **Q. Ma**, 2022: Line coupling and line mixing effects on calculated widths of symmetric-top molecules with the k-degeneracy: A theoretical study of $N_2$-, $O_2$-, and air-broadened lines of $CH_3I$. *J. Quant. Spectrosc. Radiat. Transfer*, **288**, 108273, doi:10.1016/j.jqsrt.2022.108273…….....57

9. Bowman, H., S.T. Turnock, **S.E. Bauer**, **K. Tsigaridis**, M. Deushi, N. Oshima, F.M. O'Connor, L. Horowitz, T. Wu, J. Zhang, and D.D. Parrish, 2022: Changes of anthropogenic precursor emissions drive shifts of ozone seasonal cycle throughout northern midlatitude troposphere. *Atmos. Chem. Phys.*, **22**, no. 5, 3507-3524, doi:10.5194/acp-22-3507-2022……..58

10. Brennan, M.M., S. Whitmee, **C.V. Braneon**, N. Meinsma, and R. Green, 2022: Sea level rise and city-level climate action. *Eur. J. Environ. Public Health*, **6**, no. 2, em0111, doi:10.21601/ejeph/12046…….59

11. Brown, F., G.A. Folberth, S. Sitch, **S.E. Bauer**, M. Bauters, P. Boeckx, A.W. Cheesman, M. Deushi, I. Dos Santos Vieira, C. Galy-Lacaux, J. Haywood, J. Keeble, L.M. Mercado, F.M. O'Connor, N. Oshima, **K. Tsigaridis**, and H. Verbeeck, 2022: The ozone-climate penalty over South America and Africa by 2100. *Atmos. Chem. Phys.*, **22**, no. 18, 12331-12352, doi:10.5194/acp-22-12331-2022……...…60

12. Bühler, J.C., J.M. Axelsson, F.A. Lechleitner, J. Fohlmeister, **A.N. LeGrande**, M. Midhun, J. Sjolte, M. Werner, K. Yoshimura, and K. Rehfeld, 2022: Investigating oxygen and carbon isotopic relationships in speleothem records over the last millennium using multiple isotope-enabled climate models. *Clim. Past*, **18**, no. 7, 1625-1654, doi:10.5194/cp-18-1625-2022……..…….61

13. Cammarano, D., S. Jamshidi, G. Hoogenboom, **A.C. Ruane**, D. Niyogi, and D. Ronga, 2022: Processing tomato production is expected to decrease due to the projected increase in temperature. *Nat. Food*, **3**, no. 6, 437-444, doi:10.1038/s43016-022-00521-y……..…62

14. **Carlson**, **B.E.**, **A.A. Lacis**, **G.L. Russell**, A. Marshak, and W. Su, 2022: Unique observational constraints on the seasonal and longitudinal variability of the Earth's planetary albedo and cloud distribution inferred from EPIC measurements. *Front. Remote Sens.*, **2**, 788525, doi:10.3389/frsen.2021.788525…….……63

15. **Cesana**, **G.V.**, T. Khadir, H. Chepfer, and M. Chiriaco, 2022: Southern Ocean solar reflection biases in CMIP6 models linked to cloud phase and vertical structure representations. *Geophys. Res. Lett.*, **49**, no. 22, e2022GL099777, doi:10.1029/2022GL099777……..…64

16. Chemke, R., L. Zanna, **C. Orbe**, L.T. Sentman, and L.M. Polvani, 2022: The future intensification of North Atlantic winter storms: The key role of dynamic ocean coupling. *J. Climate*, **35**, no. 8, 2407-2421, doi:10.1175/JCLI-D-21-0407.1……....65

17. **Chiang**, **F.**, **B.I. Cook**, **S.S. McDermid**, **K.D. Marvel**, **G.A. Schmidt**, **L.S. Nazarenko**, and **M.A. Kelley**, 2022: Responses of compound daytime and nighttime warm-dry and warm-humid events to individual anthropogenic forcings. *Environ. Res. Lett.*, **17**, no. 8, 084015, doi:10.1088/1748-9326/ac80ce……....66

18. Christie, D.A., E.K.H. Lee, H. Innes, P.A. Noti, B. Charnay, T.J. Fauchez, N.J. Mayne, R. Deitrick, F. Ding, J.J. Greco, M. Hammond, I. Malsky, A. Mandell, E. Rauscher, M.T. Roman, D.E. Sergeev, **L. Sohl**, M.E. Steinrueck, M. Turbet, E.T. Wolf, M. Zamyatina, and L. Carone, 2022: CAMEMBERT: A mini-Neptunes GCM intercomparison, protocol version 1.0.A CUISINES Model Intercomparison Project. *Planet. Sci. J.*, **3**, no. 11, 261, doi:10.3847/PSJ/ac9dfe……....67

19. Chrysafi, A., V. Virkki, M. Jalava, V. Sandström, J. Piipponen, M. Porkka, J.S. Lade, K. La Mere, L. Wang-Erlandsson, L. Scherer, S.L. Andersen, E. Bennett, A.K. Brauman, S.G. Cooper, A. De Palma, P. Döll, S.A. Downing, C.T. DuBois, I. Fetzer, E.A. Fulton, D. Gerten, H. Jaafar, **J. Jägermeyr**, F. Jaramillo, M. Jung, H. Kahiluoto, L. Lassaletta, W.A. Mackay, D. Mason-D'Croz, M.M. Mekonnen, K.L. Nash, A.V. Pastor, N. Ramankutty, B. Ridoutt, S. Siebert, B.I. Simmons, A. Staal, Z. Sun, A. Tobian, A. Usubiaga-Liaño, R.J. Van der Ent, A. Van Soesbergen, P.H. Verburg, Y. Wada, S. Zipper, and M. Kummu, 2022: Quantifying Earth system interactions for sustainable food production via expert elicitationion. *Nat. Sustain.*, **5**, no. 10, 830-842, doi:10.1038/s41893-022-00940-6…….....68

20. Cinner, J.E., I.R. Caldwell, L. Thiault, J. Ben, J.L. Blanchard, M. Coll, A. Diedrich, T.D. Eddy, J.D. Everett, C. Folberth, D. Gascuel, J. Guiet, G.G. Gurney, R.F. Heneghan, **J. Jägermeyr**, N. Jiddawi, R. Lahari, J. Kuange, W. Liu, O. Maury, C. Müller, C. Novaglio, J. Palacios-Abrantes, C.M. Petrik, A. Rabearisoa, D.P. Tittensor, A. Wamukota, and R. Pollnac, 2022: Potential impacts of climate change on agriculture and fisheries production in 72 tropical coastal communities. *Nat. Commun.*, **13**, no. 1, 3530, doi:10.1038/s41467-022-30991-4……..69

21. **Clifton**, **O.E.**, E.G. Patton, S. Wang, M. Barth, J. Orlando, and R.H. Schwantes, 2022: Large eddy simulation for investigating coupled canopy and turbulence influences on atmospheric chemistry: Model description and application to summer midday conditions at a temperate deciduous forest. *J. Adv. Model. Earth Syst.*, **14**, no. 10, e2022MS003078, doi:10.1029/2022MS003078……...70

22. Colosio, P., **M. Tedesco**, and E. Tellman, 2022: Flood monitoring using enhanced resolution passive microwave data: A test case over Bangladesh. *Remote Sens.*, **14**, 1180, doi:10.3390/rs14051180……....71

23. **Cook**, **B.I**, J.E Smerdon, E.R Cook, A.P. Williams, K.J Anchukaitis, J.S Mankin, K. Allen, L. Andreu-Hayles, T.R Ault, S. Belmecheri, S. Coats, B. Coulthard, B. Fosu, P. Grierson, D. Griffin, D.A Herrera, M. Ionita, F. Lehner, C. Leland, **K.D. Marvel**, M.S Morales, V. Mishra, J. Ngoma, H.T.T Nguyen, A. O'Donnell, J. Palmer, M.P Rao, M. Rodriguez-Caton, R. Seager, D.W Stahle, S. Stevenson, U.K Thapa, A.M Varuolo-Clarke, and E.K Wise, 2022: Megadroughts in the Common Era and the Anthropocene. *Nat. Rev. Earth Environ.*, **3**, no. 11, 741-757, doi:10.1038/s43017-022-00329-1…….….72

24. **Cook**, **B.I.**, A.P. Williams, and **K.D. Marvel**, 2022: Projected changes in early summer ridging and drought over the Central Plains. *Environ. Res. Lett.*, **17**, 104020, doi:10.1088/1748-9326/ac8e1a……..73

25. Cooper, V., **L.A. Roach**, J. Thomson, S. Brenner, M. Smith, M. Meylan, and C. Bitz, 2022: Wind waves in sea ice of the western Arctic and a global coupled wave-ice model. *Phil. Trans. Roy. Soc. A*, **380**, no. 2235, 20210258, doi:10.1098/rsta.2021.0258……..……..74

26. Da Silva, K.A., R.A. Snyder, M.S. Packalen, J.W. McLaughlin, **D.M. Peteet**, and S.A. Finkelstein, 2022: Mineral inputs, paleoecological change, and Holocene carbon accumulation at a boreal peatland in the Hudson Bay Lowlands, Canada. *Palaeogeogr. Palaeoclimatol. Palaeoecol.*, **596**, 110996, doi:10.1016/j.palaeo.2022.110996……...75

27. **DallaSanta**, **K.**, and L.M. Polvani, 2022: Volcanic stratospheric injections up to 160 Tg(S) yield a Eurasian winter warming indistinguishable from internal variability. *Atmos. Chem. Phys.*, **22**, no. 13, 8843-8862, doi:10.5194/acp-22-8843-2022……..……...76

28. Davis, C.C., G.M. Lyra, D.S. Park, R. Asprino, R. Maruyama, D. Torquato, **B.I. Cook**, and A.M. Ellison, 2022: New directions in tropical phenology. *Trends Ecol. Evol.*, **37**, no. 8, 683-693, doi:10.1016/j.tree.2022.05.001…….……..77

29. De Sherbinin, A., K. Grace, **S.S. McDermid**, K. Van Der Geest, **M.J. Puma**, and A. Bell, 2022: Migration theory in climate mobility research. *Front. Clim.*, **4**, 882343, doi:10.3389/fclim.2022.882343……....78

30. Diamond, M.S., P.E. Saide, P. Zuidema, **A.S. Ackerman**, S.J. Doherty, **A.M. Fridlind**, H. Gordon, C. Howes, J. Kazil, T. Yamaguchi, J. Zhang, G. Feingold, and R. Wood, 2022: Cloud adjustments from large-scale smoke-circulation interactions strongly modulate the southeast Atlantic stratocumulus-to-cumulus transition. *Atmos. Chem. Phys.*, **22**, no. 18, 12113-12151, doi:10.5194/acp-22-12113-2022……...79

31. Dueri, S., H. Brown, S. Asseng, F. Ewert, H. Webber, M. George, R. Craigie, **J.R. Guarin**, D.N.L. Pequeno, T. Stella, M. Ahmed, P.D. Alderman, B. Basso, A.G. Berger, G.B. Mujica, D. Cammarano, Y. Chen, B. Dumont, E.E. Rezaei, E. Fereres, R. Ferrise, T. Gaiser, Y. Gao, M. Garcia-Vila, S. Gayler, Z. Hochman, G. Hoogenboom, K.C. Kersebaum, C. Nendel, J.E. Olesen, G. Padovan, T. Palosuo, E. Priesack, J.W.M. Pullens, A. Rodríguez, R.P Rötter, M.R. Ramos, M.A. Semenov, N. Senapati, S. Siebert, A.K. Srivastava, C. Stöckle, I. Supit, F. Tao, P. Thorburn, E. Wang, T.K.D. Weber, L. Xiao, C. Zhao, J. Zhao, Z. Zhao, Y. Zhu, and P. Martre, 2022: Simulation of winter wheat response to variable sowing dates and densities in a high-yielding environment. *J. Exp. Bot.*, 73, no. 16, 5715-5729, doi:10.1093/jxb/erac221……..….80

32. Ebtehaj, A., M. Durand, and **M. Tedesco**, 2022: Constrained inversion of a microwave snowpack emission model using dictionary matching: Applications for GPM satellite. *IEEE Trans. Geosci. Remote Sens.*, **60**, 4302114, doi:10.1109/TGRS.2021.3115663……..…81

33. **Elsaesser, G.S.**, R. Roca, T. Fiolleau, **A.D. Del Genio**, and **J. Wu**, 2022: A simple model for tropical convective cloud shield area growth and decay rates informed by geostationary IR, GPM, and Aqua/AIRS satellite data. *J. Geophys. Res. Atmos.*, **127**, no. 10, e2021JD035599, doi:10.1029/2021JD035599…….82

34. Espinosa, Z.I., A. Sheshadri, G.R. Cain, E.P. Gerber, and **K.J. DallaSanta**, 2022: Machine learning gravity wave parameterization generalizes to capture the QBO and response to increased $CO_2$. *Geophys. Res. Lett.*, **49**, no. 8, e2022GL098174, doi:10.1029/2022GL098174……..83

35. Fan, Y., X. Wang, T. Funk, I. Rashid, B. Herman, N. Bompoti, M.S. Mahmud, M. Chrysochoou, **M. Yang**, T.M. Vadas, Y. Lei, and B. Li, 2022: A critical review for real-time continuous soil monitoring: Advantages, challenges, and perspectives. *Environ. Sci. Technol.*, **56**, no. 19, 13546-13564, doi:10.1021/acs.est.2c03562…….84

36. Fauchez, T.J., G.L. Villanueva, D.E. Sergeev, M. Turbet, I.A. Boutle, **K. Tsigaridis**, **M.J. Way**, E.T. Wolf, S.D. Domagal-Goldman, F. Forget, J. Haqq-Misra, R.K. Kopparapu, J. Manners, and N.J. Mayne, 2022: The TRAPPIST-1 Habitable Atmosphere Intercomparison (THAI). Part III: Simulated observables — The return of the spectrum. *Planet. Sci. J.*, **3**, no. 9, 213, doi:10.3847/PSJ/ac6cf1…….…85

37. **Field, R.D.**, L. Andreu-Hayles, R.D. D'Arrigo, R. Oelkers, B.H. Luckman, D. Morimoto, E. Boucher, F. Gennaretti, I. Hermoso, A. Lavergne, and M. Levesque, 2022: Tree-ring cellulose $\delta^{18}O$ records similar large-scale climate influences as precipitation $\delta^{18}O$ in the Northwest Territories of Canada. *Clim. Dyn.*, **58**, no. 3-4, 759-776, doi:10.1007/s00382-021-05932-4……...86

38. Franke, J.A., C. Müller, S. Minoli, J. Elliott, C. Folberth, C. Gardner, T. Hank, R.C. Izaurralde, **J. Jägermeyr**, C. Jones, W. Liu, S. Olin, T.A.M. Pugh, **A.C. Ruane**, H. Stephens, F. Zabel, and E. Moyer, 2022: Agricultural breadbaskets shift poleward given adaptive farmer behavior under climate change. *Glob. Change Biol.*, **28**, no. 1, 167-181, doi:10.1111/gcb.15868……..87

39. Fu, D., L. Di Girolamo, R.M. Rauber, G.M. McFarquhar, S.W. Nesbitt, J. Loveridge, Y. Hong, B. van Diedenhoven, **B. Cairns**, **M.D. Alexandrov**, P. Lawson, S. Woods, S. Tanelli, O.O. Sy, S. Schmidt, C.A. Hostetler, and A.J. Scarino, 2022: An evaluation of liquid cloud droplet effective radius derived from MODIS, airborne remote sensing and in situ measurements from CAMP$^2$Ex. *Atmos. Chem. Phys.*, **22**, no. 12, 8259-8285, doi:10.5194/acp-22-8259-2022……..…..88

40. Funk, C.C., P. Peterson, G.J. Huffman, M.F. Landsfeld, C. Peters-Lidard, F. Davenport, S. Shukla, S. Peterson, D.H. Pedreros, **A.C. Ruane**, **C.Z. Mutter**, W. Turner, L. Harrison, A. Sonnier, J. Way-Henthorne, and Husak Gregory J., 2022: Introducing and evaluating the Climate Hazards center IMErg with Stations (CHIMES) — Timely station-enhanced Integrated Multi-satellitE Retrievals for Global Precipitation Measurement. *Bull. Amer. Meteorol. Soc.*, **103**, no. 2, E429-E454, doi:10.1175/BAMS-D-

20-0245.1……...…89

41. Gao, M., K. Knobelspiesse, B. Franz, P.-W. Zhai, A. Sayer, A. Ibrahim, **B. Cairns**, O. Hasekamp, Y. Hu, V. Martins, J. Werdell, and X. Xu, 2022: Effective uncertainty quantification for multi-angle polarimetric aerosol remote sensing over ocean, Part 1: Performance evaluation and speed improvement. *Atmos. Meas. Tech.*, **15**, no. 16, 4859-4879, doi:10.5194/amt-15-4859-2022…….……..90

42. Gasperini, L., **D.M. Peteet**, E. Bonatti, E. Gambini, A. Polonia, J. Nichols, and L. Heusser, 2022: Late Glacial and Holocene environmental variability, Lago Trasimeno, Italy. *Quat. Int.*, **622**, 21-35, doi:10.1016/j.quaint.2021.10.011…….,,,.91

43. Gillmann, C., **M.J. Way**, G. Avice, D. Breuer, G.J. Golabek, D. Honing, J. Krissansen-Totton, H. Lammer, A.-C. Plesa, M. Persson, J.G. O'Rourke, A. Salvador, M. Scherf, and M.Y. Zolotov, 2022: The long-term evolution of the atmosphere of Venus: Processes and feedback mechanisms. *Space Sci. Rev.*, **218**, 56, doi:10.1007/s11214-022-00924-0…....92

44. **Glaser, D.M.**, H.E. Hartnett, D.R. Finn, S. Perez-Montaño, H. Cadillo-Quiroz, and S. Desch, 2022: Water vapor adsorption provides daily, sustainable water to soils of the hyperarid Atacama Desert. *Astrobiology*, **22**, no. 10, 1222-1238, doi:10.1089/ast.2021.0171……93

45. Grillakis, M., A. Voulgarakis, A. Rovithakis, K.D. Seiradakis, A. Koutroulis, **R.D. Field**, M. Kasoar, A. Papadopoulos, and M. Lazaridis, 2022: Climate drivers of global wildfire burned area. *Environ. Res. Lett.*, **17**, no. 4, 045021, doi:10.1088/1748-9326/ac5fa1…..94

46. **Guarin, J.R.**, P. Martre, F. Ewert, H. Webber, S. Dueri, D. Calderini, M. Reynolds, G. Molero, D. Miralles, G. Garcia, G. Slafer, F. Giunta, D. Noleto Luz Pequeno, T. Stella, M. Ahmed, P.D. Alderman, B. Basso, A.G. Berger, M. Bindi, G. Bracho Mujica, D. Cammarano, Y. Chen, B. Dumont, E. Eyshi Rezaei, E. Fereres, R. Ferrise, T. Gaiser, Y. Gao, M. Garcia-Vila, S. Gayler, Z. Hochman, G. Hoogenboom, L.A. Hunt, C. Kersebaum, C. Nendel, J. Olesen, T. Palosuo, E. Priesack, J. Pullens, A. Rodriguez, R.P. Rötter, M. Ruiz-Ramos, M.A. Semenov, N. Senapati, S. Siebert, A.K. Srivastava, C.O. Stöckle, I. Supit, F. Tao, P.J. Thorburn, E. Wang, T.K.D. Weber, L. Xiao, Z. Zhang, C. Zhao, J. Zhao, Z. Zhao, Y. Zhu, and S. Asseng, 2022: Evidence for increasing global wheat yield potential. *Environ. Res. Lett.*, **17**, no. 12, 124045, doi:10.1088/1748-9326/aca77c…….……..95

47. Hannah, W.M., K.G. Pressel, M. Ovchinnikov, and **G.S. Elsaesser**, 2022: Checkerboard patterns in E3SMv2 and E3SM-MMFv2. *Geosci. Model Dev.*, **15**, no. 15, 6243-6257, doi:10.5194/gmd-15-6243-2022……....96

48. Hausfather, Z., **K. D. Marvel**, **G.A. Schmidt**, J.W. Nielsen-Gammon, and M. Zelinka, 2022: Climate simulations: Recognize the 'hot model' problem. *Nature*, **605**, 26-29, doi:10.1038/d41586-022-01192-2…….97

49. Hedlund, J., H. Carlsen, S. Croft, C. West, Ö. Bodin, E. Stokeld, **J. Jägermeyr**, and C. Müller, 2022: Impacts of climate change on global food trade networks. *Environ. Res. Lett.*, **17**, no. 12, 124040, doi:10.1088/1748-9326/aca68b……..…..98

50. Heinicke, S., K. Frieler, **J. Jägermeyr**, and M. Mengel, 2022: Global gridded crop models underestimate yield responses to droughts and heatwaves. *Environ. Res. Lett.*, **17**, no. 4, 044026, doi:10.1088/1748-9326/ac592e……..…99

51. Hermoso de Mendoza, I., E. Boucher, F. Gennaretti, A. Lavergne, L. Andreu-Hayles, and **R.D. Field**, 2022: A new snow module improves predictions of isotope-enabled MAIDENiso forest growth model. *Geosci. Model Dev.*, **15**, no. 5, 1931-1952, doi:10.5194/gmd-15-1931-2022…….…...100

52. Hernandez-Deckers, D., T. Matsui, and **A.M. Fridlind**, 2022: Updraft dynamics and microphysics: On the added value of the cumulus thermal reference frame in simulations of aerosol-deep convection interactions. *Atmos. Chem. Phys.*, **22**, no. 2, 711-724, doi:10.5194/acp-22-711-2022……....101

53. Hochman, G., H. Zhang, L. Xia, A. Robock, S. Aleti, D. van der Mensbrugghe, and **J. Jägermeyr**, 2022: Economic incentives modify agricultural impacts of nuclear war. *Environ. Res. Lett.*, **17**, no. 5, 054003, doi:10.1088/1748-9326/ac61c7……102

54. Horvat, C., and **L.A. Roach**, 2022: WIFF1.0: A hybrid machine-learning-based parameterization of Wave-Induced sea-ice Floe Fracture. *Geosci. Model Dev.*, **15**, no. 2, 803-814, doi:10.5194/gmd-15-803-2022……..103

55. Huxley, R., B. Walsh, C. Oke, R. Bellinson, H. Bulkeley, L.L.V. Ceneviva, L.B. Correa, S. Cox, B. Giles-Corti, G. Galik, A. Gouldson, G. Karuri-Sebina, M. Mazzucato, D. Miller, A. Revi, P. Rode, **C. Rosenzweig**, C. Singh, I. Sitcov, W. Solecki, K. Trebeck, P.A. Victor, and D. Zarrilli, 2022: A research agenda for transformative urban climate action. *J. City Clim. Policy Econ.*, **1**, no. 1, 13-31, doi:10.3138/jccpe-2022.1.1.0003……104

56. Igel, A.L., H. Morrison, **S.P. Santos**, and **M. van Lier-Walqui**, 2022: Limitations of separate cloud and rain categories in parameterizing collision-coalescence for bulk microphysics schemes. *J. Adv. Model. Earth Syst.*, **14**, no. 6, e2022MS003039, doi:10.1029/2022MS00303……...105

57. Jiang, Y., **M. Yang**, W. Liu, K. Mohammadi, and G. Wang, 2022: Eco-hydrological responses to recent droughts in tropical South America. *Environ. Res. Lett.*, **17**, no. 2, 024037, doi:10.1088/1748-9326/ac507a……..……....106

58. Karambelas, A., A.M. Fiore, **D.M. Westervelt**, V.F. McNeill, C.A. Randles, C. Venkataraman, J.R. Pierce, K.R. Bilsback, and G.P. Milly, 2022: Investigating drivers of particulate matter pollution over India and the implications for radiative forcing with GEOS-Chem-TOMAS15. *J. Geophys. Res. Atmos.*, **127**, no. 24, e2021JD036195,

doi:10.1029/2021JD036195……..107

59. Kato, S., T.J. Thorsen, S.-H. Ham, N.G. Loeb, R.A. Ferrare, D.M. Winker, H. Barker, G.L. Stephens, S. Schmidt, K.G. Meyer, and **B. Cairns**, 2022: Effect of spectral variability of aerosol optical properties on direct aerosol radiative effect. *Front. Remote Sens.*, **3**, 904505, doi:10.3389/frsen.2022.904505……108

60. Kern, O.A., A. Koutsodendris, F.J. Allstädt, B. Mächtle, **D.M. Peteet**, S. Kalaitzidis, K. Christanis, and J. Pross, 2022: A near-continuous record of climate and ecosystem variability in Central Europe during the past 130 kyrs (Marine Isotope Stages 5-1) from Füramoos, southern Germany. *Quat. Sci. Rev.*, **284**, 107505, doi:10.1016/j.quascirev.2022.107505……...109

61. **Kiang, N.Y.**, W.D. Swingley, D. Gautam, J.T. Broddrick, D. Repeta, J.F. Stolz, R.E. Blankenship, B.M. Wolf, A.M. Detweiler, K.A. Miller, J.J. Schladweiler, R. Lindeman, and M.N. Parenteau, 2022: Discovery of chlorophyll *d*: Isolation and characterization of a far-red cyanobacterium from the original site of Manning & Strain (1943) at Moss Beach, California. *Microorganisms*, **10**, no. 4, 819, doi:10.3390/microorganisms10040819. **…**……...110

62. Klovenski, E.R., Y. Wang, **S.E. Bauer**, **K. Tsigaridis**, **G.S. Faluvegi**, **I. Aleinov**, **N.Y. Kiang**, A. Guenther, X. Jiang, W. Li, and N. Lin, 2022: Interactive biogenic emissions and drought stress effects on atmospheric composition in NASA GISS ModelE. *Atmos. Chem. Phys.*, **22**, no. 10, 13303-13323, doi:10.5194/acp-22-13303-2022……111

63. Kothari, K., R. Battisti, K.J. Boote, S.V. Archontoulis, A. Confalone, J. Constantin, S.V. Cuadra, P. Debaeke, B. Faye, B. Grant, G. Hoogenboom, Q. Jing, M. van der Laan, F.A. Macena da Silva, F.R. Marin, A. Nehbandani, C. Nendel, L.C. Purcell, B. Qian, **A.C. Ruane**, C. Schoving, E.H.F.M. Silva, W. Smith, A. Soltani, A. Srivastava, N.A. Vieira, S. Slone, and M. Salmerón, 2022: Are soybean models ready for climate change food impact assessments? *Eur. J. Agron.*, **135**, 126482, doi:10.1016/j.eja.2022.126482….112

64. Kumar, S., J. Kolassa, R. Reichle, W. Crow, G. de Lannoy, P. de Rosnay, N. MacBean, M. Girotto, A. Fox, T. Quaife, C. Draper, B. Forman, G. Balsamao, S. Steele-Dunne, C. Albergel, B. Bonan, J.-C. Calvet, J. Dong, **H.M. Liddy**, and B. Ruston, 2022: An agenda for land data assimilation priorities: Realizing the promise of terrestrial water, energy, and vegetation observations from space. *J. Adv. Model. Earth Syst.*, **14**, no. 11, e2022MS003259, doi:10.1029/2022MS003259……..….113

65. Kumjian, M.R., O.P. Prat, K.J. Reimel, **M. van Lier-Walqui**, and H.C. Morrison, 2022: Dual-polarization radar fingerprints of precipitation physics: A review. *Remote Sens.*, **14**, no. 15, 3706, doi:10.3390/rs14153706……..114

66. **Lacis, A.A.**, **B.E. Carlson**, **G.L. Russell**, A. Marshak, and W. Su, 2022: Unique NISTAR-based climate GCM diagnostics of the Earth's planetary albedo and spectral absorption through longitudinal data slicing. *Front. Remote Sens.*, **3**, 766917,

doi:10.3389/frsen.2022.766917……..…..…115

67. Lesk, C., W. Anderson, A. Rigden, O. Coast, **J. Jägermeyr**, **S.S. McDermid**, K.F. Davis, and M. Konar, 2022: Compound heat and moisture extreme impacts on global crop yields under climate change. *Nat. Rev. Earth Environ.*, **3**, no. 12, 872-889, doi:10.1038/s43017-022-00368-8……116

68. Li, J., **B.E. Carlson**, Y.L. Yung, D. Lv, J. Hansen, J.E. Penner, H. Liao, V. Ramaswamy, R.A. Kahn, P. Zhang, O. Dubovik, A. Ding, **A.A. Lacis**, L. Zhang, and Y. Dong, 2022: Scattering and absorbing aerosols in the climate system. *Nat. Rev. Earth Environ.*, **3**, 363-379, doi:10.1038/s43017-022-00296-7…….117

69. Li, L., N. Mahowald, J. Kok, X. Liu, M. Wu, D. Leung, D. Hamilton, L. Emmons, **Y. Huang**, J. Meng, N. Sexton, and J. Wan, 2022: Importance of different parameterization changes for the updated dust cycle modelling in the Community Atmosphere Model (version 6.1). *Geosci. Model Dev.*, **15**, no. 22, 8181-8219, doi:10.5194/gmd-15-8181-2022……..….118

70. Li, X.-Y., H. Wang, J. Chen, S. Endo, G. George, **B. Cairns**, S. Chellappan, X. Zeng, S. Kirschler, C. Voigt, A. Sorooshian, E. Crosbie, G. Chen, R.A. Ferrare, W.I. Gustafson, J.W. Hair, M.M. Kleb, H. Liu, R. Moore, D. Painemal, C. Robinson, A.J. Scarino, M. Shook, T.J. Shingler, K.L. Thornhill, **F. Tornow**, H. Xiao, L.D. Ziemba, and P. Zuidema, 2022: Large-eddy simulations of marine boundary-layer clouds associated with cold air outbreaks during the ACTIVATE campaign — Part I: Case setup and sensitivities to large-scale forcings. *J. Atmos. Sci.*, 79, no. 1, 73-100, doi:10.1175/JAS-D-21-0123.1……...….119

71. Liu, L., G.L. Schuster, H. Moosmüller, S. Stamnes, **B. Cairns**, and **J. Chowdhary**, 2022: Optical properties of morphologically complex black carbon aerosols: Effects of coatings. *J. Quant. Spectrosc. Radiat. Transfer*, **281**, 108080, doi:10.1016/j.jqsrt.2022.108080……...120

72. **Liu, Q.**, **M. Yang**, K. Mohammadi, D. Song, J. Bi, and G. Wang, 2022: Machine learning crop yield models based on meteorological features and comparison with a process-based model. *Artif. Intell. Earth Syst.*, **1**, no. 4, -e220002, doi:10.1175/AIES-D-22-0002.1…….……..121

73. Lopez, J.R., J.M. Winter, J. Elliott, **A.C. Ruane**, C. Porter, and G. Hoogenboom, Martha Anderson, Christopher Hain, 2022: Sustainable use of groundwater may dramatically reduce irrigated production of maize, soybean, and wheat. *Earth's Future*, **10**, no. 1, e2021EF002018, doi:10.1029/2021EF002018……...…122

74. Lowrie, C., A. Kruczkiewicz, S.N. McClain, **M. Nielsen**, and S.J. Mason, 2022: Evaluating the usefulness of VGI from Waze for the reporting of flash floods. *Sci. Rep.*, **12**, no. 1, 5268, doi:10.1038/s41598-022-08751-7……...…123

75. MacBean, N., **H.M. Liddy**, T. Quaife, J. Kolassa, and A. Fox, 2022: Building a land data assimilation community to tackle technical challenges in quantifying and reducing uncertainty in land model predictions. *Bull. Amer. Meteorol. Soc.*, **103**, no. 3, E733-E740, doi:10.1175/BAMS-D-21-0228.1……...…..124

76. Marston, P.L., and **M.I. Mishchenko**, 2022: Scattering by relatively small oblate spheroidal drops of water in the rainbow region: T-matrix results and geometric interpretation. *J. Quant. Spectrosc. Radiat. Transfer*, **283**, 108142, doi:10.1016/j.jqsrt.2022.108142……...125

77. **Marvel, K.D.**, and **B.I. Cook**, 2022: Using machine learning to identify novel hydroclimate states. *Phil. Trans. Roy. Soc. A*, **380**, no. 2238, 20210287, doi:10.1098/rsta.2021.0287…….…….....126

78. McConnell, K., **C.V. Braneon**, E. Glenn, N. Stamler, E. Mallen, D.P. John, R. Pandya, J. Abramowitz, G. Fernandez, and **C. Rosenzweig**, 2022: A quasi-experimental approach for evaluating the heat mitigation effects of green roofs in Chicago, Illinois. *Sustain. Cities Soc.*, **76**, 103376, doi:10.1016/j.scs.2021.103376……...127

79. McCoy, D.T., P. Field, M.E. Frazer, M.D. Zelinka, **G.S Elsaesser**, J. Mülmenstädt, I. Tan, T.A. Myers, and Z.J. Lebo, 2022: Extratropical shortwave cloud feedbacks in the context of the global circulation and hydrological cycle. *Geophys. Res. Lett.*, **49**, no. 8, e2021GL097154, doi:10.1029/2021GL097154……128

80. **McDermid, S.S.**, **E. Weng**, **M.J. Puma**, **B.I. Cook**, T. Hengl, J. Sanderman, G.J.M. De Lannoy, and **I. Aleinov**, 2022: Soil carbon losses reduce soil moisture in global climate model simulations. *Earth Interact.*, **26**, no. 1, 195-208, doi:10.1175/EI-D-22-0003.1……129

81. Meng, J., **Y. Huang**, D.M. Leung, L. Li, A.A. Adebiyi, C.L. Ryder, N.M. Mahowald, and J.F. Kok, 2022: Improved parameterization for the size distribution of emitted dust aerosols reduces model underestimation of super coarse dust. *Geophys. Res. Lett.*, **49**, no. 8, e2021GL097287, doi:10.1029/2021GL097287…….130

82. Minoli, S., **J. Jägermeyr**, S. Asseng, A. Urfels, and C. Müller, 2022: Global crop yields can be lifted by timely adaptation of growing periods to climate change. *Nat. Commun.*, **13**, no. 1, 7079, doi:10.1038/s41467-022-34411-5…….…….131

83. **Mitevski, I.**, L. Polvani, and **C. Orbe**, 2022: Asymmetric warming/cooling response to $CO_2$ increase/decrease due to non-logarithmic forcing, not feedbacks. *Geophys. Res. Lett.*, **49**, no. 5, e2021GL097133, doi:10.1029/2021GL097133…….……..132

84. Montiel, F., A.L. Kohout, and **L.A. Roach**, 2022: Physical drivers of ocean wave attenuation in the marginal ice zone. *J. Phys. Oceanogr.*, **52**, no. 5, 889-906, doi:10.1175/JPO-D-21-0240.1……..133

doi:10.1175/JPO-D-21-0240.1……..133

85. Myhre, G., B. Samset, P.M. Forster, Ø. Hodnebrog, M. Sandstad, C.W. Mohr, J. Sillmann, C.W. Stjern, T. Andrews, O. Boucher, **G.S. Faluvegi**, T. Iversen, J.-F. Lamarque, M. Kasoar, A. Kirkevåg, R. Kramer, L. Liu, J. Mülmenstädt, D. Olivié, J. Quaas, T.B. Richardson, D. Shawki, D. Shindell, C. Smith, P. Stier, T. Tang, T. Takemura, A. Voulgarakis, and D. Watson-Parris, 2022: Scientific data from precipitation driver response model intercomparison project. *Sci. Data*, **9**, no. 1, 123, doi:10.1038/s41597-022-01194-9…….……134

86. **Nazarenko, L.S.**, **N.L. Tausnev**, **G.L. Russell**, **D. Rind**, **R.L. Miller**, **G.A. Schmidt**, **S.E. Bauer**, **M.A. Kelley**, **R.A. Ruedy**, **A.S. Ackerman**, **I. Aleinov**, **M. Bauer**, R. Bleck, **V.M. Canuto**, **G.V. Cesana**, **Y. Cheng**, T.L. Clune, **B.I. Cook**, C.A. Cruz, **A.D. Del Genio**, **G.S. Elsaesser**, **G.S. Faluvegi**, **N.Y. Kiang**, D. Kim, **A.A. Lacis**, **A. Leboissetier**, **A.N. LeGrande**, **K.K. Lo**, **J. Marshall**, **E.E. Matthews**, **S.S. McDermid**, **K. Mezuman**, L.T. Murray, **V. Oinas**, **C. Orbe**, C.P. García-Pando, **J.P. Perlwitz**, **M.J. Puma**, **A. Romanou**, D.T. Shindell, S. Sun, **K. Tsigaridis**, **G. Tselioudis**, **E. Weng**, **J. Wu**, and **M.-S. Yao**, 2022: Future climate change under SSP emission scenarios with GISS-E2.1. *J. Adv. Model. Earth Syst.*, **14**, no. 7, e2021MS002871, doi:10.1029/2021MS002871…….……..…135

87. Nkwasa, A., C.J. Chawanda, **J. Jägermeyr**, and A. van Griensven, 2022: Improved representation of agricultural land use and crop management for large scale hydrological impact simulation in Africa using SWAT+. *Hydrol. Earth Syst. Sci.*, **26**, no. 1, 71-89, doi:10.5194/hess-26-71-2022……..…..136

88. Norgren, M.S., J. Wood, K.S. Schmidt, **B. van Diedenhoven**, S.A. Stamnes, L.D. Ziemba, E.C. Crosbie, M.A. Shook, A.S. Kittelman, S.E. LeBlanc, S. Broccardo, S. Freitag, and J.S. Reid, 2022: Above-aircraft cirrus cloud and aerosol optical depth from hyperspectral irradiances measured by a total-diffuse radiometer. *Atmos. Meas. Tech.*, **15**, no. 5, 1373-1394, doi:10.5194/amt-15-1373-2022……137

89. **Ottaviani, M.**, 2022: Polarization as a discriminator of light-absorbing impurities in or above snow. *Front. Remote Sens.*, **3**, 863239, doi:10.3389/frsen.2022.863239……...138

90. Pontes, G., A. Taschetto, A. Sen Gupta, A. Santoso, I. Wainer, A. Haywood, W.-L. Chan, A. Abe-Ouchi, C. Stepanek, G. Lohmann, S. Hunter, J. Tindall, **M.A. Chandler**, **L.E. Sohl**, D. Peltier, D. Chandan, Y. Kamae, K. Nisancioglu, Z. Zhang, C. Contoux, N. Tan, Q. Zhang, B. Otto-Bliesner, E. Brady, R. Feng, A. von der Heydt, M. Baatsen, and A. Oldemann, 2022: Mid-Pliocene El Niño/Southern Oscillation suppressed by Pacific intertropical convergence zone shift. *Nat. Geosci.*, **15**, no. 9, 726-734, doi:10.1038/s41561-022-00999-y…….139

91. Preece, J.R., L.J. Wachowicz, T.L. Mote, **M. Tedesco**, and X. Fettweis, 2022: Summer Greenland blocking diversity and its impact on the surface mass balance of the Greenland Ice Sheet. *J. Geophys. Res. Atmos.*, **127**, no. 4, e2021JD035489,

doi:10.1029/2021JD035489……..140

92. Raheja, G., K. Sabi, H. Sonla, E.K. Gbedjangni, C.M. McFarlane, C.G. Hodoli, and **D.M. Westervelt**, 2022: A network of field-calibrated low-cost sensor measurements of $PM_{2.5}$ in Lomé, Togo, over one to two years. *ACS Earth Space Chem.*, **6**, no. 4, 1011-1021, doi:10.1021/acsearthspacechem.1c00391.x……..……141

93. Ramos, R., **A.N. LeGrande**, M.L. Griffiths, **G.S. Elsaesser**, **D.T Litchmore**, J.F. Tierney, F.S.R. Pausata, and J Nusbaumer, 2022: Constraining clouds and convective parameterizations in a climate model from past climate. *J. Adv. Model. Earth Syst.*, **14**, no. 8, e2021MS002893, doi:10.1029/2021MS002893……..……142

94. **Roach, L.A.**, I. Eisenman, T.J. Wagner, E. Blanchard-Wrigglesworth, and C.M. Bitz, 2022: Asymmetry in the seasonal cycle of Antarctic sea ice due to insolation. *Nat. Geosci.*, **15**, no. 4, 277-281, doi:10.1038/s41561-022-00913-6……143

95. **Roach, L.A.**, and E. Blanchard-Wrigglesworth, 2022: Observed winds crucial for September Arctic sea ice loss. *Geophys. Res. Lett.*, **49**, no. 6, e2022GL097884, doi:10.1029/2022GL097884……..144

96. **Roach, L.A.**, E. Blanchard-Wrigglesworth, S. Ragen, W. Cheng, K.C. Armour, and C.M. Bitz, 2022: The impact of winds on AMOC in a fully-coupled climate model. *Geophys. Res. Lett.*, **49**, no. 24, e2022GL101203, doi:10.1029/2022GL101203…….145

97. Rovithakis, A., M.G. Grillakis, K.D. Seiradakis, C. Giannakopoulos, A. Karali, **R.D. Field**, M. Lazaridis, and A. Voulgarakis, 2022: Future climate change impact on wildfire danger over the Mediterranean: The case of Greece. *Environ. Res. Lett.*, **17**, no. 4, 045022, doi:10.1088/1748-9326/ac5f94……146

98. **Ruane, A.C.**, R. Vautard, R. Ranasinghe, J. Sillmann, E. Coppola, N. Arnell, F.A. Cruz, S. Dessai, C.E. Iles, A.K.M.S. Islam, R.G. Jones, M. Rahimi, D. Ruiz Carrascal, S.I. Seneviratne, J. Servonnat, A.A. Sörensson, M.B. Sylla, C. Tebaldi, W. Wang, and R. Zaaboul, 2022: The Climatic Impact-Driver framework for assessment of risk-relevant climate information. *Earth's Future*, **10**, no. 11, e2022EF002803, doi:10.1029/2022EF002803……..147

99. Russotto, R.D., J.D.O. Strong, S.J. Camargo, A.H. Sobel, **G.S. Elsaesser**, **M.A. Kelley**, **A.D. Del Genio**, Y. Moon, and D. Kim, 2022: Improved representation of tropical cyclones in the NASA GISS-E3 GCM. *J. Adv. Model. Earth Syst.*, **14**, no. 1, e2021MS002601, doi:10.1029/2021MS002601…….....148

100. Schiro, K.A., H. Su, F. Ahmed, N. Dai, C.E. Singer, P. Gentine, **G.S. Elsaesser**, J.H. Jiang, Y.-S. Choi, and J. David Neelin, 2022: Model spread in tropical low cloud feedback tied to overturning circulation response to warming. *Nat. Commun.*, **13**, no. 1, 7119, doi:10.1038/s41467-022-34787-4…….……..149

101. Schlosser, J.S., S. Stamnes, S.P. Burton, **B. Cairns**, E. Crosbie, B. van Diedenhoven, G. Diskin, S. Dmitrovic, R. Ferrare, J.W. Hair, C.A. Hostetler, Y. Hu, X. Liu, R.H. Moore, T. Shingler, M.A. Shook, K.L. Thornhill, E. Winstead, L. Ziemba, and A. Sorooshian, 2022: Polarimeter + lidar-derived aerosol particle number concentration. *Front. Remote Sens.*, **3**, 885332, doi:10.3389/frsen.2022.885332…….……150

102. Schmidt, F., **M.J. Way**, S. Bouley, A. Séjourné, and **I. Aleinov**, 2022: Circumpolar ocean stability on Mars 3 Gy ago. *Proc. Natl. Acad. Sci.*, **119**, no. 4, e2112930118, doi:10.1073/pnas.2112930118…….……..151

103. Schwarzwald, K., and **N. Lenssen**, 2022: The importance of internal climate variability in climate impact projections. *Proc. Natl. Acad. Sci.*, **119**, no. 42, e2208095119, doi:10.1073/pnas.2208095119……..152

104. Sebastian, M., S.K. Kompalli, V.A. Kumar, S. Jose, S.S. Babu, G. Pandithurai, S. Singh, R.K. Hooda, V.K. Soni, J.R. Pierce, V. Vakkari, E. Asmi, **D.M. Westervelt**, A.-P. Hyvärinen, and V.P. Kanawade, 2022: Observations of particle number size distributions and new particle formation in six Indian locations. *Atmos. Chem. Phys.*, **22**, no. 7, 4491-4508, doi:10.5194/acp-22-4491-2022……...153

105. Sergeev, D.E., T.J. Fauchez, M. Turbet, I.A. Boutle, **K. Tsigaridis**, **M.J. Way**, E.T. Wolf, S.D. Domagal-Goldman, F. Forget, J. Haqq-Misra, R.K. Kopparapu, F.H. Lambert, J. Manners, and N.J. Mayne, 2022: The TRAPPIST-1 Habitable Atmosphere Intercomparison (THAI). Part II: Moist cases — The two waterworlds. *Planet. Sci. J.*, **3**, no. 9, 212, doi:10.3847/PSJ/ac6cf2……..…..……154

106. Shindell, D., **G.S. Faluvegi**, L. Parsons, E. Nagamoto, and Chang J., 2022: Premature deaths in Africa due to particulate matter under high and low warming scenarios. *GeoHealth*, **6**, no. 5, e2022GH000601, doi:10.1029/2022GH000601……..……...…155

107. Silber, I., R.C. Jackson, **A.M. Fridlind**, **A.S. Ackerman**, S. Collis, J. Verlinde, and J. Ding, 2022: The Earth Model Column Collaboratory ($EMC^2$) v1.1: An open-source ground-based lidar and radar instrument simulator and subcolumn generator for large-scale models. *Geosci. Model Dev.*, **15**, no. 2, 901-927, doi:10.5194/gmd-15-901-2022……...156

108. Smith, D.M., N.P. Gillett, I.R. Simpson, P.J. Athanasiadis, J. Baehr, I. Bethke, T.A. Bilge, R. Bonnet, O. Boucher, K.L. Findell, G. Gastineau, S. Gualdi, L. Hermanson, L.R. Leung, J. Mignot, W.A. Müller, S. Osprey, O.H. Otterå, G.G. Persad, A.A. Scaife, **G.A. Schmidt**, H. Shiogama, R.T. Sutton, D. Swingedouw, S. Yang, T. Zhou, and T. Ziehn, 2022: Attribution of multi-annual to decadal changes in the climate system: The Large Ensemble Single Forcing Model Intercomparison Project (LESFMIP). *Front. Clim.*, **4**, 955414, doi:10.3389/fclim.2022.955414…….……157

109. **Tedesco, M.**, C. Hultquist, and A. de Sherbinin, 2022: A new dataset integrating public socioeconomic, physical risk, and housing data for climate justice metrics: A test-case study in Miami. *Environ. Justice*, **15**, no. 3, 149-159, doi:10.1089/env.2021.0059….158

110. **Tedesco, M.**, J.M. Keenan, and C. Hultquist, 2022: Measuring, mapping, and anticipating climate gentrification in Florida: Miami and Tampa case studies. *Cities*, **131**, 103991, doi:10.1016/j.cities.2022.103991……..…..159

111. **Tornow, F.**, **A.S. Ackerman**, **A.M. Fridlind**, **B. Cairns**, E.C. Crosbie, S. Kirschler, R.H. Moore, D. Painemal, C.E. Robinson, C. Seethala, M.A. Shook, C. Voigt, E.L. Winstead, L.D. Ziemba, P. Zuidema, and A. Sorooshian, 2022: Dilution of boundary layer cloud condensation nucleus concentrations by free tropospheric entrainment during marine cold air outbreaks. *Geophys. Res. Lett.*, **49**, no. 11, e2022GL098444, doi:10.1029/2022GL098444……...…….….160

112. Tridon, F., I. Silber, A. Battaglia, S. Kneifel, **A.M. Fridlind**, P. Kalogeras, and R. Dhillon, 2022: Highly supercooled riming and unusual triple-frequency radar signatures over McMurdo Station, Antarctica. *Atmos. Chem. Phys.*, **22**, no. 18, 12467-12491, doi:10.5194/acp-22-12467-2022……....161

113. Tubiello, F., K. Karl, A. Flammini, J. Gutschow, G. Obli-Laryea, G. Conchedda, X. Pan, S.Y. Qiu, H.H. Heiðarsdóttir, N. Wanner, R. Quadrelli, L. Souza, P. Benoit, M. Hayek, D. Sandalow, **E.A. Mencos Contreras**, **C. Rosenzweig**, J. Rosero-Moncayo, P. Conforti, and M. Torero, 2022: Pre- and post-production processes increasingly dominate greenhouse gas emissions from agri-food systems. *Earth Syst. Sci. Data*, **14**, no. 4, 1795-1809, doi:10.5194/essd-14-1795-2022……..162

114. Turbet, M., T.J. Fauchez, D.E. Sergeev, I.A. Boutle, **K. Tsigaridis**, **M.J. Way**, E.T. Wolf, S.D. Domagal-Goldman, F. Forget, J. Haqq-Misra, R.K. Kopparapu, F.H. Lambert, J. Manners, N.J. Mayne, and **L. Sohl**, 2022: The TRAPPIST-1 Habitable Atmosphere Intercomparison (THAI). Part I: Dry cases — The fellowship of the GCMs. *Planet. Sci. J.*, **3**, no. 9, 211, doi:10.3847/PSJ/ac6cf0…….….163

115. Van Diedenhoven, B., O.P. Hasekamp, **B. Cairns**, G.L. Schuster, S. Stammes, M.A. Shook, and L.D. Ziemba, 2022: Remote sensing of aerosol water fraction, dry size distribution and soluble fraction using multi-angle, multi-spectral polarimetry. *Atmos. Meas. Tech.*, **15**, no. 24, 7411-7434, doi:10.5194/amt-15-7411-2022……..164

116. Van Marle, M.J.E., D. van Wees, R.A. Houghton, **R.D. Field**, J. Verbesselt, and G.R. van der Werf, 2022: New land-use change emission estimates indicate a declining $CO_2$ airborne fraction. *Nature*, **603**, 450-454, doi:10.1038/s41586-021-04376-4……165

117. Von Salzen, K., C.H. Whaley, S.C. Anenberg, R. Van Dingenen, Z. Klimont, M.G. Flanner, R. Mahmood, S.R. Arnold, S. Beagley, R.-Y. Chien, J.H. Christensen, S. Eckhardt, A.M.L. Ekman, N. Evangeliou, **G.S. Faluvegi**, J.S. Fu, M. Gauss, W. Gong, J.L. Hjorth, U. Im, S. Krishnan, K. Kupiainen, T. Kühn, J. Langner, K.S. Law, L.

Marelle, D. Olivié, T. Onishi, N. Oshima, V.-V. Paunu, Y. Peng, D. Plummer, L. Pozzoli, S. Rao, J.-C. Raut, M. Sand, J. Schmale, M. Sigmond, M.A. Thomas, **K. Tsigaridis**, S. Tsyro, S.T. Turnock, M. Wang, and B. Winter, 2022: Clean air policies are key for successfully mitigating Arctic warming. *Commun. Earth Environ.*, **3**, no. 1, 222, doi:10.1038/s43247-022-00555-x…….166

118. **Way, M.J.**, R.E. Ernst, and J.D. Scargle, 2022: Large scale volcanism and the heat-death of terrestrial worlds. *Planet. Sci. J.*, **3**, no. 4, 92, doi:10.3847/PSJ/ac6033……..167

119. Weir, B., T. Oda, L.E. Ott, and **G.A. Schmidt**, 2022: Assessing progress toward the Paris Climate Agreement from space. *Environ. Res. Lett.*, **17**, no. 11, 111002, doi:10.1088/1748-9326/ac998c…….168

120. Weiskopf, S.R., Z. Harmáčková, C.G. Johnson, M.C. Londoño-Murcia, B.W. Miller, B.J.E. Myers, L. Pereira, M.I. Arce-Plata, J.L. Blanchard, S. Ferrier, E.A. Fulton, M. Harfoot, F. Isbell, J.A. Johnson, A.S. Mori, **E. Weng**, and I.M.D. Rosa, 2022: Increasing the uptake of ecological model results in policy decisions to improve biodiversity outcomes. *Environ. Model. Softw.*, **149**, 105318, doi:10.1016/j.envsoft.2022.105318……...169

121. Weiskopf, S.R, B.J.E Myers, M.I. Arce-Plata, J.L Blanchard, S. Ferrier, E.A Fulton, M. Harfoot, F. Isbell, J.A Johnson, A.S Mori, **E. Weng**, Z.V Harmáčková, M.C. Londoño-Murcia, B.W Miller, L.M Pereira, and I.M.D Rosa, 2022: A conceptual framework to integrate biodiversity, ecosystem function, and ecosystem service models. *BioScience*, **72**, no. 11, 1062-1073, doi:10.1093/biosci/biac074……..…..170

122. **Weng, E**., **I. Aleinov**, **R. Singh**, **M.J. Puma**, **S.S. McDermid**, **N.Y. Kiang**, **M.A Kelley**, K. Wilcox, R. Dybzinski, C.E. Farrior, S.W. Pacala, and **B.I. Cook**, 2022: Modeling demographic-driven vegetation dynamics and ecosystem biogeochemical cycling in NASA GISS's Earth system model (ModelE-BiomeE v.1.0). *Geosci. Model Dev.*, **15**, no. 22, 8153-8180, doi:10.5194/gmd-15-8153-2022……..…….171

123. Whaley, C.H., R. Mahmood, K. von Salzen, B. Winter, S. Eckhardt, S. Arnold, S. Beagley, S. Becagli, R.-Y. Chien, J. Christensen, S.M. Damani, K. Eleftheriadis, N. Evangeliou, **G.S. Faluvegi**, M. Flanner, J.S. Fu, M. Gauss, F. Giardi, W. Gong, J.L. Hjorth, L. Huang, U. Im, Y. Kanaya, S. Krishnan, Z. Klimont, T. Kühn, J. Langner, K.S. Law, L. Marelle, A. Massling, D. Olivié, T. Onishi, N. Oshima, Y. Peng, D.A. Plummer, O. Popovicheva, L. Pozzoli, J.-C. Raut, M. Sand, L.N. Saunders, J. Schmale, S. Sharma, H. Skov, F. Taketani, M.A. Thomas, R. Traversi, **K. Tsigaridis**, S. Tsyro, S. Turnock, V. Vitale, K.A. Walker, M. Wang, D. Watson-Parris, and T. Weiss-Gibbons, 2022: Model evaluation of short-lived climate forcers for the Arctic Monitoring and Assessment Programme: A multi-species, multi-model study. *Atmos. Chem. Phys.*, **22**, no. 9, 5775-5828, doi:10.5194/acp-22-5775-2022……...172

124. Williams, A.P., **B.I. Cook**, and J.E. Smerdon, 2022: Rapid intensification of the emerging southwestern North American megadrought in 2020-2021. *Nat. Clim. Change*, **12**, no. 3, 232-234, doi:10.1038/s41558-022-01290-z……173

125. Williams, A.P., B. Livneh, K.A. McKinnon, W.D. Hansen, J.S. Mankin, **B.I. Cook**, J.E. Smerdon, A.M. Varuolo-Clarke, N.R. Bjarke, C.S. Juang, and D.P. Lettenmaier, 2022: Growing impact of wildfire on western US water supply. *Proc. Natl. Acad. Sci.*, **119**, no. 10, e2114069119, doi:10.1073/pnas.2114069119……...174

126. Xia, L., A. Robock, K. Scherrer, C. Harrison, B.L. Bodirsky, I. Weindl, **J. Jägermeyr**, C. Bardeen, O.B. Toon, and R. Heneghan, 2022: Global food insecurity and famine from reduced crop, marine fishery and livestock production due to climate disruption from nuclear war soot injection. *Nat. Food*, **3**, no. 8, 586-596, doi:10.1038/s43016-022-00573-0……..…175

127. Xie, X., G. Myhre, D. Shindell, **G.S. Faluvegi**, T. Takemura, A. Voulgarakis, Z. Shi, X. Li, X. Xie, H. Liu, X. Liu, and Y. Liu, 2022: Anthropogenic sulfate aerosol pollution in South and East Asia induces increased summer precipitation over arid Central Asia. *Commun. Earth Environ.*, **3**, no. 1, 328, doi:10.1038/s43247-022-00660-x…...176

128. Yao, Y., I. Vanderkelen, D. Lombardozzi, S. Swenson, D. Lawrence**, J. Jägermeyr**, L. Grant, and W. Thiery, 2022: Implementation and evaluation of irrigation techniques in the Community Land Model. *J. Adv. Model. Earth Syst.*, **14**, no. 12, e2022MS003074, doi:10.1029/2022MS003074…….177

129. Yu, F., G. Luo, A.A. Nair, **K. Tsigaridis**, and **S.E. Bauer**, 2022: Use of machine learning to reduce uncertainties in particle number concentration and aerosol indirect radiative forcing predicted by climate models. *Geophys. Res. Lett.*, **49**, no. 16, e2022GL098551, doi:10.1029/2022GL098551…….……...178

130. Zanchettin, D., C. Timmreck, M. Khodri, A. Schmidt, M. Toohey, M. Abe, S. Bekki, J. Cole, S.-W. Fang, W. Feng, G. Hegerl, B. Johnson, N. Lebas, **A.N. LeGrande**, G.W. Mann, L. Marshall, L. Rieger, A. Robock, S. Rubinetti, **K. Tsigaridis**, and H. Weierbach, 2022: Effects of forcing differences and initial conditions on inter-model agreement in the VolMIP volc-pinatubo-full experiment. *Geosci. Model Dev.*, **15**, no. 5, 2265-2292, doi:10.5194/gmd-15-2265-2022……179

131. Zanis, P., D. Akritidis, S. Turnock, V. Naik, S. Szopa, A.K. Georgoulias, **S.E. Bauer**, M. Deushi, L.W Horowitz, J. Keeble, P. Le Sager, F.M. O'Connor, N. Oshima, **K. Tsigaridis**, and T. van Noije, 2022: Climate change penalty and benefit on surface ozone: A global perspective based on CMIP6 earth system models. *Environ. Res. Lett.*, **17**, no. 2, 024014, doi:10.1088/1748-9326/ac4a34……...180

132. Zeng, G., N.L. Abraham, A.T. Archibald, **S.E. Bauer**, M. Deushi, L.K. Emmons, P.T. Griffiths, B. Hassler, L.W. Horowitz, J. Keeble, M.J. Mills, O. Morgenstern, L.T. Murray, V. Naik, F.M. O'Connor, N. Oshima, L.T. Sentman, S. Tilmes, **K. Tsigaridis**, J.H.T. Williams, and P.J. Young, 2022: Attribution of stratospheric and tropospheric ozone changes between 1850 and 2014 in CMIP6 models. *J. Geophys. Res. Atmos.*, **127**, no. 16, e2022JD036452, doi:10.1029/2022JD036452……..181

133. Zhai, P.-W., M. Gao, B.A. Franz, P.J. Werdell, A. Ibrahim, Y. Hu, and **J. Chowdhary**, 2022: A radiative transfer simulator for PACE: Theory and applications. *Front. Remote Sens.*, **3**, 840188, doi:10.3389/frsen.2022.840188……182

134. Zheng, C., M. Ting, Y. Wu, N. Kurtz, **C. Orbe**, **P.M. Alexander**, R. Seager, and **M. Tedesco**, 2022: Turbulent heat flux, downward longwave radiation and large-scale atmospheric circulation associated with the wintertime Barents-Kara Sea extreme sea ice loss events. *J. Climate*, **35**, no. 12, 3747-3765, doi:10.1175/JCLI-D-21-0387.1……..183

135. Zhong, Q., N. Schutgens, G van der Werf, T. van Noije, **K. Tsigaridis**, **S.E. Bauer**, T. Mielonen, A. Kirkevåg, Ø. Seland, H. Kokkola, R. Checa-Garcia, D. Neubauer, Z. Kipling, H. Matsui, P. Ginoux, T. Takemura, P. Le Sager, S. Rémy, H. Bian, M. Chin, K. Zhang, J. Zhu, S.G. Tsyro, G. Curci, A. Protonotariou, B. Johnson, J.E. Penner, N. Bellouin, R.B. Skeie, and G. Myhre, 2022: Satellite-based evaluation of AeroCom model bias in biomass burning regions. *Atmos. Chem. Phys.*, **22**, no. 17, 11009-11032, doi:10.5194/acp-22-11009-2022……..184

136. Zhong, Q., N. Schutgens, G.R. van der Werf, T. van Noije, **S.E. Bauer**, **K. Tsigaridis**, T. Mielonen, R. Checa-Garcia, D. Neubauer, Z. Kipling, A. Kirkevåg, D.J.L. Olivié, H. Kokkola, H. Matsui, P. Ginoux, T. Takemura, P. Le Sager, S. Rémy, H. Bian, and M. Chin, 2022: Using modelled relationships and satellite observations to attribute modelled aerosol biases over biomass burning regions. *Nat. Commun.*, **13**, no. 1, 5914, doi:10.1038/s41467-022-33680-4…….185

137. Zhu, J., B.L. Otto-Bliesner, E.C. Brady, A. Gettelman, J.T. Bacmeister, R.B. Neale, C.J. Poulsen, J.K. Shaw, **Z.S. McGraw**, and J.E. Kay, 2022: LGM paleoclimate constraints inform cloud parameterizations and equilibrium climate sensitivity in CESM2. *J. Adv. Model. Earth Syst.*, **14**, no. 4, e2021MS002776, doi:10.1029/2021MS002776…….186

Journal of Atmospheric Sciences. Sci., vol. 79, issue no. 12, pp. 3315-3332, doi:10.1175/JAS-D-22-0125.1

# Markovian statistical model of cloud optical thickness. Part I: Theory and examples

**Alexandrov**, **M.D.**[1,2], A. Marshak[3], **B. Cairns**[1], and **A.S. Ackerman**[1], 2022

NASA Goddard Institute for Space Studies, New York, NY, USA[1]
Department of Applied Physics and Applied Mathematics, Columbia University, New York, NY, USA[2]
NASA Goddard Space Flight Center, Greenbelt, MD, USA[3]

**Abstract.** We present a generalization of the binary-value Markovian model previously used for statistical characterization of cloud masks to a continuous-value model describing 1D fields of cloud optical thickness (COT). This model has simple functional expressions and is specified by four parameters: the cloud fraction, the autocorrelation (scale) length, and the two parameters of the normalized probability density function of (nonzero) COT values (this PDF is assumed to have gamma-distribution form). Cloud masks derived from this model by separation between the values above and below some threshold in COT appear to have the same statistical properties as in binary-value model described in our previous publications. We demonstrate the ability of our model to generate examples of various cloud-field types by using it to statistically imitate actual cloud observations made by the Research Scanning Polarimeter (RSP) during two field experiments.

**Introduction.** This study follows the "Cellular Statistical Models of Broken Cloud Fields" series of papers (Alexandrov et al. 2010a,b, hereinafter CSM1 and CSM2, respectively; Alexandrov and Marshak 2017, 2019, hereinafter CSM3 and CSM4, respectively). In these series we developed statistical parameterization and modeling algorithms for cloud structure in binary-mixture framework. The approach adopted there is based on cloud-mask statistics of 1D or 2D broken cloud fields derived from observations [in the 2D case made along 1D linear transects (chords)]. Such observations consist of the lengths of cloudy and clear intervals in each transect. The cloud statistics in this approach are always finite, so it works equally well for cumulus and stratocumulus cloud fields with a smooth transition between these two types (which are symmetrical to each other under cloud–clear interchange). This is an advantage compared to, e.g., area-based characterization which yields infinite cloud areas in Sc cases and infinite clear areas in Cu cases. In CSM2 the analytical expressions derived in CSM1 were demonstrated to adequately describe the statistics of shallow, broken cloud fields generated using a realistic large-eddy simulation (LES) model. In CSM3 the results of CSM1 were interpreted in terms of the theory of Markov processes (e.g., Kulkarni 2011; Ibe 2013). This interpretation is based on the assumption that each 1D sample consisting of subsequent cloudy and clear segments is a realization of a binary Markov process, which can take only two (generally nonnumerical) values: occupied (cloudy, "•") or empty (clear, "∘"). In CSM4 the binary Markov processes framework was used for quantitative evaluation of the effects of low resolution of idealized observations on the statistics of the retrieved cloud masks.

In the above-described approach cloud mask statistics depend on the nominal threshold in continuous-value field [such as cloud optical thickness (COT)] separating "clear" from "cloudy," which is chosen rather subjectively by the investigator. In this study we want to overcome this subjectivity by turning our attention from Markovian cloud mask model to this of the underlaying continuous-value cloud fields themselves. The continuous-value fields used in this study are these of COT which can take values ranging from zero to (formally) infinity. They will be characterized in our model by four statistical parameters: the absolute (zero-threshold) cloud fraction, the autocorrelation (scale) length, and the two parameters of the normalized probability density function of nonzero COT values (this PDF is assumed to have gamma-distribution functional shape).

Our approach to COT modeling is substantially simpler than those developed in the past, in particular, compared to the following two types of stochastic models of cloud horizontal structure. The first is the bounded cascade model (**Marshak et al. 1993**, **1994**; **Cahalan 1994**) which is a nonstationary two-parameter generalization of Meneveau and Sreenivasan's *p*-models for the intermittent dissipation rate field in turbulence (**Meneveau and Sreenivasan 1987**). The second class, suggested by **Schertzer and Lovejoy (1987)**, consists of fractionally integrated cascade models where power-law filtering in Fourier space brings the spectral exponent to any prescribed value.

The Cryosphere, vol. 16, issue no. 10, pp. 4185-4199, doi:10.5194/tc-16-4185-2022

# Assessing bare ice albedo simulated by MAR over the Greenland ice sheet (2000-2021) and implications for meltwater production estimates

Antwerpen, R.[2], **M. Tedesco**[1,2], X. Fettweis, **P.M. Alexander**[1,2], and W.J. van de Berg, 2022

NASA Goddard Institute for Space Studies, New York, NY, USA[1]
Lamont-Doherty Earth Observatory, Columbia University, Palisades, NY, USA[2]

**Abstract.** Surface mass loss from the Greenland ice sheet (GrIS) has accelerated over the past decades, mainly due to enhanced surface melting and liquid water runoff in response to atmospheric warming. A large portion of runoff from the GrIS originates from exposure of the darker bare ice in the ablation zone when the overlying snow melts, where surface albedo plays a critical role in modulating the energy available for melting. In this regard, it is imperative to understand the processes governing albedo variability to accurately project future mass loss from the GrIS. Bare-ice albedo is spatially and temporally variable and contingent on non-linear feedbacks and the presence of light-absorbing constituents. An assessment of models aiming at simulating albedo variability and associated impacts on meltwater production is crucial for improving our understanding of the processes governing these feedbacks and, in turn, surface mass loss from Greenland. Here, we report the results of a comparison of the bare-ice extent and albedo simulated by the regional climate model Modèle Atmosphérique Régional (MAR) with satellite imagery from the Moderate Resolution Imaging Spectroradiometer (MODIS) for the GrIS below 70∘ N. Our findings suggest that MAR overestimates bare-ice albedo by 22.8 % on average in this area during the 2000–2021 period with respect to the estimates obtained from MODIS. Using an energy balance model to parameterize meltwater production, we find this bare-ice albedo bias can lead to an underestimation of total meltwater production from the bare-ice zone below 70∘ N of 42.8 % during the summers of 2000–2021.

**Introduction.** Global mean sea level (GMSL) rise has significantly accelerated over the past decades (Chen et al., 2017), in part as a consequence of the acceleration in Greenland ice mass loss (Aschwanden et al., 2019). Ice mass loss from the Greenland ice sheet (GrIS) was one of the largest contributors to GMSL rise in the period 1901–2018 with 17 %–32 % and will likely remain so by the end of this century (Fox-Kemper et al., 2021). According to Fox-Kemper et al. (2021), the GrIS' contribution to GMSL will constitute ∼ 17 % by 2100 for the Shared Socioeconomic Pathway SSP5-8.5 (Riahi et al., 2017). From this point of view, it is imperative to improve model representation of physical processes responsible for ice mass loss to better constrain projections of the future contribution of the GrIS. In this regard, evaluation of climate model outputs vs. observational data can provide insight into the model's ability to represent the physical processes at play and can subsequently highlight regions for model improvement (van den Broeke et al., 2017).

The total mass loss from Greenland can be separated into surface losses (e.g., runoff) and frontal losses at the terminus of outlet glaciers (e.g., calving). For the 2000–2018 period, 55 % of Greenland's mass loss originated from surface mass balance (SMB; the balance between accumulation and ablation at the ice sheet surface), and 45 % was from ice discharge from outlet glaciers (Mouginot et al., 2019). The SMB losses from the GrIS have been increasing since the late 1990s, driven primarily by an increase in melt and subsequent liquid water runoff in response to recent atmospheric warming (van den Broeke et al., 2017). An increase in summer surface air temperatures of ∼ +2 ∘C has also been observed over Greenland since the early 1990s (Hanna et al., 2012; Box, 2013). This has increased runoff by 40 %, while the contribution of changes in precipitation, sublimation, and erosion since the early 1990s are not as substantial (van den Broeke et al., 2016, 2017). The recent increase in observed runoff has also been suggested to be linked to changes in atmospheric circulations around Greenland (Hanna et al., 2014; Tedesco and Fettweis, 2020).

Atmosphere, vol. 13, issue no. 2, doi:10.3390/atmos13020332

# Spatial downscaling of GOES-R land surface temperature over urban regions: A case study for New York City

Bah, A.R[3]., H. Norouzi[3,4], S. Prakash, **R. Blake[1,2,3]**, R. Khanbilvardi, and **C. Rosenzweig[1]**, 2022

NASA Goddard Institute for Space Studies, New York, NY, USA[1]
SciSpace, LLC, New York, NY, USA[2]
The Graduate Center, City University of New York, New York, NY, USA[3]

**Abstract.** The surface urban heat island (SUHI) effect is among the major environmental issues encountered in urban regions. To better predict the dynamics of the SUHI and its impacts on extreme heat events, an accurate characterization of the surface energy balance in urban regions is needed. However, the ability to improve understanding of the surface energy balance is limited by the heterogeneity of surfaces in urban areas. This study aims to enhance the understanding of the urban surface energy budget through an innovation in the use of land surface temperature (LST) observations from remote sensing satellites. A LST database with 5–min temporal and 30–m spatial resolution is developed by spatial downscaling of the Geostationary Operational Environmental Satellites—R (GOES–R) series LST product over New York City (NYC). The new downscaling method, known as the Spatial Downscaling Method (SDM), benefits from the fine spatial resolution of Landsat–8 and high temporal resolution of GOES–R, and considers the temporal variation in LST for each land cover type separately. Preliminary results show that the SDM can reproduce the temporal and spatial variability of LST over NYC reasonably well and the downscaled LST has a spatial root mean square error (RMSE) of the order of 2 K as compared to the independent Landsat–8 observations. The SDM shows smaller RMSE of 1.93 K over the tree canopy land cover, whereas RMSE is 2.19 K for built–up areas. The overall results indicate that the SDM has potential to estimate LST at finer spatial and temporal scales over urban regions.

**Introduction.** Reliable estimates of land surface temperature (LST) are crucial for understanding the land–atmosphere energy budget, hydrological and biogeochemical cycles, climate change, as well as for land surface model data assimilation [1,2,3,4]. LST is also a key input variable for the estimation of land surface emissivity, evapotranspiration, and latent and sensible heat fluxes [5,6,7]. Differences in LST and near–surface air temperature are often difficult to characterize because LST exhibits different patterns of spatial and temporal variability than near–surface air temperature over a specific region [8].

Further, in–situ observations of LST are not uniform everywhere, and that hinders applicability due to limited spatial representation. On the other hand, satellite remote sensing provides LST estimates at uniform spatial and temporal scales globally or quasi–globally. Thermal infrared (TIR) sensors provide LST estimates at finer spatial resolution with reasonable accuracy, but they are restricted to clear–sky conditions alone. An example of one of the most widely used TIR–based LST products is obtained from the Moderate Resolution Imaging Spectroradiometer (MODIS) derived LST estimates, and it has been successfully used for numerous applications worldwide [3,4,8,9,10,11]. Microwave sensors provide LST estimates for all–weather conditions, but their spatial resolution is rather coarse. Hence, integration of both TIR– and microwave–based LST estimates could provide better estimates of LST for all–weather conditions at finer spatial and temporal scales [12,13].

Satellite–based LST estimates have been widely used for the study of surface urban heat island (SUHI) intensity and changes in their spatial extent [2,14,15,16,17]. The SUHI phenomenon is generally seen as being caused by a reduction in latent heat flux and an increase in sensible heat flux in urban areas as vegetated and evaporating soil surfaces are replaced by relatively impervious low albedo paving and building materials. However, the adequate monitoring of SUHI requires high temporal (~10–15 min) and spatial resolution (~50–100 m) LST estimates.

AGU Advances, vol. 3, issue no. 4, e2022AV000688, doi:10.1029/2022AV000688

# Clumped-isotope constraint on upper-tropospheric cooling during the Last Glacial Maximum

Banerjee, A., L.Y. Yeung, L.T. Murray, X. Tie, J.E. Tierney, and **A.N. LeGrande**[1,2], 2022

NASA Goddard Institute for Space Studies, New York, NY, USA[1]
Center for Climate Systems Research, Columbia University, New York, NY, USA[2]

**Abstract**. Ice cores and other paleotemperature proxies, together with general circulation models, have provided information on past surface temperatures and the atmosphere's composition in different climates. Little is known, however, about past temperatures at high altitudes, which play a crucial role in Earth's radiative energy budget. Paleoclimate records at high-altitude sites are sparse, and the few that are available show poor agreement with climate model predictions. These disagreements could be due to insufficient spatial coverage, spatiotemporal biases, or model physics; new records that can mitigate or avoid these uncertainties are needed. Here, we constrain the change in upper-tropospheric temperature at the global scale during the Last Glacial Maximum (LGM) using the clumped-isotope composition of molecular oxygen trapped in polar ice cores. Aided by global three-dimensional chemical transport modeling, we exploit the intrinsic temperature sensitivity of the clumped-isotope composition of atmospheric oxygen to infer that the upper troposphere (effective mean altitude 10–11 km) was 6–9°C cooler during the LGM than during the late preindustrial Holocene. A complementary energy balance approach supports a minor or negligible steepening of atmospheric lapse rates during the LGM, which is consistent with a range of climate model simulations. Proxy-model disagreements with other high-altitude records may stem from inaccuracies in regional hydroclimate simulation, possibly related to land-atmosphere feedbacks.

**Introduction**. Atmospheric lapse rates affect the emission of longwave radiation to space and thus the climate system's response to changes in greenhouse gas concentrations (Bony et al., **2006**; Soden & Held, **2006**). Accurately predicting how they and other atmospheric properties change when subject to different climate forcing, however, remains a challenge (Bony et al., **2006**, **2015**; Shepherd, **2014**; Sherwood et al., **2014**). Simulated lapse-rate responses to climate forcing differ substantially among models and they are, on average, a factor of two smaller than what proxy-based reconstructions imply for the most recent glacial period in the tropics (Farrera et al., **1999**; Kageyama et al., **2005**; Loomis et al., **2017**; Porter, **2000**; Soden & Held, **2006**). However, the high-altitude paleoclimate record is sparse and biased toward terrestrial signals; it yields few constraints on how global-mean atmospheric temperature structure changes with surface climate. A global-scale high-altitude paleotemperature proxy, unaffected by location-specific climatology, could benchmark climate model performance at high altitudes for past climates and diagnose any shortcomings in model physics. Furthermore, it could provide paleoclimatic perspectives on the lapse-rate feedback, the second-largest negative feedback in the climate system.

The Last Glacial Maximum (LGM, 21–18 ka) has been used extensively as a reference climate state for paleoclimate modeling and to constrain climate sensitivity due to its relatively recent occurrence, well-preserved proxy records, and radically different climate forcings (Braconnot et al., **2012**; Kageyama et al., **2017**, **2021**; Otto-Bliesner et al., **2006**; Schmittner et al., **2011**; Tierney et al., **2020**). Reduced greenhouse-gas concentrations and the presence of large ice sheets (Anklin et al., **1997**; Loulergue et al., **2008**; Monnin et al., **2001**; Parrenin et al., **2013**; Spahni et al., **2005**; Valdes, **2005**) led to a global-scale cooling of surface air temperatures (SATs). Estimates using model-data syntheses suggest that global-mean SATs were between 4°C and 6°C cooler than the late preindustrial Holocene (Annan & Hargreaves, **2013**; Tierney et al., **2020**), while noble gas-based low- and mid-latitude temperature estimates suggest 6°C of cooling on land (Seltzer et al., **2021**). High-altitude cooling during the LGM, however, is less well known. For example, many paleotemperature records from polar ice cores reflect climate at high elevations, but weak constraints on ice-sheet elevation histories complicate their utility as high-altitude records.

Journal of Advances in Modeling Earth Systems, vol. 14, issue no. 12, e2022MS003070,
doi:10.1029/2022MS003070

# The turning point of the aerosol era

**Bauer**, **S.E.**[1], **K. Tsigaridis**[1,2], **G.S. Faluvegi**[1,2], **L.S. Nazarenko**[1,2], **R.L. Miller**[1], **M.A. Kelley**[1], and **G.A. Schmidt**[1], 2022

NASA Goddard Institute for Space Studies, New York, NY, USA[1]
Center for Climate Systems Research, Columbia University, New York, NY, USA[2]

**Abstract.** Over the CMIP6 historical period (1850–2014), aerosols provided the largest negative forcing compared to all other climate forcings via their ability to absorb or scatter solar radiation and alter clouds. Aerosols played an important role in counterbalancing warming by greenhouse gases (GHGs). Here we study aerosol forcing trends in the CMIP6 simulations of the NASA Goddard Institute for Space Studies (GISS) ocean-atmosphere ModelE version 2.1 (GISS-E2.1-G) using a fully coupled atmospheric composition configuration, including interactive gas-phase chemistry, and either an aerosol microphysical (MATRIX) or a mass-based aerosol (OMA) module. Simulations of the CMIP6 historical period are analyzed as well as four Shared Socioeconomic Pathway (SSP) future scenarios for 2015–2100: SSP1-2.6, SSP2-4.5, SSP3-7.0, and SSP5-8.5. The main conclusion of this study is that aerosol forcing in the GISS model has reached its turning point, switching from globally increasing to a decreasing trend in the first decade of the 21st century. This result is robust, independent of which aerosol module or SSP scenario is used. Non-linear aerosol-cloud interactions dominate as a forcing agent over aerosol-radiation interactions. Aerosols' ability to counterbalance GHG forcing on the global scale is today at a level comparable to that at the beginning of the last century. In the 1980s, the decade of largest global aerosol loads, aerosols balanced up to 80% of GHG forcing. As a consequence, global warming of the last decades, which is primarily driven by greenhouse gases, has been augmented by the effect of decreasing aerosol cooling in our model. By the end of this century, following the SSP scenarios, aerosols will only counterbalance 0%–20% of GHG forcing, depending on model and on scenario.

**Introduction.** Assessing regional and global trends in aerosol forcing under past and future climate projections is crucial to improve our understanding of past and future climate change (Arias et al., **2021**; Hansen et al., **1998**). The Coupled Model Intercomparison Project Phase 6 (CMIP6) (Eyring et al., **2016**) provides forcing and emission estimates for the historical period, 1750–2014 (Hoesly et al., **2018**), and sets of future emission scenarios (Feng et al., **2020**; Gidden et al., **2019**; Meinshausen et al., **2020**; O'Neill et al., **2016**) that span from 2015 until 2300, covering multiple pathways of possible future socio-economic developments.

Calculating and understanding aerosol trends is complicated, as their time evolution depends on numerous natural and anthropogenic sources emitting various types of gaseous aerosol precursor and aerosol species that change in time and space. Translating emissions into concentrations and eventually forcings that act on the climate system in various ways such as aerosol direct (RFari) and aerosol effects on clouds (RFaci) is a complex task, which adds uncertainty in the estimates of aerosol impacts on climate.

Trends in aerosol emissions have been driven by industrialization and modernization of technology. Industrialization, which relies on the use of fossil fuel energy, has had a significant impact on the aerosol load, resulting in severe pollution episodes like the 1952 smog event in London (Bell et al., **2004**). Starting in the 1970s in the USA and in Europe, mitigation measures were implemented (Turnock, **2016**), and political change in the 1990s in Eastern Europe lead to the breakdown of many highly polluting industries, resulting in significant improvements in terms of aerosol loads and air quality. Agriculture is an emission sector that is strongly linked to population and is one of the few sectors that experiences persistent growth. Modernizations of technologies have led to large changes over the past decades in industrialized countries and more recently in Asia (Ramachandran et al., **2020**). Trends in aerosol composition and forcing have been studied in the past by modeling (Bauer et al., **2020**; Mortier et al., **2020**; Yang et al., **2018**) and satellite studies (Subba et al., **2020**; Zhao et al., **2017**).

Geophysical Research Letters, vol. 49, issue no. 14, e2022GL098632, doi:10.1029/2022GL098632

# Observation-based variability in the global ocean carbon sink from 1959-2020

Bennington, V., **L. Gloege**[1], and G.A. McKinley, 2022

NASA Goddard Institute for Space Studies, New York, NY, USA[1]

**Abstract.** Over the CMIP6 historical period (1850–2014), aerosols provided the largest negative forcing compared to all other climate forcings via their ability to absorb or scatter solar radiation and alter clouds. Aerosols played an important role in counterbalancing warming by greenhouse gases (GHGs). Here we study aerosol forcing trends in the CMIP6 simulations of the NASA Goddard Institute for Space Studies (GISS) ocean-atmosphere ModelE version 2.1 (GISS-E2.1-G) using a fully coupled atmospheric composition configuration, including interactive gas-phase chemistry, and either an aerosol microphysical (MATRIX) or a mass-based aerosol (OMA) module. Simulations of the CMIP6 historical period are analyzed as well as four Shared Socioeconomic Pathway (SSP) future scenarios for 2015–2100: SSP1-2.6, SSP2-4.5, SSP3-7.0, and SSP5-8.5. The main conclusion of this study is that aerosol forcing in the GISS model has reached its turning point, switching from globally increasing to a decreasing trend in the first decade of the 21st century. This result is robust, independent of which aerosol module or SSP scenario is used. Non-linear aerosol-cloud interactions dominate as a forcing agent over aerosol-radiation interactions. Aerosols' ability to counterbalance GHG forcing on the global scale is today at a level comparable to that at the beginning of the last century. In the 1980s, the decade of largest global aerosol loads, aerosols balanced up to 80% of GHG forcing. As a consequence, global warming of the last decades, which is primarily driven by greenhouse gases, has been augmented by the effect of decreasing aerosol cooling in our model. By the end of this century, following the SSP scenarios, aerosols will only counterbalance 0%–20% of GHG forcing, depending on model and on scenario.

**Introduction.** Assessing regional and global trends in aerosol forcing under past and future climate projections is crucial to improve our understanding of past and future climate change (Arias et al., **2021**; Hansen et al., **1998**). The Coupled Model Intercomparison Project Phase 6 (CMIP6) (Eyring et al., **2016**) provides forcing and emission estimates for the historical period, 1750–2014 (Hoesly et al., **2018**), and sets of future emission scenarios (Feng et al., **2020**; Gidden et al., **2019**; Meinshausen et al., **2020**; O'Neill et al., **2016**) that span from 2015 until 2300, covering multiple pathways of possible future socio-economic developments.

Calculating and understanding aerosol trends is complicated, as their time evolution depends on numerous natural and anthropogenic sources emitting various types of gaseous aerosol precursor and aerosol species that change in time and space. Translating emissions into concentrations and eventually forcings that act on the climate system in various ways such as aerosol direct (RFari) and aerosol effects on clouds (RFaci) is a complex task, which adds uncertainty in the estimates of aerosol impacts on climate.

Trends in aerosol emissions have been driven by industrialization and modernization of technology. Industrialization, which relies on the use of fossil fuel energy, has had a significant impact on the aerosol load, resulting in severe pollution episodes like the 1952 smog event in London (Bell et al., **2004**). Starting in the 1970s in the USA and in Europe, mitigation measures were implemented (Turnock, **2016**), and political change in the 1990s in Eastern Europe lead to the breakdown of many highly polluting industries, resulting in significant improvements in terms of aerosol loads and air quality. Agriculture is an emission sector that is strongly linked to population and is one of the few sectors that experiences persistent growth. Modernizations of technologies have led to large changes over the past decades in industrialized countries and more recently in Asia (Ramachandran et al., **2020**). Trends in aerosol composition and forcing have been studied in the past by modeling (Bauer et al., **2020**; Mortier et al., **2020**; Yang et al., **2018**) and satellite studies (Subba et al., **2020**; Zhao et al., **2017**).

Global Change Biology, vol. 28, issue no. 11, pp. 3636-3650, doi:10.1111/gcb.16132

# Global benefits of non-continuous flooding to reduce greenhouse gases and irrigation water use without rice yield penalty

Bo, Y., **J. Jägermeyr**[1,2,3], Z. Yin, Y. Jiang, J. Xu, H. Liang, and F. Zhou, 2022

NASA Goddard Institute for Space Studies, New York, NY, USA[1]
Center for Climate Systems Research, Columbia University, New York, NY, USA[2]
Potsdam Institute for Climate Impact Research (PIK), Potsdam, Germany[3]

**Abstract.** Non-continuous flooding is an effective practice for reducing greenhouse gas (GHG) emissions and irrigation water use (IRR) in rice fields. However, advancing global implementation is hampered by the lack of comprehensive understanding of GHGs and IRR reduction benefits without compromising rice yield. Here, we present the largest observational data set for such effects as of yet. By using Random Forest regression models based on 636 field trials at 105 globally georeferenced sites, we identified the key drivers of effects of non-continuous flooding practices and mapped maximum GHGs or IRR reduction benefits under optimal non-continuous flooding strategies. The results show that variation in effects of non-continuous flooding practices are primarily explained by the UnFlooded days Ratio (UFR, that is the ratio of the number of days without standing water in the field to total days of the growing period). Non-continuous flooding practices could be feasible to be adopted in 76% of global rice harvested areas. This would reduce the global warming potential (GWP) of CH4 and N2O combined from rice production by 47% or the total GWP by 7% and alleviate IRR by 25%, while maintaining yield levels. The identified UFR targets far exceed currently observed levels particularly in South and Southeast Asia, suggesting large opportunities for climate mitigation and water use conservation, associated with the rigorous implementation of non-continuous flooding practices in global rice cultivation.

**Introduction.** Rice is one of the main staple food crops, sustaining more than half of the world's population (FAO; Zhao et al., 2017). However, current rice cultivation accounts for approximately 40% of global irrigation water use (IRR) (Lampayan et al., 2015), 8% of global anthropogenic methane (CH4) emissions (Saunois et al., 2020), and 10% of global cropland nitrous oxide (N2O) emissions (Wang et al., 2020). Non-continuous flooding strategies (such as alternative wetting and drying [AWD], intermittent irrigation and midseason drainage) has been proven to be effective to reduce IRR and CH4 emissions while ensuring rice production, compared with continuous flooding (CF) conditions (Belder et al., 2004; Linquist et al., 2015). Under such practices, one or more soil aerobic periods with unflooded soil surface (water level below zero) would be introduced through drainage or applying small amounts of water regularly (Bouman et al., 2007), showing potentials to reduce both CH4 emissions and IRR. Although effects of non-continuous flooding practices on greenhouse gas (GHG) emissions, IRR, and rice yield have been extensively observed at the field scale (Carrijo et al., 2017; Jiang et al., 2019), the global magnitude and spatial pattern of co-benefits of non-continuous flooding in terms of climate mitigation and food security remain poorly understood. This is a barrier for broad promotion and implementation of non-continuous flooding practices across the rice-growing regions globally.
The GHGs and IRR reduction benefits depends on the locations and local effects of non-continuous flooding practices. Non-continuous flooding is not necessarily suitable for all rice fields because of climate constraints or yield penalty in some areas (Liang et al., 2016; Linquist et al., 2015; Yang et al., 2017). Although some studies assessed climate suitability of non-continuous flooding at regional scales (Nelson et al., 2015; Prangbang et al., 2020), environmental and yield response to non-continuous flooding adoption were rarely considered.

Journal of Quantitative Spectroscopy and Radiative Transfer, vol. 288, 108273, doi:10.1016/j.jqsrt.2022.108273

# Line coupling and line mixing effects on calculated widths of symmetric-top molecules with the k-degeneracy: A theoretical study of $N_2$-, $O_2$-, and air-broadened lines of $CH_3I$

Boulet, C., and **Q. Ma**[1,2], 2022

NASA Goddard Institute for Space Studies, New York, NY, USA[1]
Department of Applied Physics and Applied Mathematics, Columbia University, New York, NY, USA[2]

**Abstract.** Calculations of the $N_2$-, $O_2$-, and air-broadened widths, together with their temperature dependence exponents have been made for transitions of $CH_3I$ in the $\nu_5$ and $\nu_6$ bands. The calculations are based on a semi-classical line shape formalism developed by the current authors through modifying and refining the Robert-Bonamy formalism. In recent years, we have applied this formalism for linear molecules, symmetric-top molecules with inversion symmetry, and asymmetric-top molecules. For symmetric-top molecules with the k degeneracy such as $CH_3I$, the formalism has a new feature. In this case, one should consider each of the $CH_3I$ transitions labeled by $k_{i\ or\ f} \neq 0$ as a doublet. Then, one needs to consider the effects of the line mixing process between these two components. Comparisons of our theoretical predictions with some data available demonstrate a very reasonable agreement. Finally, we propose new experiments at higher perturber pressures that would enable one to check the theoretically calculated relaxation matrices and to extend the analysis to the inter-doublet mixing effects.

**Introduction.** Knowledge of spectroscopic lineshape parameters becomes more and more important for accurate interpretation of high-resolution spectra of the Earth's atmosphere. Recently, among the numerous molecules of interest, methyl **iodide** ($CH_3I$) has received an increasing interest. Indeed it is the most abundant iodine-containing compound, playing a role in various processes (destruction of the ozone layer, nuclear safety, …; see more details and references in **[1]**). To prepare an accurate detection of atmospheric $CH_3I$, numerous studies have been recently devoted, both experimentally and theoretically, to line intensities and frequencies **[2,3]** of different vibrational bands (mostly the fundamental $\nu_6$ band located at the 11 μm transparency window) as well as on self- **[4,5]**, $N_2$- **[5]**, $O_2$- **[6]** and air- **[7]** broadened widths. A more complete review can be found elsewhere **[1]**.

Among the recent theoretical analyses on air-broadening of $CH_3X$ species (with $X$ = Br, Cl, F and I), we would like to mention a series of papers by Buldyreva et al. [**1**,**[8]**, **[9]**, **[10]**] based on the semi-classical Robert-Bonamy (RB) formalism **[11]**. The main features of the RB formalism are the non-perturbative treatment of the scattering **matrix S** through the use of the linked cluster theorem, and a convenient description of classical trajectories for large impact parameters as well as for the closest approach. In the method used by Buldyreva et al. **[8]**, exact trajectories are driven by the isotropic part of the potential and an adjustable atom-atom potential was introduced to mimic the influence of short range forces.

However, one of main weaknesses of the RB formalism is that it is based on the isolated line approximation. As outlined by Cherkasov **[12]**, the operator $S_2$ is not diagonal in the linespace. As Buldyreva et al. applied the RB formalism **[1,[8], [9], [10]]**, they also assumed that the operator $S_2$ is diagonal, neglecting therefore any coupling between the transitions.

An alternative approach exists. In 2007, we found that there is a subtle derivation error in developing the RB formalism **[13]**. We have proposed a modified version of the RB formalism based on a correct way to apply the cumulant expansion. The latter is equivalent to the linked cluster theorem, but its applications are more general. At that time, the essential difference between the modified RB formalism (MRB) and the RB formalism is the location of the bath average within or outside the definition of the $S_2$ operator.

Atmospheric Chemistry and Physics, vol. 22, issue no. 5, pp. 3507-3524, doi:10.5194/acp-22-3507-2022

# Changes of anthropogenic precursor emissions drive shifts of ozone seasonal cycle throughout northern midlatitude troposphere

Bowman, H., S. Turnock, **S.E. Bauer**[1,2], **K. Tsigaridis**[1,2], M. Deushi, N. Oshima, F.M. O'Connor, L. Horowitz, T. Wu, J. Zhang, and D.D. Parrish, 2022

NASA Goddard Institute for Space Studies, New York, NY, USA[1]
Center for Climate Systems Research, Columbia University, New York, NY, USA[2]

**Abstract.** Simulations by six Coupled Model Intercomparison Project Phase 6 (CMIP6) Earth system models indicate that the seasonal cycle of baseline tropospheric ozone at northern midlatitudes has been shifting since the mid-20th century. Beginning in ∼ 1940, the magnitude of the seasonal cycle increased by ∼10 ppb (measured from seasonal minimum to maximum), and the seasonal maximum shifted to later in the year by about 3 weeks. This shift maximized in the mid-1980s, followed by a reversal – the seasonal cycle decreased in amplitude and the maximum shifted back to earlier in the year. Similar changes are seen in measurements collected from the 1970s to the present. The timing of the seasonal cycle changes is generally concurrent with the rise and fall of anthropogenic emissions that followed industrialization and the subsequent implementation of air quality emission controls. A quantitative comparison of the temporal changes in the ozone seasonal cycle at sites in both Europe and North America with the temporal changes in ozone precursor emissions across the northern midlatitudes found a high degree of similarity between these two temporal patterns. We hypothesize that changing precursor emissions are responsible for the shift in the ozone seasonal cycle; this is supported by the absence of such seasonal shifts in southern midlatitudes where anthropogenic emissions are much smaller. We also suggest a mechanism by which changing emissions drive the changing seasonal cycle: increasing emissions of NOx allow summertime photochemical production of ozone to become more important than ozone transported from the stratosphere and increasing volatile organic compounds (VOCs) lead to progressively greater photochemical ozone production in the summer months, thereby increasing the amplitude of the seasonal ozone cycle. Decreasing emissions of both precursor classes then reverse these changes. The quantitative parameter values that characterize the seasonal shifts provide useful benchmarks for evaluating model simulations, both against observations and between models.

**Introduction.** Tropospheric ozone is a harmful air pollutant and greenhouse gas. It is a secondary pollutant, formed as a photochemical product of oxidation reactions involving volatile organic compounds (VOCs), carbon monoxide (CO) and methane ($CH_4$) in the presence of oxides of nitrogen ($NO_x$). Entrainment of stratospheric ozone also contributes to tropospheric ozone concentrations. Ozone is lost from the troposphere to surface deposition and additional photochemical reactions. The processes driving ozone formation and destruction are complex, which adds difficulty to the task of understanding the impacts of tropospheric ozone on human and ecosystem health and climate change. Because ozone is not directly emitted, areas of ozone formation and enhanced concentrations are often geographically separated from emission sources. The lifetime of ozone in the troposphere is long enough – approximately 22 d averaged globally (Young et al., 2013) – that it is transported over hemispheric scales. Its lifetime is even longer above the planetary boundary layer (PBL) due to slower losses in the free troposphere (FT) and continuing formation from transported precursors (Fowler et al., 2008). At northern midlatitudes (defined here as between 30 and 60° N), prevailing westerly winds and the long lifetime of ozone result in a high degree of zonal similarity in baseline ozone concentrations (Chan et al., 2010; Parrish et al., 2014), with similar temporal changes in baseline ozone observed at multiple sites throughout that zone (Cooper et al., 2014; Parrish et al., 2020). In this work, we use the term “baseline” to denote air that has not been influenced by direct, recent continental influences – see discussion in chap. 1 of *Hemispheric Transport of Air Pollution 2010* (HTAP, 2010). Another consequence of rapid transport of ozone and its precursors is that emissions from any location in the northern midlatitude region can influence ozone concentrations throughout the zone.

European Journal of Environment and Public Health, vol. 6, issue no. 2, em0111, doi:10.21601/ejeph/12046

# Sea level rise and city-level climate action

Brennan, M.M., S. Whitmee, **C.V. Braneon**[1,2], N. Meinsma, and R. Green, 2022

NASA Goddard Institute for Space Studies, New York, NY, USA[1]
SciSpace, LLC., New York, NY, USA[2]

**Abstract.** Climate change is the greatest threat to global health in the 21st century. Rising sea levels are one particularly concerning manifestation of this and many of the world's largest cities are vulnerable to sea level rise (SLR). Thus, urban climate adaptation and mitigation policies are increasingly important to protect population health.

**Introduction.** Climate change is the greatest threat to global health in the 21st century. A warming world with rising sea levels and increased frequency of extreme weather events has numerous direct health effects including morbidity and mortality associated with extreme weather events, heat, and air pollution, but also many indirect effects such as increased spread of infectious disease, food and water insecurity, mental health impacts, and increased conflict. Currently, the impacts of climate change are intensifying and are felt on every continent, albeit disproportionately affecting those who have contributed least to the climate crisis (Watts et al., 2020). The landmark Paris Agreement agreed to hold temperatures to "well below 2°C above pre-industrial levels", and if it's possible to below 1.5°C. Unfortunately, anthropogenic activities are now estimated to have caused 1.07°C of heating and without significant reduction in greenhouse gas (GHG) emissions, it is thought likely that global warming will exceed 1.5°C between 2021 and 2040, and 2°C between 2041-2060 (IPCC, 2021). Exceeding the limits set by the Paris Agreement threatens to undermine the past 50 years of public health gains and will further exacerbate global health inequalities (Watts et al., 2020). On the contrary, adhering to the goals of the Paris Agreement with well-designed mitigation policies could generate substantial public health gains in the long term by reducing the severity of long-term climate impacts, but also in the short-term through improved air quality, better diets and increased population level physical activity (Hamilton et al., 2021). As the world is already experiencing the effects of climate change, adaptation measures are also necessary to protect population health. Cities are important settings in relation to climate change and population health for a number of reasons: Firstly, they are highly exposed to the effects of climate change due to their high concentration of industry, infrastructure and growing urban populations (UN-Habitat, 2011). Of note, the world's population is projected to grow to approximately 9.7 billion by 2050 then 10.9 billion by 2100 and more than 66% of the population are projected to reside in urban settings by 2050 (UN DESA, 2018, 2019). Secondly, cities face unique challenges such as the urban heat island effect as well as an increased risk of flooding due to concentrations of built materials and are, consequently, vulnerable to a variety of natural disasters (Masson et al., 2020; UNISDR and CRED, 2015). Lastly, global cities are estimated to be responsible for up to 70% of anthropogenic GHG emissions, although estimates vary widely depending on how emissions are counted. Regardless, there is consensus that urban areas are a significant contributor to climate change (UN-Habitat, 2011). Furthermore, it is estimated that measures taken by urban authorities could result in reductions in carbon dioxide (CO2) emissions of 50- 75% indicating that local governments are key actors in the climate crisis (Hakelberg, 2014). As cities are both vulnerable to, and drivers of climate change, it is well recognised that cities need to take a leading role in climate mitigation and adaptation. The prospects of averting climate breakdown and protecting global health seem limited without comprehensive decarbonisation and effective adaptation of urban areas (Solecki et al., 2018).

One of the most concerning manifestations o s of climate change is sea level rise (SLR). Flooding is already one of the most frequent natural disasters and carries multiple health and economic consequences (Alderman et al., 2012). Between 1995 and 2015, flooding accounted for 47% of all weather-related disasters, affecting 2.3 billion people worldwide (UNISDR and CRED, 2015). As sea levels rise, urban areas along the coasts will be threatened with increased flooding and potentially inundation.

Atmospheric Chemistry and Physics, vol. 22, issue no. vol. 18, pp. 12331-12352, doi:10.5194/acp-22-12331-2022

# The ozone-climate penalty over South America and Africa by 2100

Brown, F., G.A. Folberth, S. Sitch, **S.E. Bauer**[1,2], M. Bauters, P. Boeckx, A.W. Cheesman, M. Deushi, I. Dos Santos Vieira, C. Galy-Lacaux, J. Haywood, J. Keeble, L.M. Mercado, F.M. O'Connor, N. Oshima, **K. Tsigaridis**[1,2], and H. Verbeeck, 2022

NASA Goddard Institute for Space Studies, New York, NY, USA[1]
Center for Climate Systems Research, Columbia University, New York, NY, USA[2]

**Abstract.** Climate change has the potential to increase surface ozone (O3) concentrations, known as the "ozone–climate penalty", through changes to atmospheric chemistry, transport and dry deposition. In the tropics, the response of surface O3 to changing climate is relatively understudied but has important consequences for air pollution and human and ecosystem health. In this study, we evaluate the change in surface O3 due to climate change over South America and Africa using three state-of-the-art Earth system models that follow the Shared Socioeconomic Pathway 3-7.0 emission scenario from CMIP6. In order to quantify changes due to climate change alone, we evaluate the difference between simulations including climate change and simulations with a fixed present-day climate. We find that by 2100, models predict an ozone–climate penalty in areas where O3 is already predicted to be high due to the impacts of precursor emissions, namely urban and biomass burning areas, although on average, models predict a decrease in surface O3 due to climate change. We identify a small but robust positive trend in annual mean surface O3 over polluted areas. Additionally, during biomass burning seasons, seasonal mean O3 concentrations increase by 15 ppb (model range 12 to 18 ppb) in areas with substantial biomass burning such as the arc of deforestation in the Amazon. The ozone–climate penalty in polluted areas is shown to be driven by an increased rate of O3 chemical production, which is strongly influenced by NOx concentrations and is therefore specific to the emission pathway chosen. Multiple linear regression finds the change in NOx concentration to be a strong predictor of the change in O3 production, whereas increased isoprene emission rate is positively correlated with increased O3 destruction, suggesting NOx-limited conditions over the majority of tropical Africa and South America. However, models disagree on the role of climate change in remote, low-NOx regions, partly because of significant differences in NOx concentrations produced by each model. We also find that the magnitude and location of the ozone–climate penalty in the Congo Basin has greater inter-model variation than that in the Amazon, so further model development and validation are needed to constrain the response in central Africa. We conclude that if the climate were to change according to the emission scenario used here, models predict that forested areas in biomass burning locations and urban populations will be at increasing risk of high O3 exposure, irrespective of any direct impacts on O3 via the prescribed emission scenario.

**Introduction.** Climate change threatens to bring new pressures to the tropical forests, grasslands and agricultural lands of Africa and South America. As a result of shifts in emissions, atmospheric chemistry and meteorology, as well as changes in vegetation behaviour such as transpiration rate, surface $O_3$ concentrations are likely to change (e.g., Turnock et al., 2019; Griffiths et al., 2021; Zanis et al., 2022), which may impair or benefit human and vegetation health (Agathokleous et al., 2019; Emberson, 2020) depending on the direction of change. $O_3$ is a highly oxidising compound, formed in the atmosphere through reaction of volatile organic compounds (VOCs) or carbon monoxide (CO) with hydroxyl radicals (OH) and nitrate radicals ($NO_3$) in the presence of nitrogen oxides ($NO_x$). However, it can also be removed from the atmosphere through reactions with many of the same chemical species ($NO_x$, VOC, OH) depending on their relative concentrations. In addition to chemical pathways, $O_3$ can be removed from the lower atmosphere by dry deposition, which includes stomatal uptake by plants (Silva and Heald, 2018). Stomatal uptake of $O_3$ and subsequent ozone plant damage can lead to reduced carbon drawdown from the atmosphere (Sitch et al., 2007; Yue and Unger, 2018; Franz and Zaehle, 2021) and changes to biosphere–climate interactions (Sadiq et al., 2017). Sitch et al. (2007) showed that the tropics may be especially sensitive to high $O_3$ concentrations and therefore susceptible to large productivity losses if surface $O_3$ were to increase.

Climate of the Past, vol. 18, issue no. 7, pp. 1625-1654, doi:10.5194/cp-18-1625-2022

# Investigating oxygen and carbon isotopic relationships in speleothem records over the last millennium using multiple isotope-enabled climate models.

Bühler, J.C., J.M. Axelsson, F.A. Lechleitner, J. Fohlmeister, **A.N. LeGrande**[1,2], M. Midhun, J. Sjolte, M. Werner, K. Yoshimura, and K. Rehfeld, 2022

NASA Goddard Institute for Space Studies, New York, NY, USA[1]
Center for Climate Systems Research, Columbia University, New York, NY, USA[2]

**Abstract**. The incorporation of water isotopologues into the hydrology of general circulation models (GCMs) facilitates the comparison between modeled and measured proxy data in paleoclimate archives. However, the variability and drivers of measured and modeled water isotopologues, as well as the diversity of their representation in different models, are not well constrained. Improving our understanding of this variability in past and present climates will help to better constrain future climate change projections and decrease their range of uncertainty. Speleothems are a precisely datable terrestrial paleoclimate archives and provide well-preserved (semi-)continuous multivariate isotope time series in the lower latitudes and mid-latitudes and are therefore well suited to assess climate and isotope variability on decadal and longer timescales. However, the relationships of speleothem oxygen and carbon isotopes to climate variables are influenced by site-specific parameters, and their comparison to GCMs is not always straightforward.

Here we compare speleothem oxygen and carbon isotopic signatures from the Speleothem Isotopes Synthesis and Analysis database version 2 (SISALv2) to the output of five different water-isotope-enabled GCMs (ECHAM5-wiso, GISS-E2-R, iCESM, iHadCM3, and isoGSM) over the last millennium (850-1850 CE). We systematically evaluate differences and commonalities between the standardized model simulation outputs. The goal is to distinguish climatic drivers of variability for modeled isotopes and compare them to those of measured isotopes.

We find strong regional differences in the oxygen isotope signatures between models that can partly be attributed to differences in modeled surface temperature. At low latitudes, precipitation amount is the dominant driver for stable water isotope variability; however, at cave locations the agreement between modeled temperature variability is higher than for precipitation variability. While modeled isotopic signatures at cave locations exhibited extreme events coinciding with changes in volcanic and solar forcing, such fingerprints are not apparent in the speleothem isotopes. This may be attributed to the lower temporal resolution of speleothem records compared to the events that are to be detected. Using spectral analysis, we can show that all models underestimate decadal and longer variability compared to speleothems (albeit to varying extents).

We found that no model excels in all analyzed comparisons, although some perform better than the others in either mean or variability. Therefore, we advise a multi-model approach whenever comparing proxy data to modeled data. Considering karst and cave internal processes, e.g., through isotope-enabled karst models, may alter the variability in speleothem isotopes and play an important role in determining the most appropriate model. By exploring new ways of analyzing the relationship between the oxygen and carbon isotopes, their variability, and co-variability across timescales, we provide methods that may serve as a baseline for future studies with different models using, e.g., different isotopes, different climate archives, or different time periods.

**Introduction.** Under the current anthropogenic warming trend (Shukla et al., 2019), the interest in understanding its impacts on the mean temperature and precipitation and changes in their variability increases. Evaluating the representation of the mean state and the variability of past climate as simulated by climate models is crucial for reliable future projections (Schmidt et al., 2012).

Nature Food, vol. 3, issue no. 6, pp. 437-444, doi:10.1038/s43016-022-00521-y

# Processing tomato production is expected to decrease due to the projected increase in temperature

Cammarano, D., S. Jamshidi, G. Hoogenboom, **A.C. Ruane**[1], D. Niyogi, and D. Ronga, 2022

NASA Goddard Institute for Space Studies, New York, NY, USA[1]

**Abstract.** The global production of processing tomatoes is concentrated in a small number of regions where climate change could have a notable impact on the future supply. Process-based tomato models project that the production in the main producing countries (the United States, Italy and China, representing 65% of global production) will decrease 6% by 2050 compared with the baseline period of 1980–2009. The predicted reduction in processing tomato production is due to a projected increase in air temperature. Under an ensemble of projected climate scenarios, California and Italy might not be able to sustain current levels of processing tomato production due to water resource constraints. Cooler producing regions, such as China and the northern parts of California, stand to improve their competitive advantage. The projected environmental changes indicate that the main growing regions of processing tomatoes might change in the coming decades.

**Introduction.** Tomato is one of the world's most important vegetables in terms of cultivation area, production, commercial use and consumption1. Tomato is grown in many countries due to its adaptability to a wide range of soil and weather conditions and has also been recognized for its positive health benefits being rich in antioxidants. There are two types of cultivated tomato: one type for fresh consumption (for example, salad tomatoes), usually grown under controlled environments; and one type used for industrial transformation known as processing tomatoes (for example, canned tomatoes), which are usually grown under field conditions2. Processing tomatoes are important because they are used for tomato paste, tomato sauce, ketchup and other tomato-derived products. About 40 Mt are processed annually, making tomato the world leader for vegetable processing by weight. The main production areas are located in temperate zones around latitudes 40° N and S. Worldwide processing tomato production is concentrated in 11 major 'tomato baskets' that produce 85% of global processing tomato. Three countries—the United States (with the majority of production in California), Italy (in Foggia and Emilia-Romagna) and China (mainly in Gansu, Inner Mongolia and Xingjian)—account for 65% of global production1 (Supplementary Fig. 1).

Most of the climate change impact studies on agricultural crops have concentrated on wheat, maize, rice and potato3–7, while fruits and vegetables have not received sufficient attention. The four main agricultural crops address food security, but not nutrition security or essential vitamins and micronutrients, fibre and phytochemicals that individually or in combination may benefit human health8. The World Health Organization Global Strategy on Diet, Physical Activity and Health9 recommends that per capita fruit and vegetable consumption (excluding tubers) should exceed 400 g d−1 (ref. 9).

Most of the published research on the impacts of climate change on processing tomato has been done at regional or local level and has included agronomic and/or technological adaptations10,11. However, each study adopted different scenarios, global climate models (GCMs) and different crop modelling approaches12, making it challenging to compare results. A study that assessed the impact of cli-mate on processing tomato supply chain for the United States found that adaptation will offset the negative impact of climate change on processing tomato yield11. However, other studies on the impact of climate change on water and nutrient use efficiency of tomato in southeastern Italy reported a net negative impact on processed tomato yield2,10,13,14.

Frontiers in Remote Sensing., vol. 2, 788525, doi:10.3389/frsen.2021.788525

# Unique observational constraints on the seasonal and longitudinal variability of the Earth's planetary albedo and cloud distribution inferred from EPIC measurements

**Carlson**, **B.E.**[1], **A.A. Lacis**[1], **G.L. Russell**[1], A. Marshak[2], and W. Su[3], 2022

NASA Goddard Institute for Space Studies, New York, NY, USA[1]
NASA Goddard Space Flight Center, Greenbelt, MD, USA[2]
NASA Langley Research Center, Hampton, VA, USA[3]

**Abstract**. Thorough comparison to observations is key to developing a credible climate model forecasting capability. Deep Space Climate Observatory (DSCOVR) measurements of Earth's reflected solar and emitted thermal radiation provide a unique observational perspective that permits a more reliable model/data comparison than is possible with the otherwise available satellite data. The uniqueness is in the DSCOVR satellite's viewing geometry, which enables continuous viewing of the Earth's sunlit hemisphere from its Lissajous orbit around the Lagrangian L1 point. The key instrument is the Earth Polychromatic Imaging Camera (EPIC), which views the Earth's sunlit hemisphere with 1024-by-1024-pixel imagery in 10 narrow spectral bands from 317 nm to 780 nm, acquiring up to 22 high spatial resolution images per day. The additional feature is that the frequency of EPIC image acquisition is nearly identical to that of the climate GCM data generation scheme where climate data for the entire globe are 'instantaneously' calculated at one-hour radiation time-step intervals. Implementation of the SHS (Sunlit Hemisphere Sampling) EPIC-view geometry for the in-line GCM output data sampling establishes a precise self-consistency in the space-time data sampling between EPIC observational and GCM output data generation and sampling. The remaining problem is that the GCM generated data are radiative fluxes, while the EPIC measurements are backscatter-dependent radiances. Radiance to flux conversion is a complex problem with no simple way to convert GCM radiative fluxes into spectral radiances. The more expedient approach is to convert the EPIC spectral radiances into broadband radiances by MODIS/CERES-based regression relationships and then into solar radiative fluxes using the CERES angular distribution models. Averaging over the sunlit hemisphere fully suppresses the meteorological weather noise, but preserves the intra-seasonal and larger spatial scale variability. Longitudinal slicing by the Earth's rotation then permits a self-consistent model/data comparison of the longitudinal model/data differences in the variability of the reflected solar radiation. Ancillary EPIC Composite data provide additional cloud property information for climate model diagnostics. Comparison of EPIC-derived seasonal and longitudinal variability of the Earth's planetary albedo with the GISS ModelE2 results shows systematic overestimate of cloud reflectivity over the Pacific Ocean with corresponding underestimates over continental land areas.

**Introduction**. Model/data comparisons are essential for improved understanding of the Earth's climate system. But, as illustrated in **Figure 1**, this seemingly straightforward task is not simple. Climate GCMs and the real world are quasi-chaotic in behavior. So, there is no reason to expect agreement except for averages taken over sufficiently large space and time scales. Moreover, most climate system variables exhibit strong diurnal variability (e.g., **Eastman and Warren, 2014**). Whereas GCM output data are computed uniformly over the globe at uniform time-steps, and uniformly averaged into monthly-mean latitude-longitude tables such as the planetary albedo and total cloud cover in **Figure 1** (Left panels), the observational data typically use sequential space-time sampling from a sun-synchronous satellite track, such as the CERES planetary albedo data (Top Right), with considerable uncertainty as to how the diurnal cycle might have been averaged or referenced. The European Centre for Medium-Range Weather Forecasts Reanalysis Interim (ECMWFs ERAI) total cloud cover, which is a global re-analysis product of observations acquired over the past 3.5 decades. These data comparisons show qualitative similarity, but with substantial small-scale differences. Even for monthly-mean averages, considerable meteorological weather noise remains. By averaging data over the entire globe, the weather noise can be minimized, as in **Figure 1** Bottom.

Geophysical Research Letters, vol. 49, issue no. 22, e2022GL099777, doi:10.1029/2022GL099777




# Southern Ocean solar reflection biases in CMIP6 models linked to cloud phase and vertical structure representations

**Cesana**, **G.V.**[1,2], T. Khadir, H. Chepfer, and M. Chiriaco, 2022

NASA Goddard Institute for Space Studies, New York, NY, USA[1]
Center for Climate Systems Research, Columbia University, New York, NY, USA[2]

**Abstract.** Over the Southern Ocean (SO, 40°S–70°S), climate models have consistently underestimated solar reflection. Here we evaluate the relationship between cloud profiles, cloud phase and radiation over the SO in Coupled Model Intercomparison Project Phase 6 (CMIP6) models against Clouds and the Earth's Radiant Energy System and Cloud-Aerosol Lidar and Infrared Pathfinder Satellite Observations. We find that the lack of solar reflection is slightly improved in CMIP6 models compared to CMIP5's, attributable to a better representation of cloud fraction and phase. We show that clouds have a different vertical structure and radiative effect south and north of where the 0°C isotherm meets the surface (~55°S). Although the models capture the greater vertical extent of clouds south of 55°S, they fail to reproduce the observed increase in solar reflection, which we pinpoint to cloud phase biases. Increasing CMIP6 supercooled liquid cloud opacity should help reduce their persistent shortwave biases.

**Introduction.** Earth's climate sensitivity has increased in the most recent Coupled Model Intercomparison Project (CMIP) models, largely attributed to the response of clouds to climate change, referred to as cloud feedback, in the extratropics (Zelinka et al., **2020**). In particular, over the Southern Ocean (SO; defined as being between 40° and 70°S), the negative shortwave (SW) cloud feedback southward of about 55°S, has weakened compared to the previous CMIP exercise, while the positive SW cloud feedback northward of 55°S has strengthened, making the overall feedback more positive in models (Zelinka et al., **2020**). Around this latitude, the boundary layer (BL) typically transitions from positive temperatures on the northern side (between 40° and 55°S) to negative temperatures on the southern side (between 55° and 70°S), whereby climate model radiation schemes are the most sensitive to cloud phase transitions with substantial consequences for cloud feedbacks (Bodas-Salcedo et al., **2019**; Frey & Kay, **2018**; Gettelman et al., **2019**; Tan et al., **2016**).

For example, increasing the amount of supercooled liquid clouds in a model (Kay et al., **2016**), which are typically more opaque than their frozen counterparts (Cesana & Storelvmo, **2017**; Tsushima et al., **2006**), can help fix the long-standing lack of solar radiation reflection over the SO (Trenberth & Fasullo, **2010**). To address this problem and more generally the lack of supercooled liquid clouds reported in many Earth System Models (ESMs) (Cesana et al., **2012**, **2015**; Choi et al., **2010**; Komurcu et al., **2014**; McCoy et al., **2015**), some modeling centers have increased the relative part of liquid clouds in their CMIP6 models (Bodas-Salcedo et al., **2019**; Gettelman et al., **2019**; Kelley et al., **2020**; Madeleine et al., **2020**). It is therefore useful to determine whether ESMs properly simulate cloud phase transitions in the present-day climate—the focus of this analysis—besides reproducing the response of cloud properties to climate change.

Here we leverage the recent submission of simulated cloud phase profiles using a lidar simulator to CMIP6 to analyze and evaluate the relationship between cloud phase and radiation over the SO. The use of a lidar simulator (Cesana & Chepfer, **2013**), which mimics what a satellite-borne lidar would observe over an ESM atmosphere, offers the possibility to collectively assess CMIP6 models in a consistent manner against observations. We first evaluate how CMIP cloud fraction profiles compare with Cloud-Aerosol Lidar and Infrared Pathfinder Satellite Observations (CALIPSO) observations on a global scale. We then study the temperature dependence of the cloud phase in ESMs over the SO. And finally, we analyze how biases in liquid cloud properties may affect top-of-the-atmosphere (TOA) SW fluxes over the SO.

Journal of Climate, vol. 35, issue no. 8, pp. 2407-2421, doi:10.1175/JCLI-D-21-0407.1

# The future intensification of North Atlantic winter storms: The key role of dynamic ocean coupling

Chemke, R., L. Zanna, **C. Orbe**[1], L.T. Sentman, and L.M. Polvani, 2022

NASA Goddard Institute for Space Studies, New York, NY, USA[1]

**Abstract.** Climate models project an intensification of the wintertime North Atlantic Ocean storm track, over its downstream region, by the end of this century. Previous studies have suggested that ocean–atmosphere coupling plays a key role in this intensification, but the precise role of the different components of the coupling has not been explored and quantified. In this paper, using a hierarchy of ocean coupling experiments, we isolate and quantify the respective roles of thermodynamic (changes in surface heat fluxes) and dynamic (changes in ocean heat flux convergence) ocean coupling in the projected intensification of North Atlantic transient eddy kinetic energy (TEKE). We show that dynamic coupling accounts for nearly all of the future TEKE strengthening as it overcomes the much smaller effect of surface heat flux changes to weaken the TEKE. We further show that by reducing the Arctic amplification in the North Atlantic, ocean heat flux convergence increases the meridional temperature gradient aloft, causing a larger eddy growth rate and resulting in the strengthening of North Atlantic TEKE. Our results stress the importance of better monitoring and investigating the changes in ocean heat transport, for improving climate change adaptation strategies.

**Significance Statement.** By the end of this century, the North Atlantic Ocean storm track is projected to intensify on its eastward flank. Such intensification will have large societal impacts, mostly over western Europe. Thus, it is critical to better understand the mechanism underlying the intensification of the storm track. Here we investigate the role of ocean coupling in the future intensification of the North Atlantic storm track and find that ocean heat transport processes are responsible for the strengthening of the storm track. Our results suggest that better monitoring the changes in ocean heat transport will hopefully improve climate change adaption strategies.

**Introduction.** Midlatitude storms play a central role in the weather and climate of the extratropics. These storms not only modulate the temperature, precipitation, and winds over synoptic time scales, they also account for most of the energy (i.e., heat, moisture, and momentum) transport from low to high latitudes, and across longitudes, over multidecadal time scales. It is thus important to investigate the mechanisms associated with the midlatitude storms' response to anthropogenic emissions.

In the Southern Hemisphere, climate models project a poleward shift of midlatitude summer storm tracks, and an intensification of winter storm tracks. In the Northern Hemisphere, summer storm tracks are projected to weaken by the end of this century, while winter storm tracks to strengthen, mostly over the downstream region of the North Atlantic storm track (**Chang et al. 2012**; **Zappa et al. 2013**; **Harvey et al. 2014**; **Lehmann et al. 2014**; **Harvey et al. 2020**). This eastward extension of the North Atlantic storm track has great societal impacts, especially over western Europe (**Zappa et al. 2013**). It should be noted that previous studies have found different magnitudes of the future North Atlantic storm-track intensification, in part due to the different metrics used to define the storm track. For example, while a robust strengthening of the storm track was found using Eulerian metrics such as eddy variances (mostly at upper levels; **Chang et al. 2012**; **Coumou et al. 2015**) and sea level pressure (**Harvey et al. 2014**, **2020**), a weaker strengthening of North Atlantic storm track was found using cyclone tracking algorithms (**Zappa et al. 2013**).

Environmental Research Letters, vol. 17, issue no. 8, 084015, doi:10.1088/1748-9326/ac80ce

# Responses of compound daytime and nighttime warm-dry and warm-humid events to individual anthropogenic forcings

**Chiang, F.**[1], **B.I. Cook**[1,2], **S.S. McDermid**[1,3], **K.D. Marvel**[1,4], **G.A. Schmidt**[1], **L.S. Nazarenko**[1,4], and **M.A. Kelley**[1,5], 2022

NASA Goddard Institute for Space Studies, New York, NY, USA[1]
Lamont-Doherty Earth Observatory, Columbia University, Palisades, NY, USA[2]
Department of Environmental Studies, New York University, New York, NY, USA[3]
Center for Climate Systems Research, Columbia University, New York, NY, USA[4]
SciSpace LLC, New York, NY, USA[5]

**Abstract.** Daytime heat is often associated with reduced soil moisture and cloud cover, while nighttime heat is connected to high humidity and increased cloud cover. Due to these differing mechanisms, compound daytime and nighttime heat events may respond differently to major anthropogenic forcings (greenhouse gases, anthropogenic aerosols, land-use and land-cover change). Here, we use GISS ModelE2.1-G historical single-forcing runs from 1955 to 2014 to examine how individual anthropogenic forcings affect compound heat events—specifically warm daytime and nighttime temperatures compounded with dry precipitation or high humidity conditions. We show that greenhouse gases alone amplify the natural frequency of warm-dry events by 1.5–5 times and warm-humid events by 2–9 times in tropical and extratropical latitudes. Conversely, aerosols and land-use/land-cover change reduce the frequency of these events, resulting in more modest increases and in some regions, declines, in the historical 'all-forcings' scenario. Individually, aerosol effects are stronger and more widespread compared to land-use, oftentimes reducing the natural frequency of these events by 60%–100%. The responses of these compound events are primarily driven by changes in daytime and nighttime temperatures through large-scale warming via greenhouse gases and cooling from aerosols and land-use/land-cover change. However, changes in warm-dry events are amplified in regions with concurrent precipitation declines (e.g. Central America, Mediterranean regions) and warm-humid events are amplified by global concurrent humidity increases. Additionally, we find differences between daytime and nighttime compound responses in the historical experiment that can be traced back to the individual forcings. In particular, aerosols produce a greater cooling effect on daytime relative to nighttime temperatures, which notably results in a historical reduction of Northern Hemisphere daytime warm-dry events relative to natural conditions. Our analysis provides a more comprehensive understanding of the significant impacts of different anthropogenic climate forcings on daytime and nighttime warm-dry and warm-humid events, informing future risk and impact assessments.

**Introduction.** Human activities have caused regional and large-scale changes in the Earth's climate through several anthropogenic forcings (IPCC **2021**). Rising greenhouse gas concentrations have driven significant global temperature increases, changes in precipitation patterns, and the increasing frequency and intensity of extreme events, including heatwaves, extreme rainfall, and droughts (Hegerl *et al* **1997**, Christidis *et al* **2005**, Seneviratne *et al* **2012**, Easterling *et al* **2016**, Marvel *et al* **2019**). Anthropogenic aerosols have cooled temperatures by increasing regional albedo levels (Charlson *et al* **1992**). Aerosols have also been hypothesized to influence large-scale circulation changes through asymmetrical surface temperature changes, resulting in late 20th century drying in Northern Hemisphere monsoonal regions (Bollasina *et al* **2011**, Polson *et al* **2014**). Moreover, land cover and land management practices have driven changes in regional climate conditions. Irrigation has moderated temperatures through latent heat flux changes (Cook *et al* **2015**, Thiery *et al* **2017**, Singh *et al* **2018**), while deforestation has been linked to contrasting local and non-local climate changes (Christidis *et al* **2013**, Findell *et al* **2017**, Winckler *et al* **2019**).

The Planetary Science Journal, vol. 3, issue no. 11, 261, doi:10.3847/PSJ/ac9dfe

# CAMEMBERT: A mini-Neptunes GCM intercomparison, protocol version 1.0.A CUISINES Model Intercomparison Project

Christie, D.A., E.K.H. Lee, H. Innes, P.A. Noti, B. Charnay, T.J. Fauchez[3,4,5,] N.J. Mayne, R. Deitrick, F. Ding, J.J. Greco, M. Hammond, I. Malsky, A. Mandell[3], E. Rauscher, M.T. Roman, D.E. Sergeev, **L. Sohl[1,2]**, M.E. Steinrueck, M. Turbet, E.T. Wolf[6,7], M. Zamyatina, and L. Carone, 2022

NASA Goddard Institute for Space Studies, New York, NY, USA[1]
Center for Climate Systems Research, Columbia University, New York, NY, USA[2]
NASA Goddard Space Flight Center, Greenbelt, MD, USA[3]
Integrated Space Science and Technology Institute, American University, Washington DC, USA[4]
Goddard Space Flight Center Sellers Exoplanet Environments Collaboration, Greenbelt, MD, USA[5]
Laboratory for Atmospheric and Space Physics, Department of Atmospheric and Oceanic Sciences, University of Colorado, Boulder, CO, USA[6]
NExSS Virtual Planetary Laboratory, Seattle, WA, USA[8]

**Abstract**. With an increased focus on the observing and modeling of mini-Neptunes, there comes a need to better understand the tools we use to model their atmospheres. In this Paper, we present the protocol for the Comparing Atmospheric Models of Extrasolar Mini-Neptunes Building and Envisioning Retrievals and Transits, CAMEMBERT, project, an intercomparison of general circulation models (GCMs) used by the exoplanetary science community to simulate the atmospheres of mini-Neptunes. We focus on two targets well studied both observationally and theoretically with planned JWST cycle 1 observations: the warm GJ 1214b and the cooler K2-18b. For each target, we consider a temperature-forced case, a clear sky dual-gray radiative transfer case, and a clear sky multiband radiative transfer case, covering a range of complexities and configurations where we know differences exist between GCMs in the literature. This Paper presents all the details necessary to participate in the intercomparison, with the intention of presenting the results in future papers. Currently, there are eight GCMs participating (ExoCAM, Exo-FMS, FMS PCM, Generic PCM, MITgcm, RM-GCM, THOR, and the Unified Model), and membership in the project remains open. Those interested in participating are invited to contact the authors.

**Introduction**. Super-Earths and mini-Neptunes represent a demarcation, albeit a nebulous one, between the giant planets with their thick atmospheres dominated by hydrogen and helium and the terrestrial planets with thinner secondary atmospheres (Lopez & Fortney **2014**). The planets that have retained their hydrogen-dominated atmospheres are believed to have undergone runaway accretion during their formation in order to accumulate a thick atmosphere (Pollack et al. **1996**; Lee et al. **2014**) but have also been able to retain some or all of that atmosphere in the presence of irradiative evaporation (Owen & Jackson **2012**).

Simulating these planets with general circulation models (GCMs) presents a unique set of challenges not necessarily seen in the Earth sciences community. The primitive equations that assume hydrostatic balance, a thin atmosphere, and a constant gravitational acceleration with height, may not yield accurate results for cases where the thickness of the modeled atmosphere becomes significant relative to the radius of the planet, limiting their applicability to planets with thick atmospheres (see Tokano **2013**; Tort et al. **2015**, and Mayne et al. **2019** for discussions related to Venus and Titan, Earth, and mini-Neptunes, respectively). It has also been argued that simulations of mini-Neptunes specifically may have extremely long convergence times, potentially of 50,000 Earth days of model time or more (Wang & Wordsworth **2020**), which raises questions about the accuracy of simulations of only a few 1000 days, as are common in the exoplanetary modeling community (e.g., Charnay et al. **2015**; Mayne et al. **2017**, **2019**). These issues motivate a better understanding of the tools we use to model these planets.

Nature Sustainability, vol. 5, issue no. 10, pp. 830-842, doi:10.1038/s41893-022-00940-6

# Quantifying Earth system interactions for sustainable food production via expert elicitationion

Chrysafi, A., V. Virkki, M. Jalava, V. Sandström, J. Piipponen, M. Porkka, J.S. Lade, K. La Mere, L. Wang-Erlandsson, L. Scherer, S.L. Andersen[2], E. Bennett, A.K. Brauman, S.G. Cooper, A. De Palma, P. Döll, S.A. Downing, C.T. DuBois, I. Fetzer, E.A. Fulton, D. Gerten, H. Jaafar, **J. Jägermeyr**[1,2,3], F. Jaramillo, M. Jung, H. Kahiluoto, L. Lassaletta, W.A. Mackay, D. Mason-D'Croz, M.M. Mekonnen, K.L. Nash, A.V. Pastor, N. Ramankutty, B. Ridoutt, S. Siebert, B.I. Simmons, A. Staal, Z. Sun, A. Tobian, A. Usubiaga-Liaño, R.J. Van der Ent, A. Van Soesbergen, P.H. Verburg, Y. Wada, S. Zipper, and M. Kummu, 2022

NASA Goddard Institute for Space Studies, New York, NY, USA[1]
Potsdam Institute for Climate Impact Research, Member of the Leibniz Association, Potsdam, Germany[2]
Center for Climate Systems Research, Columbia University, New York, NY, USA[3]

**Abstract.** Several safe boundaries of critical Earth system processes have already been crossed due to human perturbations; not accounting for their interactions may further narrow the safe operating space for humanity. Using expert knowledge elicitation, we explored interactions among seven variables representing Earth system processes relevant to food production, identifying many interactions little explored in Earth system literature. We found that green water and land system change affect other Earth system processes strongly, while land, freshwater and ocean components of biosphere integrity are the most impacted by other Earth system processes, most notably blue water and biogeochemical flows. We also mapped a complex network of mechanisms mediating these interactions and created a future research prioritization scheme based on interaction strengths and existing knowledge gaps. Our study improves the understanding of Earth system interactions, with sustainability implications including improved Earth system modelling and more explicit biophysical limits for future food production.

**Introduction.** Food production is the main cause of environmental impacts such as biodiversity loss[1,2], eutrophication[3] and overexploitation of marine resources[4]. In particular, agriculture drives 80% of global deforestation and 70% of freshwater withdrawals[5]. Human pressures may have already pushed the Earth system beyond the safe operating space for humanity, as demarcated by the nine planetary boundaries describing critical Earth system processes[6,7]. Beyond these boundaries, the risk of abrupt or irreversible global environmental change increases, with the potential to push the Earth system out of its stable Holocene condition, thus threatening the capacity of humanity to develop and thrive[7,8].

Recent literature and modelling studies[9,10] provide the first quantitative estimates of an array of interactions among the Earth system processes represented by the planetary boundaries. Their findings suggest that the cascades and feedbacks of interactions amplify human impacts on the Earth system. Accounting for these interactions may narrow the estimated global safe operating space for human activities but also illuminate synergies: decreasing impacts on one Earth system process may decrease impacts on others. Given that many interactions relevant to food production are not quantified by existing studies[9,10] and that marine processes have received relatively little attention within the planetary boundaries literature[11], achieving sustainable food futures may require even greater food system reforms than previously suggested[12].

Interactions among Earth system processes are challenging to account for in food system analyses and spatially disaggregated models. The interactions and interaction strengths are partially unknown; they can be context-specific and not all control variables are suitable for spatial models. Thus, research on respecting the global safe operating space is complemented by exploring how to stay within critical limits of ecosystems at smaller scales[13]. The effects of perturbations on key

Nature Communications, vol. 13, issue no. 1, 3530, doi:10.1038/s41467-022-30991-4

# Potential impacts of climate change on agriculture and fisheries production in 72 tropical coastal communities

Cinner, J.E., I.R. Caldwell, L. Thiault, J. Ben, J.L. Blanchard, M. Coll, A. Diedrich, T.D. Eddy, J.D. Everett, C. Folberth, D. Gascuel, J. Guiet, G.G. Gurney, R.F. Heneghan, **J. Jägermeyr**[1,2,3], N. Jiddawi, R. Lahari, J. Kuange, W. Liu, O. Maury, C. Müller, C. Novaglio, J. Palacios-Abrantes, 2022

NASA Goddard Institute for Space Studies, New York, NY, USA[1]
Potsdam Institute for Climate Impact Research, Member of the Leibniz Association, Potsdam, Germany[2]
Center for Climate Systems Research, Columbia University, New York, NY, USA[3]

**Abstract.** Climate change is expected to profoundly affect key food production sectors, including fisheries and agriculture. However, the potential impacts of climate change on these sectors are rarely considered jointly, especially below national scales, which can mask substantial variability in how communities will be affected. Here, we combine socioeconomic surveys of 3,008 households and intersectoral multi-model simulation outputs to conduct a sub-national analysis of the potential impacts of climate change on fisheries and agriculture in 72 coastal communities across five Indo-Pacific countries (Indonesia, Madagascar, Papua New Guinea, Philippines, and Tanzania). Our study reveals three key findings: First, overall potential losses to fisheries are higher than potential losses to agriculture. Second, while most locations (> 2/3) will experience potential losses to both fisheries and agriculture simultaneously, climate change mitigation could reduce the proportion of places facing that double burden. Third, potential impacts are more likely in communities with lower socioeconomic status.

**Introduction.** Climate change is expected to profoundly impact key food production sectors, with the tropics expected to suffer losses in both fisheries and agriculture. For example, by 2100 tropical areas could lose up to 200 suitable plant growing days per year due to climate change[1]. Likewise, fishable biomass in the ocean could drop by up to 40% in some tropical areas[2,3]. While understanding the magnitude of losses that climate change is expected to create in key food production sectors is crucial, it is the social dimensions of vulnerability that determine the degree to which societies are likely to be affected by these changes[4,5,6,7,8]. Vulnerability is the degree to which a system is susceptible to and unable to cope with the effects of change. It is comprised of exposure (the degree to which a system is stressed by environmental or social conditions), the social dimensions of sensitivity (the state of susceptibility to harm from perturbations), and adaptive capacity (people's ability to anticipate, respond to, and recover from the consequences of these changes)[4,9]. Together, the exposure and sensitivity domains are referred to as "potential impacts", which are the focus of this article.

Incorporating key social dimensions of vulnerability is particularly important because many coastal communities simultaneously rely on both agriculture and fisheries to varying degrees[10], yet assessments of climate change impacts and the policy prescriptions that come from them often consider these sectors in isolation[1,5,11,12,13,14]. Recently, studies have begun to look at the simultaneous impacts of climate change on both fisheries and agriculture at the national level[15,16], but this coarse scale does not capture whether people simultaneously engage with- and are likely to be affected by- changes in these sectors. Indeed, whether households engage in both fisheries and agriculture[10] will determine whether people have the knowledge, skills, and capital to substitute sectors if one declines, or alternatively, make them particularly susceptible to the potential double burden of a combined decline across sectors[15]. Thus, more localised analyses incorporating key social dimensions of vulnerability are required to better understand how combined impacts to fisheries and agriculture may affect coastal communities.

Journal of Advances in Modeling Earth Systems, vol. 14, issue no. 10, e2022MS003078,
doi:10.1029/2022MS003078

# Large eddy simulation for investigating coupled canopy and turbulence influences on atmospheric chemistry: Model description and application to summer midday conditions at a temperate deciduous forest

**Clifton**, **O.E.**[1,2], E.G. Patton[2], S. Wang, M. Barth[2], J. Orlando[2], and R.H. Schwantes, 2022

NASA Goddard Institute for Space Studies, New York, NY, USA[1]
National Center for Atmospheric Research, Boulder, CO, USA[2]
Center for Climate Systems Research, Columbia University, New York, NY, USA[2]

**Abstract.** Exchanges of reactive gases between forests and the atmosphere influence tropospheric chemistry, climate, and ecosystems. Chemistry inside canopies can alter these exchanges yet understanding of the chemistry and processes influencing the chemistry is incomplete. Previous work prioritizes complex chemical mechanisms over micrometeorology in the multilayer models of forests used to understand in-canopy chemistry and its impacts. Instead, here we use a new simplified chemical mechanism and resolve turbulence in a multilayer canopy model. Specifically, we describe a new version of the National Center for Atmospheric Research large eddy simulation (LES) coupled to both a multilayer canopy model and a chemical mechanism. The mechanism has 41 reactions and 19 gases for ozone, $NO_x$ (=NO + $NO_2$), $HO_x$ (=OH + $HO_2$), and isoprene chemistry. We evaluate the mechanism against two more complex mechanisms using box modeling. We configure the LES for a temperate deciduous forest and summer midday weak-wind buoyancy-forced conditions. The multilayer canopy model necessitates estimates of reactant sources and sinks at each canopy level, and thus we describe multilayer parameterizations for dry deposition and biogenic emissions. For the first time with an LES coupled to both a multilayer canopy and chemistry, we demonstrate variability in chemical reactions due to turbulence-induced segregation of reactants inside and just above the canopy. For the cases examined here, in-canopy segregation alters reaction rates that only consider well-mixed conditions by up to −48% to +23%. For many reactions, segregation is stronger when soil NO emissions reflect the upper bound of observed values for temperate forests.

**Introduction.** Land-atmosphere exchanges of reactive gases play an important role in our earth system, influencing tropospheric chemistry, climate, and ecosystems (Arneth et al., **2011**; Barth et al., **2005**; Farmer & Riches, **2020**; Fowler et al., **2009**; He et al., **2021**; Steiner, **2020**). For example, emissions of biogenic volatile organic compounds (BVOCs) from vegetation contribute to the formation of tropospheric ozone and secondary organic aerosol, both air pollutants and short-lived climate forcers (Fehsenfeld et al., **1992**; Fiore et al., **2012**; Hallquist et al., **2009**; Henze & Seinfeld, **2006**; Trainer et al., **1987**). Air pollution and the atmospheric oxidizing capacity also depend on $NO_x$ (=NO + $NO_2$) (Crutzen, **1974, 1979**; Levy, **1971**), which has a soil source and a vegetation sink (Delaria et al., **2018**; Jacob & Bakwin, **1991**; Wang et al., **2020**; Yienger & Levy, **1995**). A key but overlooked component of forest-atmosphere chemical exchanges is turbulence.

Generally, organized eddy structures comprise turbulence in the atmospheric boundary layer (ABL), with their size and character changing with driving forces (e.g., Moeng & Sullivan, **1994**; Weckwerth et al., **1997**). Inside and just above forest canopies, turbulence is unique. Near canopy top, the mean wind profile has a hydrodynamically unstable inflection point due to vegetation absorbing momentum through its depth. ABL-scale turbulence brings high-momentum air to the canopy top, producing shear-driven canopy-scale eddies (i.e., sweeps and ejections) distinct from the background flow (Finnigan et al., **2009**; Gao et al., **1989, 1992**; Raupach et al., **1996**). In unstable conditions, buoyant plumes emanating from the ground and canopy also influence exchange between canopy layers and aloft (e.g., Brunet, **2020**; Dupont & Patton, **2012**; Patton et al., **2016**).

Remote Sensing, vol. 14, 1180, doi:10.3390/rs14051180

# Flood monitoring using enhanced resolution passive microwave data: A test case over Bangladesh

Colosio, P., **M. Tedesco**[1,2], and E. Tellman, 2022

NASA Goddard Institute for Space Studies, New York, NY, USA[1]
Lamont-Doherty Earth Observatory, Columbia University. Palisades, NY, USA[2]

**Abstract.** Monitoring floods is a major issue in water resources management and risk mitigation, especially in the Global South. Optical and radar observations, even providing a fine spatial resolution, are still limited by cloud cover interaction or insufficient temporal resolution. On the other hand, passive microwave (PMW) sensors collect information on a daily frequency with minor cloud cover interaction, but they have been historically limited in terms of spatial resolution. Here, we evaluate the capability of an enhanced spatial resolution PMW dataset (3.125 km) in monitoring spatio-temporal evolution of flood events, focusing on a major flood event that occurred in October 2005 in Bangladesh. We apply an algorithm aimed to remove the seasonal variability of surface temperature from the PMW timeseries, exploiting the difference in emissivity between dry and water-covered pixels. We assess the capability of the algorithm in capturing flood evolution and extension through the comparison with quantities obtained from optical data collected by the Moderate Resolution Imaging Spectroradiometer (MODIS) and water level measurements. We also compare the enhanced product with the historical coarser resolution dataset by means of a variogram-based analysis to evaluate the improvements in terms of spatial representation. Finally, we evaluate the possibility to extract the water fraction within a single pixel by using an Advanced Microwave Scanning Radiometer—Earth Observing System (AMSR-E) emissivity dataset and compare the estimates with MODIS-derived water fractions. Our results show that the enhanced PMW product outperforms the coarser one when compared to flood mapped from optical data based on information content, indicating that it is possible to integrate such a product into the mapping of floods at a global scale on a daily basis.

**Introduction and Background.** Flooding is a frequent hydrologic hazard, affecting everyday life and impacting social and economic systems, especially in the Global South. Structural and non-structural mitigation measurements should be based on proper knowledge of the spatial and temporal evolution of such devastating events. In this regard, the increase in the availability of radar and optical spaceborne data in recent years has allowed monitoring the spatial distribution and temporal evolution of floods with increased accuracy with respect to the previous decades [1,2,3]. Despite this, however, several major issues need to be addressed for properly capturing the spatio-temporal evolution of floods, especially in regions where in situ measurements and data infrastructures are not well developed and readily available, as in the Global South. While optical data are routinely collected at high spatial (~meters or tens of meters) and temporal (daily) resolutions, the presence of clouds within the acquired scene can often obstruct the view of the sensors, especially during floods associated with hurricanes and heavy rain. On the other hand, radar data are not limited to clear sky conditions and can collect information during cloudy conditions and without the need for solar illumination. However, current available radar datasets are characterized by a relatively coarse temporal resolution (6–12 days in the case of Sentinel-1 sensors depending on year and location) and short record (~2015–present), introducing strong limitations in monitoring the short-term evolution of floods. While radars mounted on small satellites are becoming more popular, they are still cost-prohibitive and not yet currently available at a daily timestep. Moreover, acquisitions must be tasked, limiting their access to a wide audience of researchers and utility for flood monitoring.

Nature Reviews Earth & Environment, vol. 3, issue no. 11, pp. 741-757, doi:10.1038/s43017-022-00329-1

# Megadroughts in the Common Era and the Anthropocene

**Cook**, **B.I.**[1,2], J.E Smerdon[2], E.R Cook, A.P. Williams, K.J Anchukaitis, J.S Mankin[2,3], K. Allen, L. Andreu-Hayles, T.R Ault, S. Belmecheri, S. Coats, B. Coulthard, B. Fosu, P. Grierson, D. Griffin, D.A Herrera, M. Ionita, F. Lehner, C. Leland, **K.D. Marvel**[1,4], M.S Morales, V. Mishra, J. Ngoma, H.T.T Nguyen, A. O'Donnell, J. Palmer, M.P Rao, M. Rodriguez-Caton, R. Seager[2], D.W Stahle, S. Stevenson, U.K Thapa, A.M Varuolo-Clarke[2], and E.K Wise, 2022

NASA Goddard Institute for Space Studies, New York, NY, USA[1]
Division of Ocean & Climate Physics, Lamont-Doherty Earth Observatory, Columbia University, New York, NY, USA[2]
Department of Geography, Dartmouth College, Hanover, NH, USA[3]
Center for Climate Systems Research, Columbia University, New York, NY, USA[4]

**Abstract.** Exceptional drought events, known as megadroughts, have occurred on every continent outside Antarctica over the past ~2,000 years, causing major ecological and societal disturbances. In this Review, we discuss shared causes and features of Common Era (Year 1–present) and future megadroughts. Decadal variations in sea surface temperatures are the primary driver of megadroughts, with secondary contributions from radiative forcing and land–atmosphere interactions. Anthropogenic climate change has intensified ongoing megadroughts in south-western North America and across Chile and Argentina. Future megadroughts will be substantially warmer than past events, with this warming driving projected increases in megadrought risk and severity across many regions, including western North America, Central America, Europe and the Mediterranean, extratropical South America, and Australia. However, several knowledge gaps currently undermine confidence in understanding past and future megadroughts. These gaps include a paucity of high-resolution palaeoclimate information over Africa, tropical South America and other regions; incomplete representations of internal variability and land surface processes in climate models; and the undetermined capacity of water-resource management systems to mitigate megadrought impacts. Addressing these deficiencies will be crucial for increasing confidence in projections of future megadrought risk and for resiliency planning.

**Key Points**.

- The term ‘megadrought’ is often used to refer to droughts that exceed the length of most droughts in the instrumental record, the period of climate observations largely serving as the basis for modern water-resource management and infrastructure.

- Although developing a more quantitative megadrought definition is challenging, it is suggested that the term be reserved for “persistent, multi-year drought events that are exceptional in terms of severity, duration, or spatial extent when compared to other regional droughts during the instrumental period or the Common Era”.

- Past megadroughts caused major ecological and societal disturbances over the last two millennia and were forced primarily by persistent ocean states, with possible secondary contributions from internal atmospheric variability, volcanic and solar forcing, and land–atmosphere interactions.

- Some of the most active megadrought regions in the past are also areas where anthropogenic climate change is projected to increase future drought risk through declines in precipitation, increases in evaporative demand, and/or changes in plant water use.

- Megadroughts have the potential to substantially strain modern water-management systems, although understanding of the risks of such events, and their ultimate impacts, is still limited by imperfect knowledge of past and future megadrought dynamics.

Environmental Research Letters, vol. 17, 104020, doi:10.1088/1748-9326/ac8e1a

# Projected changes in early summer ridging and drought over the Central Plains

**Cook**, **B.I.**[1,2], A.P. Williams, and **K.D. Marvel**[1], 2022

NASA Goddard Institute for Space Studies, New York, NY, USA[1]
Lamont-Doherty Earth Observatory, Palisades, New York, NY, USA[2]

**Abstract.** Early summer (May–June–July; MJJ) droughts over the Central Plains are often caused by atmospheric ridging, but it is uncertain if these events will increase in frequency or if their influence on drought severity will change in a warming world. Here, we use tree-ring based reconstructions (1500–2020 CE) of MJJ ridging and 0–200 cm soil moisture with six CMIP6 model ensembles to investigate the response of Central Plains drought dynamics to a moderate warming scenario (SSP2-4.5). By the end of the 21st century (2071–2100), precipitation increases in most models during the preceding months (February–March–April), especially over the northern part of the Central Plains, while changes during MJJ are non-robust. By contrast, vapor pressure deficit increases strongly in all models, resulting in five of the six models projecting robust median soil moisture drying and all six models projecting more rapid seasonal soil moisture declines during the transition into the summer. Major ridging events increase in frequency in some models, and there is strong agreement across all models that when ridging events do occur, they will cause more severe soil moisture drought and seasonal drying at the end of the 21st century. The median multi-model response also indicates, by the end of the 21st century, that the Central Plains will experience a three-fold increase in the risk of drought events equivalent to the most extreme droughts of the last 500 years. Our results demonstrate that even moderate warming is likely to increase early summer soil moisture drought severity and risk over the Central Plains, even in the absence of robust precipitation declines, and that drought responses to major atmospheric ridging events will be significantly stronger.

**Introduction.** Warm season droughts are a major environmental hazard in the Central Plains of the United States (Schubert *et al* **2004a**, Basara *et al* **2013**), with especially severe events occurring in 1956 (Logan *et al* **2010**), 1988 (Trenberth *et al* **1988**), 2006 (Dong *et al* **2011**), 2012 (Hoerling *et al* **2014**, Otkin *et al* **2016**), and during the 'Dust Bowl' of the 1930s (Schubert *et al* **2004b**). Central Plains droughts are typically linked to persistent atmospheric ridges that cause strong subsidence and suppress precipitation in the region (Cook *et al* **2014**, Wang *et al* **2015**, Basara *et al* **2019**, Jong *et al* **2022**) and are amplified by land-atmosphere interactions that can enhance extreme heat (Dong *et al* **2011**, Cowan *et al* **2020**) and precipitation deficits (Schubert *et al* **2004a**, Cook *et al* **2009**). The Central Plains region is also prone to quickly developing 'flash drought' events (Otkin *et al* **2018**, Pendergrass *et al* **2020**, Jong *et al* **2022**), characterized by rapid declines in soil moisture triggered by large precipitation deficits and high temperatures (Hobbins *et al* **2016**, Pendergrass *et al* **2020**).

Compared to regions with more robust drought responses to warming (e.g. southwestern North America, the Mediterranean) (Cook *et al* **2020**), projected changes in Central Plains drought in twenty-first century warming scenarios are relatively uncertain. Within the latest suite of climate model projections (Phase 6 of the Coupled Model Intercomparison Project (CMIP6)) (Eyring *et al* **2016**), there is little change in annual precipitation over the Central Plains (Cook *et al* **2020**, Ukkola *et al* **2020**), but a strong and robust shift in precipitation seasonality, characterized by large increases during the cold season and modest declines during the warm season (Marvel *et al* **2021**). Despite these complex and uncertain precipitation responses, however, some studies have found that warm season soil moisture drought risk and severity in the region will likely increase as a consequence of warming-induced increases in evaporative demand (Cook *et al* **2015**, **2020**, Marvel *et al* **2021**, Ting *et al* **2021**).

Philosophical Transactions of the Royal Society A, vol. 380, issue no. 2235, 20210258, doi:10.1098/rsta.2021.0258

# Wind waves in sea ice of the western Arctic and a global coupled wave-ice model

Cooper, V., **L.A. Roach**[1,2], J. Thomson[2], S. Brenner[2], M. Smith[2], M. Meylan, and C. Bitz, 2022

NASA Goddard Institute for Space Studies, New York, NY, USA[1]
Department of Atmospheric Sciences, University of Washington, Seattle, WA 98195, USA[2]

**Abstract.** The retreat of Arctic-sea ice is enabling increased ocean wave activity at the sea ice edge, yet the interactions between surface waves and sea ice are not fully understood. Here, we examine *in situ* observations of wave spectra spanning 2012–2021 in the western Arctic marginal ice zone (MIZ). Swells exceeding 30 cm are rarely observed beyond 100 km inside the MIZ. However, local wind waves are observed in patches of open water amid partial ice cover during the summer. These local waves remain fetch-limited between ice floes with heights less than 1 m. To investigate these waves at climate scales, we conduct experiments varying wave attenuation and generation in ice with a global model including coupled interactions between waves and sea ice. A weak high-frequency attenuation rate is required to simulate the local waves in observations. The choices of attenuation scheme and wind input in ice have a remarkable impact on the extent of wave activity across ice-covered oceans, particularly in the Antarctic. As well as demonstrating the need for stronger constraints on wave attenuation, our results suggest that further attention should be directed towards locally generated wind waves and their role in sea ice evolution.

This article is part of the theme issue 'Theory, modelling and observations of marginal ice zone dynamics: multidisciplinary perspectives and outlooks.

**Introduction.** As sea ice retreats and exposes larger open-water areas in the Arctic Ocean, interactions between ocean surface waves and sea ice may play an elevated role in the Arctic climate system [1]. Wave-ice interactions typically occur in the marginal ice zone (MIZ), the partially ice-covered region that separates interior pack ice from open ocean. The fracture of sea ice by ocean surface waves in the MIZ may affect regional climate feedbacks through enhanced sea ice melt (e.g. [2]) motivating the development of fully coupled wave-ice models in recent years (e.g. [3,4]).

However, significant uncertainty remains in our understanding of fundamental aspects of wave-ice physics [5,6]. A major obstacle is that observations of waves in polar oceans are rare and hard to obtain, and existing *in situ* datasets sample a limited range of ocean and sea ice conditions [7]. Despite recent progress (e.g. [8–10]), comprehensive datasets from remote sensing are not yet available. These observing challenges leave us with only weak constraints on the ocean surface wave climate in sea ice.

Swell, low-frequency ocean surface waves that have developed in open ocean areas, can propagate into the MIZ and decay with distance inside the sea ice edge. Many studies have considered the attenuation of swell waves in sea ice, but the theory has not yet converged on a definitive explanation [11]. A wide variety of attenuation schemes have been proposed based on different theoretical frameworks and observations [12–14], and their respective impacts on wave climate have not yet been systematically investigated.

Besides propagation of swell, ocean surface waves may also be generated inside the sea ice edge by local winds. In contrast to the large body of work on the attenuation of swell and its incorporation into numerical models, less focus has been directed toward these high-frequency wind waves. According to [15], wind waves tend to dissipate during their first 10–20km of travel into the sea ice field. However, in [16] a model was developed explaining how local wind waves can be generated anew in areas of low sea ice concentration (SIC) and sparse ice floes.

Palaeogeography, Palaeoclimatology, Palaeoecology, vol. 596, 110996, doi:10.1016/j.palaeo.2022.110996

# Mineral inputs, paleoecological change, and Holocene carbon accumulation at a boreal peatland in the Hudson Bay Lowlands, Canada

Da Silva, K.A., R.A. Snyder[2], M.S. Packalen, J.W. McLaughlin, **D.M. Peteet[1,2]**, and S.A. Finkelstein, 2022

NASA Goddard Institute for Space Studies, New York, NY, USA[1]
Lamont-Doherty Earth Observatory, Columbia University, Palisades, NY, USA[2]

**Abstract.** The Hudson Bay Lowlands (HBL) is a vast contiguous peatland extending over >370,000 km2 in Canada's boreal-subarctic and is the traditional land of the Omushkego Cree. It is currently undergoing climatic warming alongside other anthropogenic stressors and contains a large below-ground carbon pool. Understanding how climate variability and multiple stressors impact peat accumulation in this region is critical to discerning how northern peatlands will respond to future climate and land-use changes. Pollen- and macrofossil-based paleoecological reconstructions, and analyses of aluminum (Al) and titanium (Ti) fluxes in a Holocene-aged peat core (VM375) taken from a bog in the Attawapiskat watershed were conducted to link ecosystem changes with hydroclimate and long-term carbon storage. Peat initiation is dated to 5780 cal yr B.P., coincident with land emergence driven by glacial isostatic adjustment. From 4500 to 4200 cal yr B.P., apparent rate of carbon accumulation increased, and was linked to more rapid rates of peat accretion and increases in minerotrophic indicators in the pollen record. This increase in peat accretion and shift in vegetation composition co-occur with higher rates of mineral influx as shown by Ti and Al concentrations, which may have supplied nutrients. A fen to bog transition takes place ~3300 cal yr B.P., with increases in Sphagnum spores and macrofossils, and a decline in the apparent rate of carbon accumulation relative to the earlier half of the record, where paleoecological proxies indicate treed wetland and fen stages. Since peat inception, the total carbon stock of the 260-cm peat column is 110 kg C m−2. This multi-proxy record shows an association between changing peat types and variability in apparent rates of carbon accumulation and supports the hypothesis that mineral nutrients either supplied by surface hydrology or by eolian deposition played a role in Holocene peat carbon accumulation in eastern North American boreal peatlands.

**Introduction.** Peat soils are composed of partially decomposed organic matter that has accumulated as a result of complex ecohydrological interactions whereby net primary productivity exceeds the sub-surface rate of decay (Rydin and Jeglum, 2013). Globally, it has been estimated that northern peatlands store ~500 Pg of carbon (Loisel et al., 2017), with more recent analyses suggesting existing pools exceed 1000 Gt C (Nichols and Peteet, 2019), and potential interglacial pools of up to ~875 Gt (Alexandrov et al., 2020). Northern peatland regions are experiencing accelerated hydro-climatic changes in response to anthropogenic warming because of their high latitudinal position, ice-albedo feedbacks and presence of thawing permafrost (McLaughlin and Webster, 2014; Rühland et al., 2013). Peatlands have been characterized as complex adaptive systems with synergistic feedbacks that can result in self-regulating interactions between hydrology, vegetation and peat growth, however it is unclear if these self-regulating systems and large existing carbon pools can be sustained under different climate regimes (Belyea and Baird, 2006; Belyea and Malmer, 2004).

Most of the organic carbon stored in Canadian peatlands occurs in the boreal and subarctic regions (Webster et al., 2018; Zoltai and Vitt, 1995). The Hudson Bay Lowlands (HBL) is the largest continuous peatland complex in Canada (Martini, 2006; Packalen et al., 2014; Riley, 2011). The underlying geology consists mostly of Paleozoic limestone bounded to the south by Precambrian rocks of the Canadian Shield (Ontario Geological Survey, 1991).

Atmospheric Chemistry and Physics, vol. 22, issue no. 13, pp. 8843-8862, doi:10.5194/acp-22-8843-2022

# Volcanic stratospheric injections up to 160 Tg(S) yield a Eurasian winter warming indistinguishable from internal variability

**DallaSanta, K.**[1,2], and **L.M. Polvani**[1,2,3,4], 2022

NASA Goddard Institute for Space Studies, New York, NY, USA[1]
Department of Applied Physics and Applied Mathematics, Columbia University, New York, NY, USA[2]
Department of Earth and Environmental Sciences, Columbia University, New York, NY, USA[3]
Lamont-Doherty Earth Observatory, Columbia University, Palisades, NY, USA[4]

**Abstract.** Early observational and modeling work suggested that low-latitude volcanic eruptions, comparable to the one of Pinatubo in 1991 or Krakatau in 1883, cause substantial surface warming over the northern continents at mid-latitudes in winter. The proposed mechanism consists of the formation of an anomalously strong Equator-to-pole temperature gradient in the stratosphere due to the presence of volcanic aerosols in the tropics, which are accompanied by an acceleration of the stratospheric polar vortex, which then shifts the Northern Annular Mode into a positive phase, resulting in warming surface temperatures over Eurasia.

However, a large body of research in the past decade has shown that, for eruptions such as Pinatubo or Krakatau, no such warming is seen in simulations with more recent climate models which, in general, have much finer vertical and horizontal resolution than the early ones, and which have separated the forced response from the internal variability by using large ensembles of integrations. Since the proposed physical mechanism is sound, it is then possible that eruptions comparable to those of Pinatubo or Krakatau are simply too weak, but even larger ones might indeed be capable of causing Eurasian surface warming in winter.

In this study, we explore this possibility using a state-of-the-art, stratosphere-resolving climate model, forced with prescribed aerosols from the Easy Volcanic Aerosol protocol. We consider eruptions with stratospheric sulfur injections of 5, 10, 20, 40, 80, and 160 Tg(S). With 20-member ensembles, we find that with injections of 20 Tg(S) or more – roughly twice the amplitude of the Pinatubo and Krakatau eruptions – our model simulates a winter surface warming over Eurasia, which is statistically significant with a *t* test given our 20-member ensembles. However, the forced volcanic signal on Eurasian winter surface temperatures is very small, barely exceeding the $1\sigma$ range of internal variability for the 160 Tg(S) injection case, and much smaller for smaller eruptions. Most importantly, the number of eruptions needed to establish statistical significance is considerably larger than the number of eruptions known to have occurred in the past 2000 years.

**Introduction.** Large, low-latitude eruptions, such as the 1815 eruption of Mount Tambora in the Lesser Sunda Islands, can inject considerable amounts of sulfate into the lower stratosphere. Since the Brewer–Dobson circulation advects tracers upwards and polewards in the tropics (**Plumb**, **2007**), the volcanic aerosols from such eruptions have long residence times (from many months to years), making them capable of impacting surface climate in a substantial way. That impact is primarily a reduction in surface temperature, as the aerosols shield the surface from incoming solar radiation and cause cooling. It is thus not immediately obvious how such large eruptions would produce any surface *warming*.

Nonetheless, a series of observational and modeling studies, starting in the early 1990s and continuing to this day, have argued that low-latitude eruptions comparable to the one of Krakatau in 1883, or Pinatubo in 1991, do in fact cause surface warming over the Northern Hemisphere (NH) continents in the winters following the eruption.

Trends in Ecology and Evolution, vol. 37, issue no. 8, pp. 683-693, doi:10.1016/j.tree.2022.05.001

# New directions in tropical phenology

Davis, C.C., G.M. Lyra, D.S. Park, R. Asprino, R. Maruyama, D. Torquato, **B.I. Cook**[1], and A.M. Ellison, 2022

NASA Goddard Institute for Space Studies, New York, NY, USA[1]

**Abstract.** Earth's most speciose biomes are in the tropics, yet tropical plant phenology remains poorly understood. Tropical phenological data are comparatively scarce and viewed through the lens of a 'temperate phenological paradigm' expecting phenological traits to respond to strong, predictably annual shifts in climate (e.g., between subfreezing and frost-free periods). Digitized herbarium data greatly expand existing phenological data for tropical plants; and circular data, statistics, and models are more appropriate for analyzing tropical (and temperate) phenological datasets. Phylogenetic information, which remains seldom applied in phenological investigations, provides new insights into phenological responses of large groups of related species to climate. Consistent combined use of herbarium data, circular statistical distributions, and robust phylogenies will rapidly advance our understanding of tropical – and temperate – phenology.

**Phenology Research has a Temperate Zone Bias.** Phenology – the timing of key events in an organism's development or life history [1] – strongly affects individual fitness; interactions among individuals, populations, and species; the generation and maintenance of species boundaries; and how populations and species are managed [2,3]. Perhaps because of its origins in northern Europe [4,5], the study of phenology has for more than 150 years emphasized annually recurring seasonal or cyclic life-history phenomena [6].

**The Temperate Phenology Paradigm Hinders our Interpretation and Understanding of Tropical Phenology.** Applying phenological approaches and techniques from temperate regions to predicting phenology in tropical species is inadequate because in the tropics the fundamental phenological drivers are different and poorly understood; seasonal climate cues often are subtler, and species, functional, and phylogenetic diversity are much greater.

**Circular Statistics are Better for Tropical and Temperate Phenological Data.** Phenology in the temperate zone has abrupt, temperature-driven transitions that can be readily illustrated and modeled using data from truncated distributions whose endpoints are approximated by the onsets of meteorological spring and fall (i.e., the growing season or frost-free period of the year) (Figure 2A).

**Herbarium Data Greatly Expand Phenological Datasets.** Elucidating and modeling the interplay between endogenous and exogenous cues that trigger and sustain developmental shifts are required to accurately forecast the phenological responses of individuals, populations, and species to ongoing local, regional, and global climatic change. However, we lack the baseline data required to assess directions, magnitudes, and mechanisms of phenological responses to climate and climatic change for most tropical species.

**Using Herbarium Specimens to Assess and Forecast Phenological Change.** As herbarium specimens have been digitized and the associated data have been mobilized online, researchers around the world are increasingly using them to assess long-term phenological changes in hundreds of species [14,45,46,49], to document variation in phenological responses across species ranges now [14] and in the future [49], and to identify their plausible mechanistic responses to climatic and geographic factors [14].

**The Relevance of Phylogeny to Phenological Investigation.** Groups with similar phenological patterns may share a common phylogenetic history [62], but this has seldom been explored in tropical plants [63,64].

Frontiers in Climate, vol. 4, 882343, doi:10.3389/fclim.2022.882343

# Migration theory in climate mobility research

De Sherbinin, A., K. Grace, **S.S. McDermid**[1,2], K. Van Der Geest, **M.J. Puma**[1,3], and A. Bell, 2022

NASA Goddard Institute for Space Studies, New York, NY, USA[1]
Department of Environmental Studies, New York University, New York, NY, USA[2]
Center for Climate Systems Research, Columbia University, New York, NY, USA[3]

**Abstract.** The purpose of this article is to explore how migration theory is invoked in empirical studies of climate-related migration, and to provide suggestions for engagement with theory in the emerging field of climate mobility. Theory is critical for understanding processes we observe in social-ecological systems because it points to a specific locus of attention for research, shapes research questions, guides quantitative model development, influences what researchers find, and ultimately informs policies and programs. Research into climate mobility has grown out of early studies on environmental migration and has often developed in isolation from broader theoretical developments in the migration research community. As such, there is a risk that the work may be inadequately informed by the rich corpus of theory that has contributed to our understanding of who migrates; why they migrate; the types of mobility they employ; what sustains migration streams; and why they choose certain destinations over others. On the other hand, there are ways in which climate and broader environment migration research is enriching the conceptual frameworks being employed to understand migration, particularly forced migration. This paper draws on a review of 75 empirical studies and modeling efforts conducted by researchers from a diversity of disciplines, covering various regions, and using a variety of data sources and methods to assess how they used theory in their research. The goal is to suggest ways forward for engagement with migration theory in this large and growing research domain.

**Introduction.** The literature on climate migration, or what is now increasingly termed "climate mobilities" (**Boas et al., 2019**; **Cundill et al., 2021**), has grown considerably since the 2000s (**Piguet, 2021**; **Šedová et al., 2021**) and owes its origins to work on environmental migration (**Warner et al., 2010**; **Morrissey, 2012**)—a corpus that arose in isolation from the broader migration literature (**Hunter, 2005**; **Piguet, 2018**). There have been several recent reviews of the evidence for climate impacts on migration (**Borderon et al., 2019**; **Hoffmann et al., 2020**; **Šedová et al., 2021**; **Selby and Daoust, 2021**), and much has been written on the legal and conceptual ambiguities of terminology around climate migrants and "refugees" (**McAdam, 2012**; **de Sherbinin, 2020**; **Mayer, 2020**), the terminological difficulties associated with different types of mobility from voluntary to forced (**Avis, 2017**; **Piguet, 2018**), and the apolitical and ahistorical nature of the climate migration literature (**Morrissey, 2012**; **Ribot et al., 2020**). Yet, with the exception of a few authors who give the subject limited or case-specific treatment (**Hunter, 2005**; **Hugo, 2011**; **Hochleithner and Exner, 2018**; **Piguet, 2018**; **Kaczan and Orgill-Meyer, 2020**; **Zickgraf, 2021**), there has been insufficient focus on how researchers studying climate migration engage with theory. On the other hand, consensus is growing that there is a need to embed climate mobility research in migration theory (**Doevenspeck, 2011**; **Freeman, 2017**), that environmental factors have a place in migration theory, and that the climate mobility research community has much to contribute to theory-building (**Hunter and Simon, 2022**).

Theory[1] matters in empirical climate migration research because theories are formulated to elucidate causal linkages and to explain, predict, and understand phenomena. Theory is critical to the sciences, since it points to a specific locus of attention for research, shapes research questions, guides quantitative model development, and ultimately informs policies and programs. It is a vital part of "sense making" in the social sciences and, as with data and methods, continues to evolve as part of scientific advancement. However, empirical climate migration research is often critiqued because it insufficiently engages with theory, leading some to write-off the contributions as overly simplistic and environmentally deterministic (**Morrissey, 2012**). The "environmental refugees" framing prevalent in the literature of the 1990s and early 2000s is a case in point (**Myers, 1993**; **Barrios et al., 2006**). The use of theory within this framing minimized the role of the individual's abilities to make decisions within a given context shaped by conditions of the time and place.

Atmospheric Chemistry and Physics, vol. 22, issue no. 18, pp. 12113-12151, doi:10.5194/acp-22-12113-2022

# Cloud adjustments from large-scale smoke-circulation interactions strongly modulate the southeast Atlantic stratocumulus-to-cumulus transition

Diamond, M.S., P.E. Saide, P. Zuidema, **A.S. Ackerman**[1], S.J. Doherty, **A.M. Fridlind**[1], H. Gordon, C. Howes, J. Kazil, T. Yamaguchi, J. Zhang, G. Feingold, and R. Wood, 2022

NASA Goddard Institute for Space Studies, New York, NY, USA[1]

**Abstract.** Smoke from southern Africa blankets the southeastern Atlantic Ocean from June to October, producing strong and competing aerosol radiative effects. Smoke effects on the transition between overcast stratocumulus and scattered cumulus clouds are investigated along a Lagrangian (air-mass-following) trajectory in regional climate and large eddy simulation models. Results are compared with observations from three recent field campaigns that took place in August 2017: ObseRvations of Aerosols above CLouds and their intEractionS (ORACLES), CLouds and Aerosol Radiative Impacts and Forcing: Year 2017 (CLARIFY) and Layered Atlantic Smoke Interactions with Clouds (LASIC). The case study is set up around the joint ORACLES–CLARIFY flight that took place near Ascension Island on 18 August 2017. Smoke sampled upstream on an ORACLES flight on 15 August 2017 likely entrained into the marine boundary layer later sampled during the joint flight.

**Introduction**. The case is first simulated with the WRF-CAM5 regional climate model in three distinct setups: (1) FireOn, in which smoke emissions and any resulting smoke–cloud–radiation interactions are included; (2) FireOff, in which no smoke emissions are included; (3) RadOff, in which smoke emissions and their microphysical effects are included but aerosol does not interact directly with radiation. Over the course of the Lagrangian trajectory, differences in free tropospheric thermodynamic properties between FireOn and FireOff are nearly identical to those between FireOn and RadOff, showing that aerosol–radiation interactions are primarily responsible for the free tropospheric effects. These effects are non-intuitive: in addition to the expected heating within the core of the smoke plume, there is also a "banding" effect of cooler temperature (∼1–2 K) and greatly enhanced moisture (>2 g $kg^{-1}$) at the plume top. This banding effect is caused by a vertical displacement of the former continental boundary layer in the free troposphere in the FireOn simulation resulting from anomalous diabatic heating due to smoke absorption of sunlight that manifests primarily as a few hundred meters per day reduction in large-scale subsidence over the ocean.

A large eddy simulation (LES) is then forced with free tropospheric fields taken from the outputs for the WRF-CAM5 FireOn and FireOff runs. Cases are run by selectively perturbing one variable (e.g., aerosol number concentration, temperature, moisture, vertical velocity) at a time to better understand the contributions from different indirect (microphysical), "large-scale" semi-direct (above-cloud thermodynamic and subsidence changes), and "local" semi-direct (below-cloud smoke absorption) effects. Despite a more than 5-fold increase in cloud droplet number concentration when including smoke aerosol concentrations, minimal differences in cloud fraction evolution are simulated by the LES when comparing the base case with a perturbed aerosol case with identical thermodynamic and dynamic forcings. A factor of 2 decrease in background free tropospheric aerosol concentrations from the FireOff simulation shifts the cloud evolution from a classical entrainment-driven "deepening–warming" transition to trade cumulus to a precipitation-driven "drizzle-depletion" transition to open cells, however. The thermodynamic and dynamic changes caused by the WRF-simulated large-scale adjustments to smoke diabatic heating strongly influence cloud evolution in terms of both the rate of deepening (especially for changes in the inversion temperature jump and in subsidence) and in cloud fraction on the final day of the simulation (especially for the moisture "banding" effect). Such large-scale semi-direct effects would not have been possible to simulate using a small-domain LES model alone.

Journal of Experimental Botany., vol. 73, issue no. 16, pp. 5715-5729, doi:10.1093/jxb/erac221

# Simulation of winter wheat response to variable sowing dates and densities in a high-yielding environment.

Dueri, S., H. Brown, S. Asseng, F. Ewert, H. Webber, M. George, R. Craigie, **J.R. Guarin**[1,2,3], D.N.L. Pequeno, T. Stella, M. Ahmed, P.D. Alderman, B. Basso, A.G. Berger, G.B. Mujica, D. Cammarano, Y. Chen, B. Dumont, E.E. Rezaei, E. Fereres, R. Ferrise, T. Gaiser, Y. Gao[3], M. Garcia-Vila, S. Gayler, Z. Hochman, G. Hoogenboom[3,4], K.C. Kersebaum, C. Nendel, J.E. Olesen, G. Padovan, T. Palosuo, E. Priesack, J.W.M. Pullens, A. Rodríguez, R.P Rötter, M.R. Ramos, M.A. Semenov, N. Senapati, S. Siebert, A.K. Srivastava, C. Stöckle, I. Supit, F. Tao, P. Thorburn, E. Wang, T.K.D. Weber, L. Xiao, C. Zhao, J. Zhao, Z. Zhao, Y. Zhu, and P. Martre, 2022

NASA Goddard Institute for Space Studies, New York, NY, USA[1]
Center for Climate Systems Research, Columbia University, New York, NY, USA[2]
Agricultural & Biological Engineering Department, University of Florida, Gainesville, FL, USA[3]
Institute for Sustainable Food Systems, University of Florida, Gainesville, FL, USA[4]

**Abstract**. Crop multi-model ensembles (MME) have proven to be effective in increasing the accuracy of simulations in modelling experiments. However, the ability of MME to capture crop responses to changes in sowing dates and densities has not yet been investigated. These management interventions are some of the main levers for adapting cropping systems to climate change. Here, we explore the performance of a MME of 29 wheat crop models to predict the effect of changing sowing dates and rates on yield and yield components, on two sites located in a high-yielding environment in New Zealand. The experiment was conducted for 6 years and provided 50 combinations of sowing date, sowing density and growing season. We show that the MME simulates seasonal growth of wheat well under standard sowing conditions but fails under early sowing and high sowing rates. The comparison between observed and simulated in-season fraction of intercepted photosynthetically active radiation (FIPAR) for early sown wheat shows that the MME does not capture the decrease of crop above ground biomass during winter months due to senescence. Models need to better account for tiller competition for light, nutrients, and water during vegetative growth, and early tiller senescence and tiller mortality, which are exacerbated by early sowing, high sowing densities, and warmer winter temperatures.

**Introduction**. Wheat is the most traded crop commodity at the global scale and provides more than 20% of calories and protein in human diets (**Shiferaw *et al.*, 2013**; **Curtis and Halford, 2014**). For decades, the demand for cereals has been increasing, driven by world population growth and dietary change (**Alexandratos and Bruinsma, 2012**; **van Dijk *et al.*, 2021**). To meet the demand, cropping systems have to increase production while facing several challenges: risks associated with climate change, limits to cropland expansion, and increasing freshwater scarcity (**Eitelberg *et al.*, 2015**; **FAO, 2017**; **Gerten *et al.*, 2020**). Global climate change already impacts crop growth and production through increased temperatures, changing precipitation patterns, higher extent and severity of droughts, and greater frequency of extreme events, among others (**Mbow *et al.*, 2019**). Genetic improvement and agronomic management adaptation, such as optimization of sowing dates and sowing rates, are promising solutions to increase the productivity of cropping systems under global climate change (**Spiertz, 2012**; **Bai and Tao, 2017**; **Parent *et al.*, 2018**).

Adapting sowing conditions to climate change requires an understanding of how crop growth and yield development are affected by sowing date and density. Increased temperature shortens the growing season of wheat and shifts optimal sowing dates (**Tao *et al*, 2014**). Shifting sowing dates and changing sowing rates affect tiller development and tiller competition (**Spink *et al.*, 2000**). Tillering plays an important role in crop growth and yield formation. On the one hand tillers contribute to light interception and photosynthesis, on the other hand they are reservoirs of nutrients and carbohydrates, which can be remobilized to the main stem under nutrient stress (**Anderson and Garlinge, 2000**). The ability to remobilize nutrients is critical during stem elongation, when the crop is growing rapidly and nutrient demand is high (**Anderson and Garlinge, 2000**). Therefore, tillers contribute significantly to the maintenance of ear growth and grain yield.

IEEE Transactions Geosciences Remote Sensing, vol. 60, 4302114, doi:10.1109/TGRS.2021.3115663

# Constrained inversion of a microwave snowpack emission model using dictionary matching: Applications for GPM satellite

Ebtehaj, A., M. Durand, and **M. Tedesco**[1,2], 2022

NASA Goddard Institute for Space Studies, New York, NY, USA[1]
Lamont-Doherty Earth Observatory, Columbia University, Palisades, NY, USA[2]

**Abstract**. This article presents a new algorithmic framework for multilayer inversion of the dense media radiative transfer (DMRT) equations of snowpack emission, with particular emphasis on the role of high-frequency microwave channels above 60 GHz. The approach relies on dictionary matching and locally constrained least squares. The results demonstrate that the algorithm can invert the DMRT model and retrieve depth, density, and grain size of a single-layer snowpack when dependencies of density and grain size on depth are properly accounted for. However, as the number of layers increases, the sensitivity of the inversion to observation noise grows markedly. Using observations, over the Great Plains in the United States, from the microwave imager onboard the global precipitation measurement (GPM, 10–166 GHz) core satellite, the initial results demonstrate that under a clear-sky condition and no vegetation canopy, the algorithm is capable to retrieve the snow depth and water equivalent of seasonal snow with a mean absolute error (MAE) of less than 0.15 m—when compared to the high-resolution analysis data from the SNOw Data Assimilation System (SNODAS).

**Introduction**. Snowpack plays an important role in the Earth's climate system through modulating interactions between soil microbiomes, plants, and animals [1] and has a profound impact on the hydrologic cycle and water availability [2]. Global snow-cover climatology is witnessing rapid changes due to climate change [3], [4]. Trend analysis of ground-based observations [5], satellite data [6], [7], and climate models [8] demonstrate that the extent and spatiotemporal variability of snow cover [9] are changing in response to a widespread warming of air temperature and trends in precipitation patterns [10], [11]. These changes are altering the timing and magnitude of runoff [12], affecting functioning of soil processes [13], arctic biodiversity [14], and thus undermining global water and food security [15]. Microwave radiometry has been instrumental in monitoring of snowfall [16]–[18] and snow-cover physical properties [19]–[21] from space.

Microwave remote sensing of snow cover relies on a forward emission model that links snowpack multilayer physical properties (inputs) to its emission signals (outputs) in microwave bands. Different snowpack emission models [22] have been developed, including the Helsinki University of Technology (HUT) model [23], the microwave emission model for layered snowpack (MEMLS) [24], [25], as well as those based on the dense media radiative transfer (DMRT) equations [26], [27]. Recently, these modeling frameworks were represented in a single platform to determine uncertainties in simulation of snow emission through intercomparison of five different formalisms for describing the characteristics of snow microstructure [28]. Retrieval of the input physical properties of snowpack from observations of its emission signals involves an inverse problem.

Inversion of the existing microwave emission models has been widely used for retrieval of snowpack depth and water equivalent. The early attempts used forward simulations to develop empirical equations linking the snow depth to differential scattering between brightness temperatures (Tb) at 18 and 37 GHz [29].

Journal of Geophysical Research Atmospheres, vol. 127, issue no. 10, e2021JD035599, doi:10.1029/2021JD035599

# A simple model for tropical convective cloud shield area growth and decay rates informed by geostationary IR, GPM, and Aqua/AIRS satellite data

**Elsaesser**, **G.S.**[1,2], R. Roca, T. Fiolleau, **A.D. Del Genio**[1], and **J. Wu**[1,2], 2022

NASA Goddard Institute for Space Studies, New York, NY, USA[1]
Department of Applied Physics and Mathematics, Columbia University, New York, NY, USA[2]

**Abstract.** Deep convective system maximum areal extent is driven by the stratiform anvil area since convective area fractions are much less than unity when systems reach peak size. It is important to understand the processes that drive system size given the impact large systems have on rainfall and that of anvils on high cloud feedbacks. Using satellite diabatic heating and convective-stratiform information mapped to convective systems, composite analyses suggest that system maximum sizes occur at the temporal mid-point of system lifecycles with both maximum size and duration correlating with peak heating above the melting level. However, variations in system growth rates exist, with the overall smooth composites emerging as the average of highly variable system trajectories. Thus, this study focuses on understanding convective system growth rates on short (30-min) timescales via development of a simple analytical source—sink model that predicts system area changes. Growth occurs when detrained convective mass (inferred from the vertical gradient of diabatic heating and temperature lapse rates) and/or generation of convective area exceeds a sink term whose magnitude is proportional to the current cloud shield size. The model works well for systems over land and ocean, and for systems characterized by varying degrees of convective organization and duration (1.5–35 hr, with correlations often >0.8 across lifetime bins). The model may serve as a useful foundation for improved understanding of processes driving changes in tropics-wide convective system cloud shields, and further supports conceptual development and evaluation of prognostic climate model stratiform anvil area parameterizations.

**Introduction.** Mesoscale convective systems (MCSs) are the dominant sources of rainfall in the tropics (Moncrieff, **2019**; Roca et al., **2014**; Tao & Moncrieff, **2009**). MCS cloud shields comprise convective regions whose spatial aggregation may be quantified via "organization metrics" (Holloway et al., **2017**; Parker & Johnson, **2000**; Retsch et al., **2020**; Tobin et al., **2012**, **2013**) such that increased organization may be associated with larger cloud shields, longer lifetimes, and substantial rainfall accumulation (Liu, **2011**; Liu et al., **2008**; Roca & Fiolleau, **2020**; Schiro et al., **2020**). High resolution model simulations over domains populated by MCSs are frequent sources for deriving MCS radiation, cloud, and rainfall lifecycle evolutions (Feng et al., **2018**, **2021**; Hagos et al., **2013**). Observational composite MCS evolutions can be derived by mapping orbital-level satellite-estimated radiation, cloud, rainfall, and environment characteristics to the life stages of IR-tracked MCSs (as in Bouniol et al., **2016**; Feng et al., **2012**; Fiolleau & Roca, **2013b**; Futyan & Del Genio, **2007**; Machado et al., **1998**; Machado & Laurent, **2004**; Roca et al., **2017**; Roca et al., **2020**; Vant-Hull et al., **2016**), or by mapping in situ environmental data to scanning radar-identified MCSs (e.g., Wang et al., **2019**; Wang et al., **2020**). One such compositing analysis has revealed that MCSs over the open ocean cool the sea surface temperature (SST), a signature that lasts for days (Duncan et al., **2014**) and is likely to affect the subsequent development of convection.

MCS convective regions are characterized by diabatic heating profiles whose magnitudes are positive throughout most of the troposphere, though spread over a smaller area, while the extensive moderately raining stratiform anvil region is characterized by widespread positive heating that peaks above the melting level with diabatic cooling below (Elsaesser et al., **2010**; Feng et al., **2018**; Liu et al., **2015**) attributed to melting snow and precipitation evaporation below cloud base.

Geophysical Research Letters, vol. 49, issue no. 8, e2022GL098174, doi:10.1029/2022GL098174

# Machine learning gravity wave parameterization generalizes to capture the QBO and response to increased $CO_2$

Espinosa, Z.I., A. Sheshadri, G.R. Cain, E.P. Gerber, and **K.J. DallaSanta**[1,2], 2022

NASA Goddard Institute for Space Studies, New York, NY, USA[1]
Universities Space Research Association, Columbia, MD, USA[2]

**Abstract.** We present single-column gravity wave parameterizations (GWPs) that use machine learning to emulate non-orographic gravity wave (GW) drag and demonstrate their ability to generalize out-of-sample. A set of artificial neural networks (ANNs) are trained to emulate the momentum forcing from a conventional GWP in an idealized climate model, given only one view of the annual cycle and one phase of the Quasi-Biennial Oscillation (QBO). We investigate the sensitivity of offline and online performance to the choice of input variables and complexity of the ANN. When coupled with the model, moderately complex ANNs accurately generate full cycles of the QBO. When the model is forced with enhanced $CO_2$, its climate response with the ANN matches that generated with the physics based GWP. That ANNs can accurately emulate an existing scheme and generalize to new regimes given limited data suggests the potential for developing GWPs from observational estimates of GW momentum transport

**Introduction.** Atmospheric gravity waves (GWs) play an important role in surface climate (Palmer et al., **1986**) and a leading-order role in driving the middle atmospheric circulation and its variability (Fritts & Alexander, **2003**). By transporting momentum, GWs impact the mean climatology (Bretherton, **1969**; Sato & Hirano, **2019**) and atmospheric variability, affecting storm tracks (Fritts & Nastrom, **1992**) and stratospheric dynamics (Antonita et al., **2007**; Kang et al., **2018**; Limpasuvan et al., **2012**). Since much of the GW spectrum is too fine to be captured at current model resolutions, models typically mimic its effects on the resolved circulation via explicit gravity wave parameterizations (GWPs) (Fritts & Alexander, **2003**; Richter et al., **2010**).

Incorporating a realistic representation of these effects in numerical models, however, remains challenging for several reasons. The true GW momentum flux is not well-constrained by observational or intermodel studies (Geller et al., **2013**) and GWs are generated by a variety of sources, including orography, convection, and frontogenesis (Fritts & Alexander, **2003**), many of which must be parameterized themselves, that vary greatly in their representation across models. Hence the details of GWPs differ greatly between models (Butchart et al., **2018** ), and even small changes within the same model can lead to diverging regional climate projections (Schirber, **2015**). Given these limitations, GWPs are optimized toward maximizing global forecast skill scores (Alexander et al., **2019**) or "tuned" to reduce climatological biases (Garcia et al., **2017**). Projections of the tropospheric and stratospheric circulations' response to anthropogenic forcing are sensitive to uncertainties in GWPs (Polichtchouk et al., **2018**; Sigmond & Scinocca, **2010**), requiring continued development of GWP and the need for more observational constraints on their behavior.

An alternative approach to physics-based parameterization has emerged in the form of machine learning (ML). ML has been employed to parameterize processes such as convection (Gentine et al., **2018**; Rasp et al., **2018**) and radiation (Brenowitz & Bretherton, **2018**; Roh & Song, **2020**). Matsuoka et al. (**2020**) demonstrated that a convolutional neural network can estimate the GW structure over Hokkaido, Japan when trained on high-resolution reanalysis data and Chantry et al. (**2021**) used an artificial neural network (ANN) to emulate a non-orographic GWP in a weather forecasting system for seasonal prediction.

Environmental Science & Technology, vol. 56, issue no. 19, pp. 13546-13564, doi:10.1021/acs.est.2c03562

# A critical review for real-time continuous soil monitoring: Advantages, challenges, and perspectives

Fan, Y.[2], X. Wang[2], T. Funk[2], I. Rashid[2], B. Herman[2], N. Bompoti[2], M.S. Mahmud, M. Chrysochoou[2], **M. Yang[1,2]**, T.M. Vada[2]s, Y. Lei, and B. Li[2], 2022

NASA Goddard Institute for Space Studies, New York, NY, USA[1]
Department of Civil and Environmental Engineering, University of Connecticut, Storrs, Connecticut, USA[2]

**Abstract.** Most soil quality measurements have been limited to laboratory-based methods that suffer from time delay, high cost, intensive labor requirement, discrete data collection, and tedious sample pretreatment. Real-time continuous soil monitoring (RTCSM) possesses a great potential to revolutionize field measurements by providing first-hand information for continuously tracking variations of heterogeneous soil parameters and diverse pollutants in a timely manner and thus enable constant updates essential for system control and decision-making. Through a systematic literature search and comprehensive analysis of state-of-the-art RTCSM technologies, extensive discussion of their vital hurdles, and sharing of our future perspectives, this critical review bridges the knowledge gap of spatiotemporal uninterrupted soil monitoring and soil management execution. First, the barriers for reliable RTCSM data acquisition are elucidated by examining typical soil monitoring techniques (e.g., electrochemical and spectroscopic sensors). Next, the prevailing challenges of the RTCSM sensor network, data transmission, data processing, and personalized data management are comprehensively discussed. Furthermore, this review explores RTCSM data application for updating diverse strategies including high-fidelity soil process models, control methodologies, digital soil mapping, soil degradation, food security, and climate change mitigation. Finally, the significance of RTCSM implementation in agricultural and environmental fields is underscored through illuminating future directions and perspectives in this systematic review.

**Introduction**. Through complex interactions with air, water, nutrients, and organisms, soil plays a vital role on the earth which includes storing water and nutrients, sustaining food security, contributing to biodiversity, supplying antibiotics used to fight diseases, improving resilience to floods and droughts, and protecting the planet from climate change.1 The United States Environmental Protection Agency (U.S. EPA) has prioritized the promotion of soil health with respect to nutrient cycling, water infiltration, bioremediation, contamination removal, and carbon sequestration. The Food and Agriculture Organization (FAO) also underscores the significance of soil health to maintain a diverse community of soil organisms, to control plant disease, insect and weed pests, and ultimately to improve crop production. Nevertheless, soil health has been jeopardized globally by numerous pollution sources including industrial chemicals, domestic and municipal wastes, agrochemicals, pharmaceuticals, pathogens, and petroleum-derived products. These pollutants are released to the environment either accidentally (e.g., oil spills and/or leaching from landfills) or intentionally (e.g., the use of fertilizers and pesticides, irrigation with untreated wastewater, and land application of biosolids). In the past decade, emerging contaminants (ECs) such as pharmaceuticals, endocrine disruptors, hormones, and microplastics have drawn high concern in terms of soil usage and food safety. Given the significance of sustaining soil health and fertility and minimizing soil contamination, continuous monitoring and expeditious assessment of soil quality, soil nutrient/contaminant dynamics, and soil mechanics become essential.

Traditional soil measurement techniques are primarily laboratory-based analysis such as ion chromatography (IC), inductively coupled plasma-optical emission spectrometry/ mass spectrometry (ICP-OES/MS), gas chromatography−mass spectrometry (GC-MS), and chemiluminescence. Although these methods have high accuracy and low detection limit, the time and effort associated with the sampling, transfer, pretreatment, and analysis processes are enormous. Furthermore, these methods are unable to obtain soil data in a real-time, continuous, and in situ mode, resulting in information deficiency hindering decision-making for precaution, prevention, and management.

The Planetary Science Journal, vol. 3, issue no. 9, pp. 213, doi:10.3847/PSJ/ac6cf1

# The TRAPPIST-1 Habitable Atmosphere Intercomparison (THAI). Part III: Simulated observables — The return of the spectrum

Fauchez, T.J.[1,2,3,4], G.L. Villanueva[1], D.E. Sergeev, M. Turbet, I.A. Boutle, **K. Tsigaridis[5,6]**, **M.J. Way[4,5,7]**, E.T. Wolf[4,8,9], S.D. Domagal-Goldman[1,4,9], F. Forget, J. Haqq-Misra[9,10], R.K. Kopparapu[1,4,9], J. Manners, and N.J. Mayne, 2022

NASA Goddard Space Flight Center, 8800 Greenbelt Road, Greenbelt, MD, USA[1]
Goddard Earth Sciences Technology and Research (GESTAR), Universities Space Research Association (USRA), Columbia, MD, USA[2]
American University, College of Arts and Sciences, Washington, DC, USA[3]
Goddard Space Flight Center Sellers Exoplanet Environments Collaboration, Greenbelt, MD, USA[4]
NASA Goddard Institute for Space Studies, New York, NY, USA[5]
Center for Climate Systems Research, Columbia University, New York, NY, USA[6]
Theoretical Astrophysics, Department of Physics and Astronomy, Uppsala University, Uppsala, Sweden[7]
Laboratory for Atmospheric and Space Physics, University of Colorado Boulder, Boulder, CO, USA[8]
NASA NExSS Virtual Planetary Laboratory, Seattle, WA, USA[9]
Blue Marble Space Institute of Science, Seattle, WA, USA[10]

**Abstract.** The TRAPPIST-1 Habitable Atmosphere Intercomparison (THAI) is a community project that aims to quantify how differences in general circulation models (GCMs) could impact the climate prediction for TRAPPIST-1e and, subsequently, its atmospheric characterization in transit. Four GCMs have participated in THAI: ExoCAM, LMD-Generic, ROCKE-3D, and the UM. This paper, focused on the simulated observations, is the third part of a trilogy, following the analysis of two land planet scenarios (Part I) and two aquaplanet scenarios (Part II). Here we show a robust agreement between the simulated spectra and the number of transits estimated to detect the land planet atmospheres. For the cloudy aquaplanet ones, a $5\sigma$ detection of $CO_2$ could be achieved in about 10 transits if the atmosphere contains at least 1 bar of $CO_2$. That number can vary by 41%–56% depending on the GCM used to predict the terminator profiles, principally due to differences in the cloud deck altitude, with ExoCAM and LMD-G producing higher clouds than ROCKE-3D and UM. Therefore, for the first time, this work provides "GCM uncertainty error bars" of ∼50% that need to be considered in future analyses of transmission spectra. We also analyzed the intertransit spectral variability. Its magnitude differs significantly between the GCMs, but its impact on the transmission spectra is within the measurement uncertainties. THAI has demonstrated the importance of model intercomparison for exoplanets and also paved the way for a larger project to develop an intercomparison meta-framework, namely, the Climates Using Interactive Suites of Intercomparisons Nested for Exoplanet Studies.

**Introduction.** At the dawn of terrestrial exoplanet atmospheric characterization with the James Webb Space Telescope (JWST), predicting the detectability of the atmospheres of such planets is crucial in order to prepare for observations and maximize the scientific return. JWST Guaranteed Time Observations (GTOs) and Cycle 1 proposals have already been selected. While $CO_2$ can be potentially detectable from Cycle 1, it is unlikely that enough transits would be accumulated for any single target to characterize in depth the atmosphere of a terrestrial exoplanet (Fauchez et al. **2019**; Lustig-Yaeger et al. **2019**; Pidhorodetska et al. **2020**) in the habitable zone (HZ; see, e.g., Kopparapu et al. **2013**) of M-dwarf stars. The presence of $CO_2$ has been shown to be the best proxy (Fauchez et al. **2019**; Lustig-Yaeger et al. **2019**; Turbet et al. **2020**) for the detection of a potentially habitable atmosphere owing to its strong absorption band in the mid-infrared (MIR) at 4.3 $\mu$m and in the far-infrared at ∼15 $\mu$m. However, a $5\sigma$ detection under cloudy conditions would likely require more than a dozen transits, even for the most favorable HZ terrestrial planet, TRAPPIST-1e (Fauchez et al. **2019**).

Climate Dynamics, vol. 58, issue no. 3-4, pp. 759-776, doi:10.1007/s00382-021-05932-4

# Tree-ring cellulose $\delta^{18}O$ records similar large-scale climate influences as precipitation $\delta^{18}O$ in the Northwest Territories of Canada

**Field**, **R.D.**[1,2], L. Andreu-Hayles, R.D. D'Arrigo, R. Oelkers, B.H. Luckman, D. Morimoto, E. Boucher, F. Gennaretti, I. Hermoso, A. Lavergne, and M. Levesque, 2022

NASA Goddard Institute for Space Studies, New York, NY, USA[1]
Department of Applied Physics and Applied Mathematics, Columbia University, New York, NY, USA[2]

**Abstract.** Stable oxygen isotopes measured in tree rings are useful for reconstructing climate variability and explaining changes in physiological processes occurring in forests, complementing other tree-ring parameters such as ring width. Here, we analyzed the relationships between different climate parameters and annually resolved tree-ring $\delta^{18}O$ records ($\delta^{18}O_{TR}$) from white spruce (*Picea glauca* [Moench]Voss) trees located near Tungsten (Northwest Territories, Canada) and used the NASA GISS ModelE2 isotopically-equipped general circulation model (GCM) to better interpret the observed relationships. We found that the $\delta^{18}O_{TR}$ series were primarily related to temperature variations in spring and summer, likely through temperature effects on the precipitation $\delta^{18}O$ in spring, and evaporative enrichment at leaf level in summer. The GCM simulations showed significant positive relationships between modelled precipitation $\delta^{18}O$ over the study region and surface temperature and geopotential height over northwestern North America, but of stronger magnitudes during fall-winter than during spring–summer. The modelled precipitation $\delta^{18}O$ was only significantly associated with moisture transport during the fall-winter season. The $\delta^{18}O_{TR}$ showed similar correlation patterns to modelled precipitation $\delta^{18}O$ only during spring–summer when water matters more for trees, with significant positive correlations with surface temperature and geopotential height, but no correlations with moisture transport. Overall, the $\delta^{18}O_{TR}$ records for northwestern Canada reflect the same significant large-scale climate patterns as precipitation $\delta^{18}O$ for spring–summer, and therefore have potential for reconstructing past atmospheric dynamics in addition to temperature variability in the region.

**Introduction.** Tree rings have been used to reconstruct climate, particularly temperature, over northwestern North America prior to the instrumental period, primarily using tree-ring width (TRW) and maximum latewood density (MXD) data for the past millennium (Anchukaitis et al. **2012**; Briffa et al. **2004**; D'Arrigo et al. **2014**). Such records have also been used to generate indices of patterns of large-scale atmospheric-ocean circulation, such as the Aleutian Low, or the Pacific Decadal Oscillation (PDO) for the north Pacific sector (e.g. D'Arrigo et al. **2001**; Gaglioti et al. **2019**; Villalba et al. **2011**). Tree-ring density proxies such as MXD have been shown to have a more stable and robust temperature signal than ring-width chronologies from the same trees, and thus have been used to generate temperature reconstructions for a variety of northern sites, e.g. in British Columbia (Wilson and Luckman **2003**), at latitudinal treeline at Firth River in Alaska (Anchukaitis et al. **2012**; Andreu-Hayles et al. **2011a**) and in the Yukon (Morimoto **2015**), as well as for the Northern Hemisphere (Anchukaitis et al. **2017**; Wilson et al. **2016**). Blue intensity (BI), a novel proxy for density, has been used to produce reconstructions in Yukon (Wilson et al. **2019**) and the Gulf of Alaska (Wilson et al. **2017**), among other locations.

The isotopic composition of stable oxygen ($\delta^{18}O$, ratio of $^{18}O$–$^{16}O$ relative to a standard) measured in cellulose from tree rings can be used as another climate proxy and can provide complementary and unique information relative to TRW and MXD/BI data. This isotopic information includes, for example, physiological insights into tree response to environmental changes in boreal and other terrestrial ecosystems (e.g. Andreu-Hayles et al. **2011b**; Barber et al. **2000**; Levesque et al. **2017**), information about the source water used by the tree (e.g. Gessler et al. **2014**; McCarroll and Loader **2004**), and climate variability (e.g. Andreu-Hayles et al. **2017**; Gennaretti et al. **2017**).

Global Change Biology, vol. 28, issue no. 1, pp. 167-181, doi:10.1111/gcb.15868

# Agricultural breadbaskets shift poleward given adaptive farmer behavior under climate change

Franke, J.A., C. Müller, S. Minoli[3], J. Elliott, C. Folberth, C. Gardner, T. Hank, R.C. Izaurralde, **J. Jägermeyr[1,3]**, C. Jones, W. Liu, S. Olin, T.A.M. Pugh, **A.C. Ruane[1]**, H. Stephens, F. Zabel, and E. Moyer, 2022

NASA Goddard Institute for Space Studies, New York, NY, USA[1]
Center for Climate Systems Research, Columbia University, New York, NY, USA[2]
Potsdam Institute for Climate Impact Research (PIK), Member of the Leibniz Association, Potsdam, Germany[3]

**Abstract.** Modern food production is spatially concentrated in global "breadbaskets." A major unresolved question is whether these peak production regions will shift poleward as the climate warms, allowing some recovery of potential climate-related losses. While agricultural impacts studies to date have focused on currently cultivated land, the Global Gridded Crop Model Intercomparison Project (GGCMI) Phase 2 experiment allows us to assess changes in both yields and the location of peak productivity regions under warming. We examine crop responses under projected end of century warming using seven process-based models simulating five major crops (maize, rice, soybeans, and spring and winter wheat) with a variety of adaptation strategies. We find that in no-adaptation cases, when planting date and cultivar choices are held fixed, regions of peak production remain stationary and yield losses can be severe, since growing seasons contract strongly with warming. When adaptations in management practices are allowed (cultivars that retain growing season length under warming and modified planting dates), peak productivity zones shift poleward and yield losses are largely recovered. While most growing-zone shifts are ultimately limited by geography, breadbaskets studied here move poleward over 600 km on average by end of the century under RCP 8.5. These results suggest that agricultural impacts assessments can be strongly biased if restricted in spatial area or in the scope of adaptive behavior considered. Accurate evaluation of food security under climate change requires global modeling and careful treatment of adaptation strategies.

**Introduction.** While agriculture is widespread on the Earth's surface, food production is spatially concentrated: 80% of global cereals (and soybeans) and nearly half of total global calories are produced from just ~3% of ice-free land surface area (SPAM, International Food Policy Research Institute, **2019**), largely concentrated in temperate "breadbaskets" or "rice bowls." From the beginnings of modern climate science, there has been concerns that climate change would drive these regions of optimal cultivation poleward, causing significant economic disruptions. Newman (**1980**) estimated that a 1°C increase in daily temperature could shift the North American maize belt poleward by 175 km, and other studies in the 1980s found similar effects (e.g., Blasing & Solomon, **1983**; Rosenzweig, **1985**; Warrick, **1988**). A large body of work since then has continued this approach of evaluating potential changes in agricultural suitability (e.g., Akpoti et al., **2019**, and references therein). While many studies use suitability rules based only on mean temperature and precipitation (e.g., Caviezel et al., **2017**; Hannah et al., **2020**; King et al., **2018**), others incorporate soil characteristics (e.g., Zabel et al., **2014**) or employ more complex climate suitability approaches (e.g., He & Zhou, **2012**; Hoffman et al., **2020**; Kogo et al., **2019**; Ramirez-Cabral et al., **2017**; Zhang et al., **2017**). In economics, rule-based suitability maps have been used to investigate how future climate-driven changes in production across countries may impact the global food trade (e.g., Costinot et al., **2016**; Hertel, **2018**). However, while climate change is already modifying the spatial distributions of many species of plants and animals (e.g., Parmesan, **2006**, and references therein), evidence for real-world shifts in agricultural growing zones is more limited (Sloat et al., **2020**).

Despite the concern about shifting "breadbaskets", nearly all modeling assessments of the impacts of climate change on crop yields consider production only on currently cultivated land (e.g., Muller & Robertson, **2014**). Many studies of future yields use statistical models trained on historical records of crop yields and weather, an approach that can only produce predictions over regions where those records exist (e.g., Anderson et al., **2019**; Gaupp et al., **2020**; Kornhuber et al., **2020**; Moore, Baldos, Hertel, et al., **2017**; Qin et al., **2020**; Schlenker & Roberts, **2009**).

Atmospheric Chemistry and Physics, vol. 22, issue no. 12, 8259-8285, doi:10.5194/acp-22-8259-2022

# An evaluation of liquid cloud droplet effective radius derived from MODIS, airborne remote sensing and in situ measurements from CAMP$^2$Ex

Fu, D., L. Di Girolamo, R.M. Rauber, G.M. McFarquhar, S.W. Nesbitt, J. Loveridge, Y. Hong, B. van Diedenhoven, **B. Cairns**[1], **M.D. Alexandrov**[1], P. Lawson, S. Woods, S. Tanelli[2], O.O. Sy, S. Schmidt, C.A. Hostetler[3], and A.J. Scarino, 2022

NASA Goddard Institute for Space Studies, New York, NY, USA[1]
NASA Jet Propulsion Laboratory, Pasadena, CA, USA[2]
NASA Langley Research Center, Hampton, VA, USA[4]

**Abstract.** The cloud drop effective radius ($R_e$) of the drop size distribution derived from passive satellite sensors is a key variable used in climate research. Validation of these satellite products has often taken place under stratiform cloud conditions that favor the assumption of cloud horizontal homogeneity used by the retrieval techniques. However, many studies have noted concerns with respect to significant biases in retrieved $R_e$ arising from cloud heterogeneity, for example, in cumulus cloud fields. Here, we examine data collected during the 2019 "Cloud, Aerosol and Monsoon Processes Philippines Experiment" (CAMP$^2$Ex), which, in part, targeted the objective of providing the first detailed evaluation of $R_e$ retrieved across multiple platforms and techniques in a cumulus and congestus cloud region. Our evaluation consists of cross-comparisons of $R_e$ between the Moderate Resolution Imaging Spectroradiometer (MODIS) onboard the Terra satellite, the Research Scanning Polarimeter (RSP) onboard the NASA P-3 aircraft, and in situ measurements from both the NASA P-3 and Learjet aircraft that are all taken in close spatiotemporal proximity to the same cloud fields. A particular advantage of our approach lies in the capability of the RSP to retrieve $R_e$ using a bi-spectral MODIS approach and a polarimetric approach, which allows for the evaluation of bi-spectral and polarimetric $R_e$ retrievals from an airborne perspective using the same samples.

Averaged over all P-3 flight segments examined here for warm clouds, the RSP polarimetric method, the in situ method, and the bias-adjusted MODIS method of Fu et al. (2019) show a comparable median (mean ± standard deviation) for the $R_e$ samples of 9.6 (10.2 ± 4.0) µm, 11.0 (13.6 ± 11.3) µm, and 10.4 (10.8 ± 3.8) µm, respectively. These values are far lower than the values of 15.1 (16.2 ± 5.5) µm and 17.2 (17.7 ± 5.7) µm from the bi-spectral retrievals of RSP and MODIS, respectively. Similar results are observed when $R_e$ is segregated by cloud-top height and in detailed case studies. The clouds sampled during CAMP$^2$Ex consist of mostly small (mean transect length ~ 1.4 km) and low clouds (mean cloud-top height ~ 1 km), which had more numerous small clouds than the trade wind cumuli sampled in past field campaigns such as Rain in Shallow Cumulus over the Ocean (RICO) and the Indian Ocean Experiment (INDOEX). The overestimates of $R_e$ from the RSP bi-spectral technique compared with the polarimetric technique increased as cloud size and cloud optical depth decreased. Drizzle, cloud-top bumpiness, and solar zenith angle, however, are not closely correlated with the overestimate of bi-spectral $R_e$. For shallow clouds that dominated the liquid cloud cover for the CAMP$^2$Ex region and period, we show that 3-D radiative transfer and cloud heterogeneity, particularly for the optically thin and small clouds, appear to be the leading cause of the large positive biases in bi-spectral retrievals. Because this bias varies with the underlying structure of the cloud field, caution continues to be warranted in studies that use bi-spectral $R_e$ retrievals in cumulus cloud fields.

**Introduction.** Satellite-retrieved cloud properties have been critical in advancing the understanding of the role of clouds in the Earth's climate system. However, the role of clouds in a changing climate still remains a dominant source of uncertainty in climate change predictions (IPCC, 2013). Efforts to improve the accuracy of our satellite record of cloud properties continue to be called for (Ohring et al., 2005; NASEM, 2018).

Bulletin of the American Meteorological Society, vol. 103, issue no. 2, pp. E429-E454, doi:10.1175/BAMS-D-20-0245.1

# Introducing and evaluating the Climate Hazards center IMErg with Stations (CHIMES) — Timely station-enhanced Integrated Multi-satellitE Retrievals for Global Precipitation Measurement

Funk, C.C., P. Peterson, G.J. Huffman[1], M.F. Landsfeld, C. Peters-Lidard[1], F. Davenport, S. Shukla, S. Peterson, D.H. Pedreros, **A.C. Ruane[2]**, **C.Z. Mutter[2,3]**, W. Turner, L. Harrison, A. Sonnier, J. Way-Henthorne, and J. Husak Gregory, 2022

NASA Goddard Space Flight Center, Greenbelt, MD, USA[1]
NASA Goddard Institute for Space Studies, New York, NY, USA[2]
Center for Climate Systems Research, Columbia University, New York, NY, USA[3]

**Abstract.** As human exposure to hydroclimatic extremes increase and the number of in situ precipitation observations declines, precipitation estimates, such as those provided by the Integrated Multisatellite Retrievals for Global Precipitation Measurement (GPM) (IMERG) mission, provide a critical source of information. Here, we present a new gauge-enhanced dataset [the Climate Hazards Center IMERG with Stations (CHIMES)] designed to support global crop and hydrologic modeling and monitoring. CHIMES enhances the IMERG Late Run product using an updated Climate Hazards Center (CHC) high-resolution climatology ($CHP_{clim}$) and low-latency rain gauge observations. $CHP_{clim}$ differs from other products because it incorporates long-term averages of satellite precipitation, which increases $CHP_{clim}$'s fidelity in data-sparse areas with complex terrain. This fidelity translates into performance increases in unbiased $IMERG_{late}$ data, which we refer to as CHIME. This is augmented with gauge observations to produce CHIMES. The CHC's curated rain gauge archive contains valuable contributions from many countries. There are two versions of CHIMES: preliminary and final. The final product has more copious and better-curated station data. Every pentad and month, bias-adjusted $IMERG_{late}$ fields are combined with gauge observations to create pentadal and monthly $CHIMES_{prelim}$ and $CHIMES_{final}$. Comparisons with pentadal, high-quality gridded station data show that $IMERG_{late}$ performs well ($r = 0.75$) but has some systematic biases which can be reduced. Monthly cross-validation results indicate that unbiasing increases the variance explained from 50% to 63% and decreases the mean absolute error from 48 to 39 mm month$^{-1}$. Gauge enhancement then increases the variance explained to 75%, reducing the mean absolute error to 27 mm month$^{-1}$.

**Introduction.** Accurate, timely, unbiased, consistent gauge-enhanced satellite precipitation can help understand and manage agricultural and hydrologic risks. Unfortunately, the number of global gauge observations is very low, covering an area of less than a single football field or soccer pitch (**Kidd et al. 2017**). Globally, the number of gauges1 has declined between 1981 and 2021, from about 32,000 to 14,000, while in Africa, the corresponding figures are just 3,400 and 600. These declines are caused by a combination of data policy and decaying observation and transmission systems. Precipitation thus remains a leading source of uncertainty for agroclimatic risk assessments and related agricultural modeling applications (**Ruane et al. 2021**). Gridded satellite rainfall datasets, therefore, provide a key resource for understanding weather, providing effective early warning, and assessing changes in extremes in a warming world (**Kirschbaum et al. 2017**). There are three primary categories of satellites used to study and quantify precipitation from space. The oldest category dates back to the Television and Infrared Observation Satellite (TIROS), which launched in 1960 and hosted imagers capable of capturing visible and infrared wavelength Earth observations (EOs). Modern descendants of TIROS occupy geostationary orbits over the equator. Circling in step with Earth's rotation, they provide continuous information about cloud-top temperatures (**Janowiak et al. 2001**; **Knapp et al. 2011**). These geostationary infrared (GEO-IR) observations, however, do not directly observe precipitation, but rather, just the highest layer of clouds and/or the land surface.

Atmospheric Measurement Techniques, vol. 15, issue no. 16, pp. 4859-4879, doi:10.5194/amt-15-4859-2022

# Effective uncertainty quantification for multi-angle polarimetric aerosol remote sensing over ocean, Part 1: Performance evaluation and speed improvement

Gao, M.[1,2], K. Knobelspiesse[1], B. Franz[1], P.-W. Zhai, A. Sayer[1,3], A. Ibrahim[1], **B. Cairns[4]**, O. Hasekamp, Y. Hu[1], V. Martins[3,5], J. Werdell[1], and X. Xu[3,5], 2022

NASA Goddard Space Flight Center, Greenbelt, MD, USA[1]
Science Systems and Applications, Inc., Greenbelt, MD, USA[2]
Goddard Earth Sciences Technology and Research (GESTAR) II, University of Maryland, Baltimore County, Baltimore, MD, USA[3]
NASA Goddard Institute for Space Studies, New York, NY, USA[4]
JCET and Physics Department, University of Maryland, Baltimore County, Baltimore, MD, USA[5]

**Abstract.** Multi-angle polarimetric (MAP) measurements can enable detailed characterization of aerosol microphysical and optical properties and improve atmospheric correction in ocean color remote sensing. Advanced retrieval algorithms have been developed to obtain multiple geophysical parameters in the atmosphere–ocean system. Theoretical pixel-wise retrieval uncertainties based on error propagation have been used to quantify retrieval performance and determine the quality of data products. However, standard error propagation techniques in high-dimensional retrievals may not always represent true retrieval errors well due to issues such as local minima and the nonlinear dependence of the forward model on the retrieved parameters near the solution. In this work, we analyze these theoretical uncertainty estimates and validate them using a flexible Monte Carlo approach. The Fast Multi-Angular Polarimetric Ocean coLor (FastMAPOL) retrieval algorithm, based on efficient neural network forward models, is used to conduct the retrievals and uncertainty quantification on both synthetic HARP2 (Hyper-Angular Rainbow Polarimeter 2) and AirHARP (airborne version of HARP2) datasets. In addition, for practical application of the uncertainty evaluation technique in operational data processing, we use the automatic differentiation method to calculate derivatives analytically based on the neural network models. Both the speed and accuracy associated with uncertainty quantification for MAP retrievals are addressed in this study. Pixel-wise retrieval uncertainties are further evaluated for the real AirHARP field campaign data. The uncertainty quantification methods and results can be used to evaluate the quality of data products, as well as guide MAP algorithm development for current and future satellite systems such as NASA's Plankton, Aerosol, Cloud, ocean Ecosystem (PACE) mission.

**Introduction.** Satellite remote sensing has revolutionized Earth observation capabilities and plays a significant role in studying atmosphere, ocean, and land systems. Remote sensing techniques have advanced rapidly to provide highly accurate geophysical property retrievals by utilizing the rich information content of observations at multiple spectral bands, viewing angles, and polarization states. Multi-angle polarimeters (MAPs) are particularly well suited to characterize aerosol microphysical properties (**Mishchenko and Travis**, **1997**; **Chowdhary et al.**, **2001**; **Hasekamp and Landgraf**, **2007**; **Knobelspiesse et al.**, **2012**). Improved aerosol characterization helps reduce uncertainties in aerosol radiative forcing estimates and thereby advances our understanding of Earth's climate (**Bender**, **2020**; **IPCC**, **2022**). Furthermore, better quantification of the aerosol path radiance in the atmosphere reduces error in the retrieval of spectral water-leaving radiances from ocean color remote sensing systems (**Mobley et al.**, **2016**; **Mobley**, **2022**), which is important for the study of aquatic phytoplankton dynamics, marine ecosystems, and the global carbon cycle (**Frouin et al.**, **2019**; **Groom et al.**, **2019**).

Quaternary International, vol. 622, pp. 21-35, doi:10.1016/j.quaint.2021.10.011

# Late Glacial and Holocene environmental variability, Lago Trasimeno, Italy

Gasperini, L.[2], **D.M. Peteet[1,3]**, E. Bonatti[2,3], E. Gambini, A. Polonia[2], J. Nichols[3], and L. Heusser, 2022

NASA Goddard Institute for Space Studies, New York, NY, USA[1]
Istituto di Scienze Marine, CNR, Bologna, Italy[2]
Lamont-Doherty Earth Observatory, Palisades, NY, USA[3]

**Abstract.** Lago Trasimeno (central Italy), 10 km wide and < 6m deep, fills a basin of **tectonic** origin, and is one of Europe's few endorheic lakes. We report on a multidisciplinary stratigraphic study based on **seismic reflection** profiles and two **sediment cores**, aimed at providing information on the vegetational, lithological, and climate history of this area. Trace elements, palynology, macrofossils, **organic carbon**, and C isotopes, coupled with AMS C-14 dating, describe environmental changes from Late-Glacial to present. The base of the cores records a Late-Glacial steppic vegetation (Poaceae, *Artemisia*, Amaranthaceae), with dry and cold conditions and a high charcoal/pollen ratio. An ensuing shift to a warmer and moister climate is shown by the rise of *Pinus* and *Quercus*, and shallow water aquatics such as *Nitella*. **Early Holocene** warming, indicated by *Quercus*, Oleaceae, *Corylus*, and *Betula*, is followed by a hiatus suggesting one or more severe drought events between 9000 and 3000 yr BP. Late **Holocene** presence of *Alnus* and *Fagus* indicates increased moisture, probably in winter, which would have increased lake level. Heavy metal pollution indicators (Pb, Cu, Zn) in the upper portion of the cores imply industrialization. Due to its location, to intensive and uninterrupted anthropogenic impacts since proto historical times, and to its shallow depths, Lago Trasimeno provides an important observation point for climate and environmental changes in the central **Mediterranean region** during and before **Holocene** times.

**Introduction.** Lago Trasimeno (43°09′N; 12°06′E), a large (~120 km$^2$) and unusually shallow (~3–6 m deep) circular lake (Fig. 1), located in the Umbria Region of central Italy, is the largest lake of peninsular Italy. One of the few endorheic lakes in Europe, Lago Trasimeno has no natural outlets; thus, seasonal flooding and desiccation events reflect local precipitation/evaporation and regional climatic variations (Cattuto et al., 2011). The shallow depth, the flat bottom morphology, and the absence of natural outflows and dams along its shorelines, caused periodical floods since ancient times, only partially attenuated by the creation of an artificial outflow in the XV century. Due to its location, Lago Trasimeno has been a natural crossroad since proto-historical times. The fields of Lago Trasimeno are well known as the site of a historic battle, when Carthaginians led by Hannibal defeated the Roman Legions in 217 BC. The location of the site, one of the largest ambushes in military history (16,500 dead), is controversial (Susini, 1960), although recent work points strongly towards the northwestern shores of Lago Trasimeno near the village of Tuoro (Brizzi and Gambini, 2008), as suggested by the presence of cremation pits and by historical reports. The concentration of ~29,000 Carthaginians and ~15,000 Romans in such a small area would have significantly impacted the lake and surrounding environment. However, despite the Battle's historical significance, little is known about possible effects on the lake. Using molecular markers as proxies for human and livestock occurrence, a recent study (Kirchgeog, 2015) identified evidence of the 217 BC Trasimeno battle in sediment core TR13_001. The lake acts today as a carbon sink due to the extensive reed (*Phragmites*, *Scirpus*, *Carex*) beds that line its shore (Landucci et al., 2011; Giardino et al., 2015).

The name *Trasimeno* apparently alludes to periodic severe droughts during the Bronze age (Ancillotti, 2008), as confirmed by archeological findings (Gambini, 2002; Angelini et al., 2014). Lake level oscillation, with alternating periods of drought and flood, continued during historical times and constituted a problem before the creation of the artificial outlet (Gambini, 1995, 2002).

Space Science Reviews, vol. 218, issue no. 56, doi:10.1007/s11214-022-00924-0

# The long-term evolution of the atmosphere of Venus: Processes and feedback mechanisms

Gillmann, C., **M.J. Way**[1,2], G. Avice, D. Breuer, G.J. Golabek, D. Honing, J. Krissansen-Totton, H. Lammer, A.-C. Plesa, M. Persson, J.G. O'Rourke, A. Salvador, M. Scherf, and M.Y. Zolotov, 2022

NASA Goddard Institute for Space Studies, New York, NY, USA[1]
Theoretical Astrophysics, Department of Physics and Astronomy, Uppsala University, Uppsala, Sweden[2]

**Abstract.** This work reviews the long-term evolution of the atmosphere of Venus, and modulation of its composition by interior/exterior cycling. The formation and evolution of Venus's atmosphere, leading to contemporary surface conditions, remain hotly debated topics, and involve questions that tie into many disciplines. We explore these various inter-related mechanisms which shaped the evolution of the atmosphere, starting with the volatile sources and sinks. Going from the deep interior to the top of the atmosphere, we describe volcanic outgassing, surface-atmosphere interactions, and atmosphere escape. Furthermore, we address more complex aspects of the history of Venus, including the role of Late Accretion impacts, how magnetic field generation is tied into long-term evolution, and the implications of geochemical and geodynamical feedback cycles for atmospheric evolution. We highlight plausible end-member evolutionary pathways that Venus could have followed, from accretion to its present-day state, based on modeling and observations. In a first scenario, the planet was desiccated by atmospheric escape during the magma ocean phase. In a second scenario, Venus could have harbored surface liquid water for long periods of time, until its temperate climate was destabilized, and it entered a runaway greenhouse phase. In a third scenario, Venus's inefficient outgassing could have kept water inside the planet, where hydrogen was trapped in the core and the mantle was oxidized. We discuss existing evidence and future observations/missions required to refine our understanding of the planet's history and of the complex feedback cycles between the interior, surface, and atmosphere that have been operating in the past, present or future of Venus.

**Introduction and Overview.** *In situ* and remote studies of Venus, numerical modelling and experimental work, as well as comparison with the Earth, inform us about the current state of Venus and can provide clues on its past (Fig. 1). Despite past missions and advances in computational models and experimental techniques, many uncertainties remain when it comes to which exact evolutionary pathway Venus has followed. The observation of Venus has challenged many of our assumptions on the evolution and present-day state of terrestrial planets. For example, before observations revealed its surface environment, Venus was imagined to be warm but temperate, while its surface proved to be dry and hot enough to melt lead (see O'Rourke et al. **2022**). The planet was thought to be geologically moribund or even dead, but data for the atmosphere and surface from numerous missions indicate that Venus might instead be an active world.

These advances, however, highlight the many gaps in our understanding of Venus. This is even more evident when it comes to Venus' past and its long-term evolution. Whether Venus could have sustained temperate surface conditions at any time during its evolution and for how long this could have lasted, is not known. Whether Venus could have had a magnetic field in the past, and when and why the core dynamo stopped operating is also unknown. What convection regime is most representative for the interior dynamics of Venus, if and how it changed over the planet's history, and what became of Venus's water, are difficult to constrain with current data (see Rolf et al. **2022**, for a detailed review). Even Venus' present-day mantle convection regime is peculiar, lacking the subduction zones and the clear dichotomy between continental and oceanic crust we see on Earth, it also displays more traces of horizontal motion and deformation than the clear stagnant lids operating on Mars and Mercury. For these reasons we label it as single plate planet in this manuscript. In fact, one of the main challenges for reconstructing Venus' evolution is that many observations defy straightforward interpretation. Instead, present-day measurements depend on the cumulative effects of many mechanisms. A good example of this is the high D/H ratio measured for the atmosphere of Venus, indicative of strong fractionation relative to the Earth (Donahue et al. **1982**; De Bergh et al. **1991**).

Astrobiology, vol. 22, issue no. 10, pp. 1222-1238, doi:10.1089/ast.2021.0171

# Water Vapor Adsorption Provides Daily, Sustainable Water to Soils of the Hyperarid Atacama

**Glaser, D.M.**[1,2], H.E. Hartnett[2], D.R. Finn, S. Perez-Montaño, H. Cadillo-Quiroz[2,3], and S. Desch, 2022

NASA Goddard Institute for Space Studies, New York, NY, USA[1]
School of Molecular Sciences, Arizona State University, Tempe, Arizona, USA[2]
Biodesign Institute, Arizona State University, Tempe, Arizona, USA[3]

**Abstract.** Water is necessary for all life on Earth. Water is so critical that organisms have developed strategies to survive in hyperarid environments. These regions with extremely low water availability are also unique analogs in which to study the physicochemical conditions of extraterrestrial environments such as Mars. We have identified a daily, sustainable cycle of water vapor adsorption (WVA) and desorption that measurably affects soil water content (SWC) in the hyperarid region of the Atacama Desert in southern Perú. We pair field-based soil temperature and relative humidity soil profiles with laboratory simulations to provide evidence for a daily WVA cycle. Using our WVA model, we estimate that one adsorptive period—one night—increases SWC by 0.2–0.3 mg/g of soil (~30 μm rainfall). We can plausibly rule out other water inputs during our field campaign that could account for this water input, and we provide evidence that this WVA cycle is driven by solar heating and maintained by atmospheric water vapor. The WVA may also serve to retain water from infrequent rain events in these soils. If the water provided by WVA in these soils is bioavailable, it could have significant implications for the microorganisms that are endemic to hyperarid environments.

**Introduction.** Water is necessary for all known life on Earth. However, life has developed strategies to survive all sorts of environments from freshwater lakes and tropical rainforests to hypersaline lakes and hyperarid deserts. In the search for life elsewhere, NASA has pursued a "follow the water" strategy to investigate the most probable targets for life contingent on the presence of liquid water. Our nearest neighbors in the solar system are dry, inhospitable places. However, scientists have been searching over the past several decades for life on these dry planets.

Mars is an extraordinarily dry planet, having lost virtually all its surface water ~1 Ga through interaction with the solar wind (Terada *et al.*,**2009**; Kite, **2019**). Water on modern Mars, though scarce, is almost entirely present as ice located in the polar caps and in the subsurface of higher latitudes (Piqueux *et al.*,**2019**). Smaller non-ice reservoirs of water include (1) atmospheric vapor (~20–160 ppmv) (Savijärvi *et al.*,**2015**; Fedorova *et al.*,**2021**), (2) ephemeral deliquescent brines (Rennó *et al.*,**2009**; Toner and Catling, **2018**), and (3) regolith adsorbed vapor (~0.5–1.5 weight percent [wt %]) (Beck *et al.*,**2010**; Steele *et al.*,**2017**). Recent work has also incited a robust debate as to the presence of hypersaline lakes in the subsurface below the southern polar cap (Lauro *et al.*,**2021**; Smith *et al.*,**2021**).

Hyperarid environments (defined as an aridity index, the ratio of evapotranspiration to rain, of ≤0.05) (Bastin *et al.*,**2017**) are one of the best terrestrial analogs from which to understand the physical and chemical conditions on Mars and, eventually, arid exoplanets. The hyperarid, ecological region of the Atacama Desert, which spans Perú and Chile, is one of the driest environments on Earth and is a reasonably accessible place that mimics aspects of martian conditions (Houston and Hartley, **2003**; Narvaez-Montoya *et al.*,**2022**).

Water inputs to the Atacama soils are rare and meager (~2 mm/year) due to the rain shadow effect from the Andes (Houston and Hartley, **2003**). Rain and fog events occur between ~1 and 10 times per year on average, respectively (McKay *et al.*, 2003; Valdivia-Silva *et al.*, 2012). Despite the infrequency of rain and fog events, viable cells are found in the top tens of cm in these soils (Navarro-Gonzalez *et al.*,**2003**; Valdivia-Silva *et al.*,**2011**; Schulze-Makuch *et al.*,**2018**).

Environmental Research Letters, vol. 17, issue no. 4, 045021, doi:10.1088/1748-9326/ac5fa1

# Climate drivers of global wildfire burned area

Grillakis, M., A. Voulgarakis, A. Rovithakis, K.D. Seiradakis, A. Koutroulis, **R.D. Field**[1,2], M. Kasoar, A. Papadopoulos, and M. Lazaridis, 2022

NASA Goddard Institute for Space Studies, New York, NY, USA[1]
Department of Applied Physics and Applied Mathematics, Columbia University, New York, NY, USA[2]

**Abstract.** Wildfire is an integral part of the Earth system, but at the same time it can pose serious threats to human society and to certain types of terrestrial ecosystems. Meteorological conditions are a key driver of wildfire activity and extent, which led to the emergence of the use of fire danger indices that depend solely on weather conditions. The Canadian Fire Weather Index (FWI) is a widely used fire danger index of this kind. Here, we evaluate how well the FWI, its components, and the climate variables from which it is derived, correlate with observation-based burned area (BA) for a variety of world regions. We use a novel technique, according to which monthly BA are grouped by size for each Global Fire Emissions Database (GFED) pyrographic region. We find strong correlations of BA anomalies with the FWI anomalies, as well as with the underlying deviations from their climatologies for the four climate variables from which FWI is estimated, namely, temperature, relative humidity, precipitation, and wind. We quantify the relative sensitivity of the observed BA to each of the four climate variables, finding that this relationship strongly depends on the pyrographic region and land type. Our results indicate that the BA anomalies strongly correlate with FWI anomalies at a GFED region scale, compared to the strength of the correlation with individual climate variables. Additionally, among the individual climate variables that comprise the FWI, relative humidity and temperature are the most influential factors that affect the observed BA. Our results support the use of the composite fire danger index FWI, as well as its sub-indices, the Build-Up Index (BUI) and the Initial Spread Index (ISI), comparing to single climate variables, since they are found to correlate better with the observed forest or non-forest BA, for the most regions across the globe.

**Introduction.** Due to the existence of vegetation, atmospheric oxygen, and the widespread presence of ignition sources, wildfire has been an integral part of many of the Earth's terrestrial ecosystems [1]. Wildfires comprise a significant source of greenhouse gases and aerosols playing a key role in atmospheric radiative forcing and air quality [2–4]. In densely populated regions with extensive wildland-urban interface, wildfires usually have a direct impact in terms of fire suppression financial cost, homes and infrastructure damages, crops and livestock losses and, most importantly, human losses, injuries, long-term health implications [5] and other socioeconomic impacts [6].
Wildfire activity is controlled by weather and climate parameters either in a time window of several months by controlling biomass growth and snowpack accumulation and hence fire fuel availability, or in shorter term by determining vegetation and duff layer moisture content and, hence, their flammability [7–10]. Analyzing wildfire activity at a global scale for different ecoregions, Abatzoglou *et al* [11] showed that climate variability can explain one-third of the interannual variability in burned area (BA), highlighting the controlling role of climate parameters. Further studies at a global scale have shown that temperature related indicators are the best climate predictors for BA [12, 13]. Furthermore, climate forcings on wildfire activity vary by climatic region. For example, large boreal forest fires of North America, have been correlated to weather patterns that associate with strong winds, and low precipitation conditions [14]. Ying *et al* [15], indicated that the most important climate related ignition factor for the Chinese province of Yunnan is relative humidity. For Europe, significant correlation has been detected between large wildfires and high temperature for Spain [16, 17], as well as for Italy [18], but also for Greece, along with other variables [19] such as humidity and high pressure. Further studies have shown that severe fire weather conditions associate with specific synoptic-scale atmospheric circulation patterns [20, 21]. Additional factors affecting wildfire activity and the resulting BA include land-use modification Kelley *et al* [22], as well as human fire ignitions and fire suppression media [23].

Environmental Research Letters, vol. 17, issue no. 12, 124045, doi:10.1088/1748-9326/aca77c

# Evidence for increasing global wheat yield potential

**Guarin, J.R.**, P. Martre, F. Ewert, H. Webber, S. Dueri, D. Calderini, M. Reynolds, G. Molero, D. Miralles, G. Garcia, G. Slafer, F. Giunta, D. Noleto Luz Pequeno, T. Stella, M. Ahmed, P.D. Alderman, B. Basso, A.G. Berger, M. Bindi, G. Bracho Mujica, D. Cammarano, Y. Chen, B. Dumont, E. Eyshi Rezaei, E. Fereres, R. Ferrise, T. Gaiser, Y. Gao[2], M. Garcia-Vila, S. Gayler, Z. Hochman, G. Hoogenboom[2,4], L.A. Hunt, C. Kersebaum, C. Nendel, J. Olesen, T. Palosuo, E. Priesack, J. Pullens, A. Rodriguez, R.P. Rötter, M. Ruiz-Ramos, M.A. Semenov, N. Senapati, S. Siebert, A.K. Srivastava, C.O. Stöckle, I. Supit, F. Tao, P.J. Thorburn, E. Wang, T.K.D. Weber, L. Xiao, Z. Zhang, C. Zhao, J. Zhao, Z. Zhao, Y. Zhu, and S. Asseng, 2022

NASA Goddard Institute for Space Studies, New York, NY, USA[1]
Agricultural & Biological Engineering Department, University of Florida, Gainesville, FL, USA[2]
Center for Climate Systems Research, Columbia University, New York, NY, USA[3]
Institute for Sustainable Food Systems, University of Florida, Gainesville, FL, USA[4]

**Abstract.** Wheat is the most widely grown food crop, with 761 Mt produced globally in 2020. To meet the expected grain demand by mid-century, wheat breeding strategies must continue to improve upon yield-advancing physiological traits, regardless of climate change impacts. Here, the best performing doubled haploid (DH) crosses with an increased canopy photosynthesis from wheat field experiments in the literature were extrapolated to the global scale with a multi-model ensemble of process-based wheat crop models to estimate global wheat production. The DH field experiments were also used to determine a quantitative relationship between wheat production and solar radiation to estimate genetic yield potential. The multi-model ensemble projected a global annual wheat production of 1050 ± 145 Mt due to the improved canopy photosynthesis, a 37% increase, without expanding cropping area. Achieving this genetic yield potential would meet the lower estimate of the projected grain demand in 2050, albeit with considerable challenges.

**Introduction.** The global demand for food is continuously increasing and agricultural production must follow to ensure future global food security [1–5]. Wheat (*Triticum aestivum* L.) is one of the most important crops contributing to global food security, providing approximately 20% of calories and protein in the human diet [6]. Although global wheat production has continued to increase over recent decades [7], the rate of yield improvement has stagnated or declined in certain regional wheat-producing areas (e.g. Eastern Europe, Central India, and Western Australia) [8] and projected yield gains fall below the predicted future grain demand [3, 9, 10]. Grain production increases between 35%–56% (30%–62% when accounting for climate change) are needed to meet the projected global food demand by 2050 (relative to 2010 food demand) [11], while endeavoring to improve environmental sustainability and land preservation [2, 12]. Breeding new cultivars to further increase yield potential in high-yielding environments [13] is one approach to address the food security challenge [14], with the advantage that yields in poorer growing conditions could still increase [6, 15]. Investment in yield improvements and intensification can also mitigate greenhouse gas emissions [16]. Improving physiological traits that have a profound influence on the growth and yield of wheat, such as radiation use efficiency (RUE, biomass accumulation per unit of radiation intercepted by crop canopies), is of paramount importance to meeting the future grain demand [17, 18]. Estimates from the literature show that the RUE of current wheat could be increased by up to 50% under favorable crop-growing conditions [6, 19]. Doubled haploid (DH) crosses with modified traits such as RUE, light extinction coefficient, fruiting efficiency, grain filling duration, and grain size can increase yield potential compared to conventional wheat cultivars [15, 20, 21].

Global wheat yield gap analyses examine the difference between the potential yield (yield of well-adapted wheat cultivars grown with sufficient water and nutrients and without abiotic and biotic stress) and the average actual yield reported by farmers under conventional management practices [22]. Quantifying the yield potential provides a benchmark for future crop production and a guide for the sustainable intensification of agriculture. However, global yield potential analyses have not yet considered the improved genetic yield potential from advancements in physiological traits which would quantify the extent of potential genetic improvements.

Geoscientific Model Development, vol. 15, issue no. 15, pp. 6243-6257, doi:10.5194/gmd-15-6243-2022

# Checkerboard patterns in E3SMv2 and E3SM-MMFv2

Hannah, W.M., K.G. Pressel, M. Ovchinnikov, and **G.S. Elsaesser**[1,2], 2022

NASA Goddard Institute for Space Studies, New York, NY, USA[1]
Department of Applied Physics and Applied Mathematics, Columbia University, New York, NY, USA[2]

**Abstract.** An unphysical checkerboard pattern is identified in E3SMv2 and E3SM-MMF that is detectable across a wide range of timescales, from instantaneous snapshots to multi-year averages. A detection method is developed to quantify characteristics of the checkerboard signal by cataloguing all possible configurations of the eight adjacent neighbors for each cell on the model's cubed sphere grid using daily mean data. The checkerboard pattern is only found in cloud-related quantities, such as precipitation and liquid water path. Instances of pure and partial checkerboard are found to occur more often in E3SMv2 and E3SM-MMF when compared to satellite data re-gridded to the model grid. Continuous periods of partial checkerboard state are found to be more persistent in both models compared to satellite data, with E3SM-MMF exhibiting more persistence than E3SMv2. The checkerboard signal in E3SMv2 is found to be a direct consequence of the recently added deep convective trigger condition based on dynamically generated CAPE (DCAPE). In E3SM-MMF the checkerboard signal is found to be associated with the "trapping" of cloud-scale fluctuations within the embedded cloud-resolving model. Solutions to remedy this issue are discussed.

**Introduction.** The representation of moist convection is a critically important feature of an atmospheric general circulation model (GCM), but these processes are often parameterized with simplified models because explicitly simulating all scales of moist convection is too computationally expensive. The multi-scale modeling framework (MMF), or super-parameterization, was conceived as an economical way to include an explicit representation of some scales of moist convection in a GCM by embedding a cloud-resolving model (CRM) in each column of the parent GCM(**Grabowski and Smolarkiewicz**, **1999**; **Grabowski**, **2001**; **Randall et al.**, **2003**; **Khairoutdinov et al.**, 2005).

The embedded CRM significantly increases the model's overall computational cost, but the overall cost is still orders of magnitude lower than a global convection-resolving model. The way in which the two models of an MMF are coupled allows unique algorithmic and hardware acceleration methods that bring the cost in line with traditional GCMs (**Hannah et al.**, **2020**).

A notable trade-off of the MMF method is that there is a "scale gap" between the resolved scales of the GCM and CRM where neither model represents the relevant processes (see Fig. **1**). The MMF method couples the two models through forcing and feedback tendencies formulated such that the domain mean thermodynamic state of the CRM and its parent GCM columns cannot drift apart. A related consequence of the scale gap is that the internal spatial variability of the CRM cannot be advected by the GCM flow and remain "trapped" in the CRM. Thus, the propagation of signals organized within the CRM can only happen indirectly through the coupling of the CRM domain mean (**Pritchard et al.**, **2011**).

Most MMF results in the literature use a global host model with a finite-volume grid that produces a smooth solution (**Khairoutdinov et al.**, **2005**; **Benedict and Randall**, **2009**). However, results from the MMF configuration of the DOE Energy Exascale Earth System Model (E3SM-MMF) revealed a strong grid-imprinting signal related to the use of the spectral element grid (**Hannah et al.**, **2020**). This problem is hypothesized to be related to "cusps" in the solution that can form due to discontinuous derivatives at the shared spectral element edges. These occasional cusps lead to noise in the vertical velocity field (**Herrington et al.**, **2019b**), which the embedded CRMs in E3SM-MMF are notably more sensitive to compared to traditional convective parameterizations. The analysis of **Hannah et al.** (**2020**) did not relate the grid-imprinting signal to the trapping of CRM fluctuations, but a connection could not be ruled out.

Nature, vol. 605, pp. 26-29, doi:10.1038/d41586-022-01192-2

# Climate simulations: Recognize the 'hot model' problem

Hausfather, Z., **K. D. Marvel**[1,2], **G.A. Schmidt**[1], J.W. Nielsen-Gammon, and M. Zelinka, 2022

NASA Goddard Institute for Space Studies, New York, NY, USA[1]
Center for Climate Systems Research, Columbia University, New York, NY, USA[2]

**Abstract.** The sixth and latest IPCC assessment weights climate models according to how well they reproduce other evidence. Now the rest of the community should do the same.

**Introduction.** Computer models that project future climates are widely used for adaptation, mitigation and resilience planning. More than 50 such models were assessed and compared in the latest round of the Coupled Model Intercomparison Project, phase 6 (CMIP6), run by the World Climate Research Programme[1]. It is crucial that researchers know the best way to use those outputs to provide consistent information for climate science and policy.

We are climate modelers and analysts who develop, distribute and use these projections. We know scientists must treat them with great care. Users beware: a subset of the newest generation of models are 'too hot'[2] and project climate warming in response to carbon dioxide emissions that might be larger than that supported by other evidence[3–7]. Some suggest that doubling atmospheric $CO_2$ concentrations from pre-industrial levels will result in warming above 5 °C, for example. This was not the case in previous generations of simpler models.

Earth is a complicated system of interconnected oceans, land, ice and atmosphere, and no computer model could ever simulate every aspect of it exactly. Models vary in their complexity, and each makes different assumptions about and approximations of processes that happen on small scales, such as cloud formation.

The CMIP6 models include more sophisticated treatments of ice, water and clouds than earlier ones did, including those in phase 5 (CMIP5). The latest models also include a wider variety of physical processes than before. As models become more realistic, they are expected to converge. In the meantime, individual improvements can affect how sensitive the models are to certain warming processes, in ways that are often impossible to predict.

The Intergovernmental Panel on Climate Change (IPCC), to its credit, has recognized this 'hot model' problem. Scientists contributing to the main sections of its Sixth Assessment Report (AR6; published over the past few months) reconciled the newest climate models with key observational constraints on global mean warming, sea-level rise and ocean heat content, and other analyses. They applied statistics to determine the most reasonable projections, consistent with many lines of evidence, which they call 'assessed warming'.

Unfortunately, little guidance was made available for scientists wishing to study projections in other contexts. We are concerned that in the absence of such guidance, much of the scientific literature is at risk of reporting projections that are inconsistent with the approach taken by the IPCC, and that are overly influenced by the hot models.

Studies that cover monthly or daily extremes or regional climate impacts, for example, are instead left to use the full set of CMIP6 models. And simply taking an average of those leads to higher projections of warming than the IPCC's assessed-warming averages. As a result, some studies have reported projections that might be inconsistent with AR6 assessments. Findings that show projected climate change will be 'worse than we thought' are often attributable to the hot models in CMIP6.

It is important to emphasize that, whereas unduly hot outcomes might be unlikely, this does not mean that global warming is not a serious threat. Multiple lines of evidence establish that the planet is more than 1 °C warmer than it was before the Industrial Revolution, and that further warming poses severe risks to society and the natural world. ]

Environmental Research Letters, vol. 17, issue no. 12, 124040, doi:10.1088/1748-9326/aca68b

# Impacts of climate change on global food trade networks

Hedlund, J., H. Carlsen, S. Croft, C. West, Ö. Bodin, E. Stokeld, **J. Jägermeyr**[1,2,3], and C. Müller[3], 2022

NASA Goddard Institute for Space Studies, New York, NY, USA[1]
Center for Climate Systems Research, Columbia University, New York, NY, USA[2]
Potsdam Institute for Climate Impact Research (PIK), Potsdam, Germany[3]

**Abstract.** Countries' reliance on global food trade networks implies that regionally different climate change impacts on crop yields will be transmitted across borders. This redistribution constitutes a significant challenge for climate adaptation planning and may affect how countries engage in cooperative action. This paper investigates the long-term (2070–2099) potential impacts of climate change on global food trade networks of three key crops: wheat, rice and maize. We propose a simple network model to project how climate change impacts on crop yields may be translated into changes in trade. Combining trade and climate impact data, our analysis proceeds in three steps. First, we use network community detection to analyse how the concentration of global production in present-day trade communities may become disrupted with climate change impacts. Second, we study how countries may change their network position following climate change impacts. Third, we study the total climate-induced change in production plus import within trade communities. Results indicate that the stability of food trade network structures compared to today differs between crops, and that countries' maize trade is least stable under climate change impacts. Results also project that threats to global food security may depend on production change in a few major global producers, and whether trade communities can balance production and import loss in some vulnerable countries. Overall, our model contributes a baseline analysis of cross-border climate impacts on food trade networks.

**Introduction.** Higher temperatures will significantly modify the production of crops (Parry *et al* **2004**, Wheeler and Braun **2013**, Challinor *et al* **2016**, Bezner Kerr *et al* **2022**). This impact constitutes a threat not only to individual producing countries but, because of an acceleration in countries' dependence on overseas trade for food supply, also to global food security (D'Odorico *et al* **2014**, Janssens *et al* **2020**). Disrupted production in one or a few countries can induce changes in the food trade network as a whole (Puma *et al* **2015**), which is a primary example of cross-border impacts of climate change (Bren D'Amour *et al* **2016**, Hedlund *et al* **2018**, Adams *et al* **2021**, Carter *et al* **2021**, Lager and Benzie **2022**). Such redistribution of global climate risk constitutes a significant challenge for climate adaptation with regards to international cooperation (Challinor *et al* **2017**).

Global food trade networks consist of densely connected trade communities (Torreggiani *et al* **2018**, Gutiérrez-Moya *et al* **2021**), in which countries (i.e. nodes) have a higher number of within-community trade relationships (i.e. links) than they have relations with countries outside their community. Networks with clearly distinguishable, but only loosely connected, communities can have stabilising effects on certain changes within networks, such as limiting 'domino effects' of risks (May *et al* **2008**, Scheffer *et al* **2012**). However, the extent to which climate change impacts may change the structure of trade networks remains unknown.

This paper investigates how trade patterns between countries may be disrupted and reoriented under potential long-term (2070–2099) climate change impacts on food production. Using trade data for three key staple crops (wheat, rice and maize), we propose a baseline model for analysing potential structural redistributions of global food trade networks as a consequence of climate-induced production changes. We test the model for the three crops and develop projections by linking data on future climate impacts and current trade. Projected results are compared to present-day trade in order to assess the relative levels of disruption. For this, we use network community detection and functional cartography to analyse how trade community structures and countries' network roles change following adjustments to countries' trade patterns. The analysis is especially focused on identifying differences in structural changes across the selected key staple crops, and how trade might be concentrated differently compared to present-day. Our analysis is not a prediction of future trade.

Environmental Research Letters, vol. 17, issue no. 4, 044026, doi:10.1088/1748-9326/ac592e

# Global gridded crop models underestimate yield responses to droughts and heatwaves

Heinicke, S.[2], K. Frieler[2], **J. Jägermeyr[1,2,3]**, and M. Mengel[2], 2022

NASA Goddard Institute for Space Studies, New York, NY, USA[1]
Potsdam Institute for Climate Impact Research (PIK), Potsdam, Germany[2]
Center for Climate Systems Research, Columbia University, New York, NY, USA[3]

**Abstract.** Extreme events can lead to crop yield declines, resulting in financial losses and threats to food security, and the frequency and intensity of such events is projected to increase. As global gridded crop models (GGCMs) are commonly used to assess climate change impacts on agricultural yields, there is a need to understand whether these models are able to reproduce the observed yield declines. We evaluated 13 GGCMs from the Inter-Sectoral Impact Model Intercomparison Project and compared observed and simulated impact of past droughts and heatwaves on yields for four crops (maize, rice, soy, wheat). We found that most models detect but underestimate the impact of droughts and heatwaves on yield. Specifically, the drought signal was detected by 12 of 13 models for maize and all models for wheat, while the heat signal was detected by eleven models for maize and six models for wheat. To investigate whether the difference between simulated and observed yield declines is due to a misrepresentation of simulated exposure to heat or water scarcity (i.e., misrepresentation of growing season), we analysed the relationship between average discrepancies between observed and simulated yield losses, and average simulated exposure to extreme weather conditions across all crop models. We found a positive correlation between simulated exposure to heat and model performance for heat waves but found no correlation for droughts. This suggests that there is a systematic underestimation of yield responses to heat and drought and not only a misrepresentation of exposure. Assuming that performance for the past indicates models' capacity to project future yield impacts, models likely underestimate future yield decline from climate change. High-quality temporally and spatially resolved observational data on growing seasons will be highly valuable to further improve crop models' capacity to adequately respond to extreme weather events.

**Introduction.** Crop yields are strongly impacted by weather conditions (Frieler *et al* **2017**, Müller *et al* **2017**, FAO **2018**). Especially extreme weather events, such as droughts and heatwaves, can have detrimental impacts on crop yields (Lesk *et al* **2016**). Yield variability in turn affects food supply and prices (FAO **2018**), and ultimately livelihoods of farmers and those consumers that spend a large proportion of their income on food. As more than 20% of food is traded internationally (D'Odorico *et al* **2014**), local production shocks can have global impacts especially for countries relying on food imports, such as during the 2008/2010 spike in food prices (Maetz *et al* **2011**).

Over the last decades, the frequency and strength of extreme weather events increased substantially, and this trend will likely continue (Morales *et al* **2020**, Perkins-Kirkpatrick and Lewis **2020**). In addition, the likelihood of multiple regions being affected at the same time is increasing, which could exacerbate negative impacts on agricultural production (Gaupp *et al* **2020**). To inform agricultural practices, spatial planning, or the development of insurance policies for farmers, there is a need to better understand yield responses to weather disturbances to improve future projections under climate change.

Global gridded crop models (GGCMs) have been developed to assess how climate change and agricultural management might impact crop yields (Müller *et al* **2017**, Jägermeyr *et al* **2021**). To enable model intercomparison the Agricultural Model Intercomparison and Improvement Project (AgMIP) and the Inter-Sectoral Impact Model Intercomparison Project (ISIMIP) provide common modelling protocols describing a harmonized simulation setup. It has been tested how much of the annual variability of crop yields can be explained by weather fluctuations with strong differences in performance between countries, crops and models (Frieler *et al* **2017**, Müller *et al* **2017**, **2019**).

Geoscientific Model Development, vol. 15, issue no. 5, pp. 1931-1952, doi:10.5194/gmd-15-1931-2022

# A new snow module improves predictions of isotope-enabled MAIDENiso forest growth model

Hermoso de Mendoza, I., E. Boucher, F. Gennaretti, A. Lavergne, L. Andreu-Hayles, and **R.D. Field**[1,2], 2022

NASA Goddard Institute for Space Studies, New York, NY, USA[1]
Applied Physics and Applied Mathematics, Columbia University, New York, NY, USA[2]

**Abstract.** The representation of snow processes in forest growth models is necessary to accurately predict the hydrological cycle in boreal ecosystems and the isotopic signature of soil water extracted by trees, photosynthates and tree-ring cellulose. Yet, most process-based models do not include a snow module; consequently, their simulations may be biased in cold environments. Here, we modified the MAIDENiso model to incorporate a new snow module that simulates snow accumulation, melting and sublimation, as well as thermal exchanges driving freezing and thawing of the snow and the soil. We tested these implementations in two sites in eastern and western Canada for black spruce (*Picea mariana* (Mill.) B.S.P.) and white spruce (*Picea glauca* (Moench) Voss) forests, respectively. The new snow module improves the skills of the model to predict components of the hydrological cycle. The MAIDENiso model is now able to reproduce the spring discharge peak and to simulate stable oxygen isotopes in tree-ring cellulose more realistically than in the original snow-free version of the model. The new implementation also results in simulations with a higher contribution from the source water on the oxygen isotopic composition of the simulated cellulose, leading to more accurate estimates of cellulose isotopic composition. Future work may include the development of inverse modelling with this new version of MAIDENiso to produce robust reconstructions of the hydrological cycle and isotope processes in cold environments.

**Introduction.** In boreal regions of Canada and Alaska, snow represents about 30 %–50 % of total precipitation (**Mesinger et al.**, **2006**). This feature has a notable influence on hydrological and ecological system functioning in these cold environments (**Beria et al.**, **2018**). From a hydrological perspective, snowpack dynamics greatly influence water infiltration in soils, groundwater and aquifer replenishment, runoff production, and water supplies to both natural and artificial water bodies during spring flood (**Li et al.**, **2017**; **Barnhart et al.**, **2016**; **Berghuijs et al.**, **2014**). From an ecological perspective, snowpack accumulation protects exposed plant tissues and organs against cold winds (**Boivin and Bégin**, **1997**). Snowmelt contributes to mitigate the negative impacts of droughts on tree growth (**St. George et al.**, **2009**), while affecting photosynthesis (**Perkins and Swetnam**, **1996**; **Peterson and Peterson**, **1994**). Snowpack dynamics also have the potential to alter heat fluxes, temperature and depth of freezing in soils, all of which can impact the timing of critical ecophysiological processes that drive growth in high-latitude forest stands.

For decades, tree-ring proxies such as ring widths (**Nicault et al.**, **2015**; **Ols et al.**, **2018**), wood density (**Boucher et al.**, **2017**) or stable isotope ratios of tree-ring cellulose (**Naulier et al.**, **2015b**, **2014**; **Porter et al.**, **2014**) have been used to track inter-annual changes in forest response to climate variability. Most studies emphasized the dominant role of summer temperatures on key ecophysiological processes controlling proxy formation.

This has helped to clarify the response mechanisms of the boreal forest to growing-season temperatures (**Gennaretti et al.**, **2017a**) and enabled long, millennial summer temperature reconstructions to be produced in this region (**Gennaretti et al.**, **2017a**, **b**; **Naulier et al.**, **2015a**). However, despite their ecological and hydrological significance, snow-related processes were rarely taken into account in these tree-ring studies (**Coulthardet al.**, **2021**; **Woodhouse**, **2003**; **Huang et al.**, **2019**; **Zhu et al.**, **2021**).

Atmospheric Chemistry and Physics, vol. 22, issue no. 2, pp. 711-724, doi:10.5194/acp-22-711-2022

# Updraft dynamics and microphysics: On the added value of the cumulus thermal reference frame in simulations of aerosol-deep convection interactions

Hernandez-Deckers, D., T. Matsui[1,2], and **A.M. Fridlind[3]**, 2022

Mesoscale Atmospheric Processes Laboratory, NASA Goddard Space Flight Center, Greenbelt, MD, USA[1]
Earth System Science Interdisciplinary Center – ESSIC, University of Maryland, College Park, MD, USA[2]
NASA Goddard Institute for Space Studies, New York, NY, USA[3]

**Abstract.** One fundamental question about atmospheric moist convection processes that remains debated is whether, or under which conditions, a relevant variability in background aerosol concentrations may have a significant dynamical impact on convective clouds and their associated precipitation. Furthermore, current climate models must parameterize both the microphysical and the cumulus convection processes, but this is usually implemented separately, whereas in nature there is a strong coupling between them. As a first step to improve our understanding of these two problems, we investigate how aerosol concentrations modify key properties of updrafts in eight large-eddy-permitting regional simulations of a case study of scattered convection over Houston, Texas, in which convection is explicitly simulated and microphysical processes are parameterized. Dynamical and liquid-phase microphysical responses are investigated using the following two different reference frames: static cloudy updraft grid cells versus tracked cumulus thermals. In both frameworks, we observe the expected microphysical responses to higher aerosol concentrations, such as higher cloud number concentrations and lower rain number concentrations. In terms of the dynamical responses, both frameworks indicate weak impacts of varying aerosol concentrations relative to the noise between simulations over the observationally derived range of aerosol variability for this case study. On the other hand, results suggest that thermals are more selective than cloudy updraft grid cells in terms of sampling the most active convective air masses. For instance, vertical velocity from thermals is significantly higher at upper levels than when sampled from cloudy updraft grid points, and several microphysical variables have higher average values in the cumulus thermal framework than in the cloudy updraft framework. In addition, the thermal analysis is seen to add rich quantitative information about the rates and co-variability of microphysical processes spatially and throughout tracked thermal lifecycles, which can serve as a stronger foundation for improving sub-grid scale parameterizations.

**Introduction.** The net impacts of atmospheric aerosol concentration on deep convective cloud systems and their environment remain highly uncertain, with mixed results that do not generally yield conclusive answers yet (e.g., **Khain et al.**, **2008**; **Tao et al.**, **2012**). All else being equal, a higher aerosol concentration generally corresponds to more condensation nuclei at any given supersaturation, which, in turn, is expected to produce more but smaller cloud droplets within a convective updraft. This may delay the occurrence of initial warm precipitation formation due to a less efficient collision–coalescence process, enhancing latent heat release above the freezing level (**Rosenfeld et al.**, **2008**). However, when or if this has a substantial impact on the amount or intensity of cold precipitation is not clear due to the uncertainties of subsequent ice and mixed-phase microphysics (e.g., **Korolev et al.**, **2020**) and the complex morphology and feedback of deep convective clouds under various environmental conditions (e.g., **Tao et al.**, **2012**; **Fan et al.**, **2016**; **Abbott and Cronin**, 2021). One approach, to reduce such complexities to some degree, is to focus on aerosol–cloud interactions in relatively isolated convective cells (e.g., **Fridlind et al.**, **2019**), where the various mechanisms by which aerosol may impact updraft properties remain operative.

The recent Aerosol, Cloud, Precipitation and Climate (ACPC) working group model intercomparison project (MIP) compared regional model simulations of such scattered convection in response to a realistic dynamic range of ambient aerosol concentration profiles with similar large-scale forcing.

Environmental Research Letters, vol. 17, issue no. 5, 054003, doi:10.1088/1748-9326/ac61c7

# Economic incentives modify agricultural impacts of nuclear war

Hochman, G., H. Zhang, L. Xia, A. Robock, S. Aleti, D. van der Mensbrugghe, and **J. Jägermeyr**[1,2,3], 2022

NASA Goddard Institute for Space Studies, New York, NY, USA[1]
Center for Climate Systems Research, Columbia University, New York, NY, USA[2]
Potsdam Institute for Climate Impact Research (PIK), Potsdam, Germany[3]

**Abstract.** A nuclear war using less than 1% of the current global nuclear arsenal, which would inject 5 Tg of soot into the stratosphere, could produce climate change unprecedented in recorded human history and significant impacts on agricultural productivity and the economy. These effects would be most severe for the first five years after the nuclear war and may last for more than a decade. This paper calculates how food availability would change by employing the Environmental Impact and Sustainability Applied General Equilibrium model. Under a robust world trading system, global food availability would drop by a few percentage points. If the war would destabilize trade, it would magnify by several times the negative ramifications of land productivity shocks on food availability. If exporting countries redirect production to domestic consumption at the expense of importing countries, it would lead to the destabilization of international trade. The analysis suggests that economic models aiming to inform policymakers require both economic behavior analysis and biophysical drivers. Policy lessons derived from a crop model can be significantly nuanced when coupled with economic feedback derived from economic models. Through the impact on yield, farmers could shift production among crops and reallocate land use to maximize profits, showing the importance of general equilibrium effects such as product and input substitution and international trade. Although the global impact on corn and soybean production would be significant when just considering crop production, it could be considerably smaller under the economic model. However, this would be at the expense of other sectors, including livestock. In addition, the costs borne from disruptions to climate would vary significantly across regions, with significant adverse effects in high latitude regions. The severity of the shocks in the high-latitude areas would marginalize the farmers' product and input substitution ability.

**Introduction.** Natural and anthropogenic aerosols in the stratosphere can profoundly impact agriculture and world food trade through their effects on climate, and ultimately may produce famine. While significant volcanic eruptions cause natural aerosol layers, anthropogenic aerosols may be the outcome of fires caused by a nuclear war. Previous work showed that a nuclear war between India and Pakistan, using less than 1% of the global nuclear arsenal, could create climate disruption with significant effects (Toon *et al* **2019**). Crop models project that a scenario that produced 5 Tg of stratospheric soot could lead to reductions in agricultural production of maize, wheat, rice, and soybean by 13 (±1) %, 11 (±8) %, 3 (±5) %, and 17 (±2) % over five years (Jägermeyr *et al* **2020**). However, changes in agricultural productivity would likely be modified by economic activity, including adaptation by farmers and trade, affecting the ultimate availability of food and the possibility of regional famine.

While focusing on the 5 Tg scenario studied extensively in the literature (Robock *et al* **2007a**, Toon *et al* **2007a**, Stenke *et al* **2013**, Mills *et al* **2014**), the results here serve as an example to potentially much larger injections and impacts—e.g. a nuclear war between the U.S. and Russia that leads to a nuclear winter, with virtually all agriculture shut down and global famine (Robock *et al* **2007b**, Coupe *et al* **2019**). However, it is important to analyze the impacts of smaller injections, to understand how catastrophic local nuclear war could be.

As far as we know, this work is the first to use computable general economic (CGE) models to show the impacts of a nuclear war on food availability and food insecurity, both within and between regions. Through the CGE we detail the potential economic responses to the food production shock and highlight the importance of modeling the economy in its entirety. We use a CGE model, the Environmental Impact and Sustainability Applied General Equilibrium (Envisage) model (van der Mensbrugghe **2018**).

Geoscientific Model Development, vol. 15, issue no. 2, pp. 803-814, doi:10.5194/gmd-15-803-2022

# WIFF1.0: A hybrid machine-learning-based parameterization of Wave-Induced sea-ice Floe Fracture

Horvat, C., and **L.A. Roach**[1,2], 2022

NASA Goddard Institute for Space Studies, New York, NY, USA[1]
Department of Atmospheric Sciences, University of Washington, Seattle, WA, USA[2]

**Abstract.** Ocean surface waves play an important role in maintaining the marginal ice zone, a heterogenous region occupied by sea ice floes with variable horizontal sizes. The location, width, and evolution of the marginal ice zone are determined by the mutual interaction of ocean waves and floes, as waves propagate into the ice, bend it, and fracture it. In previous work, we developed a one-dimensional "superparameterized" scheme to simulate the interaction between the stochastic ocean surface wave field and sea ice. As this method is computationally expensive and not bitwise reproducible, here we use a pair of neural networks to accelerate this parameterization, delivering an adaptable, computationally inexpensive, reproducible approach for simulating stochastic wave–ice interactions. Implemented in the sea ice model CICE, this accelerated code reproduces global statistics resulting from the full wave fracture code without increasing computational overheads. The combined model, Wave-Induced Floe Fracture (WIFF v1.0), is publicly available and may be incorporated into climate models that seek to represent the effect of waves fracturing sea ice.

**Introduction.** Sea ice is a composite of individual pieces called floes. Floes are discrete solid pieces of sea ice with horizontal geometric length scales (sizes) ranging from meters to tens of kilometers. Yet in climate model simulations, sea ice is treated as a continuum field (**Hibler**, **1979**; **Golden et al.**, **2020**). To represent the effect of changes to sea ice floe geometry in climate models, modeling centers have started to incorporate prognostic sub-grid-scale parameterizations of the sea ice floe size distribution (FSD) as a core aspect of their model physics (**Horvat and Tziperman**, **2015**; **Zhang et al.**, **2015**; **Roach et al.**, **2018b**; **Boutin et al.**, **2018**; **Bateson et al.**, **2020**; **Hunke et al.**, **2019**). The FSD is a probability distribution $f(r)$, where $f(r)\mathrm{d}r$ is the percentage of a grid area comprised of floes with a size between $r$ and $r+\mathrm{d}r$. The integral of $f(r)$ over all positive $r$ is equal to the sea ice concentration, $c$.

One major advantage of simulating a sub-grid-scale FSD is it permits the representation of coupled interactions between sea ice floes and ocean surface waves. Ocean surface waves propagate into, are attenuated by, and fracture sea ice in regions known as the marginal ice zone (MIZ, **Wadhams et al.**, **1988**; **Langhorne et al.**, **1998**; **Squire et al.**, **1995**). Wave-affected sea-ice-covered regions are observed to be several million square kilometers in size in both hemispheres, impacting up to half of the sea ice cover depending on the season and hemisphere (**Horvat et al.**, **2020**). When waves propagate into and fracture sea ice, there is no direct change to sea ice concentration or thickness. Instead, this fracture process alters sea ice floe sizes, increasing the sensitivity of the sea ice to external thermodynamic or dynamic forcing (**Steele**, **1992**; **Feltham et al.**, **2006**; **Horvat et al.**, **2016**; **Horvat and Tziperman**, **2017**) and altering the attenuation of ocean wave energy (**Perrie and Hu**, **1996**; **Meylan et al.**, **2021**). Thus, there is a hypothesized coupling between sea ice loss and wave activity – waves propagate into the ice, fracturing it, causing it to melt, and enhancing wave propagation (**Kohout et al.**, **2011**; **Asplin et al.**, **2012**, **2014**). Floe fracture by waves is the dominant process driving changes in floe perimeter in summer months when the most lateral melting occurs (**Roach et al.**, **2019**).

In a climate model, coupled wave–ice feedbacks are related to two sub-grid-scale distributions: the FSD, $f(r)$, and the ocean surface wave spectrum, $S(\lambda)$, where $\lambda$ is the wavelength and (units $\mathrm{m}^2$) is the wave energy per square meter, with for $H_s$ the significant wave height (**Michel**, **1968**). Heuristic parameterizations have been developed to relate bulk properties of the ocean surface wave field to the FSD – generally assuming that fractured floes follow a power-law distribution (**Williams et al.**, **2013**; **Zhang et al.**, **2015**; **Bateson et al.**, **2020**).

Journal of City Climate Policy and Economy, vol. 1, issue no. 1, pp. 13-31, doi:10.3138/jccpe-2022.1.1.0003

# A research agenda for transformative urban climate action

Huxley, R., B. Walsh, C. Oke, R. Bellinson, H. Bulkeley, L.L.V. Ceneviva, L.B. Correa, S. Cox, B. Giles-Corti, G. Galik, A. Gouldson, G. Karuri-Sebina, M. Mazzucato, D. Miller, A. Revi, P. Rode, **C. Rosenzweig**[1,2], C. Singh, I. Sitcov, W. Solecki, K. Trebeck, P.A. Victor, and D. Zarrilli, 2022

NASA Goddard Institute for Space Studies, New York, NY, USA[1]
Center for Climate Systems Research, Columbia University, New York, NY, USA[2]

**Abstract.** This commentary from the Journal Editorial Board sets out the research agenda for the journal and invites contributions. We want to elicit and synthesize research- and practice-based knowledge toward the goal of resilient, equitable cities in a world with less than 1.5°C of warming, focusing on the transformational change needed to achieve this goal. Within this focus, we set out two primary areas that are pivotal to demonstrate the economic and political strategies necessary to stop climate breakdown: ecologically and socially viable and just economic systems; and purposeful, progressive, and inclusive government and governance. We set out key principles of transformational change and invite a plurality of conceptualizations, particularly emphasizing the need and potential of drawing on emerging thinking at regional, national, and international levels and applying it to city-scale. We outline the need for action-oriented, policy-relevant research in collaboration with city actors, tackling priority challenges in real-time, as well as an openness to new knowledge, perspectives, and contributors. We aim to catalyze and realize the opportunity to combine collective city action with academic (re-)thinking and research activism, in order to empower mayors with the evidence and narrative to create sustainable, thriving cities.

**Introduction.** Cities both contribute to climate change—they are responsible for 67%–72% of greenhouse gas emissions (**Lwasa et al., 2022**)—, and are vulnerable to the impacts of it with 55% of the world's population living in cities (**UN DESA, 2019**). Every tenth of a degree in warming exposes these urban populations to increased climate risks such as heat waves, water stress, and food insecurity (**Intergovernmental Panel on Climate Change [IPCC], 2018**), with devastating human and ecosystem impacts (**WHO, 2020**).

The central role of cities[1] in addressing climate change has never been more clear (**van der Heijden et al., 2019**). They are increasingly recognized as key agents of change to influence national and global climate action, and key to reaching global goals (**Frey & Calderón Ramírez, 2018**; **IPCC, 2018**).

Cities are rising to this challenge, setting ambitious targets and climate plans (**GCoM, 2021**). However, there is a significant gap in implementation of urban climate targets (**Walsh et al., 2022**) and accelerated implementation is needed to keep warming below 1.5°C.

With this in mind, this commentary sets out the Journal of City Climate Policy and Economy's research agenda focused on how to achieve transformational change in order to support the goal of resilient and equitable cities in a world with less than 1.5°C of warming. The journal will explore both how we achieve this process of transformational change and by—and for whom—it is being defined, with what consequences (see **Figure 1**).

We aim to create a space to explore transformative urban climate action, to reinvent our economic approaches and to reinvigorate purposeful city government and governance. We welcome contributions that apply a range of frameworks and thinking at the city-scale, and draw on diverse forms of knowledge, to support urban decision-makers to achieve transformational change and attain their climate goals. We are particularly interested in city administrations while also recognizing that collaboration and coordination is needed across all sectors and levels of government. We invite research that is action-oriented, policy relevant, and timely—we cannot wait to act, so research must be done in parallel with action and in pace with politics.

Journal of Advances in Modeling Earth Systems, vol. 14, issue no. 6, e2022MS003039, doi:10.1029/2022MS00303

# Limitations of separate cloud and rain categories in parameterizing collision-coalescence for bulk microphysics schemes.

Igel, A.L., H. Morrison, **S.P. Santos**[1,2], and **M. van Lier-Walqui**[1,2], 2022

NASA Goddard Institute for Space Studies, New York, NY, USA[1]
Center for Climate Systems Research, Columbia University, New York, NY, USA[2]

**Abstract.** Warm rain collision-coalescence has been persistently difficult to parameterize in bulk microphysics schemes. We use a flexible bulk microphysics scheme with bin scheme process parameterizations, called AMP, to investigate reasons for the difficulty. AMP is configured in a variety of ways to mimic bulk schemes and is compared to simulations with the bin scheme upon which AMP is built. We find that an important limitation in traditional bulk schemes is the use of separate cloud and rain categories. When the drop size distribution is instead represented by a continuous distribution, the simulation of cloud-to-rain conversion is substantially improved. We also find large sensitivity to the threshold size to distinguish cloud and rain in traditional schemes; substantial improvement is found by decreasing the threshold from 40 to 25 μm. Neither the use of an assumed functional form for the size distribution nor the choice of predicted distribution moments has a large impact on the ability of AMP to simulate rain production. When predicting four total moments of the liquid drop size distribution, either with a traditional two-category, two-moment scheme with a reduced size threshold, or a four-moment single-category scheme, errors in the evolution of mass and the cloud size distribution are similar, but the single-category scheme has a substantially better representation of the rain size distribution. Optimal moment combinations for the single-category approach are investigated and appear to be linked more to the information content they provide for constraining the size distributions than to their correlation with collision-coalescence rates.

**Introduction.** The representation of warm phase collision-coalescence in global weather and climate models (GCMs) is notoriously challenging and is often a large source of disagreement between models and observations. Several studies have found that GCMs produce too much light rain and potentially not enough heavy rain (Jing et al., **2017**; Kay et al., **2018**) and that these errors can lead to a substantial bias in the cloud radiative forcing (Mülmenstädt et al., **2021**). Due to these known issues, improving the parameterization of collision-coalescence rates is an active area of current research.

Liquid water in the bulk microphysics schemes used in cloud-resolving and global climate models is typically represented by an artificial division into two categories, one for small cloud droplets and one for larger rain drops. This is based on widespread observations that the liquid water mass distribution is often bimodal and the idea that cloud and rain drops generally grow by different processes (vapor diffusion for the former and collision-coalescence for the latter). With a few exceptions (Szyrmer et al., **2005**; Y. L. Kogan & Belochitski, **2012**; Morrison et al., **2020**), the drop size distribution (DSD) of each category is assumed to follow a theoretical distribution function, most commonly the gamma distribution (e.g., Clark, **1974**; Khairoutdinov & Kogan, **2000**; Morrison et al., **2005**; Seifert & Beheng, **2001**; Walko et al., **1995**). Bulk schemes then predict one to three moments of the DSD, or integral quantities of these functions. Most commonly these are the 0th moment (M0) of the size distribution, which corresponds to the total number concentration, the third moment (M3), which is proportional to the mass mixing ratio, and possibly the sixth moment (M6), which is proportional to the radar reflectivity factor.

With this basic framework for representing cloud liquid water in bulk schemes, warm phase collision-coalescence is forced to be divided into two main processes, namely auto-conversion, the self-collection of cloud droplets to make rain, and accretion, the collection of cloud droplets by raindrops.

Environmental Research Letters, vol. 17, issue no. 2, 024037, doi:10.1088/1748-9326/ac507a

# Eco-hydrological responses to recent droughts in tropical South America

Jiang, Y.[2,3], **M. Yang[1,2]**, W. Liu[2], K. Mohammadi[2], and G. Wang[2,3], 2022

NASA Goddard Institute for Space Studies, New York, NY, USA[1]
Department of Civil and Environmental Engineering, University of Connecticut, Storrs, CT, USA[2]
Center for Environmental Sciences and Engineering, University of Connecticut, Storrs, CT, USA[3]

**Abstract.** This study assesses the ecohydrological effects of recent meteorological droughts in tropical South America based on multiple sources of data and investigates the possible mechanisms underlying the drought response and recovery of different ecohydrological systems. Soil drought response and recovery lag behind the meteorological drought, with delays longer in the dry region (Nordeste) than in the wet region (Amazonia), and longer in deep soil than in shallow soil. Evapotranspiration (ET) and vegetation in Nordeste are limited by water under normal conditions and decrease promptly in response to the onset of shallow soil drought. In most of the Amazon where water is normally abundant, ET and vegetation indices follow an increase-then-decrease pattern, increase at the drought onset due to increased sunshine and decrease when the drought is severe enough to cause a shift from an energy-limited regime to a water-limited regime. After the demise of meteorological droughts, ET and vegetation rapidly recover in Nordeste with the replenishment of shallow soil moisture (SM) but take longer to recover in southern Amazon due to their dependence on deep SM storage. Following severe droughts, the negative anomalies of ET and vegetation indices in southern Amazon tend to persist well beyond the end of soil drought, indicating drought-induced forest mortality that is slow to recover from. Findings from this study may have implications on the possibility of a future forest dieback as drought is projected to become more frequent and more severe in a warmer climate.

**Introduction.** Drought is a major natural hazard characterized by below-normal precipitation over a period of months to years, which has devastating impacts on agriculture, water resources, and the economy (Dai **2011**, Sheffield *et al* **2012**, Smith and Matthews **2015**). Globally, drought is projected to increase in frequency and severity, mainly as a result of decreasing rainfall and increasing evaporation in a warmer climate (Wang **2005**, Sheffield and Wood **2008b**, Dai **2013**, Naumann *et al* **2018**, Su *et al* **2018**). Observational data have already shown an increasing trend of drought frequency and severity, despite the debates on the magnitude of changes (Sheffield *et al* **2012**, Dai **2013**, Trenberth *et al* **2014**). At the regional scale, as a critical component of the global ecosystem, tropical South America has experienced repeated severe and widespread droughts over the past two decades. El Niño-Southern Oscillation and warm anomalies in the tropical North Atlantic are two main drivers of meteorological droughts over tropical South America (Zeng *et al* **2008**, Coelho *et al* **2012**, Jimenez *et al* **2018**, Panisset *et al* **2018**). In the Amazon rainforest, extreme droughts in 2005, 2010 and 2016 were all considered one-in-100 year events, contributing to an increasing trend of drought severity and spatial extent during the past 20 years (Jiménez-Muñoz *et al* **2016**). The Nordeste region also experienced two major droughts in 2007 and 2012 (Marengo *et al* **2017**); the extreme drought in 2012 reached the strongest intensity in 2012/2013 but lasted until 2015 at a somewhat lower intensity. The prolonged 2012 drought was followed by the unprecedented drought in 2016 to produce severe and long-lasting water deficits in Northeast Brazil (Erfanian *et al* **2017**), putting the regional ecosystem at risk.

Soil moisture (SM) is an important pathway for precipitation anomalies to influence the regional ecosystem. Low SM inhibits latent heat flux and thus enhances sensible heat flux, leading to warmer air in the lower atmosphere (Wang *et al* **2007**, Seneviratne *et al* **2010**, Liu *et al* **2014**, Stocker *et al* **2019**). In turn, higher temperature increases the vapor pressure deficit (VPD) and evaporative demand, which may accelerate evapotranspiration (ET) and further deplete SM (Ruosteenoja *et al* **2018**).

Journal of Geophysical Research Atmospheres, vol. 127, issue no. 24, e2021JD036195, doi:10.1029/2021JD036195

# Investigating drivers of particulate matter pollution over India and the implications for radiative forcing with GEOS-Chem-TOMAS15

Karambelas, A.[2,3], A.M. Fiore[2,4], **D.M. Westervelt[1,2]**, V.F. McNeill, C.A. Randles, C. Venkataraman, J.R. Pierce, K.R. Bilsback, and G.P. Milly[2], 2022

NASA Goddard Institute for Space Studies, New York, NY, USA[1]
Lamont-Doherty Earth Observatory, Columbia University, Palisades, NY, USA[2]
Northeast States for Coordinated Air Use Management, Boston, MA, USA[3]
Department of Earth and Environmental Sciences, Columbia University, New York, NY, USA[4]

**Abstract.** Ambient fine particulate matter ($PM_{2.5}$) concentrations in India frequently exceed 100 μg/m$^3$ during fall and winter pollution episodes. We use the GEOS-Chem chemical transport model with the TwO-Moment Aerosol Sectional microphysics scheme with 15 size bins (TOMAS15) to assess $PM_{2.5}$ composition and impacts on radiation and cloud condensation nuclei (CCN) during pollution episodes as compared to the seasonal (October-December) average. We conduct high resolution (0.25° × 0.3125°) nested-domain simulations over India for short-duration, high-$PM_{2.5}$ episodes in the fall of 2015 and 2017. The simulations capture the magnitude and spatial patterns of pollution episodes measured by surface monitors ($r^2_{PM2.5}$ = 0.69) although aerosol optical depth is underestimated. During the episodes, near-surface organic matter (OM), black carbon (BC), and secondary inorganic aerosol concentrations increase from seasonal averages by up to 36, 7, and 7 μg/m$^3$, respectively. Episodic aerosol increases enhance cooling by lowering the top-of-atmosphere clear-sky direct radiative effect ($DRE_{TOA}$) during the 2015 episode (−6 W/m$^2$), with a smaller impact during the 2017 episode (−1 W/m$^2$). Differences in $DRE_{TOA}$ reflect larger increases in scattering aerosols in the column during the 2015 episode (+17 mg/m$^2$) than in 2017 (+13 mg/m$^2$), while absorbing aerosol column enhancements are smaller (+3 mg/m$^2$) in both years. Changes in shortwave radiation at the surface ($SW_{sfc}$) are spatially similar to $DRE_{TOA}$ and mostly negative during both episodes. CCN enhancements (0.2% supersaturation) during these episodes occur across the western Indo-Gangetic Plain, coincident with higher $PM_{2.5}$ concentrations. Changes in $DRE_{TOA}$, $SW_{sfc}$, and CCN during high-$PM_{2.5}$ episodes may have implications for crops, the hydrologic cycle, and surface temperature.

**Introduction.** In recent decades, ambient air pollution in India has grown increasingly worse alongside population growth, economic development, urbanization, and motorization with the limited implementation or enforcement of regulations on air pollutant emissions. One such pollutant, fine particulate matter with diameters smaller than 2.5 μm ($PM_{2.5}$), regularly exceeds India's National Ambient Air Quality Standard (NAAQS) of 40 μg/m$^3$ for annual mean $PM_{2.5}$. Approximately 58% of districts experience $PM_{2.5}$ concentrations greater than the India NAAQS (Chowdhury et al., **2019**), and up to 99.9% of the population lives in areas exceeding the World Health Organization (WHO) annual mean guideline of 10 μg/m$^3$. Anthropogenic source sectors contribute approximately 60% of India's annual average population-weighted $PM_{2.5}$ concentrations (Venkataraman et al., **2018**).

In addition to its role in air pollution, PM (also referred to as aerosols) affects climate by altering the energy balance of the planet through its interactions with radiation and clouds. In this way, aerosols exert a radiative forcing (IPCC, **2013**) on climate, which can lead to disruptions in the monsoon (Dave et al., **2017**; Westervelt et al., **2020**) and agriculture (Burney & Ramanathan, **2014**; Gupta et al., **2017**). The climate impacts from PM depend on the composition, size (diameter), and mass, and are thus expected to vary in space and time as the balance of PM sources, and their overall magnitude, change. For example, strong seasonal variations in concentrations and composition will affect bulk optical properties as the mix of black carbon (BC; strongly absorbing) and sulfate (strongly scattering) varies (Bellouin et al., **2016**).

Frontiers in Remote Sensing, vol. 3, 904505, doi:10.3389/frsen.2022.904505

# Effect of spectral variability of aerosol optical properties on direct aerosol radiative effect

Kato, S.[1], T.J. Thorsen[1], S.-H. Ham, N.G. Loeb[1], R.A. Ferrare[1], D.M. Winker[1], H. Barker, G.L. Stephens[2,3], S. Schmidt, K.G. Meyer[4], and **B. Cairns**[5], 2022

NASA Langley Research Center, Science Directorate, Hampton, VA, USA[1]
Jet Propulsion Laboratory, California Institute of Technology, Pasadena, CA, USA[2]
Department of Physics, University of Oxford, Oxford, United Kingdom[3]
NASA Goddard Space Flight Center, Greenbelt, MD, USA[4]
NASA Goddard Institute for Space Studies, New York, NY, USA[5]

**Abstract.** Aerosol optical properties depend on wavelength as well as both mixing ratios and size distributions of components that make up a particular type of aerosol. This study examines impacts on direct aerosol radiative effect (DARE) for desert, clean maritime, and polluted maritime aerosol types over the ocean when their optical properties are determined by various combinations of observations made by active (i.e., lidar) and passive (e.g., shortwave spectrometer) satellite sensors. Spectral optical properties are perturbed by altering mixing ratios of components that define aerosol types with assumptions that components within an aerosol type are fixed and only one aerosol type is present in the atmosphere. When 532 nm depolarization ratio from the lidar is used to identify desert aerosol, the uncertainty in the mean DARE due to spectral optical property variabilities is 10%. When the 532 nm depolarization and lidar ratios are used to identify clean and polluted maritime aerosols, uncertainties in mean DARE are, respectively, 4 and 18%. When scattering optical thicknesses are also known to within ± 3% at four passive imager wavelengths (340 nm, 546 nm, 966 nm, and 1,657 nm), uncertainty in the polluted maritime DARE decreases to 8%. Uncertainties in the instantaneous top-of-atmosphere (TOA) reflected irradiances derived from observed broadband radiances and angular distribution models are also estimated. When TOA irradiances are derived solely from the nadir view, their uncertainties can be reduced if aerosol type can be identified, and aerosol type dependence is considered in the radiance to irradiance conversion. This is especially so for aerosols with a large fraction of non-spherical particles, such as desert aerosols.

**Introduction.** Particles suspended in the atmosphere scatter and absorbed solar radiation. Some particles are anthropogenic in origin and others are produced naturally, although the separation is not always distinct. The influence of natural and anthropogenic particles on the amount of energy input to Earth is the aerosol direct radiative effect. Because they alter Earth's radiation budget, it is important to understand how much of aerosol change since the beginning of the Industrial Age can be attributed to changes in the aerosol radiative effect and how predicted changes in aerosol emissions will alter the Earth's radiation budget in the future (**Bellouin et al., 2020**). Despite the importance of quantifying the aerosol radiative effect for future climate predictions, estimates have a larger uncertainty. Global annual mean direct aerosol radiative effect estimates range from −3.1 to −0.61 $Wm^{-2}$ for all-sky and −6.5 to −2.3 $Wm^{-2}$ for clear-sky conditions (**Yu et al., 2006**). A similar range of clear-sky direct aerosol radiative effects of −5.5 to −3.8 $Wm^{-2}$ (±1σ) is also reported in a recent study by **Thorsen et al. (2020)**.

Satellites provide observations of aerosols and radiation on a global scale that can be used to derive an estimate of the aerosol direct radiative effect. Basically, there are two ways to estimate the direct aerosol radiative effect at the top of the atmosphere (TOA) using satellite observations. The first approach is to use a combination of broadband irradiances derived from broadband radiance observations combined with imager (e.g., MODIS) derived aerosol optical thicknesses or modeled irradiances under a pristine condition. This approach was used in, for example, **Loeb and Kato (2002)**, **Loeb and Manalo-Smith (2008)**, and **Zhang et al. (2005)**. Recently, **Loeb et al. (2021)** used TOA and surface irradiance observations to derive the trend of direct aerosol radiative effects.

Quaternary Science Reviews, vol. 284, 107505, doi:10.1016/j.quascirev.2022.107505

# A near-continuous record of climate and ecosystem variability in Central Europe during the past 130 kyrs (Marine Isotope Stages 5-1) from Füramoos, southern Germany

Kern, O.A., A. Koutsodendris, F.J. Allstädt, B. Mächtle, **D.M. Peteet**[1,2], S. Kalaitzidis, K. Christanis, and J. Pross, 2022

NASA Goddard Institute for Space Studies, New York, NY, USA[1]
Lamont-Doherty Earth Observatory, Columbia University, Palisades, NY, USA[2]

**Abstract.** Due to a general scarcity of archives and a lack of temporally highly resolved records, the response of Central European ecosystems to abrupt climate change during the **Late Pleistocene** – and notably the **Last Glacial** – has remained insufficiently explored. To contribute to a better understanding of the impact of short-term climate variability on ecosystems in Central Europe north of the Alps during that time, we present a new, near-continuous pollen record from Füramoos, southern Germany. Except for a hiatus from 28 to 20 ka BP, the record spans the past 130 kyrs in centennial-scale resolution. Our pollen dataset is augmented by sedimentological (i.e., XRF core scanning, loss on ignition, and **maceral** analysis) and macro botanical data. This new record represents the yet most complete, temporally highest resolved reconstruction of **terrestrial ecosystem** dynamics in Central Europe for the Last Glacial period.

Our results show that **temperate forests** thrived at Füramoos during full interglacial conditions (i.e., **MIS** 5e and MIS 1), **boreal forests** developed during the early glaciation (MIS 5 d–5a), and a tundra vegetation prevailed during full glacial conditions (MIS 4–2). Fourteen transient expansions (contractions) of tree and shrub populations that are synchronous with increases (decreases) in weathering intensity can be firmly attributed to specific Greenland **Interstadials** (Greenland Stadials) of the NGRIP ice-core record. By comparing individual expansions/contractions of tree and shrub populations with Greenland $\delta^{18}O_{ice}$ ice-core and North Atlantic sea-surface temperature (SST) data, we show that during interstadials **vegetation dynamics** in Central Europe were closely linked to SSTs in the North Atlantic and decoupled from the climate recorded in Greenland; during stadials, the opposite pattern prevailed. We attribute these patterns to changes in AMOC strength and associated latitudinal shifts of the **polar front**.

**Introduction.** The **Late Pleistocene** (Marine Isotope Stages [MIS] 5e–2, ca. 130–14 ka BP) marks a period of extreme climate variability characterized by warmer-than-today interglacial climates during MIS 5e, remarkably cold conditions during the MIS 4 and MIS 2 glacials, and pronounced short-term **climate oscillations** during MIS 3 (**Rasmussen et al., 2014**). Because near-future climate change is projected to occur at rates comparable to those of the millennial-scale climate oscillations of the Late Pleistocene (**Masson-Delmotte et al., 2021**), understanding the consequences of such climatic change for **terrestrial ecosystems** is important for extending the lead time for adaptation (**Alley et al., 2003**; **O'Neill et al., 2017**).

The millennial-scale climate oscillations during Late Pleistocene glaciations, and notably during MIS 3, comprise transient warming episodes known as Greenland **Interstadials** (GI), also termed Dansgaard-Oeschger events (D-O events; **Dansgaard et al., 1993**). Although the exact physical origin of GI has remained uncertain (**Bereiter et al., 2012**; **Zhang et al., 2014**), they have been successfully predicted by modeling approaches (**Galbraith and de Lavergne, 2019**; **Zhang et al., 2017**), and it has become clear that their occurrence across the northern hemisphere is quasi-synchronous (**Corrick et al., 2020**).

Microorganisms, vol. 10, issue no. 4, pp. 819, doi:10.3390/microorganisms10040819

# Discovery of chlorophyll *d*: Isolation and characterization of a far-red cyanobacterium from the original site of Manning & Strain (1943) at Moss Beach, California

**Kiang, N.Y.**[1,2], W.D. Swingley[2,3], D. Gautam[3], J.T. Broddrick[4], D. Repeta, J.F. Stolz, R.E. Blankenship, B.M. Wolf, A.M. Detweiler[4,5], K.A. Miller, J.J. Schladweiler[3], R. Lindeman, and M.N. Parenteau[2,4], 2022

NASA Goddard Institute for Space Studies, New York, NY, USA[1]
Virtual Planetary Laboratory, Nexus for Exoplanet System Science, NASA Astrobiology Program, USA[2]
Department of Biological Sciences, Northern Illinois University, DeKalb, IL, USA[3]
NASA Ames Research Center, Moffett Field, CA, USA[4]
Bay Area Environmental Research Institute, Moffett Field, CA, USA[5]

**Abstract.** We have isolated a chlorophyll-d-containing cyanobacterium from the intertidal field site at Moss Beach, on the coast of Central California, USA, where Manning and Strain (1943) originally discovered this far-red chlorophyll. Here, we present the cyanobacterium's environmental description, culturing procedure, pigment composition, ultrastructure, and full genome sequence. Among cultures of far-red cyanobacteria obtained from red algae from the same site, this strain was an epiphyte on a brown macroalgae. Its Qy in vivo absorbance peak is centered at 704–705 nm, the shortest wavelength observed thus far among the various known Acaryochloris strains. Its Chl a/Chl d ratio was 0.01, with Chl d accounting for 99% of the total Chl d and Chl a mass. TEM imagery indicates the absence of phycobilisomes, corroborated by both pigment spectra and genome analysis. The Moss Beach strain codes for only a single set of genes for producing allophycocyanin. Genomic sequencing yielded a 7.25 Mbp circular chromosome and 10 circular plasmids ranging from 16 kbp to 394 kbp. We have determined that this strain shares high similarity with strain S15, an epiphyte of red algae, while its distinct gene complement and ecological niche suggest that this strain could be the closest known relative to the original Chl d source of Manning and Strain (1943). The Moss Beach strain is designated Acaryochloris sp. (marina) strain Moss Beach.

**Introduction.** Chlorophyll *d* (Chl *d*) is a far-red-absorbing chlorophyll, which Manning and Strain [1] first discovered off the coast of Central California, and assumed to be a pigment of the red macroalgae growing in the intertidal zone. It was not until more than 50 years later that Miyashita, et al. [2] found Chl *d* to be not an accessory pigment of algae, but a primary photopigment of a cyanobacterium, which they named *Acaryochloris marina* (type-strain MBIC11017). They discovered that Chl *d* replaces nearly all chlorophyll *a* (Chl *a*) in these organisms, enabling them to perform oxygenic photosynthesis at long wavelengths in the far-red/near-infrared [3]. This discovery overturned long-held wisdom about the primacy of chlorophyll *a* and the photon energy limits for oxygenic photosynthesis.

Li and Chen [4] and Allakhverdiev, et al. [5] provided detailed reviews of the molecular structures of the different chlorophylls, and of research to characterize the position and function of Chl *d* in Photosystems I and II (PSI and PSII). Whereas Chl *a* possesses a vinyl group at the C3 position of the chlorin macrocycle, with its Soret and $Q_y$ bands peaking in absorbance at 435 and 666 nm, respectively, in methanol, Chl *d* instead possesses a formyl group, such that its Soret band is broadened with two peaks at 401 and 460 nm, and the $Q_y$ peak is at 697–698 nm. PSI in *A. marina* turns out to have a Chl *d* homodimer for the special pair [6], while in Photosystem II (PSII) it remains to be confirmed whether the special pair is a Chl *a*/Chl *d* heterodimer [7] or a Chl *d*/Chl *d* homodimer [8]. Mielke, et al. [9] resolved questions as to whether *A. marina* could have inefficiencies in the use of long-wavelength photons due to recombinations, showing that the photon-energy-storage efficiency in *A. marina* is comparable to or higher than that of Chl *a* organisms. They found *A. marina* MBIC 11017 had 40 ± 1% thermal storage efficiency compared to that measured in Chl *a* organisms (ranging from 34.1 ± 1% in *Synechococcus leopoliensis* to 43 ± 2% in an alga, *Chlorella vulgaris*, Cha and Mauzerall [10]).

Atmospheric Chemistry and Physics, vol. 22, issue no. 10, pp. 13303-13323, doi:10.5194/acp-22-13303-2022

# Interactive biogenic emissions and drought stress effects on atmospheric composition in NASA GISS ModelE

Klovenski, E.R., Y. Wang, **S.E. Bauer**[1], **K. Tsigaridis**[1,2], **G.S. Faluvegi**[1,2], **I. Aleinov**[1,2], **N.Y. Kiang**[1], A. Guenther, X. Jiang, W. Li, and N. Lin, 2022

NASA Goddard Institute for Space Studies, New York, NY, USA[1]
Center for Climate Systems Research, Columbia University, New York, NY, USA[2]

**Abstract.** Drought is a hydroclimatic extreme that causes perturbations to the terrestrial biosphere and acts as a stressor on vegetation, affecting emissions patterns. During severe drought, isoprene emissions are reduced. In this paper, we focus on capturing this reduction signal by implementing a new percentile isoprene drought stress ($y_d$) algorithm in NASA GISS ModelE based on the MEGAN3 (Model of Emissions of Gases and Aerosols from Nature Version 3) approach as a function of a photosynthetic parameter ($V_{c,max}$) and water stress ($\beta$). Four global transient simulations from 2003–2013 are used to demonstrate the effect without $y_d$ (Default_ModelE) and with online $y_d$ (DroughtStress_ModelE). DroughtStress_ModelE is evaluated against the observed isoprene measurements at the Missouri Ozarks AmeriFlux (MOFLUX) site during the 2012 severe drought where improvements in the correlation coefficient indicate it is a suitable drought stress parameterization to capture the reduction signal during severe drought. The application of $y_d$ globally leads to a decadal average reduction of ∼2.7 %, which is equivalent to ∼14.6 Tg $yr^{-1}$ of isoprene. The changes have larger impacts in regions such as the southeastern US. DroughtStress_ModelE is validated using the satellite ΩHCHO column from the Ozone Monitoring Instrument (OMI) and surface $O_3$ observations across regions of the US to examine the effect of drought on atmospheric composition. It was found that the inclusion of isoprene drought stress reduced the overestimation of ΩHCHO in Default_ModelE during the 2007 and 2011 southeastern US droughts and led to improvements in simulated $O_3$ during drought periods. We conclude that isoprene drought stress should be tuned on a model-by-model basis because the variables used in the parameterization responses are relative to the land surface model hydrology scheme (LSM) and the effects of $y_d$ application could be larger than seen here due to ModelE not having large biases of isoprene during severe drought.

**Introduction.** In present-day conditions terrestrial ecosystems release about 1000 Tg C $yr^{-1}$ of biogenic volatile organic compounds (BVOCs) into the atmosphere, and there is an additional smaller emission from marine ecosystems (Guenther et al., 2012). The majority of BVOCs emitted from vegetation are isoprene and monoterpenes (Guenther et al., 2006, 2012). Representing over half of emitted BVOCs, isoprene is the dominant species globally with reported ranges of 440–600 Tg C $yr^{-1}$ (Guenther et al., 2012) and high emission factors from some, but not all, broadleaf trees including species of oak, willow, palm oil, and eucalyptus (Benjamin et al., 1996; Geron et al., 2000). Isoprene is produced from carbon substrates generated during photosynthesis and contributes to abiotic stress tolerance from water and temperature stress (Loreto and Sharkey, 1990; Monson et al., 2021). Isoprene emissions peak during warm, sunnier months of the growing season (March–October) (Opacka et al., 2021). Isoprene has a chemical lifetime of approximately 1 h via oxidation by the hydroxyl radical (OH), producing organic aerosols and oxidation products that contribute to ozone ($O_3$) formation (Carlton et al., 2009). Biogenic isoprene emissions affect atmospheric composition and climate and in turn depend on environmental factors including light, temperature, photosynthetically active radiation (PAR), leaf area index (LAI), water stress, ambient $O_3$, and $CO_2$ concentrations. Thus, the response of isoprene emissions to weather extremes and changing climates is highly uncertain.

Drought is a common abiotic stress to terrestrial ecosystems characterized by low soil moisture, usually associated with high temperature and low precipitation. However, even boreal forests undergo winter drought due to frozen soils. Recent work has shown a strong correlation between drought severity and fine-mode aerosols in the US and estimated that regions undergoing severe drought see up to 17 % surface enhancement of aerosols during the growing season (Wang et al., 2017).

European Journal of Agronomy, vol. 135, 126482, doi:10.1016/j.eja.2022.126482

# Are soybean models ready for climate change food impact assessments?

Kothari, K., R. Battisti, K.J. Boote, S.V. Archontoulis, A. Confalone, J. Constantin, S.V. Cuadra, P. Debaeke, B. Faye, B. Grant, G. Hoogenboom, Q. Jing, M. van der Laan, F.A. Macena da Silva, F.R. Marin, A. Nehbandani, C. Nendel, L.C. Purcell, B. Qian, **A.C. Ruane**[1], C. Schoving, E.H.F.M. Silva, W. Smith, A. Soltani, A. Srivastava, N.A. Vieira, S. Slone, and M. Salmerón, 2022

NASA Goddard Institute for Space Studies, New York, NY, USA[1]

**Abstract.** An accurate estimation of crop yield under climate change scenarios is essential to quantify our ability to feed a growing population and develop agronomic adaptations to meet future food demand. A coordinated evaluation of yield simulations from process-based eco-physiological models for climate change impact assessment is still missing for soybean, the most widely grown **grain legume** and the main source of protein in our food chain. In this first soybean multi-model study, we used ten prominent models capable of simulating soybean yield under varying temperature and atmospheric $CO_2$ concentration [$CO_2$] to quantify the uncertainty in soybean yield simulations in response to these factors. Models were first parametrized with high quality measured data from five contrasting environments. We found considerable variability among models in simulated yield responses to increasing temperature and [$CO_2$]. For example, under a + 3 °C temperature rise in our coolest location in Argentina, some models simulated that yield would reduce as much as 24%, while others simulated yield increases up to 29%. In our warmest location in Brazil, the models simulated a yield reduction ranging from a 38% decrease under + 3 °C temperature rise to no effect on yield. Similarly, when increasing [$CO_2$] from 360 to 540 ppm, the models simulated a yield increase that ranged from 6% to 31%. Model calibration did not reduce variability across models but had an unexpected effect on modifying yield responses to temperature for some of the models. The high uncertainty in model responses indicates the limited applicability of individual models for climate change food projections. However, the ensemble mean of simulations across models was an effective tool to reduce the high uncertainty in soybean yield simulations associated with individual models and their parametrization. Ensemble mean yield responses to temperature and [$CO_2$] were similar to those reported from the literature. Our study is the first demonstration of the benefits achieved from using an ensemble of grain legume models for climate change food projections and highlights that further soybean model development with experiments under elevated [$CO_2$] and temperature is needed to reduce the uncertainty from the individual models.

**Introduction.** Soybean (*Glycine max* L. (Merr.) is globally the fifth most widely grown crop and first among legumes. Future soybean yield projections are essential to develop management adaptations and inform policymakers to ensure sufficient and sustainable productivity of this major crop. Uncertainties in crop yield projections that hinder effective planning and adaptation to a changing climate are attributed to multiple sources. First, there is uncertainty associated with different climate scenarios from global climate circulation models that is based on a range of trajectories of future greenhouse gas emissions (**Moss et al., 2010, Müller et al., 2021**, **Qian et al., 2020**). Additionally, there is uncertainty associated with the responses from different process-based eco-physiological models that are typically used to estimate crop yield under a changing climate (**Müller et al., 2021, Ruane et al., 2016**). The Agricultural Model Inter-comparison and Improvement Project (AgMIP) was established to quantify and reduce uncertainties in projections of agricultural production by facilitating multi-model analyses and improvement of existing crop models **Rosenzweig et al., 2013**). While there have been prior crop multi-model comparison studies in wheat (**Asseng et al., 2013**), maize (**Bassu et al., 2014**), rice (**Li et al., 2015**), sugarcane (**Marin et al., 2015**), and potato (**Fleisher et al., 2017**), this type of coordinated effort, comparing responses of crop models to key climate change factors, is still missing for soybean and other legume crops. In a prior assessment of future yield projections from global gridded crop models, there was a higher variability for soybean than for the other major crops (**Jägermeyr, 2021, Rosenzweig et al., 2014**). Thus, there is a pressing need to address this scientific gap and for a coordinated pilot multi-model evaluation to support global yield projections for soybean.

Journal of Advances in Modeling Earth Systems, vol. 14, issue no. 11, e2022MS003259,
doi:10.1029/2022MS003259

# An agenda for land data assimilation priorities: Realizing the promise of terrestrial water, energy, and vegetation observations from space

Kumar, S.[1], J. Kolassa[2,3], R. Reichle[2], W. Crow, G. de Lannoy, P. de Rosnay, N. MacBean, M. Girotto, A. Fox, T. Quaife, C. Draper, B. Forman, G. Balsamao, S. Steele-Dunne, C. Albergel, B. Bonan, J.-C. Calvet, J. Dong, **H.M. Liddy[4,5]**, and B. Ruston, 2022

Hydrological Sciences Lab, NASA Goddard Flight Center, Greenbelt, MD, USA[1]
Global Modeling and Assimilation Office, NASA Goddard Space Flight Center, Greenbelt, MD, USA[2]
Science Systems and Applications, Inc, Lanham, MD, USA[3]
NASA Goddard Institute for Space Studies, New York, NY, USA[4]
Center for Climate Systems Research, Columbia University, New York, NY, USA[5]

**Abstract.** The task of quantifying spatial and temporal variations in terrestrial water, energy, and vegetation conditions is challenging due to the significant complexity and heterogeneity of these conditions, all of which are impacted by climate change and anthropogenic activities. To address this challenge, Earth Observations (EOs) of the land and their utilization within data assimilation (DA) systems are vital. Satellite EOs are particularly relevant, as they offer quasi-global coverage, are non-intrusive, and provide uniformity, rapid measurements, and continuity. The past three decades have seen unprecedented growth in the number and variety of land remote sensing technologies launched by space agencies and commercial companies around the world. There have also been significant developments in land modeling and DA systems to provide tools that can exploit these measurements. Despite these advances, several important gaps remain in current land DA research and applications. This paper discusses these gaps, particularly in the context of using DA to improve model states for short-term numerical weather and sub-seasonal to seasonal predictions. We outline an agenda for land DA priorities so that the next generation of land DA systems will be better poised to take advantage of the significant current and anticipated shifts and advancements in remote sensing, modeling, computational technologies, and hardware resources.

**Introduction and Premise.** Warmer global temperatures associated with climate change have been shown to lead to more uncertainties in water availability both regionally and globally (Barnett et al., **2005**; Berg et al., **2016**; Konapala et al., **2020**; Milly et al., **2005**; Wu et al., **2020**). There is increasing evidence for an uneven distribution of changes in key water flux rates such as precipitation and evaporation leading to more intense and frequent extreme events, with the lack of predictability in water availability exacerbating water scarcity (Cook et al., **2018**; Oki & Kanae, **2006**; Trenberth et al., **2014**), water excess and natural disasters. The scientific literature shows that changes in atmospheric moisture transport will lead to consequences such as longer droughts in arid and semi-arid regions, more intense precipitation and snowfall, and earlier snow melt, among other changes (J. Huang et al., **2016**; Ingram, **2016**; Trenberth et al., **2003**; Wainwright et al., **2021**). Additionally, anthropogenic factors such as agricultural water use and industrial expansion, reservoir management, deforestation, and wetland drainage have not only quickened the pace of land transformation, but have also contributed to, often unpredictable, changes in the water, energy, and carbon cycles (Haddeland et al., **2014**; McDonald et al., **2011**; Mehran et al., **2017**; Vorosmarty & Sahagian, **2000**; Wood et al., **1997**). Given the urgent need to understand the variability in water cycle fluxes, there have been several efforts to develop inventories of key water cycle fluxes (L'Ecuyer et al., **2015**; Rodell et al., **2015**; Trenberth et al., **2007**; Vargas Godoy et al., **2021**). The combined use of modeling and remote sensing estimates of water and energy states and fluxes is a key feature of these studies, which typically report closure of water and energy budgets with relatively small residuals and uncertainty (~4%–8%) at coarse (monthly or larger) temporal scales. However, these studies also note that the imbalances and closure errors increase with increasing spatial and temporal resolution; consequently, concurrent high-quality Earth observations are needed to further constrain the modeled estimates and enable reliable assessment of water, energy, and carbon cycle budgets.

Remote Sensing, vol. 14, issue no. 15, pp. 3706, doi:10.3390/rs14153706

# Dual-polarization radar fingerprints of precipitation physics: A review

Kumjian, M.R., O.P. Prat, K.J. Reimel, **M. van Lier-Walqui**[1], and H.C. Morrison, 2022

NASA Goddard Institute for Space Studies, New York, NY, USA[1]

**Abstract.** This article reviews how precipitation microphysics processes are observed in dual-polarization radar observations. These so-called "fingerprints" of precipitation processes are observed as vertical gradients in radar observables. Fingerprints of rain processes are first reviewed, followed by processes involving snow and ice. Then, emerging research is introduced, which includes more quantitative analysis of these dual-polarization radar fingerprints to obtain microphysics model parameters and microphysical process rates. New results based on a detailed rain shaft bin microphysical model are presented, and we conclude with an outlook of potentially fruitful future research directions.

**Introduction.** Dual-polarization radar observations are a valuable resource for studies of precipitation microphysics. The value of such observations arises by virtue of the information about hydrometeor shapes, sizes, orientations, and phase (liquid, ice) obtained through probing clouds and precipitation with two orthogonal polarizations (see, e.g., [1,2,3,4,5,6,7]).

Dual-polarization radar data have been widely and successfully used for a broad spectrum of applications. For example, there is a rich literature of studies developing and applying hydrometeor classification algorithms (HCAs), also referred to as hydrometeor identification or particle identification algorithms, which categorize individual pixels in graphical displays of radar data by the inferred dominant backscattering hydrometeor type. Such HCAs have been implemented using a variety of techniques, including theoretically or empirically determined thresholds for the different polarimetric radar variables that correspond to various hydrometeor types (e.g., [8,9,10]), fuzzy logic or neuro-fuzzy logic approaches (e.g., [1,11,12,13,14,15,16,17,18,19,20,21], among many others), and more data-driven approaches such as hierarchical clustering or support vector machines (e.g., [22,23,24,25,26], among many others). There is a good review of these approaches in [27]. While useful for spot-checking model distributions of hydrometeors (e.g., [28]), these types of HCAs provide only limited direct information about ongoing microphysical processes; one would have to infer processes from independent algorithmic classifications of nearby pixels. For example, a pixel classified as "snow aggregates" adjacent to one identified as "ice crystals" could imply aggregation, etc. In addition, HCAs often have different species categories than are used in models, making even such simple comparisons challenging (e.g., drizzle, different rainfall intensities, and "big drops" in HCAs compared to a single "rain category" in model microphysics schemes). Finally, although grounded in theoretical and empirical studies, there still exists uncertainty in the HCA classifications. As such, although HCAs are useful for qualitatively understanding the structure of precipitating systems, which can be leveraged for other applications such as rainfall estimation (e.g., [29]), other approaches should be considered for insights into microphysical processes.

There are also numerous studies proposing and applying retrievals of microphysically useful quantities from the dual-polarization radar variables. This includes estimates of precipitation rates (e.g., see the recent review in this collection [30]), raindrop size distribution parameters (e.g., [31,32,33]), ice water content and snow particle size distribution parameters [34,35,36,37,38,39]. These retrievals generally map the radar variables to important microphysical quantities through empirically or theoretically derived relationships. Such retrievals can be useful for comparisons to numerical model simulations because the retrieved quantities often are closely related to or directly predicted or diagnosed from model output. However, uncertainties in these types of retrievals often are unquantified, and many require a priori assumptions that introduce additional potential sources of error (e.g., [40])

Frontiers in Remote Sensing, vol. 3, 766917, doi:10.3389/frsen.2022.766917

# Unique NISTAR-based climate GCM diagnostics of the Earth's planetary albedo and spectral absorption through longitudinal data slicing

**Lacis, A.A.**[1], **B.E. Carlson**[1], **G.L. Russell**[1], A. Marshak[2], and W. Su[3], 2022

NASA Goddard Institute for Space Studies, New York, NY, USA[1]
NASA Goddard Space Flight Center, Greenbelt, MD, USA[2]
NASA Langley Research Center, Hampton, VA, United States[3]

**Abstract.** Deep Space Climate Observatory (DSCOVR) measurements of Earth's reflected solar and emitted thermal radiation permit a unique model/data comparison perspective that is not readily available from other satellite data. The key factor is the unique Lissajous orbital viewing geometry from the Lagrangian L1 point, which enables a continuous view of Earth's sunlit hemisphere. The National Institute of Standards and Technology Advanced Radiometer (NISTAR) is the DSCOVR Mission energy budget instrument, which views the reflected and emitted radiation of the Earth's sunlit hemisphere by means of single pixel active cavity full-spectrum (Band-A, 0.2–100 μm) and filtered solar wavelength (Band-B, 0.2–4.0 μm; and Band-C, 0.7–4.0 μm) radiometer measurements. An additional solar wavelength photodiode channel (0.3–1.1 μm) provides a calibration reference. The objective of this study is the assessment of climate GCM performance via direct model/data comparisons. Such comparisons are difficult due to quasi-chaotic natural variability present in real-world observational data and in climate GCM simulations. This is where the unique DSCOVR viewing geometry makes possible the longitudinal data slicing methodology for more direct model/data comparison. The key point of the longitudinal slicing approach is that data integration over the entire sunlit hemisphere eliminates the quasi-chaotic meteorological weather-scale noise, while preserving intra-seasonal and planetary-scale variability. The rotation of the Earth that retrieves this climate-style, large-scale longitudinal and seasonal variability. The hemispheric averaging is accomplished automatically in NISTAR measurements with its single-pixel view of the Earth. For climate GCMs, this requires implementing the Sunlit Hemisphere Sampling (SHS) scheme to operate on the GCM run-time output data, utilizing the DSCOVR Satellite Ephemeris data to assure precise viewing geometry between NISTAR measurements and GCM output data, while averaging out the meteorological weather noise. However, GCM generated data are radiative fluxes, while NISTAR (and EPIC) measurements are near-backscattered radiances. Conversing NISTSR measurements into radiative fluxes cannot be accomplished using NISTAR data alone, even with detailed support from conventional satellite data. But the identical viewing geometry of Earth's sunlit hemisphere, and synergistic analyses of EPIC data make it feasible for this conversion of NISTAR near-backscatter radiances into radiative fluxes.

**Introduction.** **Figure 1** is a schematic representation of the NISTAR and EPIC measurements from the Lagrangian L1 point 1.4 to 1.6 × $10^6$ km from the Earth in the direction of the Sun, where the disk-image of the Earth is roughly the size of the Moon as viewed from Earth. To be specific, the DSCOVR Satellite is not precisely located at the Lagrangian L1 point. The DSCOVR Satellite is actually orbiting around the Lagrangian L1 point in a Lissajous orbit (**Koon et al., 2000**) as shown in **Figure 2**. The Lissajous orbit is forever evolving in shape with a roughly 6-month period. The solar illumination of the earth is determined by the Solar Ephemeris whereby (in the GCM simulations) the grid-box local solar zenith angle changes are updated on an hourly basis, as is the seasonal change in solar irradiance due to the Earth's orbital motion around the Sun. But, for viewing Earth from the Lissajous orbit, the DSCOVR Satellite viewing geometry must conform to the specification given by the DSCOVR Satellite Ephemeris.

Nature Reviews Earth and Environment, vol. 3, issue no. 12, pp. 872-889, doi:10.1038/s43017-022-00368-8

# Compound heat and moisture extreme impacts on global crop yields under climate change

Lesk, C.[6,7], W. Anderson[1,2], A. Rigden, O. Coast, **J. Jägermeyr[3,4,5]**, **S.S. McDermid[3,8]**, K.F. Davis, and M. Konar, 2022

NASA Goddard Space Flight Center, Greenbelt, MD, USA
Earth System Science Interdisciplinary Center, University of Maryland, College Park, MD, USA[2]
NASA Goddard Institute for Space Studies, New York, NY, USA[3]
Center for Climate Systems Research, Columbia University, New York, NY, USA[4]
Potsdam Institute for Climate Impacts Research (PIK), Member of the Leibniz Association, Potsdam, Germany[5]
Neukom Institute for Computational Science, Dartmouth College, Hanover, NH, USA[6]
Department of Geography, Dartmouth College, Hanover, NH, USA[7]
Department of Environmental Studies, New York University, New York, NY, USA[8]

**Abstract.** Extreme heat, drought and moisture excess are increasingly co-occurring within a single growing season, impacting crop yields in global breadbasket regions. In this Review, we synthesize understanding of compound heat and moisture extremes, their impacts on global crop yields and implications for adaptation. Heat and moisture extremes and their impacts become compounded through crop-physiological interactions, heat–moisture couplings in the climate system and crop–atmosphere interactions. Since around 2000, these compound extremes, and hot droughts in particular, have been linked to especially poor harvests (up to 30% yield losses) in regions such as India, Ethiopia, the USA, Europe and Russia. However, in some cases, combinations of crop stresses might generate compensating effects. Compound extremes are projected to increase in frequency and amplitude in the future, but owing to the biophysical interdependence among temperature, water and crop physiology, the net yield effects of such future compound extremes remain uncertain. Accordingly, compound extremes will necessitate comprehensive agricultural adaptation strategies geared towards multi-stress resilience, as adaptations that work for single climate stresses could be maladaptive under combined stresses. An integrated understanding of heat and water in soil–plant–atmosphere dynamics is urgently needed to understand risks and suitably adapt cropping systems to compounding climate impacts.

**Introduction.** Productive crops underpin the global food system, stable commodity prices and rural livelihoods. Climate is a major driver of staple crop production variability, accounting for up to 50% of year-to-year variation in global crop yields, particularly via extreme events3. As climate-related hazards mount, extreme heat, drought (precipitation or soil moisture deficits) and excess moisture are increasingly co-occurring in space and time. Such combined stressors, or ‘compound extremes’ (multiple, potentially interacting hazards that generate multiple, potentially interacting impacts, contributing to societal or environmental risk) can have unique and particularly severe crop impacts. The myriad complex interactions involved in compound temperature and moisture extremes pose a challenge to understanding how climate variability affects crop yield. For example, early efforts to statistically model empirical crop–climate relationships revealed a particular sensitivity of staple crop yields to extreme heat. Although extreme temperatures can directly damage crop tissue and reduce yield capacity, they can also induce moisture stress by raising the evaporative demand of the atmosphere (vapour pressure deficit (VPD)). Land-surface drying also often amplifies high air temperatures, physically linking the two extremes. Furthermore, responses of crop physiology to combined drought and heat stresses are distinct from those of the individualstresses14,15 and often more severe16. Such connections between water and heat in the physics of climate extremes and their impacts on crop biology raise the potential for compound, interactive effects of changing precipitation, temperature, soil moisture and VPD.

Future changes in crop productivity will also depend on the evolution of many climate variables and their interactions under anthropogenic greenhouse gas increase. However, projections of some of these variables are highly uncertain.

Nature Reviews Earth and Environment, vol. 3, pp. 363-379, doi:10.1038/s43017-022-00296-7

# Scattering and absorbing aerosols in the climate system

Li, J., **B.E. Carlson**[1], Y.L. Yung, D. Lv, J. Hansen, J.E. Penner, H. Liao, V. Ramaswamy, R.A. Kahn[3], P. Zhang, O. Dubovik, A. Ding, **A.A. Lacis**[1], L. Zhang, and Y. Dong, 2022

NASA Goddard Institute for Space Studies, New York, NY, USA[1]
Center for Climate Systems Research, Columbia University, New York, NY, USA[2]
Earth Sciences Division, NASA Goddard Space Flight Center, Greenbelt, MD, USA[3]

**Abstract.** Tropospheric anthropogenic aerosols contribute the second-largest forcing to climate change, but with high uncertainty owing to their spatio-temporal variability and complicated optical properties. In this Review, we synthesize understanding of aerosol observations and their radiative and climate effects. Aerosols offset about one-third of the warming effect by anthropogenic greenhouse gases. Yet, in regions and seasons where the absorbing aerosol fraction is high — such as South America and East and South Asia — substantial atmospheric warming can occur. The internal mixing and the vertical distribution of aerosols, which alters both the direct effect and aerosol–cloud interactions, might further enhance this warming. Despite extensive research in aerosol–cloud interactions, there is still at least a 50% spread in total aerosol forcing estimates. This ongoing uncertainty is linked, in part, to the poor measurement of anthropogenic and natural aerosol absorption, as well as the little-understood effects of aerosols on clouds. Next-generation, space-borne, multi-angle polarization and active remote sensing, combined with in situ observations, offer opportunities to better constrain aerosol scattering, absorption and size distribution, thus, improving models to refine estimates of aerosol forcing and climate effects.

**Introduction.** Aerosols are small liquid or solid particles suspended in the atmosphere[1]. They can be emitted directly (such as dust, sea salt, black carbon (BC) and volcanic aerosols) or formed indirectly through chemical reactions (including sulfate, nitrate, ammonium and secondary organic aerosols). Owing to their relatively short lifetime, aerosol concentrations typically peak near their sources. Desert regions (such as North Africa and the Middle East), industrial regions (such as East and South Asia) and biomass-burning regions (such as South America and South Africa) are, therefore, characterized by high mass concentrations (Fig. 1). Aerosols exhibit complicated compositions and vary substantially in shape and size, typically ranging between 0.01 and 10 μm (ref.[2]). Depending on these structural and compositional characteristics, aerosols can scatter and/or absorb shortwave radiation, as quantified through the single-scattering albedo (SSA; Table 1). Purely scattering aerosols include sulfates, nitrates, ammonium and sea-salt particles, whereas absorbing aerosols are primarily BC, with dust and organic carbon partly absorbing in the ultraviolet (UV) spectrum[3].

Aerosols have a direct bearing on Earth's energy balance and, therefore, on climate. For instance, aerosol scattering, and absorption alters the radiation balance and atmospheric stability through perturbations to the vertical temperature profile. Aerosols can further serve as cloud condensation nuclei (CCN) or ice-nucleating particles (INPs), which modify the reflectivity and lifetime of clouds through microphysical processes. Collectively, these influences are quantified as aerosol forcing: the change of net radiative flux at a specified level of the atmosphere, often assessed relative to estimated pre-industrial conditions[4].

Globally, anthropogenic aerosols are estimated to produce a net cooling $\sim -1.3 \pm 0.7\ \mathrm{W\ m^{-2}}$ at the top of the atmosphere; $-0.3 \pm 0.3\ \mathrm{W\ m^{-2}}$ is attributed to the aerosol–radiation interaction (ARI), $-1.0 \pm 0.7\ \mathrm{W\ m^{-2}}$ to aerosol–cloud interactions, $\sim -1.15\ \mathrm{W\ m^{-2}}$ to total forcing from scattering aerosols and $\sim +0.12\ \mathrm{W\ m^{-2}}$ to BC[4]. This combined aerosol forcing offsets roughly one-third of the warming from anthropogenic greenhouse gases (GHGs). However, the large spread in the estimated aerosol forcing leads to large discrepancies in climate sensitivity[5,6]. Thus, aerosols are considered to be the largest contributor of uncertainty in quantifying present-day climate change[4].

Geoscientific Model Development, vol. 15, issue no. 22, pp. 8181-8219, doi:10.5194/gmd-15-8181-2022

# Importance of different parameterization changes for the updated dust cycle modelling in the Community Atmosphere Model (version 6.1)

Li, L., N. Mahowald, J. Kok[2], X. Liu, M. Wu, D. Leung[2], D. Hamilton, L. Emmons, **Y. Huang[1,2,3]**, J. Meng[2], N. Sexton, and J. Wan, 2022

NASA Goddard Institute for Space Studies, New York, NY, USA[1]
Department of Atmospheric and Oceanic Sciences, University of California, Los Angeles, CA, USA[2]
Earth Institute, Columbia University, New York, NY, USA[3]

**Abstract.** The Community Atmosphere Model (CAM6.1), the atmospheric component of the Community Earth System Model (CESM; version 2.1), simulates the life cycle (emission, transport, and deposition) of mineral dust and its interactions with physio-chemical components to quantify the impacts of dust on climate and the Earth system. The accuracy of such quantifications relies on how well dust-related processes are represented in the model. Here we update the parameterizations for the dust module, including those on the dust emission scheme, the aerosol dry deposition scheme, the size distribution of transported dust, and the treatment of dust particle shape. Multiple simulations were undertaken to evaluate the model performance against diverse observations, and to understand how each update alters the modeled dust cycle and the simulated dust direct radiative effect. The model–observation comparisons suggest that substantially improved model representations of the dust cycle are achieved primarily through the new more physically-based dust emission scheme. In comparison, the other modifications induced small changes to the modeled dust cycle and model–observation comparisons, except the size distribution of dust in the coarse mode, which can be even more influential than that of replacing the dust emission scheme. We highlight which changes introduced here are important for which regions, shedding light on further dust model developments required for more accurately estimating interactions between dust and climate.

**Introduction.** Mineral dust accounts for most aerosol mass in the Earth's atmosphere and plays an important role in different aspects of the coupled Earth–human–climate system. For example, dust modifies the radiative budget and atmospheric dynamics via direct, semi-direct, and indirect interactions with radiation (Sokolik and Toon, 1996; Miller and Tegen, 1999; Pérez et al., 2006; Li and Sokolik, 2018a) and clouds (DeMott et al., 2003; Rosenfeld et al., 2001; Shi and Liu, 2019). In addition, the deposition of mineral dust perturbs the energy budget by darkening snow and glacial ice sheets directly due to the relatively darker color of dust particles (Skiles et al., 2018; Sarangi et al., 2020) and indirectly by providing nutrients (e.g., phosphorus) to snow algae (McCutcheon et al., 2021). Dust deposited onto land and ocean can also affect the biogeochemistry by adding nutrients (iron and phosphorus) and/or pollutants to ecosystems (Martin et al., 1990; Swap et al., 1992; Shinn et al., 2000; Tie and Cao, 2009; Mahowald, 2011; Mahowald et al., 2017, 2010; Hamilton et al., 2020).

To quantify the climate and biogeochemical impacts of dust, accurately reproducing the dust cycle (e.g., emission, transport, and deposition) with models is required. However, previous studies have shown substantial differences between the modeled dust cycle and observations (e.g., surface dust concentration and dust deposition) (Albani et al., 2014; C. Wu et al., 2020). These uncertainties in the dust cycle modeling, as well as uncertainties in optical properties due primarily to dust size and mineral composition, suggest a large uncertainty in estimating the dust direct radiative effect (DRE) (Kok et al., 2017; Li et al., 2021).

Journal of the Atmospheric Sciences, vol. 79, issue no. 1, pp. 73-100, doi:10.1175/JAS-D-21-0123.1

# Large-eddy simulations of marine boundary-layer clouds associated with cold air outbreaks during the ACTIVATE campaign — Part I: Case setup and sensitivities to large-scale forcings

Li, X.-Y., H. Wang, J. Chen, S. Endo, G. George, **B. Cairns**[1,2], S. Chellappan, X. Zeng[3], S. Kirschler, C. Voigt, A. Sorooshian, E. Crosbie[3,4], G. Chen[3], R.A. Ferrare[3], W.I. Gustafson, J.W. Hair, M.M. Kleb[3], H. Liu, R. Moore[3,4], D. Painemal[3,4], C. Robinson[4], A.J. Scarino[3,4], M. Shook[4], T.J. Shingler[3], K.L. Thornhill[3,4], **F. Tornow**[1,5], H. Xiao, L.D. Ziemba, and P. Zuidema, 2022

NASA Goddard Institute for Space Studies, New York, NY, USA[1]
Brookhaven National Laboratory, Upton, NY, USA[2]
NASA Langley Research Center, Hampton, VA, USA[3]
Science Systems and Applications, Inc., Hampton, VA, USA[4]
Center for Climate Systems Research, Earth Institute, Columbia University, New York, NY, USA[5]

**Abstract.** Large-eddy simulation (LES) is able to capture key boundary layer (BL) turbulence and cloud processes. Yet, large-scale forcing and surface turbulent fluxes of sensible and latent heat are often poorly prescribed for LESs. We derive these quantities from measurements and reanalysis obtained for two cold-air outbreak (CAO) events during Phase I of the Aerosol Cloud Meteorology Interactions over the Western Atlantic Experiment (ACTIVATE) in February–March 2020. We study the two contrasting CAO cases by performing LES and test the sensitivity of BL structure and clouds to large-scale forcings and turbulent heat fluxes. Profiles of atmospheric state and large-scale divergence and surface turbulent heat fluxes obtained from ERA5 data agree reasonably well with those derived from ACTIVATE field measurements for both cases at the sampling time and location. Therefore, we adopt the time-evolving heat fluxes, wind, and advective tendencies profiles from ERA5 data to drive the LES. We find that large-scale thermodynamic advective tendencies and wind relaxations are important for the LES to capture the evolving observed BL meteorological states characterized by the hourly ERA5 data and validated by the observations. We show that the divergence (or vertical velocity) is important in regulating the BL growth driven by surface heat fluxes in LESs. The evolution of liquid water path is largely affected by the evolution of surface heat fluxes. The liquid water path simulated in LES agrees reasonably well with the ACTIVATE measurements. This study paves the path to investigate aerosol–cloud–meteorology interactions using LES informed and evaluated by ACTIVATE field measurements.

**Introduction.** When viewed from space, about 70% of Earth's surface is covered by clouds (**Schneider et al. 2017**). Clouds, the regulator of the radiative heating and cooling of the planet (**Ramanathan et al. 1989**), represent a major complication in the current modeling of the climate system (**Schneider et al. 2017; Stevens and Bony 2013**; **Bony et al. 2017**). One of the most challenging problems of cloud–climate interactions is to understand how cloud microphysical processes affect atmospheric water and radiation budgets, such as how precipitation efficiency affects radiative properties of stratocumulus clouds (**Boucher et al. 2013**).

The western North Atlantic Ocean (WNAO) region has attracted decades of atmospheric research due to the complex atmospheric system (**Painemal et al. 2021**), pollution outflow from North America (**Corral et al. 2021**), and accessibility by aircraft and ships. However, the subject of aerosol–cloud interaction (ACI) is the least investigated among all the field campaign measurements over the WNAO (**Sorooshian et al. 2020**) partly because of the complicated chemical, physical, and dynamical processes in this region. ACI involves processes from the formation of nanometer-sized aerosols to the life cycle of kilometer-sized clouds, which covers a scale range of about $10^{12}$. Such a scale separation coupled with turbulence poses great challenge for both measurements and numerical modeling.

Journal of Quantitative Spectroscopy and Radiative Transfer, vol. 281, 108080, doi:10.1016/j.jqsrt.2022.108080

# Optical properties of morphologically complex black carbon aerosols: Effects of coatings.

**Liu**, **L.**[1,2], G.L. Schuster[3], H. Moosmüller, S. Stamnes[3], **B. Cairns**[1], and **J. Chowdhary**[1,2], 2022

NASA Goddard Institute for Space Studies, New York, NY, USA[1]
Center for Climate Systems Research, Columbia University, New York, NY, USA[2]
NASA Langley Research Center, Hampton, VA, USA[3]

**Abstract.** Optical properties are computed for fractal-like aggregate black carbon (BC) aerosols coated with different substances. Two models are used for these aerosols: (i) the coated aggregate model (model I), where coating is added to the voids and surroundings of BC fractal-like aggregates; and (ii) the closed-cell aggregate model (model II), where coating is added concentrically to each monomer of BC fractal-like aggregates. Our results favor choosing the coated aggregate model (model I) to simulate scattering and absorption by coated BC aerosols because this model is morphologically more realistic, and because this model yields mass absorption cross section (MAC) and backscattering linear depolarization ratio (LDR) values that are consistent with field measurements. Moreover, the corresponding computed degree of linear polarization (DoLP) and LDR values are very sensitive to changes in the coating volume fraction (fvol) and the coating refractive index ($m$). With the same absorbing BC core, the MAC value increases steadily with increasing fvol and $m$ values. For example, using a density of 1.8 g/cm$^3$ and BC refractive index 1.95 + i0.79, the calculated MAC values for uncoated BC aggregates range from 6.2 to 6.8 m$^2$/g at 0.55 µm. When coating material is applied to the BC aggregates, the calculated MAC values for model I particles increase to between 9.8 and 13.2 m$^2$/g (depending on $m$) when fvol = 87.5%. The backscattering LDR values also tend to increase with the increasing $m$ values for the shapes and sizes considered in our study. For model I particles, the backscattering LDR values span a wide range of 4.2–27.8% at a wavelength of 0.35 µm at fvol = 87.5% when $m$ increases from 1.33 to 1.55. Our results are relevant to analyses of polarimetric and lidar observations of smoke particles, especially when these particles undergo hygroscopic growth.

**Introduction.** Black carbon (BC) aerosol is an important contributor to climate forcing and ranks as the second-largest human-made cause of global warming. Knowledge of the **optical properties** of BC particles is essential not only for accurately assessing their direct and indirect radiative effects, but also for a variety of applications including remote sensing, environmental studies, optical diagnostics for industrial aerosol processes such as combustion, and astrophysical phenomena involving the effects of **interstellar grains** on light propagation and scattering **[1], [2], [3], [4], [5], [6], [7], [8], [9], [10], [11], [12], [13], [14], [15].**

Freshly emitted BC particles are fractal-like aggregates, typically consisting of tens to hundreds of carbonaceous **spherules** (monomers) with diameters of about a few tens of nanometers **[16], [17], [18], [19]**. After release into the atmosphere, fresh BC aerosols undergo aging processes during which they tend to mix with various ambient materials and often become coated or partially coated. The most common coating materials are secondary organic compounds, sulfate, sulphuric acid, nitrate, sea salt, and water **[19], [20], [21], [22], [23], [24], [25], [26].**

Accurately modeling the optical properties of BC particles internally mixed with other aerosol species is a challenging task. These properties are complex functions of many factors, including size and shape of the BC aerosols, **refractive index**, mixing state, position of BC particle within the host, and the amount and **composition** of the coating material. Thanks to the rapid growth of computer processing power coupled with the availability of efficient numerically-exact computer solvers for the **Maxwell equations**, much recent progress has been made in studying the radiative properties of atmospheric BC aerosols. Please see Kahnert and Kanngießer **[27]** and the long list of references therein for an overview. The multi-sphere superposition T-matrix method (MSTM) **[28], [29], [30], [31], [32], [33], [34]** and the **discrete dipole approximation** (DDA) **[35], [36], [37], [38], [39]** are the two most frequently used techniques for accurate calculations of light scattering and absorption by morphologically complex non-homogenous particles.

Artificial Intelligence Earth Systems, vol. 1, issue no. 4, -e220002, doi:10.1175/AIES-D-22-0002.1

# Machine learning crop yield models based on meteorological features and comparison with a process-based model

Liu, Q.[1], **M. Yang[1,2,3]**, K. Mohammadi[2,3], D. Song[2], J. Bi[2], and G. Wang[2,3], 2022

NASA Goddard Institute for Space Studies, New York, NY, USA[1]
Department of Civil and Environmental Engineering, University of Connecticut, Storrs, CT, USA[2]
Institute of the Environment, University of Connecticut, Storrs, Connecticut[3]

**Abstract**. A major challenge for food security worldwide is the large interannual variability of crop yield, and climate change is expected to further exacerbate this volatility. Accurate prediction of the crop response to climate variability and change is critical for short-term management and long-term planning in multiple sectors. In this study, using maize in the U.S. Corn Belt as an example, we train and validate multiple machine learning (ML) models predicting crop yield based on meteorological variables and soil properties using the leaving-one-year-out approach, and compare their performance with that of a widely used process-based crop model (PBM). Our proposed long short-term memory model with attention ($LSTM_{att}$) outperforms other ML models (including other variations of LSTM developed in this study) and explains 73% of the spatiotemporal variance of the observed maize yield, in contrast to 16% explained by the regionally calibrated PBM; the magnitude of yield prediction errors in $LSTM_{att}$ is about one-third of that in the PBM. When applied to the extreme drought year 2012 that has no counterpart in the training data, the $LSTM_{att}$ performance drops but still shows advantage over the PBM. Findings from this study suggest a great potential for out-of-sample application of the $LSTM_{att}$ model to predict crop yield under a changing climate.

**Introduction**. Feeding the rapidly increasing global population is a grand challenge of the twenty-first century. A major obstacle to global food security is the crop yield loss caused by extreme weather events such as drought, flood, and heatwaves, which is expected to be exacerbated by the changing climate as warming increases the frequency and severity of weather extremes. Accurate estimation and prediction of regional and global crop productivity and crop response to climate variability, change, and extremes are crucial for developing agricultural policies, setting international food aid priorities, forecasting and analyzing global trade trends, and identifying effective strategies for climate change adaptation. Remote sensing of the actual crop growth status offers a powerful yield predictor and is the basis of numerous crop yield models using machine learning or other statistical approaches (Battude et al. 2016; Fieuzal et al. 2017; Geipel et al. 2014; Khaki et al. 2021; Shahhosseini et al. 2019). However, remote sensing data are not available for long-lead seasonal prediction and future projections. To address this challenge, here we explore different approaches to crop yield prediction based on growing season meteorological forcing and soil properties, focusing on machine learning and its comparison with process-based modeling.

Most past studies estimating crop yield projection based on growing season meteorological variables made use of classical statistical approaches such as multivariate regression (e.g., Lobell et al. 2020; Yang et al. 2020). While many variables that influence crop growth and productivity were considered, temperature and precipitation are the most commonly used as yield predictors (e.g., Schlenker and Roberts 2009). Typically, these models used meteorological statistics (e.g., mean) during the growing season (or its part), which cannot capture the impact of extreme weather conditions during some critical stages of crop development that may have a disproportionate impact on crop yield. Another challenge facing conventional statistical models is the uncertain applicability to historically unprecedented events, as it is not clear whether the observed predictors and relationships can be extrapolated.

Process-based crop models offer a preferred alternative for studying climate change impact on crop yield, especially in the context of future projections (e.g., Bassu et al. 2014; Franke et al. 2020; Qian et al. 2019; Rosenzweig et al. 2018, 2014). Process-based models (PBMs) take meteorological variables (e.g., air temperature and humidity, precipitation, and solar radiation) and soil properties as inputs, parameterize crop physiological and phenological processes, and entail a large number of cultivar-specific parameters that have to be calibrated based on field.

Earth's Future, vol. 10, issue no. 1, e2021EF002018, doi:10.1029/2021EF002018

# Sustainable use of groundwater may dramatically reduce irrigated production of maize, soybean, and wheat

Lopez, J.R., J.M. Winter, J. Elliott, **A.C. Ruane**[1], C. Porter, and G. Hoogenboom, Martha Anderson, Christopher Hain[2], 2022

NASA Goddard Institute for Space Studies, New York, NY, USA[1]
NASA Marshall Space Flight Center, Huntsville, AL, USA[2]

**Abstract**. Groundwater extraction in the United States (US) is unsustainable, making it essential to understand the impacts of limited water use on irrigated agriculture. To improve this understanding, we integrated a gridded crop model with satellite observations, recharge estimates, and water survey data to assess the effects of sustainable groundwater withdrawals on US irrigated agricultural production. The gridded crop model agrees with satellite-based estimates of evapotranspiration (R2 = 0.68), as well as survey data from the United States Department of Agriculture (R2 = 0.82–0.94 for county-level production and 0.37–0.54 for county-level yield). Using the optimistic assumption that groundwater extraction equals effective aquifer recharge rate, we find that sustainable groundwater use decreases US irrigated production of maize, soybean, and winter wheat by 20%, 6%, and 25%, respectively. Using a more conservative assumption of groundwater availability, US irrigated production of maize, soybean, and winter wheat decreases by 45%, 37%, and 36%, respectively. The wide range of simulated losses is driven by considerable uncertainty in surface water and groundwater interactions, as well as accounting for the many aspects of sustainability. Our results demonstrate the vulnerability of US irrigated agriculture to unsustainable groundwater pumping, highlighting the difficulty of expanding or even maintaining irrigated food production in the face of climate change, population growth, and shifting dietary demands. These findings are based on reducing pumping by fallowing irrigated farmland; however, alternate pumping reduction strategies or technological advances in crop genetics and irrigation could produce different results.

**Introduction.** Groundwater extraction in much of the United States (US) is unsustainable (USDA, **2018**; Dieter et al., **2018**; Maupin et al., **2014**; Reitz et al., **2017**). Combined, the two major aquifers in the US, the High Plains and Central Valley, were depleted by approximately 12.5 and 3.1 $km^3$ per year between 2003 and 2013, respectively (Famiglietti, **2014**). This depletion is equivalent to 15% of total US groundwater extraction in 2010 (Maupin et al., **2014**). Between 2010 and 2015, groundwater withdrawals for irrigation increased by 16% (Dieter et al., **2018**). This increase was primarily driven by four states, California, Arkansas, Nebraska, and Idaho, that already had substantial groundwater use for irrigation and further increased irrigation groundwater use by 26%–59% (Dieter et al., **2018**). Overall, irrigation used 67% of total US groundwater extraction in 2015 (Dieter et al., **2018**), and groundwater use exceeds groundwater recharge across 15% of the contiguous US (Reitz et al., **2017**). Groundwater extraction for irrigation must substantially decrease for US agricultural production to be sustainable but doing so would have a negative impact on both the US and world food supplies. The US is responsible for 36% of global maize production, 35% of global soybean production, and 8% of global wheat production (USDA, **2018**). In the US, approximately 17% of total maize production comes from irrigated agriculture, as well as 12% of total soybean and wheat production (USDA-NASS, **2017**). These three crops occupy 52% (maize 22%, soybean 17%, and wheat 13%) of US irrigated agricultural area (Dieter et al., **2018**). The tension between increasing food production and using water sustainably raises two critical questions: how much groundwater can be extracted while still irrigating sustainably, and what would the impacts of irrigating sustainably be on agricultural production?

Multiple studies have approximated sustainable groundwater extraction for agriculture using the concept of safe aquifer yield (Hahn et al., **1997**; Miles & Chambet, **1995**; Voudouris, **2006**). Safe aquifer yield is defined as the estimated sustainable groundwater extraction rate and based on aquifer recharge rates (Miles & Chambet, **1995**).

Scientific Reports, vol. 12, issue no. 1, pp. 5268, doi:10.1038/s41598-022-08751-7

# Evaluating the usefulness of VGI from Waze for the reporting of flash floods

Lowrie, C., A. Kruczkiewicz, S.N. McClain, **M. Nielsen**[1,2], and S.J. Mason, 2022

NASA Goddard Institute for Space Studies, New York, NY, USA[1]
Department of Earth and Environmental Science, Columbia University, New York, USA[2]

**Abstract.** Using volunteered geographic information (VGI) to supplement disaster risk management systems, including forecasting, risk assessment, and disaster recovery, is increasingly popular. This attention is driven by difficulties in detection and characterization of hazards, as well as the rise of VGI appropriate for characterizing specific forms of risk. Flash-flood historical records, especially those that are impact-based, are not comprehensive, leading to additional barriers for flash-flood research and applications. In this paper we develop a method for associating VGI flood reporting clusters against authoritative data. Using Hurricane Harvey as a case study, VGI reports are assimilated into a spatial analytic framework that derives spatial and temporal clustering parameters supported by associations between Waze's community-driven emergency operations center and authoritative reports. These parameters are then applied to find previously unreported likely flash flood-events. This study improves the understanding of the distribution of flash flooding during Hurricane Harvey and shows potential application to events in other areas where Waze data and reporting from official sources, such as the National Weather Service, are available.

**Introduction. Flash flood warning procedures in the United States.** In the United States, the National Weather Service (NWS) mandate requires warnings for a variety of severe weather types, including flash floods. Meteorologists at local NWS Weather Forecast Offices develop standard operating procedures for warning issuance based on understanding of the area, potential socioeconomic impacts and available meteorological data[1,2,3]. Warnings for flash floods are issued as geographic 'storm-based' (as opposed to county-based) polygons with a time duration, typically on the order of 3–10 h, and can cover as much as several hundred square kilometers or as little as 10 s of square kilometers[4]. During the warning duration, or soon after it expires, the forecast-office staff undertakes a confirmation process to verify whether or not a flash flood is taking or has taken place within the issued warning extent[5]. While the intent is to assess temporal overlap of any flash-flood warning with any potential flash flood[6], there can be significant challenges in doing so with a high level of confidence, due in large part to the sparseness of sensors relative to the spatial and temporal scales of flash floods[7,8]. In addition to sensors, confirmations of a flash flood are derived from reports gathered primarily from specialists—trained storm watchers, law enforcement, and emergency management—but also from social media, local businesses, and news coverage[2,9,10]. If a flash-flood event is confirmed, the NWS Weather Forecast Office that issued the warning creates a Local Storm Report (LSR) containing a spatial–temporal point. LSRs are intended to be issued during the duration of the storm, to inform risk mitigation and response actions. Typically, a single confirmed report within the extent of the warning polygon is considered sufficient for verification, which speaks to the incentive to verify the warning, however this presents challenges in delineating the spatial extent and estimating the full impact of a flash flood[11]. After any subsequent meteorological phenomena pass, the Storm Data publication[12] is created, which is intended to be the final source of truth for historical records.

Relative to other natural hazards in the US, there is a paucity in observational data for flash floods[13]. Compared to other flood types, historical records for flash floods are more likely to have significant gaps[14,15]. However, recent advances in unified flood and flash-flood data systems highlight the need for additional data sources to supplement reporting systems[16]. In the United States in 2005, only 46% of flash-flood warnings were verified[17]. Of the 54% of warnings that went unverified, it is unclear how many were false positives and how many coincided with actual, but unreported, flash-flood events.

Bulletin of the American Meteorological Society, vol. 103, issue no. 3, pp. E733-E740, doi:10.1175/BAMS-D-21-0228.1

# Building a land data assimilation community to tackle technical challenges in quantifying and reducing uncertainty in land model predictions

MacBean, N., **H.M. Liddy**[1,2], T. Quaife, J. Kolassa[3], and A. Fox, 2022

NASA Goddard Institute for Space Studies, New York, NY, USA[1]
Center for Climate Systems Research, Columbia University, New York, NY, USA[2]
Global Modeling and Assimilation Office, NASA Goddard Space Flight Center, Greenbelt, and Science Systems and Applications, Inc., Lanham, MD, USA[3]

**Abstract.** The regional to global-scale process-based land models that form part of numerical weather prediction (NWP) systems or Earth system models (ESMs) have rapidly increased in their complexity over the past few decades (**Prentice et al. 2015**; **Fisher and Koven, 2020**). In parallel, there is a growing wealth of terrestrial observations that can be used to confront land models, including long-running observation/experiment campaigns [e.g., NSF Long-Term Ecological Research (LTER) sites and DOE Next-Generation Ecosystem Experiments–Tropics (NGEE-Tropics) and Arctic] and satellite missions or products [e.g., Landsat and MODIS from NASA, ESA Climate Change Initiative (CCI) Soil Moisture], the synthesis of site-based and experimental manipulation data into networks [e.g., FLUXNET, Integrated Carbon Observation System (ICOS), the International Soil Moisture Network, SAPFLUXNET, Drought-Net, Free Air $CO_2$ Enrichment (FACE)], novel ground-based observations (e.g., tree ring data, carbonyl sulfide, radiocarbon measurements), and a new array of space-based observations of global carbon, water, and energy cycles [e.g., hyperspectral and lidar instruments such as Global Ecosystem Dynamics Investigation (GEDI) and Hyperspectral Imager Suite (HISUI) on the International Space Station (ISS), and solar induced fluorescence from platforms like the *Orbiting Carbon Observatory 2* (*OCO-2*) and Tropospheric Monitoring Instrument (TROPOMI)] at higher spatial, temporal, and spectral resolutions than ever before. Despite the increasing complexity of models and density of land-based data, uncertainty in land model projections remains high.

While there has been a concerted effort to use terrestrial observations for model evaluation, the number of studies that use these data for quantifying and reducing uncertainty in land model parameters and states via a statistical data assimilation (DA) framework is small in comparison. This is primarily due to the computational expense and technical challenges associated with implementing such a global-scale land DA system. However, land models urgently need to be confronted with a wide range of data to optimize model parameters, initialize surface states, and to address model structural uncertainty. Without such efforts, we cannot quantify or reduce uncertainty associated with individual model projections, and the intermodel spread in weather forecasts and predictions of land–atmospheric interactions or carbon–climate feedbacks will remain high (**Arora et al. 2020**).

**The challenge of developing land DA systems.** A number of land modeling groups spanning different modeling communities [carbon, hydrology, land surface modeling (LSM)/ESM, and NWP] have devoted significant resources into developing global-scale land DA systems. However, this technical development work does not get the level of exposure in the literature or in conference talks commensurate with the resources needed to complete that work because publications and presentations are naturally focused on scientific questions. For the same reason, development of DA systems is typically not the focus of grant proposals nor calls for proposals by funding agencies. Nonetheless, their development can consume much of the time on a given research project due to the considerable complexities and technical challenges faced when implementing DA methods within land models. As a result, this largely hidden work and advancement of "best practices" or solutions for technical challenges are not widely publicized or discussed at scientific meetings.

Journal of Quantitative Spectroscopy and Radiative Transfer, vol. 283, 108142, doi:10.1016/j.jqsrt.2022.108142

# Scattering by relatively small oblate spheroidal drops of water in the rainbow region: T-matrix results and geometric interpretation

Marston, P.L., and **M.I. Mishchenko**[1], 2022

NASA Goddard Institute for Space Studies, New York, NY, USA[1]

**Abstract.** Late in 1999 Michael Mishchenko carried out T-matrix calculations of light scattered by oblate spheroidal drops of water at Marston's request. The purpose of the investigation was to determine if the caustic features, known by that time to be visible in the far-field scattering near the primary rainbow region for horizontally illuminated relatively large drops, would also be present in T-matrix calculations of the scattering by small drops. The axis of rotational symmetry of the drop was taken to be vertical, and the illumination was taken to be horizontal. Scattering into the relevant angular region was evaluated for drop aspect ratios D/H = 1, 1.23, 1.311, and 1.37 where D denotes the equatorial diameter and H the vertical diameter. The results are limited to polarized monochromatic illumination with ka = 140 where a = D/2 and k = 2π/λ with λ being the wavelength of the illumination. As expected from geometrical analysis, a horizontal "V" shaped caustic is visible for D/H = 1.311. The T-matrix results, gray-tone intensity displays provided by Mishchenko, remain instructive.

**Introduction.** The main purpose of this paper is to report some T-matrix light scattering calculations carried out by Michael Mishchenko in autumn 1999 at the request of the corresponding author. A secondary purpose is to recall how Michael's scientific hospitality made this interaction possible and to explain how these results remained unreported to the present time. The calculations concern the caustics visible in the far-field light scattering by oblate spheroidal drops of water discovered in 1984 by Marston and Trinh **[1]**. The calculations were an outgrowth of Marston having met Michael at the *Conference on Light Scattering by Non-spherical Particles: Theory, Measurements, and Applications* (29 September - 1 October 1998) that he helped convene **[2].** It is appropriate to include here a brief overview of the related research available at that time. Some additional discussion is given concerning related subsequent developments concerning this field of research. For reasons explained in **Section 3**, Michael's calculations were limited to spheroids that were small relative to the drops observed in **[1]**. These results were presented at the online *Electromagnetic and Light Scattering Conference (ELS-XIX)* in the session *Michael Mishchenko's Scientific Legacy* in July 2021 **[3]**.

Concerning the broader context of the interaction with Michael to be described, Marston became aware of some of Michael's publications on scattering in the 1990s as evidenced by some early signed reprints from Michael in his possession. He arranged to attend the aforementioned 1998 meeting through the encouragement of both Michael and a mutual associate, W.P. Arnott **[4]**, **[5]**. Michael helped to arrange for Marston's accommodations during that meeting.

**Generalized rainbows and physical optics of spheroidal drops as of 1998**. Though a summary of Marston's 1998 presentation is available **[6]**, some additional perspective will be helpful. An early investigation of the effect of the shape of ultrasonically levitated liquid drops on the light scattering near the primary rainbow concerned the situation where the illumination was along the symmetry axis of the drop **[7]**, **[8]**. The drops were xylene levitated in water and set into low-frequency vibration using modulated radiation pressure **[9]**, **[10]**, **[11]**. The shape oscillations resulted in associated oscillating shifts of the rainbow angle of the type originally considered by Möbius **[12]**.

Philosophical Transactions of the Royal Society A, vol. 380, issue no. 2238, 20210287, doi:10.1098/rsta.2021.0287

# Using machine learning to identify novel hydroclimate states

**Marvel**, **K.D.**[1,2], and **B.I. Cook**[1], 2022

NASA Goddard Institute for Space Studies, New York, NY, USA[1]
Center for Climate Systems Research, Columbia University, New York, NY, USA[2]

**Abstract.** Anthropogenic climate change is expected to alter drought risk in the future. However, droughts are not uncommon or unprecedented, as documented in tree-ring-based reconstructions of the summer average Palmer drought severity index (PDSI). Using an unsupervised machine-learning method trained on these reconstructions of pre-industrial climate, we identify outliers: years in which the spatial pattern of PDSI is unusual relative to 'normal' variability. We show that in many regions, outliers are more frequently identified in the twentieth and twenty-first centuries. This trend is more pronounced when the regional drought atlases are combined into a single global dataset. By definition, outlier patterns at the 10% level are expected to occur once per decade, but from 1950 to 2000 more than 6 years per decade are identified as outliers in the global drought atlas (GDA). Extending the GDA through 2020 using an observational dataset suggests that anomalous global drought conditions are present in 80% of years in the twenty-first century. Our results indicate, without recourse to climate models, that the world is more frequently experiencing drought conditions that are highly unusual in the context of past natural climate variability.

Sustainable Cities and Society, vol. 76, 103376, doi:10.1016/j.scs.2021.103376

# A quasi-experimental approach for evaluating the heat mitigation effects of green roofs in Chicago, Illinois

McConnell, K., **C.V. Braneon**[1,2], **E. Glenn**[1,3], N. Stamler, E. Mallen, D.P. John, R. Pandya, J. Abramowitz, G. Fernandez, and **C. Rosenzweig**[1,4], 2022

NASA Goddard Institute for Space Studies, New York, NY, USA[1]
SciSpace LLC., Bethesda, MD, USA[2]
The City College of the City University of New York, New York, NY, USA[3]
Center for Climate Systems Research, Columbia University, New York, NY, USA[4]

**Abstract**. In the coming decades, millions of urban residents will be exposed to increasingly deadly heat extremes. As an adaptive response to rising temperatures, many cities have begun to install vegetated" green" roofs, which now vary widely in structure and size, and have generally been shown to have cooling capacity. Yet, little research has been done to differentiate which types of green roofs are most effective at reducing urban heat. We present a method to evaluate the cooling effects associated with green infrastructure that draws on publicly available satellite imagery and open-source software for analysis. Based on a quasi-experimental research design that integrates social and physical science approaches, this technique is able to identify the cooling effects of green infrastructure against background warming trends associated with urbanization and climate change. We demonstrate this method at three green roof sites across the City of Chicago, finding that the study sites with larger, intensive green roofs accompanied by diverse **plant species** have greater cooling benefits than the extensive, **monoculture** green roof. Our low-cost method can aid policymakers and planners in empirically evaluating the cooling capacity of green roofs in their own communities.

**Introduction.** The growth of urban populations and expansion of urban land cover alongside rising global temperatures mean that millions of people will be exposed to potentially deadly urban heat in the coming century (Hoegh-Guldberg et al., 2018). Green infrastructure projects – such as vegetated roofs, greenspaces, street trees, and vertical greenery – are a critical means of adapting to these rising temperatures (Bowler et al., 2010, Gill et al., 2007), and are now widely advanced as a heat mitigation strategy by researchers, urban planners, and policymakers (Norton et al., 2015, Zhang et al., 2020). Yet, there is still a limited scholarly understanding of which types of green infrastructure are most effective at reducing urban heat (Bartesaghi Koc, Osmond, & Peters, 2018), and whether their heat mitigation performance varies across climatic regions. Given that local governments often have limited city budgets for climate planning (Aylett, 2015), comparative research that evaluates the relative effectiveness of different types of green infrastructure projects can provide pragmatic guidance for planners working on the ground. Since at least the 1960s, vegetated or "green" roofs have been advanced as a key form of green infrastructure that can reduce building energy use and urban heat (Oberndorfer et al., 2007, Shafique et al., 2018). As green roofs have spread, the term itself has come to encompass a diverse assortment of vegetated roof types that vary in plant and substrate type, species diversity, size, and upkeep. Broadly, green roofs can be categorized as either "intensive" or "extensive", with intensive roofs being characterized by a variety of shrubs, trees, and other herbaceous plants requiring deeper soil and irrigation. Extensive roofs tend to have shallower soil and host low-lying plants such as *Sedum* species, which require little to no irrigation (Heusinger and Weber, 2017, Zheng et al., 2021). Limited experimental research suggests that these characteristics can all affect the cooling capacity of a given green roof (Blanusa et al., 2013, MacIvor and Lundholm, 2011). Given the wide range of green roofs available, more detailed, comparative evaluations of green roof impacts are needed to aid decision-makers in selecting the optimal roof type for their site (Mahdiyar, Tabatabaee, Abdullah, & Marto, 2018).

Geophysical Research Letters, vol. 49, issue no. 8, e2021GL097154, doi:10.1029/2021GL097154

# Extratropical shortwave cloud feedbacks in the context of the global circulation and hydrological cycle

McCoy, D.T., P. Field, M.E. Frazer, M.D. Zelinka, **G.S Elsaesser**[1,2], J. Mülmenstädt, I. Tan, T.A. Myers, and Z.J. Lebo, 2022

NASA Goddard Institute for Space Studies, New York, NY, USA[1]
Department of Applied Physics and Applied Mathematics, Columbia University, New York, NY, USA[2]

**Abstract.** Shortwave (SW) cloud feedback ($SW_{FB}$) is the primary driver of uncertainty in the effective climate sensitivity (ECS) predicted by global climate models (GCMs). ECS for several GCMs participating in the sixth assessment report exceed 5K, above the fifth assessment report "likely" maximum (4.5K) due to extratropical $SW_{FB}$'s that are more positive than those simulated in the previous generation of GCMs. Here we show that across 57 GCMs Southern Ocean $SW_{FB}$ can be predicted from the sensitivity of column-integrated liquid water mass (LWP) to moisture convergence and to surface temperature. The response of LWP to moisture convergence and the response of albedo to LWP anti-correlate across GCMs. This is because GCMs that simulate a larger response of LWP to moisture convergence tend to have higher mean-state LWPs, which reduces the impact of additional LWP on albedo. Observational constraints suggest a modestly negative Southern Ocean $SW_{FB}$— inconsistent with extreme ECS.

**Introduction.** The Shortwave (SW) cloud feedback ($SW_{FB}$) represents the central uncertainty in the future warming and effective climate sensitivity (ECS) predicted by global climate models (GCMs). Uncertainty in $SW_{FB}$ is a function of the parameterizations of cloud processes necessitated by the relatively coarse resolution of GCMs. Most GCMs transition from a positive $SW_{FB}$ in the subtropics to a negative $SW_{FB}$ poleward of 50°, albeit with substantial uncertainty in magnitude (Gordon & Klein, **2014**; Terai et al., **2016**; Zelinka et al., **2016**, **2020**). Several CMIP6 GCMs with very high ECS (>5K) have emerged owing to a more positive extratropical $SW_{FB}$ (Bjordal et al., **2020**; Frey & Kay, **2018**; Zelinka et al., **2020**) and this feature needs to be evaluated.

**Different mechanisms have been put forward to explain negative extratropical $SW_{FB}$:**

1. Replacement of susceptible cloud ice with more reflective liquid (McCoy et al., **2014b**; Senior & Mitchell, 1993; Tsushima et al., **2006**)
2. Suppression of ice hydrometeor sinks of cloud through reduced glaciation (Ceppi, Hartmann, & Webb, **2016**; Field & Heymsfield, **2015**; Kay et al., **2014**; McCoy et al., **2015**; Mülmenstädt et al., **2021**; Tan & Storelvmo, **2019**; Tsushima et al., **2006**)
3. Enhanced air-sea exchange of aerosol precursors (Bodas-Salcedo et al., **2019**)
4. Strongly increasing adiabatic water content at cold temperatures (Betts & Harshvardhan, **1987**; Frazer & Ming, **2022**; Terai et al., **2019**)
5. Increased extratropical moisture convergence driving enhanced condensation (McCoy et al., **2019**, **2020**)

We focus on the last of these processes. This is motivated by previous studies that found that changes in surface temperature ($T_{skin}$) and moisture convergence could be used to explain changes in extratropical cloudiness with minor contributions from other terms such as boundary layer stability and subsidence (McCoy et al., **2020**).

It is difficult to untangle the effects of increased local $T_{skin}$ on clouds as it may act through several of the processes listed above. One probable explanation is that increased $T_{skin}$ acts to enhance buoyancy fluxes in the boundary layer, reducing cloud condensate (Bretherton & Blossey, **2014**). This mechanism has been found to be important to boundary layer cloud changes across the subtropics (Klein et al., **2017**; Myers & Norris, **2016**; Myers et al., **2021**). Here we treat $T_{skin}$ variations as a proxy for all processes not related to moisture convergence, such as inversion strength as well as other boundary layer processes (Terai et al., **2016**, **2019**).

Earth Interactions, vol. 26, issue no. 1, pp. 195-208, doi:10.1175/EI-D-22-0003.1

# Soil carbon losses reduce soil moisture in global climate model simulations

**McDermid**, **S.S.**[1,2], **E. Weng**[1,3], **M.J. Puma**[1,3], **B.I. Cook**[1,4], T. Hengl, J. Sanderman, G.J.M. De Lannoy, and **I. Aleinov**, 2022

NASA Goddard Institute for Space Studies, New York, NY, USA[1]
Department of Environmental Studies, New York University, New York, NY, USA[2]
Center for Climate Systems Research, Columbia University, New York, NY, USA[3]
Lamont-Doherty Earth Observatory, Columbia University, Palisades, NY, USA[4]

**Abstract.** Most agricultural soils have experienced substantial soil organic carbon losses in time. These losses motivate recent calls to restore organic carbon in agricultural lands to improve biogeochemical cycling and for climate change mitigation. Declines in organic carbon also reduce soil infiltration and water holding capacity, which may have important effects on regional hydrology and climate. To explore the regional hydroclimate impacts of soil organic carbon changes, we conduct new global climate model experiments with NASA Goddard Institute for Space Studies ModelE that include spatially explicit soil organic carbon concentrations associated with different human land management scenarios. Compared to a "no land use" case, a year 2010 soil degradation scenario, in which organic carbon content (OCC; weight %) is reduced by a factor of ~0.12 on average across agricultural soils, resulted in soil moisture losses between 0.5 and 1 temporal standard deviations over eastern Asia, northern Europe, and the eastern United States. In a more extreme idealized scenario where OCC is reduced uniformly by 0.66 across agricultural soils, soil moisture losses exceed one standard deviation in both hemispheres. Within the model, these soil moisture declines occur primarily due to reductions in porosity (and to a lesser extent infiltration) that overall soil water holding capacity. These results demonstrate that changes in soil organic carbon can have meaningful, large-scale effects on regional hydroclimate and should be considered in climate model evaluations and developments. Further, this also suggests that soil restoration efforts targeting the carbon cycle are likely to have additional benefits for improving drought resilience.

**Introduction.** Land-use and land-cover change, especially through agricultural expansion and industrialization, has resulted in soil organic matter losses across many important crop and pasture regions (**Sanderman et al. 2017**; **Scholes et al. 2018**). Hereafter, we refer primarily to soil organic matter in terms of stored soil organic carbon (SOC), as this constitutes a major portion (~58%) of total organic matter in soils. The global SOC stock to 1 m depth amounts to ~1500 PgC, although significant spatial variation exists (**Zomer et al. 2017**). The weight fraction of organic carbon content (OCC) of most agricultural soils is <2% of the total mass of soil material and concentrated in the upper soil layers (**Oldfield et al. 2019**). Consequently, small OCC changes are associated with relatively large declines in stocks of SOC, and these changes have significant impacts on soil ecosystem services (**Lal et al. 2011**). Since the dawn of agriculture (~12 000 years), global SOC stocks have declined by an estimated ~116 PgC as a consequence of land-use change (**Sanderman et al. 2017**). These losses have had significant impacts on nutrient retention and cycling in agricultural systems, with implications for reduced productivity (**Lal et al. 2011**; **Oldfield et al. 2019**), while also contributing to rising atmospheric greenhouse gas concentrations (**Lal 2015**; **Lal et al. 2015**; **Houghton and Nassikas 2017**). In light of this, there is growing interest in rebuilding soil carbon stocks on agricultural land through improved management to mitigate anthropogenic climate change (**Chabbi et al. 2017**; **Amelung et al. 2020**; **Bossio et al. 2020**; **Zomer et al. 2017**; **Paustian et al. 2016**).

Additionally, there are also important *biogeophysical* impacts of SOC changes, particularly related to soil–water dynamics in managed agroecosystems (**Arenas-Calle et al. 2021**). Higher SOC content increases porosity and stabilizes soil aggregates, thereby increasing soil water holding capacity and plant available water (**Intergovernmental Technical Panel on Soils 2015**).

Geophysical Research Letters, vol. 49, issue no. 8, e2021GL097287, doi:10.1029/2021GL097287

# Improved parameterization for the size distribution of emitted dust aerosols reduces model underestimation of super coarse dust

Meng, J., **Y. Huang**[1,2,3], D.M. Leung[3], L. Li, A.A. Adebiyi[3,4], C.L. Ryder, N.M. Mahowald, and J.F. Kok[3], 2022

NASA Goddard Institute for Space Studies, New York, NY, USA[1]
Earth Institute, Columbia University, New York, NY, USA[2]
Department of Atmospheric and Oceanic Sciences, University of California, Los Angeles, CA, USA[3]
Department of Life & Environmental Sciences, University of California, Merced, CA, USA[4]

**Abstract.** Aircraft measurement campaigns have revealed that super coarse dust (diameter >10 μm) surprisingly accounts for approximately a quarter of aerosols by mass in the atmosphere. However, most global aerosol models either underestimate or do not include super coarse dust abundance. To address this problem, we use brittle fragmentation theory to develop a parameterization for the emitted dust size distribution that includes emission of super coarse dust. We implement this parameterization in the Community Earth System Model (CESM) and find that it brings the model in good agreement with aircraft measurements of super coarse dust close to dust source regions. However, the CESM still underestimates super coarse dust in dust outflow regions. Thus, we conclude that the model underestimation of super coarse atmospheric dust is in part due to the underestimation of super coarse dust emission and likely in part due to errors in deposition processes.

**Introduction.** Mineral dust is an important component of the Earth system, impacting Earth's radiation budget, clouds, precipitation, biogeochemistry, and air quality (Balkanski et al., **2021**; Chen et al., **2019**; Guieu et al., **2019**; Jickells et al., **2005**; Kosmopoulos et al., **2017**; Meng et al., **2021**). Because all these impacts depend sensitively on dust size (Mahowald et al., **2014**), global aerosol models need to accurately represent the dust particle size distribution (PSD) to quantify the various dust impacts on the Earth system. Recent dust PSD measurements have indicated that super coarse (diameter >10 μm) dust particles are more prevalent than previously thought (Ryder et al., **2018**, **2019**; van der Does et al., **2018**; Varga et al., **2021**). Indeed, recent model estimates suggest an atmospheric load of ~10 Tg of super coarse dust, which represents about a quarter of the total atmospheric loading of particulate matter and adds an estimated warming effect of around 0.10 W $m^{-2}$ by absorbing both short-wave and long-wave radiation (Adebiyi & Kok, **2020**; Di Biagio et al., **2020**; Kok et al., **2017**, **2021**). However, some current models do not include super coarse dust (Checa-Garcia et al., **2021**; Wu et al., **2020**; Zhao et al., **2022**). Other models that do represent super coarse dust underestimate their abundance by over an order of magnitude (Adebiyi & Kok, **2020**). This omission or underestimation of super coarse dust by models hinder our quantitative understanding of how dust aerosols affect the current and future climates (Adebiyi & Kok, **2020**; Di Biagio et al., **2020**; Ryder et al., **2019**).

Because the underestimation of super coarse dust by models could be due to an underestimation of super coarse dust emission, we develop a new parameterization of the PSD of emitted dust that accounts for the emission of super coarse dust (Section **2**). We implement this new parameterization in the Community Earth System Model (CESM, version 1.2) and evaluate the simulated atmospheric dust PSD with in situ aircraft measurements (Sections **3** and **4**). We find that the CESM with this new parameterization reproduces the abundance of super coarse dust close to dust source regions. We also discuss possible reasons why the model still underestimates super coarse dust further from source regions (Section **5**).

Nature Communications, vol. 13, issue no. 1, pp. 7079, doi:10.1038/s41467-022-34411-5

# Global crop yields can be lifted by timely adaptation of growing periods to climate change

Minoli, S.[3], **J. Jägermeyr**[1,2,3], S. Asseng, A. Urfels, and C. Müller[3], 2022

NASA Goddard Institute for Space Studies, New York, NY, USA[1]
Center for Climate Systems Research, Columbia University, New York, NY, USA[2]
Potsdam Institute for Climate Impact Research (PIK), Member of the Leibniz Association, Potsdam, Germany[3]

**Abstract.** Adaptive management of crop growing periods by adjusting sowing dates and cultivars is one of the central aspects of crop production systems, tightly connected to local climate. However, it is so far underrepresented in crop-model based assessments of yields under climate change. In this study, we integrate models of farmers' decision making with biophysical crop modeling at the global scale to simulate crop calendars adaptation and its effect on crop yields of maize, rice, sorghum, soybean and wheat. We simulate crop growing periods and yields (1986-2099) under counterfactual management scenarios assuming no adaptation, timely adaptation or delayed adaptation of sowing dates and cultivars. We then compare the counterfactual growing periods and corresponding yields at the end of the century (2080-2099). We find that (i) with adaptation, temperature-driven sowing dates (typical at latitudes >30°N-S) will have larger shifts than precipitation-driven sowing dates (at latitudes <30°N-S); (ii) later-maturing cultivars will be needed, particularly at higher latitudes; (iii) timely adaptation of growing periods would increase actual crop yields by ~12%, reducing climate change negative impacts and enhancing the positive $CO_2$ fertilization effect. Despite remaining uncertainties, crop growing periods adaptation require consideration in climate change impact assessments.

**Introduction.** Plant phenology is the sequence of morphological and physiological events in the annual plant growth cycle. As the onset and rate of progress of phenological events are primarily driven by temperature and day length, the rising global temperatures due to climate change alter the timing of plants' phenology. Phenological records of the recent past in Europe show that the responses of plants to temperature increase have determined earlier and faster phenological progress of both wild and cultivated plants[1,2]. Faster-growing cycles associated with higher temperatures are considered one of the main mechanisms of climate change impacts on crop yields[3,4].

However, the phenology of annual crops depends also on farmers' decisions on sowing dates and varietal choice[5,6,7]. Annual crops have growing-period durations (here defined as days from sowing to maturity) of less than a year. They are thus exposed only to a fraction of the annual weather[8], and farmers manage crops to enhance yields and resource use by growing them during the most favorable part of the year. Through plant domestication and breeding, humans have artificially modified the response of cultivated varieties (cultivars) to temperature and day length and by that, have expanded the area where crop species can be grown[8,9]. Farmers can thus draw from a vast assortment of cultivars that differ by their thermal time (maturity classes), photoperiod (long-day, short-day or day-neutral) and vernalization requirements (vernalizing, non-vernalizing or facultative), which are considered central for adapting cropping systems to changing climatic conditions[9].

It is essential to accurately represent growing periods in crop simulation models for estimating yield responses to climatic factors[10]. At the global scale, calibration of crop growing periods to reported historical crop calendars[11,12,13] has been shown to improve simulation of observed interannual yield variability[14,15]. However, for climate impact assessments, previous studies have not assessed farmers' adaptive behavior and relied on observation-based static crop calendars, thereby either assuming unchanged sowing dates and cultivar selection[13,16], or simply adapting crop cultivars to regain the duration of the reference growing period that is otherwise shortened with accelerated phenology under climate change[17].

Geophysical Research Letters, vol. 49, issue no. 5, e2021GL097133, doi:10.1029/2021GL097133

# Asymmetric warming/cooling response to $CO_2$ increase/decrease due to non-logarithmic forcing, not feedbacks

**Mitevski**, **I.**[2], L. Polvani[2], and **C. Orbe**[2], 2022

NASA Goddard Institute for Space Studies, New York, NY, USA[1]
Department of Applied Physics and Applied Mathematics, Columbia University, New York, NY, USA[2]

**Abstract.** We explore the $CO_2$ dependence of effective climate sensitivity ($S_G$) with symmetric abrupt and transient $CO_2$ forcing, spanning the range 1/8×, 1/4×, 1/2×, 2×, 4×, and 8×$CO_2$, using two state-of-the-art fully coupled atmosphere-ocean-sea-ice-land models. In both models, under abrupt $CO_2$ forcing, we find an asymmetric response in surface temperature and $S_G$. The surface global warming at 8×$CO_2$ is more than one third larger than the corresponding cooling at 1/8×$CO_2$, and $S_G$ is $CO_2$ dependent, increasing non-monotonically from 1/8×$CO_2$ to 8×$CO_2$. We find similar $CO_2$ dependence in the transient runs, forced with $-1\%yr^{-1}CO_2$ and $+1\%yr^{-1}CO_2$ up to 1/8×$CO_2$ and 8×$CO_2$, respectively. The non-logarithmic radiative forcing—not the changing feedbacks—primarily explains the dependence of $S_G$ on $CO_2$, particularly at low $CO_2$ levels. The changing feedbacks, however, explain $S_G$'s non-monotonic behavior.

**Introduction.** Equilibrium climate sensitivity (ECS) is the global mean surface temperature change after the doubling of $CO_2$ concentrations from pre-industrial (PI) levels. ECS is perhaps the most important metric in climate science, and it has been extensively investigated in the literature (Sherwood et al., **2020**). An important question is whether the amount of warming for each $CO_2$ doubling (which we refer to as the effective climate sensitivity, $S_G$) is constant or not (i.e., whether it is $CO_2$ dependent). Necessary conditions for a constant $S_G$ are (a) that the radiative forcing of the climate system for each $CO_2$ doubling is constant and (b) that the net radiative feedback does not change with $CO_2$ levels. This question has been investigated in many modeling studies (Bloch-Johnson et al., **2021**; Meraner et al., **2013**; Mauritsen et al., **2019**; Sherwood et al., **2020**), which have reported that $S_G$ is indeed $CO_2$ dependent. Most of these studies find that $S_G$ increases at higher $CO_2$ levels and that the change in feedbacks, not the change in $CO_2$ radiative forcing, is the primary driver of $S_G$ $CO_2$ dependence.

An alternative approach to using climate models to investigate the dependency of $S_G$ on $CO_2$ is to seek observational constraints from reconstructions of past climates. In particular, most studies conclude that $S_G$ inferred from paleoclimate records does depend on $CO_2$ (Anagnostou et al., **2016**, **2020**; Caballero & Huber, **2013**; Farnsworth et al., **2019**; Friedrich et al., **2016**; Shaffer et al., **2016**; Zhu et al., **2019**), although a few studies disagree (e.g., Martínez-Botí et al., **2015**). An ideal period to study the $S_G$ from past climate is the Last Glacial Maximum (LGM), approximately 21 kyr ago, when the Earth was roughly 6K colder than PI conditions (Tierney et al., **2020**). The LGM period is of particular interest because the climate system was in a quasi-equilibrium state, the climate forcings were large, and the surface temperature reconstructions are relatively well-constrained (Zhu & Poulsen, **2021**). However, when considering the LGM and other periods in Earth's past, one needs to account for how the feedbacks in those past climate states differ from the feedbacks operating in the modern state: hence the challenge in using paleoclimate-based estimates to constrain $S_G$.

While modeling and paleoclimatic evidence suggest that $S_G$ depends on $CO_2$, a systematic exploration of the symmetry over a wide range of $CO_2$ forcing has yet to be performed. The question thus remains: is the climate system response symmetric across a broad range of positive (warm) and negative (cold) $CO_2$ forcings? The question of symmetry was examined recently by Chalmers et al. (2022), who compared 1/2× and 2×CO2 simulations performed with the CESM1-CAM5 model and found that global surface temperatures warm 20% more than they cool.

Journal of Physical Oceanography, vol. 52, issue no. 5, pp. 889-906, doi:10.1175/JPO-D-21-0240.1

# Physical drivers of ocean wave attenuation in the marginal ice zone

Montiel, F., A.L. Kohout, and **L.A. Roach**[1,2,3], 2022

NASA Goddard Institute for Space Studies, New York, NY, USA[1]
Center for Climate Systems Research, Columbia University, New York, NY, USA[2]
Department of Atmospheric Sciences, University of Washington, Seattle, Washington, USA[3]

**Abstract.** Despite a recent resurgence of observational studies attempting to quantify the ice-induced attenuation of ocean waves in polar oceans, the physical processes governing this phenomenon are still poorly understood. Most analyses have attempted to relate the spatial rate of wave attenuation to wave frequency but have not considered how this relationship depends on ice, wave, and atmospheric conditions. An in-depth analysis of the wave-buoy data collected during the 2017 Polynyas, Ice Production, and Seasonal Evolution in the Ross Sea (PIPERS) program in the Ross Sea is conducted. Standard techniques are used to estimate the spatial rate of wave attenuation $\alpha$, and the influence of a number of potential physical drivers on its dependence on wave period $T$ is investigated. A power law is shown to consistently describe the $\alpha(T)$ relationship, in line with other recent analyses. The two parameters describing this relationship are found to depend significantly on sea ice concentration, mean wave period, and wind direction, however. Looking at cross correlations between these physical drivers, three regimes of ice-induced wave attenuation are identified, which characterize different ice, wave, and wind conditions, and very possibly different processes causing this observed attenuation. This analysis suggests that parameterizations of ice-induced wave decay in spectral wave models should be piecewise, so as to include their dependence on local ice, wave, and wind conditions.

**Introduction.** The Southern Ocean has experienced the most intense changes in ocean wave activity resulting from the observed increase in extreme weather events caused by climate change (**Young et al. 2011**; **Young and Ribal 2019**). As the frequency and magnitude of large wave events continue to grow under projected climate change scenarios (**Meucci et al. 2020**), it has been conjectured that sea ice morphology will be increasingly affected by the climatology of ocean waves at high latitudes (**Kohout et al. 2014**). Both the growth and melt seasonal sea ice cycles are impacted by local wave conditions, e.g., as pancake ice is more likely to form in a wavy sea (**Shen et al. 2001**; **Roach et al. 2018c**; **Nose et al. 2021**), while wave-induced sea ice breakup magnifies the thawing rate of the ice cover in spring and summer (**Bennetts et al. 2017**; **Roach et al. 2018b**, **2019**). The outer band of the ice cover where ocean waves and sea ice dynamics are strongly coupled is referred to as the marginal ice zone (MIZ).

In turn, the extent to which sea ice dynamics respond to changes in wave conditions depends significantly on how quickly wave energy attenuates with distance from the ice edge in the MIZ. This spatial rate of ice-induced wave attenuation is understood to be governed by (i) a conservative multiple scattering process (**Montiel et al. 2016**) and (ii) a collection of dissipative physical processes, e.g., under-ice turbulence and overwash (e.g., **Voermans et al. 2019**; **Nelli et al. 2020**). Despite a recent explosion of research in the modeling and observation of these phenomena (**Squire 2020**), much remains to be understood with regards to their relative importance as a function of ice and wave conditions. Using spectral wave modeling, **Ardhuin et al. (2020)** argue that dissipation caused by anelastic ice deformations dominates over other processes in explaining the observed attenuation of significant wave height in the Ross Sea winter MIZ. In particular, these authors suggest attenuation caused by scattering in a broken ice field is negligible, as long-crested, low-frequency waves travel nearly unaffected by the presence of sea ice under such conditions, confirming similar earlier findings in the Arctic Ocean (**Ardhuin et al. 2016**). However, the spatial rate of wave energy attenuation, usually referred to as the attenuation coefficient and denoted by $\alpha(T)$, depends on the wave period $T$, so that different mechanisms are likely to govern attenuation in different spectral bands of the wave spectrum, with scattering only important at short wave periods.

Scientific Data, vol. 9, issue no. 1, pp. 123, doi:10.1038/s41597-022-01194-9

# Scientific data from precipitation driver response model intercomparison project

Myhre, G., B. Samset, P.M. Forster, Ø. Hodnebrog, M. Sandstad, C.W. Mohr, J. Sillmann, C.W. Stjern, T. Andrews, O. Boucher, **G.S. Faluvegi**[1,2], T. Iversen, J.-F. Lamarque, M. Kasoar, A. Kirkevåg, R. Kramer[3,4], L. Liu, J. Mülmenstädt, D. Olivié, J. Quaas, T.B. Richardson, D. Shawki, D. Shindell, C. Smith, P. Stier, T. Tang, T. Takemura, A. Voulgarakis, and D. Watson-Parris, 2022

NASA Goddard Institute for Space Studies, New York, NY, USA[1]
Center for Climate Systems Research, Columbia University, New York, NY, USA[2]
Climate and Radiation Laboratory, NASA Goddard Space Flight Center, Greenbelt, MD, USA[3]
Universities Space Research Association, 7178 Columbia Gateway Drive, Columbia, MD, USA[4]

**Abstract.** his data descriptor reports the main scientific values from General Circulation Models (GCMs) in the Precipitation Driver and Response Model Intercomparison Project (PDRMIP). The purpose of the GCM simulations has been to enhance the scientific understanding of how changes in greenhouse gases, aerosols, and incoming solar radiation perturb the Earth's radiation balance and its climate response in terms of changes in temperature and precipitation. Here we provide global and annual mean results for a large set of coupled atmospheric-ocean GCM simulations and a description of how to easily extract files from the dataset. The simulations consist of single idealized perturbations to the climate system and have been shown to achieve important insight in complex climate simulations. We therefore expect this data set to be valuable and highly used to understand simulations from complex GCMs and Earth System Models for various phases of the Coupled Model Intercomparison Project.

**Background & Summary.** The Precipitation Driver Response Model Intercomparison Project (PDRMIP)1 was launched in November 2013 in an effort to improve our insight on how various mechanisms that perturb the planetary radiation balance induce precipitation changes. This includes the most important anthropogenic climate drivers such as greenhouse gases and aerosols as well as natural changes in the solar incoming radiation.

The motivation for PDRMIP arose from climate model simulations showing that the global and annual mean precipitation changes occurring on a fast time scale, of the order of months to a few years, depend on the atmospheric absorption and are strongly dependent on climate drivers, whereas the slow response, on order of decades to centuries, is dependent on the temperature change and independent of climate drivers2,3. The physical reason for these relationships is energy constraints4,5,6. The link between precipitation changes and climate sensitivity due to perturbation of the radiation balance by a climate driver is strong, but the diversity between climate models is not fully settled7.

PDRMIP includes idealised experiments of large and abrupt changes in all major greenhouse gases and aerosols. The experiment setup allows for diagnosing perturbations to the radiation balance and the precipitation changes both on a fast and a slow timescale. Twelve modelling groups have submitted PDRMIP results. Analyses of the PDRMIP results are being conducted by groups contributing to PDRMIP as well as groups outside the core PDRMIP modelling groups.

The PDRMIP data are valuable in several aspects, their main purpose was to contribute to the understanding of precipitation changes, but the data also yield insights into radiative forcing, climate feedbacks and surface temperature changes. The results from PDRMIP have so far given improved knowledge of how the climate drivers influence the hydrological sensitivity and extreme precipitation on a regional and global scale8,9,10,11,12,13,14,15,16. One main result from the PDRMIP analysis is that black carbon in the atmosphere has a weak surface temperature response caused by a strong negative rapid adjustment17,18. Two studies have provided important knowledge on the effective radiative forcing (ERF) concept19,20.

Journal of Advances in Modeling Earth Systems, vol. 14, issue no. 7, e2021MS002871,
doi:10.1029/2021MS002871



# Future climate change under SSP emission scenarios with GISS-E2.1

**Nazarenko**, **L.S.**[1,2], **N.L. Tausnev**[1,3], **G.L. Russell**[1], **D. Rind**, **R.L. Miller**[1,4], **G.A. Schmidt**[1], **S.E. Bauer**[1], **M.A. Kelley**[1], **R.A. Ruedy**[1,3], **A.S. Ackerman**[1], **I. Aleinov**[1,5], **M. Bauer**[1,5], R. Bleck, **V.M. Canuto**[1], **G.V. Cesana**[1,5], **Y. Cheng**[1,5], T.L. Clune[6], **B.I. Cook**[1], C.A. Cruz[6,7], **A.D. Del Genio**[1], **G.S. Elsaesser**[1,4], **G.S. Faluvegi**[1,5], **N.Y. Kiang**[1], D. Kim, **A.A. Lacis**[1], **A. Leboissetier**[1,3], **A.N. LeGrande**[1], **K.K. Lo**[1,3], **J. Marshall**, **E.E. Matthews**[1], **S.S. McDermid**[1,8], **K. Mezuman**[1,5], L.T. Murray, **V. Oinas**[1,3], **C. Orbe**[1], C.P. García-Pando, **J.P. Perlwitz**[1,9], **M.J. Puma**[1,5], **A. Romanou**[1], D.T. Shindell, S. Sun, **K. Tsigaridis**[1,5], **G. Tselioudis**[1], **E. Weng**[1,5], **J. Wu**[1,4], and **M.-S. Yao**[1,3], **2022**

NASA Goddard Institute for Space Studies, New York, NY, USA[1]
Center for Climate Systems Research, Columbia University, New York, NY, USA[2]
SciSpace, LLC., New York, NY, USA[3]
Department of Applied Physics and Applied Mathematics, Columbia University, New York, NY, USA[4]
Center for Climate Systems Research, Earth Institute, Columbia University, New York, NY, USA[5]
Goddard Space Flight Center, Greenbelt, MD, USA[6]
SSAI, Greenbelt, MD, USA[7]
Department of Environmental Studies, New York University, New York, NY, USA[8]
Climate, Aerosol, and Pollution Research, LLC., Bronx, NY, USA[9]

**Abstract.** This paper presents the response to anthropogenic forcing in the GISS-E2.1 climate models for the 21st century Shared Socioeconomic Pathways emission scenarios within the Coupled Model Intercomparison Project Phase 6 (CMIP6). The experiments were performed using an updated and improved version of the NASA Goddard Institute for Space Studies (GISS) coupled general circulation model that includes two different versions for atmospheric composition: A non-interactive version (NINT) with prescribed composition and a tuned aerosol indirect effect and the One-Moment Aerosol model (OMA) version with fully interactive aerosols which includes a parameterized first indirect aerosol effect on clouds. The effective climate sensitivities are 3.0°C and 2.9°C for the NINT and OMA models, respectively. Each atmospheric version is coupled to two different ocean general circulation models: The GISS ocean model (E2.1-G) and HYCOM (E2.1-H). We describe the global mean responses for all future scenarios and spatial patterns of change for surface air temperature and precipitation for four of the marker scenarios: SSP1-2.6, SSP2-4.5, SSP4-6.0, and SSP5-8.5. By 2100, global mean warming ranges from 1.5°C to 5.2°C relative to 1,850–1,880 mean temperature. Two high-mitigation scenarios SSP1-1.9 and SSP1-2.6 limit the surface warming to below 2°C by the end of the 21st century, except for the NINT E2.1-H model that simulates 2.2°C of surface warming. For the high emission scenario SSP5-8.5, the range is 4.6–5.2°C at 2100. Due to about 15% larger effective climate sensitivity and stronger transient climate response in both NINT and OMA CMIP6 models compared to CMIP5 versions, there is a stronger warming by 2100 in the SSP emission scenarios than in the comparable Representative Concentration Pathway (RCP) scenarios in CMIP5. Changes in sea ice area are highly correlated to global mean surface air temperature anomalies and show steep declines in both hemispheres, with the largest sea ice area decreases occurring during September in the Northern Hemisphere in both E2.1-G (−1.21 × 106 km2/°C) and E2.1-H models (−0.94 × 106 km2/°C). Both coupled models project decreases in the Atlantic overturning stream function by 2100. The largest decrease of 56%–65% in the 21st century overturning stream function is produced in the warmest scenario SSP5-8.5 in the E2.1-G model, comparable to the reduction in the corresponding CMIP5 GISS-E2 RCP8.5 simulation. Both low-end scenarios SSP1-1.9 and SSP1-2.6 also simulate substantial reductions of the overturning (9%–37%) with slow recovery of about 10% by the end of the 21st century (relative to the maximum decrease at the middle of the 21st century).

Hydrology and Earth System Sciences, vol. 26, issue no. 1, pp. 71-89, doi:10.5194/hess-26-71-2022

# Improved representation of agricultural land use and crop management for large scale hydrological impact simulation in Africa using SWAT+

Nkwasa, A., C.J. Chawanda, **J. Jägermeyr**[1,2,3], and A. van Griensven, 2022

NASA Goddard Institute for Space Studies, New York, NY, USA[1]
Center for Climate Systems Research, Columbia University, New York, NY, USA[2]
Climate Resilience, Potsdam Institute for Climate Impact Research (PIK), Member of the Leibniz Association, Potsdam, Germany[3]

**Abstract.** To date, most regional and global hydrological models either ignore the representation of cropland or consider crop cultivation in a simplistic way or in abstract terms without any management practices. Yet, the water balance of cultivated areas is strongly influenced by applied management practices (e.g., planting, irrigation, fertilization, and harvesting). The SWAT+ (Soil and Water Assessment Tool) model represents agricultural land by default in a generic way, where the start of the cropping season is driven by accumulated heat units. However, this approach does not work for tropical and subtropical regions such as sub-Saharan Africa, where crop growth dynamics are mainly controlled by rainfall rather than temperature. In this study, we present an approach on how to incorporate crop phenology using decision tables and global datasets of rainfed and irrigated croplands with the associated cropping calendar and fertilizer applications in a regional SWAT+ model for northeastern Africa.

We evaluate the influence of the crop phenology representation on simulations of leaf area index (LAI) and evapotranspiration (ET) using LAI remote sensing data from Copernicus Global Land Service (CGLS) and WaPOR (Water Productivity through Open access of Remotely sensed derived data) ET data, respectively. Results show that a representation of crop phenology using global datasets leads to improved temporal patterns of LAI and ET simulations, especially for regions with a single cropping cycle. However, for regions with multiple cropping seasons, global phenology datasets need to be complemented with local data or remote sensing data to capture additional cropping seasons. In addition, the improvement of the cropping season also helps to improve soil erosion estimates, as the timing of crop cover controls erosion rates in the model. With more realistic growing seasons, soil erosion is largely reduced for most agricultural hydrologic response units (HRUs), which can be considered as a move towards substantial improvements over previous estimates. We conclude that regional and global hydrological models can benefit from improved representations of crop phenology and the associated management practices. Future work regarding the incorporation of multiple cropping seasons in global phenology data is needed to better represent cropping cycles in areas where they occur using regional to global hydrological models.

**Introduction.** Even though cropland cultivation covers over 40 % of the planet's ice-free land surface, most regional and global hydrological model applications overlook the necessity of addressing crop phenological development and/or distinguishing between different crops (Chen and Xie, 2012; Srivastava et al., 2020). In some regional applications (e.g., Schuol and Abbaspour, 2006; Schuol et al., 2008; Chawanda et al., 2020), the model applications consider one uniform generic crop as a simplification for agricultural land use representation despite the existing wide variety of crops in agricultural land use (Sood and Smakhtin, 2015). Using a uniform generic crop for agricultural land use modelling fails to account for any variability in vegetation attributes, such as leaf area index (LAI), corresponding to several crops in real-world scenarios (Viña et al., 2011). Detailed agricultural land use representation in hydrological models is important as heterogeneity in agricultural land use can have a significant effect on hydrological fluxes such as evapotranspiration (ET) and soil moisture (Srivastava et al., 2020).

Atmospheric Measurement Techniques, vol. 15, issue no. 5, pp. 1373-1394, doi:10.5194/amt-15-1373-2022

# Above-aircraft cirrus cloud and aerosol optical depth from hyperspectral irradiances measured by a total-diffuse radiometer

Norgren, M.S., J. Wood, K.S. Schmidt, **B. van Diedenhoven**[1,2], S.A. Stamnes[3], L.D. Ziemba[3], E.C. Crosbie[3], M.A. Shook[3], A.S. Kittelman, S.E. LeBlanc[4,5], S. Broccardo[4,5,6], S. Freitag, and J.S. Reid, 2022

NASA Goddard Institute for Space Studies, New York, NY, USA[1]
SRON Netherlands Institute for Space Research, Utrecht, the Netherlands[2]
NASA Langley Research Center, Hampton, VA, USA[3]
NASA Ames Research Center, Moffett Field, CA, USA[4]
Bay Area Environmental Research Institute, Moffett Field, CA, USA[5]
Universities Space Research Association, Columbia, MD, USA[6]

**Abstract.** This study develops the use of spectral total and diffuse irradiance measurements, made from a prototype hyperspectral total-diffuse sunshine pyranometer (SPN-S), to retrieve layer fine-mode aerosol ($\tau_{aer}$) and total optical depths from airborne platforms. Additionally, we use spectral analysis in an attempt to partition the total optical depth into its $\tau_{aer}$ and cirrus cloud optical depth ($\tau_{cld}$) components in the absence of coarse-mode aerosols. Two retrieval methods are developed: one leveraging information in the diffuse irradiance and the other using spectral characteristics of the transmitted direct beam, with each approach best suited for specific cloud and aerosol conditions. The SPN-S has advantages over traditional sun photometer systems, including no moving parts and a low cost. However, a significant drawback of the instrument is that it is unable to measure the direct-beam irradiance as accurately as sun photometers. To compensate for the greater measurement uncertainty in the radiometric irradiances, these retrieval techniques employ ratioed inputs or spectral information to reduce output uncertainty. This analysis uses irradiance measurements from the SPN-S and the solar spectral flux radiometer (SSFR) aboard the National Aeronautics and Space Administration's (NASA) P-3 aircraft during the 2018 deployment of the ObseRvations of Aerosols above CLouds and their intEractionS (ORACLES) campaign and the 2019 Cloud, Aerosol and Monsoon Processes Philippines Experiment (CAMP$^2$Ex) mission to quantify above-aircraft cirrus $\tau_{cld}$ and derive vertical profiles of layer $\tau_{aer}$. Validation of the $\tau_{aer}$ retrieval is accomplished by comparison with co-located measurements of direct solar irradiance made by the Sky-Scanning Sun-Tracking Atmospheric Research (4STAR) and in situ measurements of aerosol optical depth. For the aggregated 2018 ORACLES results, regression between the SPN-S-based method and sun photometer $\tau_{aer}$ values yields a slope of 0.96 with an $R^2$ of 0.96, while the root mean square error (RMSE) is $3.0 \times 10^{-2}$. When comparing the retrieved $\tau_{aer}$ to profiles of integrated in situ measurements of optical extinction, the slope, $R^2$, and RMSE values for ORACLES are 0.90, 0.96, and $3.4 \times 10^{-2}$, and for CAMP$^2$Ex they are 0.94, 0.97, and, $3.4 \times 10^{-2}$, respectively.

**Introduction.** Clouds and aerosol particles both play important roles in controlling the flux of solar radiation through the Earth's atmosphere. Despite their relevance to the broader climate system and Earth's radiative balance, significant uncertainty exists in quantifying the optical properties of atmospheric systems containing one or both constituents. Traditional passive remote sensing methods retrieve aerosol properties in the absence of clouds (Holben et al., 1998; Levey et al., 2013). This is because when clouds are thick their radiative signal is large in relation to the aerosol signal, and when clouds are thin it is difficult to separate the two signals. For automated aerosol optical depth ($\tau_{aer}$) retrievals, the challenge of cloud detection and removal is a significant hurdle to overcome (Smirnov et al., 2000; Remer et al., 2012; Spencer et al., 2019; Yang et al., 2019). Advanced methods, such as the spectral deconvolution algorithm (SDA), have been developed to differentiate between fine- and coarse-mode $\tau_{aer}$ using spectral sun photometry data (O'Neill et al., 2003), though these techniques are limited when cirrus is present (Smirnov et al., 2018). Conversely, retrieval of cloud optical depth ($\tau_{cld}$) tends to be insensitive to the aerosol loading of the local environment because clouds are often much thicker optically than aerosols. A common exception to this occurs when thin cirrus clouds are present.

Frontiers in Remote Sensing, vol. 3, pp. 863239, doi:10.3389/frsen.2022.863239

# Polarization as a discriminator of light-absorbing impurities in or above snow

**Ottaviani**, **M.**[1,2], 2022

NASA Goddard Institute for Space Studies, New York, NY, USA[1]
Terra Research Inc, Hoboken, NJ, USA[2]

**Abstract.** This conceptual study presents advanced radiative transfer computations of light polarization originating from a snowpack consisting of non-spherical grains and variable content of light-absorbing impurities, either embedded in the snowpack or (with the same optical properties) lofted above it in the form of atmospheric aerosols. The results highlight the importance of considering shapes other than spherical for the snow grains, which otherwise can lead to non-negligible errors in the retrieval of snow albedo from remote sensing observations. More importantly, it is found that polarimetric measurements provide a means to partition light-absorbing impurities embedded in the snowpack from absorbing aerosols aloft, a task traditionally prohibitive for sensors capable exclusively of measurements of total reflectance. Heritage techniques to obtain snow grain size from shortwave infrared observations of total reflectance are well established, as are those that leverage polarimetric, multi-angular observations across the entire optical spectrum to characterize the optical and microphysical properties of atmospheric aerosols. The polarization signatures of near-infrared (e.g., 864 nm) observations carry critical information on snow grain shape. The prospected launch of space-borne polarimeters with proven accuracy, therefore, advocates for the development of data inversion schemes, to boost the accuracy of simultaneous retrievals of atmospheric and surface parameters in the polar and snow-covered regions, critical to climate studies.

**Introduction.** The scientific interest in quantifying the surface energy and mass balance (SEMB) of the ice sheets is obvious when considering the potential impacts on global climate of variations in the brightness of such regions (**Hansen and Nazarenko, 2004**; **Fettweis et al., 2008**; **van den Broeke et al., 2011**; **Rae et al., 2012**; **Van Angelen et al., 2012**; **Tedesco et al., 2013**; **Alexander et al., 2014**; **Colgan et al., 2014**). On the other hand, upper estimates of the projected sea level rise are still very uncertain because of poor knowledge of ice sheet dynamics and the SEMB in the polar areas (**Van Angelen et al., 2012**), which demand a better characterization of their albedo.

As the albedo of snow-covered regions depends on the microphysical and optical properties of the constituent ice crystals (**Wiscombe and Warren, 1980**; **Aoki et al., 2000**; **Bartelt and Lehning, 2002**; **Flanner and Zender, 2006**; **Bougamont et al., 2007**; **Dang et al., 2016**; **He et al., 2018**), and on the content of light-absorbing impurities (LAIs) (**Warren and Wiscombe, 1980**; **Hansen and Nazarenko, 2004**; **Dumont et al., 2014**), a better knowledge of such properties and their evolution is a high-priority objective for the remote sensing of the cryosphere (**Tedesco et al., 2013**; **Dumont et al., 2014**). In developing techniques for the retrieval of these climatologically relevant parameters (**Krabill et al., 2004**; **Comiso, 2006**; **Zwally and Giovinetto, 2011**; **Zatko et al., 2013**), particular attention has been given to the Greenland ice sheet (GrIS) (**Hori et al., 2007**; **Tedesco et al., 2011**, **2013**; **Box et al., 2012**), for which quantitative explanations of the ascertained mass losses are still lacking (**Velicogna, 2009**). Aerosol (especially black carbon) transport (**Dumont et al., 2014**; **Tedesco et al., 2016**) and deposition (**Doherty et al., 2014**), consolidation of LAIs (including black and organic carbon, and dust) through melt and scavenging, exposure of bare ice, and biogenic contributions cause large variations in the albedo of the GrIS and deeply affect its SEMB, especially in the topographically complex coastal region known as the ablation zone (**Alexander et al., 2014**; **Schmale et al., 2021**).

Nature Geoscience, 15, issue no. 9, pp. 726-734, doi:10.1038/s41561-022-00999-y

# Mid-Pliocene El Niño/Southern Oscillation suppressed by Pacific intertropical convergence zone shift.

Pontes, G., A. Taschetto, A. Sen Gupta, A. Santoso, I. Wainer, A. Haywood, W.-L. Chan, A. Abe-Ouchi, C. Stepanek, G. Lohmann, S. Hunter, J. Tindall, **M.A. Chandler**[1,2], **L.E. Sohl**[1,2], D. Peltier, D. Chandan, Y. Kamae, K. Nisancioglu, Z. Zhang, C. Contoux, N. Tan, Q. Zhang, B. Otto-Bliesner, E. Brady, R. Feng, A. von der Heydt, M. Baatsen, and A. Oldemann, 2022

NASA Goddard Institute for Space Studies, New York, NY, USA[1]
Center for Climate Systems Research, Columbia University, New York, NY, USA[2]

**Abstract.** The El Niño/Southern Oscillation (ENSO), the dominant driver of year-to-year climate variability in the equatorial Pacific Ocean, impacts climate pattern across the globe. However, the response of the ENSO system to past and potential future temperature increases is not fully understood. Here we investigate ENSO variability in the warmer climate of the mid-Pliocene (~3.0–3.3 Ma), when surface temperatures were ~2–3 °C above modern values, in a large ensemble of climate models—the Pliocene Model Intercomparison Project. We show that the ensemble consistently suggests a weakening of ENSO variability, with a mean reduction of 25% (±16%). We further show that shifts in the equatorial Pacific mean state cannot fully explain these changes. Instead, ENSO was suppressed by a series of off-equatorial processes triggered by a northward displacement of the Pacific intertropical convergence zone: weakened convective feedback and intensified Southern Hemisphere circulation, which inhibit various processes that initiate ENSO. The connection between the climatological intertropical convergence zone position and ENSO we find in the past is expected to operate in our warming world with important ramifications for ENSO variability.

**Main.** El Niño/Southern Oscillation (ENSO) warm (El Niño) and cold (La Niña) events cause substantial changes in weather patterns and ocean circulation, impacting agriculture, fisheries, coral bleaching and cyclogenesis, among a host of other impacts[1]. Given its pronounced socioeconomic impacts and potential predictability of a few seasons in advance, ENSO has been under intense investigation[2]. Whether and how ENSO changes in response to greenhouse gases and other external forcing may be studied by investigating past, present and future climates with palaeo-reconstructions, instrumental records, theory and numerical simulations. There is a lack of consensus among climate models in general as to how ENSO variability will respond to future warming[3,4], although models that better capture ENSO nonlinearity tend to simulate enhanced variability in the eastern equatorial Pacific[5] and increased frequency of extreme events[6,7]. These changes in ENSO properties are linked to changes in the Pacific mean state marked by a weakened Walker circulation, increased upper-ocean stratification, reduced zonal sea surface temperature (SST) gradient and equatorially enhanced warming that causes the intertropical convergence zone (ITCZ) to be displaced equatorward[7,8,9].

Studies based on palaeo-reconstructions have also suggested that ENSO activity is sensitive to the mean climate. A synthesis of mid-Holocene (~6 thousand years ago (ka)) records indicates a 33% reduction in ENSO amplitude in the eastern Pacific during this period[10]. ENSO activity over the past millennium was shown to be weaker when compared with the past half century[11], potentially suggesting global warming-related changes. Furthermore, there is evidence of significantly reduced ENSO variability during the Last Glacial Maximum[12] (~21 ka). Proxy data for the Pliocene (~5 to ~3 million years ago (Ma)) are controversial with regard to tropical Pacific changes[13,14,15,16]. A Pliocene El Niño-like mean state has been hypothesized to reduce ENSO variability[17], although there is evidence of significant interannual variability during this period[18,19], whose magnitude could be comparable to the late Holocene[20]. As such, tropical Pacific mean-state changes during the Pliocene and how they have impacted ENSO activity remain uncertain.

Journal of Geophysical Research Atmospheres, vol. 27, issue no. 4, e2021JD035489, doi:10.1029/2021JD035489

# Summer Greenland blocking diversity and its impact on the surface mass balance of the Greenland Ice Sheet.

Preece, J.R., L.J. Wachowicz, T.L. Mote, **M. Tedesco**[1,2,3], and X. Fettweis, 2022

NASA Goddard Institute for Space Studies, New York, NY, USA[1]
Lamont-Doherty Earth Observatory, Columbia University, Palisades, NY, USA[2]
Data Science Institute, Columbia University, New York, NY, USA[3]

**Abstract.** The increase in Greenland Ice Sheet (GrIS) surface runoff since the turn of the century has been linked to a rise in Greenland blocking frequency. However, a range of synoptic patterns can be considered blocked flow and efforts that summarize all blocking types indiscriminately likely fail to capture consequential differences in GrIS response. To account for these differences, we employ ERA5 reanalysis to identify summer blocking using two independent blocking metrics: the Greenland Blocking Index (GBI) and the blocking index of Pelly and Hoskins (2003, **https://doi.org/10.1175/1520-0469(2003)060<0743:ANPOB>2.0.CO;2**). We then conduct a self-organizing map analysis to objectively classify synoptic conditions during Greenland blocking episodes and identify three primary blocking types: (a) a high-amplitude Omega block, (b) a lower-amplitude, stationary summer ridge, and (c) a cyclonic wave breaking pattern. Using Modèle Atmosphérique Régional output, we document the spatiotemporal progression of the surface energy and mass balance for each blocking type. Relative to all blocking episodes, summer ridge patterns produce more melt over the southern ice sheet, Omega blocks produce more melt across the northern ice sheet, and cyclonic wave breaking patterns produce more melt in northeast Greenland. Our results indicate that the recent trend in summer Greenland blocking was largely driven by an increase in Omega patterns and suggest that Omega blocks have played a central role in the recent acceleration of GrIS mass loss. Furthermore, the GBI exhibited a relative bias toward Omega patterns, which may help explain why it has measured stronger trends in summer Greenland blocking than other blocking metrics.

**Introduction.** Atmospheric blocking is characterized by a pronounced, quasi-stationary anticyclone that diverts incoming synoptic disturbances that would otherwise bring a change in weather conditions. In summer, persistent, widespread subsidence within the blocking ridge suppresses cloud cover and increases radiative warming at the surface, resulting in warm extremes (Tedesco et al., **2016**; Tedesco & Fettweis, **2020**; Woollings et al., **2018**). Given their impact on summer surface temperature more broadly, it is not surprising that blocking anticyclones over Greenland show a strong association with Greenland Ice Sheet (GrIS) surface melt and runoff over synoptic-to-decadal timescales (Ballinger et al., **2019**; Häkkinen et al., **2014**; Hanna et al., **2013**, **2014**; Hermann et al., **2020**; McLeod & Mote, **2016**). Indeed, Greenland blocking was instrumental in promoting exceptional surface melt in 2012 and 2019 that extended to Summit Station (Cullather et al., **2020**; Hanna et al., **2021**; Nghiem et al., **2012**; Tedesco & Fettweis, **2020**)—a phenomenon that has occurred, on average, only once every 153 years throughout most of the Holocene (Alley & Anandakrishnan, **1995**).

Blocking events encourage melt through their spatially varying influence on the surface energy balance (SEB). The poleward extension of the blocking ridge transports warm, moist air aloft that may then be mixed through the stable boundary layer to the surface (van den Broeke & Gallée, **1996**; Duynkerke & van den Broeke, **1994**; Gorter et al., **2014**). Southerly flow along the upstream flank of the blocking anticyclone often generates strong water vapor transport to northern Greenland through the Davis Strait (Ballinger et al., **2019**; Barrett et al., **2020**; Mattingly et al., **2018**; Ward et al., **2020**). Not only can this warm, southerly flow amplify turbulent heat flux along the western ablation zone (van den Broeke & Gallée, **1996**), but as it rounds the crest of the ridge and ascends the northwest ice sheet, it cools adiabatically and generates cloud cover that enhances downwelling longwave radiation over high elevations of the northern ice sheet (Hahn et al., **2020**; Mattingly et al., **2020**; Ward et al., **2020**).

ACS Earth Space Chemistry, vol. 6, issue no. 4, pp. 1011-1021, doi:10.1021/acsearthspacechem.1c00391

# A network of field-calibrated low-cost sensor measurements of $PM_{2.5}$ in Lomé, Togo, over one to two years.

Raheja, G.[2,3], K. Sabi, H. Sonla, E.K. Gbedjangni, C.M. McFarlane[2], C.G. Hodoli, and **D.M. Westervelt**[1,2,3], 2022

NASA Goddard Institute for Space Studies, New York, NY, USA[1]
Lamont-Doherty Earth Observatory of Columbia University, Palisades, NY, USA
Department of Earth and Environmental Science, Columbia University, New York, NY, USA[3]

**Abstract.** Air pollution is a leading cause of global premature mortality and is especially prevalent in many low- and middle-income countries (LMICs). In sub-Saharan Africa, preliminary monitoring networks, satellite retrievals of air-quality-relevant species, and air quality models show ambient fine particulate matter ($PM_{2.5}$) concentrations that far exceed the World Health Organization guidelines, yet many areas remain largely unmonitored and understudied. Deploying a network of five low-cost PurpleAir $PM_{2.5}$ monitors over 2 years (2019–2021), we present the first multiyear ambient air pollution monitoring data results from Lomé, Togo, a major West African coastal city with a population of about 1.4 million people. The full-study time period network-wide mean measured daily $PM_{2.5}$ concentration is 23.5 $\mu g\ m^{-3}\ m^{-3}$. The strong regional influence of the dry and dusty Harmattan wind increases the local average $PM_{2.5}$ concentration by up to 58% during December through February, but the diurnal and weekly trends in $PM_{2.5}$ are largely controlled by local influences. At all sites, more than 87% of measured days exceeded the new WHO Daily $PM_{2.5}$ guidelines; these first measurements highlight the need for air quality improvement in a rapidly growing urban metropolis.

**Introduction.** Air pollution is a burgeoning global health crisis. In 2019, it rose from the fifth to the fourth leading risk factor for premature death, associated with 6.67 million premature deaths **(1)** and up to 6 million premature births. **(2)** Exposure to $PM_{2.5}$, which is a form of air pollution composed of inhalable particulate matter smaller than 2.5 μm in aerodynamic diameter, is linked to asthma, ischemic heart disease, type II diabetes, lung cancer, and other deleterious health effects. **(1)** These particles are emitted from vehicles, coal-burning power plants, waste incineration, and other anthropogenic and natural sources. **(1)** Thus far, most academic research, monitoring, and media attention regarding $PM_{2.5}$ exposure have been largely focused on the United States, Europe, and recently, China. **(3,4)** Additional research is vital and urgent for other regions where air pollution levels might be even higher.

In particular, countries in Asia, Africa, and the Middle East face the highest levels of ambient $PM_{2.5}$. **(1,5)** Over the past decade, regions in sub-Saharan Africa have seen drastic increases in $PM_{2.5}$ concentrations, while high-income countries in Europe and North America have seen steady declines. **(1,6)** Recent research shows that 1.1 million premature deaths were attributable to air pollution across the African continent in 2019; **(7)** in the same year, over 8000 premature deaths were attributed to air pollution in Togo, a West African nation with a population of 8.3 million. **(8)** These deaths are coupled with hundreds of thousands more cumulatively in neighboring West African countries including Nigeria and Ghana. **(8,9)** Diseases attributable to chronic air pollution exposure in a small handful of West African countries lead to a cumulative loss of over 5 million years of healthy life. **(10)**

However, these estimated health impact numbers are extremely uncertain and preliminary in areas where neither air quality nor public health data are available. While in Europe and the United States, the mean population distance of a person to a $PM_{2.5}$ monitor is approximately 0–50 km, the global mean population distance of a person to a $PM_{2.5}$ monitor is about 220 km. **(3)** This metric is largely influenced by the sparsity of monitors in low- and middle-income countries (LMICs). **(3)** Throughout the entire African continent, approximately 400 million children live in areas with no reliable air quality monitoring, making actual impacts uncertain. **(11)**

Journal of Advances in Modeling Earth Systems, vol. 14, issue no. 8, e2021MS002893,
doi:10.1029/2021MS002893

# Constraining clouds and convective parameterizations in a climate model from past climate.

Ramos, R., **A.N. LeGrande**[1,2], M.L. Griffiths, **G.S. Elsaesser**[1,2], **D.T Litchmore**[1,2], J.F. Tierney, F.S.R. Pausata, and J Nusbaumer, 2022

NASA Goddard Institute for Space Studies, New York, NY, USA[1]
Center for Climate Systems Research, Columbia University, New York, NY, USA[2]

**Abstract.** Cloud and convective parameterizations strongly influence uncertainties in equilibrium climate sensitivity. We provide a proof-of-concept study to constrain these parameterizations in a perturbed parameter ensemble of the atmosphere-only version of the Goddard Institute for Space Studies Model E2.1 simulations by evaluating model biases in the present-day runs using multiple satellite climatologies and by comparing simulated δ18O of precipitation (δ18Op), known to be sensitive to parameterization schemes, with a global database of speleothem δ18O records covering the Last Glacial Maximum (LGM), mid-Holocene (MH) and pre-industrial (PI) periods. Relative to modern interannual variability, paleoclimate simulations show greater sensitivity to parameter changes, allowing for an evaluation of model uncertainties over a broader range of climate forcing and the identification of parts of the world that are parameter sensitive. Certain simulations reproduced absolute δ18Op values across all time periods, along with LGM and MH δ18Op anomalies relative to the PI, better than the default parameterization. No single set of parameterizations worked well in all climate states, likely due to the non-stationarity of cloud feedbacks under varying boundary conditions. Future work that involves varying multiple parameters sets simultaneously with coupled ocean feedbacks will likely provide improved constraints on cloud and convective parameterizations.

**Introduction.** Cloud and convective processes vary at scales significantly smaller than a general circulation model (GCM) grid box, requiring them to be parameterized on simulated grid-scale variables (Boucher et al., **2013**). Because such parameterizations employ different assumptions (Lopez, **2007**), representation of cloud and convective effects in climate models inherently hold large uncertainties. Cloud and convective parameterizations, aside from aerosol schemes and aerosol-cloud interactions (Meehl et al., **2020**), are considered the leading source of inter-model spread in equilibrium climate sensitivity (ECS) estimates (Dufresne & Bony, **2008**; Sherwood et al., **2014**; Webb et al., **2015**; Zelinka et al., **2020**) and consequently the broad range of future climate projections (Flato et al., **2013**; Sherwood et al., **2014**). The latest generation of climate models participating in Coupled Model Intercomparison Project Phase 6 (CMIP6) have an average ECS value of 3.9°C and range from 1.8°C to 5.6°C (Zelinka et al., **2020**), which is higher and more variable than the CMIP5 models (i.e., mean of 3.3°C and range of 1.5°C–4.5°C (Flato et al., **2013**; Knutti et al., **2017**) and estimates from the Intergovernmental Panel on Climate Change Assessment Report 6 (i.e., mean of 3°C with a very likely range of 2°C–5°C (Hausfather et al., **2022**; IPCC, **2021**).

Paleoclimate evidence provides additional constraints on ECS by offering an independent test of climate model performance. Colder and warmer intervals of well-known forcings and fairly stable climate states relative to the present instrumental period such as the Last Glacial Maximum (LGM; 21 ka or kilo-years before present) and the mid-Pliocene warm period (mPWP; 3.3–3.0 Ma or million years before present) indicate an ECS range of 1.5°C–5°C with a maximum likelihood of 2.5°C (Sherwood et al., **2020**). Based on temperature changes provided by paleorecords and known responses to climate forcings during these time periods, these joint yet independent paleoconstraints on ECS argue against extreme estimates of 1.2°C and greater than 6°C (Sherwood et al., **2014**; Zhu & Poulsen, **2020**). In another example, proxy-model comparison using the Community Earth System Model version 2 – one such model that reports an ECS greater than 5°C in the CMIP6 models – reveals that their simulated LGM cooling is excessive and not realistic relative to proxy reconstructions and previous model simulations, highlighting the cloud feedback-related source of their overestimated ECS (Zhu et al., **2021**).

Nature Geoscience, vol. 15, issue no. 4, pp. 277-281, doi:10.1038/s41561-022-00913-6

# Asymmetry in the seasonal cycle of Antarctic sea ice due to insolation.

**Roach**, **L.A.**[1,2], I. Eisenman, T.J. Wagner, E. Blanchard-Wrigglesworth[2], and C.M. Bitz[2], 2022

NASA Goddard Institute for Space Studies, New York, NY, USA[1]
Department of Atmospheric Sciences, University of Washington, Seattle, WA, USA[2]

**Abstract. T**he mean seasonal cycle of Antarctic sea-ice extent is asymmetric, with the period of ice retreat being approximately two months shorter than the period of ice advance. This feature is largely consistent in observations from year to year and across different satellite products. The asymmetry is also broadly reproduced by comprehensive climate models across generations from CMIP3 to CMIP6, with limited impacts from internal variability. Using a range of idealized climate models of varying complexity, we show that the seasonal cycle in top-of-atmosphere incident solar radiation drives the asymmetry. Because insolation in southern high latitudes departs from a sinusoid by having a narrow peak of intense brightness in summer and a long period of low light in winter, there is rapid summer ice retreat and gradual winter ice advance. This simple physical explanation is markedly different from those proposed in previous studies.

**Main.** The seasonal growth and melt of Antarctic Sea ice represents one of the largest annual surface cover changes on Earth. Antarctic sea ice is a key driver of the upper ocean freshwater budget[1] and the formation of Antarctic Bottom Water[2], which is a main component of the global ocean circulation. Changes in the sea-ice cover can have impacts on the Antarctic Ice Sheet[3]; Antarctic sea ice also plays a role in marine ecosystems and primary production[4]. The phase delay of sea ice relative to insolation influences the fraction of sunlight reflected annually back to space, a key component of Earth's energy budget.

There is a striking asymmetry in the seasonal cycle of Antarctic sea-ice extent between fast decay during ~5 months of the year and slow growth during the remaining ~7 months (ref. 5). This is not mirrored in the Arctic, where the durations of sea-ice retreat and advance are more similar (Supplementary Fig. 1). Much previous work has attempted to explain the enigma of this seasonal asymmetry in Antarctic sea-ice extent (see ref. 5 for a recent review). One of the main mechanisms put forward previously, based on an energy budget analysis from observations, is that upwelling and associated warm surface waters accelerate sea-ice melt[6,7]. An alternative mechanism, based on connections identified in observations, has the asymmetry caused by processes in the atmosphere rather than the ocean, with the semi-annual oscillation of the atmospheric low-pressure trough that surrounds the Antarctic continent creating patterns of convergence and divergence of Antarctic sea ice that favour fast ice retreat[8,9,10,11,12]. In this article, we systematically investigate the physical mechanism responsible for this asymmetry using observations and a range of climate models.

**Observations and Comprehensive Climate Models**. The observed mean seasonal cycle in Antarctic sea-ice extent is plotted in Fig. 1 (see **Methods** for details). The seasonal asymmetry can be readily seen in the plot. As a measure of this asymmetry, we define $\delta_I$ as the difference in length between the ice advance and retreat periods, with positive values indicating a shorter retreat season. In other words, $\delta_I$ is the duration of the advance season (that is, time from minimum to maximum ice extent) minus the duration of the retreat season (that is, time from maximum to minimum). In Fig. 1, the summer minimum occurs on 24 February, and the winter maximum occurs on 20 September. This implies that the retreat period is 51 days shorter than the growth period: $\delta_I = 51$ days for the mean seasonal cycle. This value is broadly consistent from year to year, across satellite data products and for both sea-ice extent and sea-ice area (Supplementary Figs. 1b and 2).

Geophysical Research Letters, vol. 49, issue no. 6, e2022GL097884, doi:10.1029/2022GL097884

# Observed winds crucial for September Arctic sea ice loss

**Roach**, **L.A.**[1,2], and E. Blanchard-Wrigglesworth[2], 2022

NASA Goddard Institute for Space Studies, New York, NY, USA[1]
Department of Atmospheric Sciences, University of Washington, Seattle, WA, USA[2]

**Abstract.** Arctic sea ice has declined strikingly over the past 40 years under climate change. The physical processes driving these changes and the relative roles of external forcing versus natural variability remain under debate, partly due to lack of confidence in the simulation of Arctic Sea ice by coupled climate models. Here, we nudge a widely used CMIP5-class model (CESM1) toward observed winds above the boundary layer. These simulations reproduce observed Arctic trend patterns and Arctic-average interannual fluctuations in near-surface temperature. We find that atmospheric circulation plays a crucial role in September Arctic Sea ice loss and sea ice interannual variability. Trends in the observed atmospheric circulation that are not part of the modeled forced response cause approximately 20%–25% of the modeled September Sea ice decline, which is in close agreement with the observed trend. However, our simulations do not capture sea ice loss in other seasons, pointing to important model biases in winter and spring.

**Introduction.** Over the satellite era, observations show rapid Arctic surface warming (Box et al., **2019**) and extensive sea ice decline (Comiso et al., **2017**). Annual-minimum (September) Arctic sea ice extent has declined by approximately 40% over the past 40 years, alongside substantial thinning (Kwok, **2018**), with implications for Arctic coastal communities (Cooley et al., **2020**; Molnár et al., **2020**), atmospheric (Screen & Simmonds, **2010**; Vihma, **2014**) and oceanic (Armitage et al., **2020**; Timmermans & Marshall, **2020**) circulation. Decadal trends in Arctic surface temperature and sea ice are driven by greenhouse gas (Notz & Stroeve, **2016**) and aerosol (Gagné et al., **2017**) emissions, volcanic forcing (Rosenblum & Eisenman, **2016**; Slawinska & Robock, **2018**), and natural internal variability, yet the contribution of each to the observed trend is still a matter of debate. Previous work has found that internal variability has accelerated sea ice loss, but estimates of the contribution of internal variability to September Arctic sea ice loss over the satellite period range widely, from 20% to 50% (Day et al., **2012**; Ding et al., **2017**, **2019**; Fox-Kemper et al., **2021**; Kay et al., **2011**; Notz & Marotzke, **2012**; Stroeve et al., **2007**, **2012**).

A variety of physical processes impact Arctic sea ice loss, although there is no consensus on which are the most important. These processes include the sea ice albedo feedback (Perovich et al., **2007**), atmospheric temperature fluctuations (Olonscheck et al., **2019**), moisture intrusions (Boisvert et al., **2016**), ocean heat input (Polyakov et al., **2017**), cloud feedbacks (Kay et al., **2008**), and the dynamic impact of winds on sea ice (Ogi et al., **2010**). A portion of the observed summer sea ice decline in recent decades has been linked to a high pressure anomaly over northeastern Canada and Greenland that has warmed and moistened the Arctic atmosphere (Ding et al., **2017**, **2019**), which in turn has been linked both to a Pacific-Arctic teleconnection (Baxter et al., **2019**) and to melting of the Greenland ice sheet (Hahn et al., **2018**). However, a more robust understanding of Arctic summer sea ice loss has been hindered by a lack of confidence in the ability of coupled climate models to represent the governing processes (Bonan & Blanchard-Wrigglesworth, **2020**; Luo et al., **2021**; Mahlstein & Knutti, **2012**; Notz & Stroeve, **2016**; Rosenblum & Eisenman, **2017**; SIMIP, **2020**; Winton, **2011**).

Here, we perform novel experiments designed to understand the role of observed circulation variability in observed Arctic Sea ice loss by nudging model winds toward observed wind anomalies at high latitudes and above the boundary layer.

Geophysical Research Letters, vol. 49, issue no. 24, e2022GL101203, doi:10.1029/2022GL101203

# The impact of winds on AMOC in a fully-coupled climate model

**Roach**, **L.A.**[1,2], E. Blanchard-Wrigglesworth, S. Ragen, W. Cheng, K.C. Armour, and C.M. Bitz, 2022

NASA Goddard Institute for Space Studies, New York, NY, USA[1]
Center for Climate Systems Research, Columbia University, New York, NY, USA[2]

**Abstract.** Here we investigate the role of the atmospheric circulation in the Atlantic Meridional Overturning Circulation (AMOC) by comparing a fully-coupled large ensemble, a forced-ocean simulation, and new experiments using a fully-coupled global climate model where winds above the boundary layer are nudged toward reanalysis. When winds are nudged north of 45°N, agreement with RAPID array observations of AMOC at 26.5°N improves across several metrics. The phasing of interannual variability is well-captured due to the response of the local Ekman component in both wind-nudging and forced-ocean simulations, however the variance remains underestimated. The mean AMOC strength is substantially reduced relative to the fully-coupled model large ensemble, which is biased high, due to the impact of winds on surface buoyancy fluxes over the subpolar gyre. Nudging winds toward observations also reduces the 1979–2016 trend in AMOC, suggesting that improvement in the representation of the high-latitude atmosphere is important for projecting long-term AMOC changes.

**Introduction.** The Atlantic Meridional Overturning Circulation (AMOC) is a system of currents that extends from the Southern Ocean to the Nordic Seas, transporting warm water northward near the surface and cold water southward at depth. It is a fundamental component of the global climate system, impacting a host of climate phenomena from Arctic sea ice to the Indian Monsoon (see Zhang et al. (**2019**) for a review of climate impacts). AMOC is projected to weaken over the 21st century (Cheng et al., **2013**; Weijer et al., **2020**), but with low confidence in the timing and magnitude of the decline (Fox-Kemper et al., **2021**).

Many previous studies highlight the importance of atmospheric circulation for variability in AMOC across timescales (see Buckley and Marshall (**2016**) for a review). It is understood that interannual AMOC variability is primarily driven by momentum forcing, while decadal and longer timescales are primarily driven by buoyancy forcing (e.g., Larson et al., **2020**; Roberts et al., **2013**; Yeager and Danabasoglu, **2014**). AMOC variability at 26.5°N is dominated by sub-annual to interannual variations in momentum forcing through local winds (Kostov et al., **2021**; Larson et al., **2020**; Roberts et al., **2013**; Yeager & Danabasoglu, **2014**). On longer timescales, there is a contribution from non-local buoyancy forcing, largely from subpolar latitudes (Delworth et al., **2016**; Kostov et al., **2021**; Yeager & Danabasoglu, **2014**). Changes in atmospheric circulation drive changes in both buoyancy and momentum forcing, with a dominant role for the North Atlantic Oscillation (NAO) and its associated turbulent heat fluxes (e.g., Oldenburg et al., 2021; Oldenburg et al., **2022**).

The most recent generation of coupled climate models simulate a large range of mean AMOC strengths (Fox-Kemper et al., **2021**; Weijer et al., **2020**) and generally underestimate interannual and decadal variability (Fox-Kemper et al., **2021**; Roberts et al., **2014**; Wang et al., **2017**; Yan et al., **2018**). Because of the wide-ranging climate impacts arising from AMOC, understanding why coupled climate models differ from observations is critical for interpreting and improving global climate projections over the 21st century. A "nudging," or "relaxation," approach has been widely used previously to diagnose the origin of errors in atmospheric variables (e.g., Jung et al., **2010**; Jung et al., **2014**; Liu et al., **2021**). For example, Jung et al. (**2010**) nudge various model fields toward reanalysis over different spatial domains to diagnose the remote impact of error reduction in those regions on winds and geopotential heights. Roach and Blanchard-Wrigglesworth (**2022**) apply wind-nudging north of 60°N to a fully-coupled climate model to highlight biases in sea ice trends that cannot be ascribed to biases in atmospheric circulation. Nudging the winds in a coupled climate model toward observed winds constrains the circulation but permits the atmosphere to respond thermodynamically to surface conditions.

Environmental Research Letters, vol. 17, issue no. 4, pp. 045022, doi:10.1088/1748-9326/ac5f94

# Future climate change impact on wildfire danger over the Mediterranean: The case of Greece

Rovithakis, A., M.G. Grillakis, K.D. Seiradakis, C. Giannakopoulos, A. Karali, **R.D. Field**[1,2], M. Lazaridis, and A. Voulgarakis, 2022

NASA Goddard Institute for Space Studies, New York, NY, USA[1]
Department of Applied Physics and Applied Mathematics, Columbia University, New York, NY, USA[2]

**Abstract.** Recent studies have shown that temperature and precipitation in the Mediterranean are expected to change, contributing to longer and more intense summer droughts that even extend out of season. In connection to this, the frequency of forest fire occurrence and intensity will likely increase. In the present study, the changes in future fire danger conditions are assessed for the different regions of Greece using the Canadian fire weather index (FWI). Gridded future climate output as estimated from three regional climate models from the Coordinated Regional Downscaling Experiment are utilized. We use three representative concentration pathways (RCPs) consisting of an optimistic emissions scenario where emissions peak and decline beyond 2020 (RCP2.6), a middle-of-the-road scenario (RCP4.5) and a pessimistic scenario, in terms of mitigation where emissions continue to rise throughout the century (RCP8.5). Based on established critical fire FWI threshold values for Greece, the future change in days with critical fire danger were calculated for different areas of Greece domains. The results show that fire danger is expected to progressively increase in the future especially in the high-end climate change scenario with southern and eastern regions of Greece expected to have up to 40 additional days of high fire danger relative to the late 20th century, on average. Crete, the Aegean Islands, the Attica region, as well as parts of Peloponnese are predicted to experience a stronger increase in fire danger.

**Introduction.** Extreme wildfire events can have devastating consequences for ecosystems (Andela *et al* **2018**), the atmospheric environment (Voulgarakis and Field **2015**), human health (Chuvieco *et al* **2018**) and the economy (Nielsen-Pincus *et al* **2014**). Fire can be both a natural and an anthropogenic disturbance process prevalent across most land surfaces with regular ignitions from humans particularly in agricultural areas where it is often used as a tool (Abatzoglou *et al* **2018**). In southern Greece, a wildfire in August 2007 resulted in a loss of 84 human lives more than 3000 destroyed houses and 270 000 ha of burnt area. The second deadliest wildfire event ever in the country (102 casualties) has been the recent wildfire in eastern Attica (July 2018), which burned an area of ∼1250 ha (Lagouvardos *et al* **2019**).

Mediterranean ecosystems are considered fire-prone, with severe associated economic and environmental damages every year (Turco *et al* **2018**). Although Mediterranean vegetation is able to cope with fire, land use changes in the area burned and the consequent changes in fire recurrence can have consequences at landscape level. Thus, understanding changes in fire regime and their relation to climate is a key factor for predicting the future of Mediterranean ecosystems (Pausas **2004**).

Drought events of unforeseen spatial extent and duration, are projected to occur up to twice per decade in the future, regardless of the degree of mitigation for Europe (Grillakis **2019**). Such climate-driven changes are expected to increase the risk of fire occurrence (Carvalho *et al* **2011**, Dupuy *et al* **2020**), reduce the time intervals between fire events (Pausas **2004**) and lengthen the duration of the fire season (Goss *et al* **2020**). Current trends in the Mediterranean climate and more specifically in Greece, indicate an increase in summer droughts due to global warming (Tramblay *et al* **2020**). Studies have consistently reported that climate change is expected to increase summer temperatures especially in the southern parts of Europe by the end of the 21st century. Projections regarding the southeastern Mediterranean region for the end of the century have shown an increase of 1.7 °C–2.5 °C for the moderate climate change scenario (RCP4.5) and 3.5 °C–5 °C for the higher-end scenario (RCP 8.5) (Zittis *et al* **2019**).

Earth's Future, vol. 10, issue no. 11, e2022EF002803, doi:10.1029/2022EF002803

# The Climatic Impact-Driver framework for assessment of risk-relevant climate information

**Ruane**, **A.C.**[1], R. Vautard, R. Ranasinghe, J. Sillmann, E. Coppola, N. Arnell, F.A. Cruz, S. Dessai, C.E. Iles, A.K.M.S. Islam, R.G. Jones, M. Rahimi, D. Ruiz Carrascal, S.I. Seneviratne, J. Servonnat, A.A. Sörensson, M.B. Sylla, C. Tebaldi, W. Wang, and R. Zaaboul, 2022

NASA Goddard Institute for Space Studies, New York, NY, USA[1]

**Abstract.** The climate science and applications communities need a broad and demand-driven concept to assess physical climate conditions that are relevant for impacts on human and natural systems. Here, we augment the description of the "climatic impact-driver" (CID) approach adopted in the Working Group I (WGI) contribution to the Intergovernmental Panel on Climate Change (IPCC) Sixth Assessment Report. CIDs are broadly defined as "physical climate system conditions (e.g., means, events, and extremes) that affect an element of society or ecosystems. Depending on system tolerance, CIDs and their changes can be detrimental, beneficial, neutral, or a mixture of each across interacting system elements and regions." We give background information on the IPCC Report process that led to the development of the 7 CID types (heat and cold, wet and dry, wind, snow and ice, coastal, open ocean, and other) and 33 distinct CID categories, each of which may be evaluated using a variety of CID indices. This inventory of CIDs was co-developed with WGII to provide a useful collaboration point between physical climate scientists and impacts/risk experts to assess the specific climatic phenomena driving sectoral responses and identify relevant CID indices within each sector. The CID Framework ensures that a comprehensive set of climatic conditions informs adaptation planning and risk management and may also help prioritize improvements in modeling sectoral dynamics that depend on climatic conditions. CIDs contribute to climate services by increasing coherence and neutrality when identifying and communicating relevant findings from physical climate research to risk assessment and planning activities.

**Introduction.** Continuing advances in climate change assessment have led to stronger interactions between the physical climate science community (with a focus on process understanding) and the climate impacts and risk communities (devoted to working with stakeholders to understand the implications of observed and future climate changes on affected systems). For the sake of efficient decision making, it is crucial that climate information is produced with a prior knowledge of its application through science and decision making interactions (Doblas-Reyes, et al., **2021**; Lemos et al., **2012**; Meinke et al., **2006**; Ranasinghe et al., **2021**). A process of "co-production" extending from these communities to stakeholders serves as a model to shift from a supply oriented (or "top-down") climate science assessment toward assessments driven by the demand for useful climate information (ISO, **2018**; Jones & Preston, **2011**; New et al., **2022**; Pulkkinen et al., **2022**). This process is cemented by sustained engagement and a recognition of context and values that shape diverse decision processes, including the identification, gathering, processing and delivery of climate information in a manner that complements stakeholders' perception of risk and motivation for action.

A common framework guiding climate information development has been a long-time challenge of the Intergovernmental Panel on Climate Change (IPCC) in creating coherent assessments across Working Groups. The IPCC has long fostered a neutral approach on climate information, for example, developing the "Reasons for Concern" framework in its Third Assessment Report (O'Neill et al., **2017**; Smith et al., **2001**). The IPCC adopted a cross-Working Group framework characterizing risk as an intersection of hazard, vulnerability and exposure in its Special Report on Climate Extremes (SREX; IPCC, **2012**; see also Zscheischler et al., **2018**). The Fifth Assessment Report (AR5) emphasized that good scientific and technical information is necessary but not sufficient for decision making given that actions are decided in particular contexts, with specific aims, and weighing multiple motivations under uncertainty (Jones et al., **2014**; Kolstad et al., **2014**; Kunreuther et al., **2014**).

Journal of Advances in Modeling Earth Systems, vol. 14, issue no. 1, e2021MS002601,
doi:10.1029/2021MS002601

# Improved representation of tropical cyclones in the NASA GISS-E3 GCM

Russotto, R.D.[3], J.D.O. Strong[3], S.J. Camargo[3], A.H. Sobel[2,3], **G.S. Elsaesser[1,2]**, **M.A. Kelley[1,4]**, **A.D. Del Genio[1]**, Y. Moon, and D. Kim, 2022

NASA Goddard Institute for Space Studies, New York, NY, USA[1]
Department of Applied Physics and Applied Mathematics, Columbia University, New York, NY, USA[2]
Lamont-Doherty Earth Observatory, Columbia University, Palisades, NY, USA[3]
SciSpace LLC, New York, NY, USA[4]

**Abstract.** The next-generation global climate model from the NASA Goddard Institute for Space Studies, GISS-E3, contains many improvements to resolution and physics that allow for improved representation of tropical cyclones (TCs) in the model. This study examines the properties of TCs in two different versions of E3 at different points in its development cycle, run for 20 years at 0.5° resolution, and compares these TCs with observations, the previous generation GISS model, E2, and other climate models. E3 shares many TC biases common to global climate models, such as having too few tropical cyclones, but is much improved from E2. E3 produces strong enough TCs that observation-based wind speed thresholds can now be used to detect and track them, and some storms now reach hurricane intensity; neither of these was true of E2. Model development between the first and second versions of E3 further increased the number and intensity of TCs and reduced TC count biases globally and in most regions. One-year sensitivity tests to changes in various microphysical and dynamical tuning parameters are also examined. Increasing the entrainment rate for the more strongly entraining plume in the convection scheme increases the number of TCs (though also affecting other climate variables, and in some cases increasing biases). Variations in divergence damping did not have a strong effect on simulated TC properties, contrary to expectations based on previous studies. Overall, the improvements in E3 make it more credible for studies of TC activity and its relationship to climate.

**Introduction.** Tropical cyclones (TCs) are among Earth's most potent natural hazards affecting life and property. There is much interest in how these storms will change as a consequence of anthropogenic global warming but predicting these changes with global climate models (GCMs) has proven challenging due in part to the dependence of TC dynamics on processes that are unresolved at such models' typical spatial resolutions. All else being equal, higher horizontal resolution in GCMs typically improves TC activity characteristics (Moon, Kim, Camargo, Wing, Sobel, et al., **2020**; Murakami & Sugi, **2010**; Shaevitz et al., **2014**; Vidale et al., **2021**; Walsh et al., **2013**; Wehner et al., **2015**), but models with similar resolutions can still vary widely in their representations of TC activity (Camargo et al., **2020**), as differences in the model configuration such as the convection scheme (Duvel et al., **2017**; Kim et al., **2012**; Murakami et al., **2012**; Vitart et al., **2001**), dynamical core (Reed et al., **2015**), and coupling to the ocean (Li & Sriver, **2018**; Scoccimarro et al., **2017**; Zarzycki, **2016**) also affect TC properties. Given these differences between GCMs, and the rapid increase of computational expense with resolution, some progress in understanding changing TCs in future climates is being gained using models run at resolutions of about half a degree (currently, a plausible compromise between computational expense and TC simulation fidelity), in single-model large ensembles (Yoshida et al., **2017**) and in multi-model ensembles including the U.S. Climate Variability and Predictability Program (CLIVAR) Hurricane Working Group experiments (Shaevitz et al., **2014**; Walsh et al., **2015**) and HighResMIP (Haarsma et al., **2016**; Roberts et al., **2020a**, **2020b**), an endorsed project of the Coupled Model Intercomparison Project (CMIP) Phase 6 (Eyring et al., **2016**).

Nature Communications, vol. 13, issue no. 1, pp. 7119, doi:10.1038/s41467-022-34787-4

# Model spread in tropical low cloud feedback tied to overturning circulation response to warming.

Schiro, K.A., H. Su, F. Ahmed, N. Dai, C.E. Singer, P. Gentine, **G.S. Elsaesser**[1,2], J.H. Jiang, Y.-S. Choi, and J. David Neelin, 2022

NASA Goddard Institute for Space Studies, New York, NY, USA[1]
Department of Applied Physics and Applied Mathematics, Columbia University, New York, NY, USA[2]

**Abstract.** Among models participating in the Coupled Model Intercomparison Project phase 6 (CMIP6), here we show that the magnitude of the tropical low cloud feedback, which contributes considerably to uncertainty in estimates of climate sensitivity, is intimately linked to tropical deep convection and its effects on the tropical atmospheric overturning circulation. First, a reduction in tropical ascent area and an increased frequency of heavy precipitation result in high cloud reduction and upper-tropospheric drying, which increases longwave cooling and reduces subsidence weakening, favoring low cloud reduction (Radiation-Subsidence Pathway). Second, increased longwave cooling decreases tropospheric stability, which also reduces subsidence weakening and low cloudiness (Stability-Subsidence Pathway). In summary, greater high cloud reduction and upper-tropospheric drying (negative longwave feedback) lead to a more positive cloud feedback among CMIP6 models by contributing to a greater reduction in low cloudiness (positive shortwave feedback). Varying strengths of the two pathways contribute considerably to the intermodel spread in climate sensitivity.

**Introduction.** Across generations of climate model intercomparisons, uncertainty in estimates of the projected warming in response to increasing greenhouse gases has persisted[1,2]. While tremendous progress has been made in modeling the Earth system in individual climate models, our ability to narrow the inter-model spread in equilibrium climate sensitivity (ECS), the equilibrium response in global-mean surface temperature to a doubling of carbon dioxide, is still limited. Critical to making significant progress in reducing such uncertainty is explaining the intermodel spread in the strength of the cloud feedback.

Low cloud changes have long been a root cause of uncertainty in ECS through their radiative effects[3,4,5,6,7,8,9,10,11,12,13,14]. Low-level clouds efficiently reflect incoming solar radiation back to space while only weakly reducing the longwave emission of terrestrial radiation to space, thereby exerting a strong cooling effect on the planet. A decrease in low cloud fraction (LCF) or cloud optical depth with warming would amplify the positive radiative forcing from increasing greenhouse gases by allowing more solar radiation to reach Earth's surface[15], constituting a positive feedback.

The latest generation of models participating in the coupled model intercomparison project Phase 6 (CMIP6) exhibit a wider range and higher multi-model-mean ECS than CMIP5 models[2]. The upward shift in ECS can be traced back to stronger positive low cloud feedback in the extratropics[2], while the tropical (30°S-30°N) low cloud feedback in both trade cumulus and stratocumulus regimes continues to be a dominant source of inter-model differences in ECS[16,17.] Moreover, Zelinka et al[18] found that the feedbacks with largest uncertainties in expert assessments and the largest bias across the CMIP6 ensemble are from tropical marine low cloudiness and tropical anvil cloud area. In this study, we consider whether the uncertainty in tropical marine low cloud and anvil cloud area feedbacks might be physically related to one another.

Frontiers in Remote Sensing, vol. 3, 885332, doi:10.3389/frsen.2022.885332

# Polarimeter + lidar-derived aerosol particle number concentration

Schlosser, J.S.[1], S. Stamnes[1], S.P. Burton[1], **B. Cairns[1]**, E. Crosbie[1,3], B. Van Diedenhoven, G. Diskin[1], S. Dmitrovic, R. Ferrare[1], J.W. Hair[1], C.A. Hostetler[1], Y. Hu[1], X. Liu[1], R.H. Moore[1], T. Shingler[1], M.A. Shook[1], K.L. Thornhill, E. Winstead, L. Ziemba, and A. Sorooshian, 2022

NASA Langley Research Center, Hampton, VA, USA[1]
NASA Goddard Institute for Space Studies, New York, NY, USA[2]
Science Systems and Applications, Inc., Lanham, MD, USA[3]

**Abstract.** In this study, we propose a simple method to derive vertically resolved aerosol particle number concentration ($N_a$) using combined polarimetric and lidar remote sensing observations. This method relies on accurate polarimeter retrievals of the fine-mode column-averaged aerosol particle extinction cross section and accurate lidar measurements of vertically resolved aerosol particle extinction coefficient such as those provided by multiwavelength high spectral resolution lidar. We compare the resulting lidar + polarimeter vertically resolved $N_a$ product to *in situ* $N_a$ data collected by airborne instruments during the NASA aerosol cloud meteorology interactions over the western Atlantic experiment (ACTIVATE). Based on all 35 joint ACTIVATE flights in 2020, we find a total of 32 collocated *in situ* and remote sensing profiles that occur on 11 separate days, which contain a total of 322 cloud-free vertically resolved altitude bins of 150 m resolution. We demonstrate that the lidar + polarimeter $N_a$ agrees to within 106% for 90% of the 322 vertically resolved points. We also demonstrate similar agreement to within 121% for the polarimeter-derived column-averaged $N_a$. We find that the range-normalized mean absolute deviation (NMAD) for the polarimeter-derived column-averaged $N_a$ is 21%, and the NMAD for the lidar + polarimeter-derived vertically resolved $N_a$ is 16%. Taken together, these findings suggest that the error in the polarimeter-only column-averaged $N_a$ and the lidar + polarimeter vertically resolved $N_a$ are of similar magnitude and represent a significant improvement upon current remote sensing estimates of $N_a$.

**Introduction.** Aerosol particle number concentration ($N_a$) is an important aerosol microphysical property for many applications including air quality and aerosol–cloud interactions. Historically, $N_a$ has been difficult to retrieve from remote sensing measurements that are sensitive to the aerosol scattering cross section, which scales with $N_a$ to the first power and particle diameter (D) to a higher power. Thus, uncertainty in the aerosol size distribution translates directly into a much greater uncertainty in the retrieved $N_a$ than would be the case when trying to retrieve the higher order moments of the aerosol population (e.g., surface area and volume) (**Knobelspiesse et al., 2011**; **Georgoulias et al., 2020**). While still limited to optically-active particles (i.e., D $\gtrsim$ 150 nm), the combination of next-generation polarimeter and lidar measurements makes the retrieval of $N_a$ possible. First, multi-angle, multichannel polarimeter observations, such as those from the research scanning polarimeter (RSP), allow for accurate retrieval of column-averaged fine- and coarse-mode aerosol properties (**Cairns et al., 1999**; **Stamnes et al., 2018**). Second, multiwavelength high spectral resolution lidar (HSRL-2) measurements provide accurate, vertically resolved measurements of aerosol extinction and depolarization (**Hair et al., 2008**). The HSRL-2 observations also provide accurate (within ~30 m) retrieval of the mixed layer height (MLH, **Scarino et al., 2014**).

A previous study demonstrated a median relative bias between HSRL-2 lidar- and in situ–derived $N_a$ of 33% and 47%; the lidar-derived $N_a$ was retrieved by inverting HSRL-2–only aerosol products to produce vertically resolved $N_a$ (**Sawamura et al., 2017**; **Müller et al., 2019**). In this study, we demonstrate a simple yet powerful method that uses combined lidar and polarimeter aerosol products to derive vertically resolved $N_a$ in the troposphere that has a median relative bias of 30%.

Proceedings of the National Academy of Sciences, vol. 119, issue no. 4, e2112930118,
doi:10.1073/pnas.2112930118

# Circumpolar ocean stability on Mars 3 Gy ago

Schmidt, F., **M.J. Way**[1,2,3], S. Bouley, A. Séjourné, and **I. Aleinov**[1,4], 2022

NASA Goddard Institute for Space Studies, New York, NY, USA[1]
Goddard Space Flight Center Sellers Exoplanet Environments Collaboration, Greenbelt, MD, USA[2]
Theoretical Astrophysics, Department of Physics and Astronomy, Uppsala University, Uppsala, Sweden[3]
Center for Climate Systems Research, Columbia University, New York, NY, USA[4]

**Abstract.** What was the nature of the Late Hesperian climate, warm and wet or cold and dry? Formulated this way the question leads to an apparent paradox since both options seem implausible. A warm and wet climate would have produced extensive fluvial erosion, but few valley networks have been observed at the age of the Late Hesperian. A too cold climate would have kept any northern ocean frozen most of the time. A moderate cold climate would have transferred the water from the ocean to the land in the form of snow and ice. But this would prevent tsunami formation, for which there is some evidence. Here, we provide insights from numerical climate simulations in agreement with surface geological features to demonstrate that the Martian climate could have been both cold and wet. Using an advanced general circulation model (GCM), we demonstrate that an ocean can be stable, even if the Martian mean surface temperature is lower than 0 ∘°C. Rainfall is moderate near the shorelines and in the ocean. The southern plateau is mostly covered by ice with a mean temperature below 0 ∘°C and a glacier return flow back to the ocean. This climate is achieved with a 1-bar $CO_2$-dominated atmosphere with 10% $H_2$. Under this scenario of 3 Ga, the geologic evidence of a shoreline and tsunami deposits along the ocean/land dichotomy are compatible with ice sheets and glacial valleys in the southern highlands.

**Introduction.** The possibility of a late Martian Ocean is a topic of debate with strong implications on the habitability of the Red Planet (**1**). A recent review (**2**) discusses this controversy. There is evidence of Martian paleo-shorelines (**3**) in Deuteronilus Mensae (sometimes noted contact 2) in a geometry closely corresponding to the current equipotential height (**4**). The Deuteronilus shoreline seems to have formed during the last stage of the true polar wander induced by Tharsis (**5**). A northern ocean is also supported by specific radar properties (**6**), smooth surface roughness (**7**), and a fractal analysis of the topography (**8**). Crater count dating of the Vastitas Borealis Formation near Deuteronilus Mensae is 3.5 Ga (**9**) but the ocean may have been more recent. Detailed studies in Kasei Valles imply that such an ocean rose in elevation (~1,000 m) between ca. 3.6 and 3.2 Ga (**10**). Along this shoreline, candidate tsunami deposits have been identified at an age of 3 Ga (**11**, **12**) with at least two impact events. The Lomonosov crater morphology is coherent with an impact in shallow water, at the very same age as the tsunami deposits (**13**), and it is thus the most probable source.

The stability of an ocean in a warm and wet scenario, even transient, at 3 Ga has been questioned since intense and widespread rainfall in such a scenario appeared inconsistent with the few observed dendritic valley networks from this time (**14**, **15**). In previous work, a cold and wet Mars seemed impossible since the long-term stability of an ocean (open or ice covered) in such a scenario has never been achieved by a three-dimensional general circulation model (3D-GCM) (**14**–**19**). Mainly the water was found to accumulate in the form of ice in the southern highlands, but no glacier/ice sheet processes were considered in these studies.

Cool and wet scenarios in the case of a faint young sun (at the Noachian-Hesperian boundary at 3.6 Ga) demonstrate that the ocean freezes for pressures below 1 bar and yet predict intense rainfall when the global average temperature is higher than 0 ∘°C (**20**). Nevertheless, liquid brines are possible in this case but only with significant anti-freezing properties (**21**). An investigation with two-dimensional (2D) simulations for early Mars argues for a warm and semiarid early Mars (**22**) but stresses the need for a coupled ocean/atmosphere model.

Proceedings of the National Academy of Sciences, vol. 119, issue no. 42, e2208095119,
doi:10.1073/pnas.2208095119

# The importance of internal climate variability in climate impact projections

Schwarzwald, K.[2], and **N. Lenssen**[1,2], 2022

NASA Goddard Institute for Space Studies, New York, NY, USA[1]
Lamont-Doherty Earth Observatory of Columbia University, Palisades, NY, USA[2]

**Abstract.** Uncertainty in climate projections is driven by three components: scenario uncertainty, inter-model uncertainty, and internal variability. Although socioeconomic climate impact studies increasingly take into account the first two components, little attention has been paid to the role of internal variability, although underestimating this uncertainty may lead to underestimating the socioeconomic costs of climate change. Using large ensembles from seven coupled general circulation models with a total of 414 model runs, we partition the climate uncertainty in classic dose–response models relating county-level corn yield, mortality, and per-capita gross domestic product to temperature in the continental United States. The partitioning of uncertainty depends on the time frame of projection, the impact model, and the geographic region. Internal variability represents more than 50% of the total climate uncertainty in certain projections, including mortality projections for the early 21st century, although its relative influence decreases over time. We recommend including uncertainty due to internal variability for many projections of temperature-driven impacts, including early-century and midcentury projections, projections in regions with high internal variability such as the Upper Midwest United States, and impacts driven by nonlinear relationships.

**Introduction.** Studies on the socioeconomic impacts of climate change have historically underestimated climate uncertainty, leading to overconfident projections of the resulting impacts (1, 2). Uncertainty in simulations of the future climate may arise from three major sources: 1) scenario uncertainty, representing differences in plausible future greenhouse gas emissions trajectories; 2) (climate) model uncertainty, representing differences in model responses to the same scenario inputs; and 3) internal variability (3). Currently, state-of-the-art analyses of future climate impacts account for scenario uncertainty by using projections from multiple future scenarios and model uncertainty by using a multi-model ensemble of projections from coupled general circulation models (CGCMs) (1, 2, 4–6). However, uncertainty due to internal variability is rarely taken into account despite the evidence that internal variability is an important component of total climate uncertainty for at least the first 50 y of projections (3, 7–9).

Internal variability consists of the naturally occurring variations in climate on timescales from daily weather to multidecadal processes due to interactions between various components of the Earth system. Internal variability is made up of components that are predictable, such as the El Niño–Southern Oscillation (10), as well as irreducible uncertainty due to the chaotic nature of the system (11). In the continental United States (CONUS), for example, increased likelihood of droughts and higher temperatures occurs during and following El Niño events in the Pacific Northwest (12, 13), following La Niña events in the Midwest (14, 15), and during the positive phase of the Atlantic Multidecadal Oscillation (16–18). In addition, internal variability leads to variability in trends of temperature, particularly over the northern and eastern CONUS (19, 20). The current best available estimates of the true internal variability of the Earth's climate system come from multi-model ensembles of initial-condition large ensembles (LEs), where a CGCM is run multiple times with slight perturbations to the initial conditions to sample the distribution of its possible climate outcomes, conditioned on the same emissions scenario (21). The LEs used in this study provide generally realistic simulations of historical temperature variability over CONUS (22).

Atmospheric Chemistry and Physics, vol. 22, issue no. 7, pp. 4491-4508, doi:10.5194/acp-22-4491-2022

# Observations of particle number size distributions and new particle formation in six Indian locations.

Sebastian, M., S.K. Kompalli, V.A. Kumar, S. Jose, S.S. Babu, G. Pandithurai, S. Singh, R.K. Hooda, V.K. Soni, J.R. Pierce, V. Vakkari, E. Asmi, **D.M. Westervelt**[1,2], A.-P. Hyvärinen, and V.P. Kanawade, 2022

NASA Goddard Institute for Space Studies, New York, NY, USA[1]
Division of Ocean and Climate Physics, Lamont-Doherty Earth Observatory, Palisades, New York, USA[2]

**Abstract.** Atmospheric new particle formation (NPF) is a crucial process driving aerosol number concentrations in the atmosphere; it can significantly impact the evolution of atmospheric aerosol and cloud processes. This study analyses at least 1 year of asynchronous particle number size distributions from six different locations in India. We also analyze the frequency of NPF and its contribution to cloud condensation nuclei (CCN) concentrations. We found that the NPF frequency has a considerable seasonal variability. At the measurement sites analyzed in this study, NPF frequently occurs in March–May (pre-monsoon, about 21 % of the days) and is the least common in October–November (post-monsoon, about 7 % of the days). Considering the NPF events in all locations, the particle formation rate ($J_{SDS}$) varied by more than 2 orders of magnitude (0.001–0.6 $cm^{-3}$ $s^{-1}$) and the growth rate between the smallest detectable size and 25 nm ($GR_{SDS\text{-}25\,nm}$) by about 3 orders of magnitude (0.2–17.2 nm $h^{-1}$). We found that $J_{SDS}$ was higher by nearly 1 order of magnitude during NPF events in urban areas than mountain sites. $GR_{SDS}$ did not show a systematic difference. Our results showed that NPF events could significantly modulate the shape of particle number size distributions and CCN concentrations in India. The contribution of a given NPF event to CCN concentrations was the highest in urban locations ($4.3 \times 10^3$ $cm^{-3}$ per event and $1.2 \times 10^3$ $cm^{-3}$ per event for 50 and 100 nm, respectively) as compared to mountain background sites ($2.7 \times 10^3$ $cm^{-3}$ per event and $1.0 \times 10^3$ $cm^{-3}$ per event, respectively). We emphasize that the physical and chemical pathways responsible for NPF and factors that control its contribution to CCN production require in situ field observations using recent advances in aerosol and its precursor gaseous measurement techniques.

**Introduction.** Cooling by atmospheric aerosols offsets a significant fraction of the radiative forcing of greenhouse gases (Paasonen et al., 2013) directly by scattering and absorbing solar radiation and indirectly by altering cloud microphysical properties via activation of cloud condensation nuclei (CCN; Rosenfeld et al., 2014; Sarangi et al., 2018). New particle formation (NPF), as a result of gas-to-particle conversion, is the largest source of aerosol numbers to the terrestrial atmosphere (Kulmala et al., 2007; Zhang et al., 2012). While nucleated particles from NPF are initially very small molecular clusters (1–2 nm; Kerminen et al., 2012), these molecular clusters can grow to large sizes within a few hours to a few days and ultimately reach CCN active sizes (> 50–100 nm; Pierce and Adams, 2007; Westervelt et al., 2013). Thus, CCN forms the direct microphysical link between aerosols and clouds and plays a vital role in the hydrological cycle and climate.

In India, several intensive field campaigns such as the Indian Ocean Experiment (INDOEX; Ramanathan et al., 2001), Indian Space Research Organization (ISRO)-Geosphere-Biosphere Programme (GBP)-Land campaign II (Tripathi et al., 2006; Tare et al., 2006), and Integrated Campaign for Aerosols, gases, and Radiation Budget (ICARB; Moorthy et al., 2008; Nair et al., 2020; Kompalli et al., 2020) have measured sub-micron particle number size distributions (PNSDs). There are also short- and long-term field observations of sub-micron PNSDs in a variety of diverse locations in India (Hyvärinen et al., 2010; Kanawade et al., 2014a; Shika et al., 2020; Tripathi et al., 1988; Komppula et al., 2009; Singh et al., 2004; Moorthy et al., 2011; Babu et al., 2016; Kompalli et al., 2018). However, there are sparse studies in India characterizing seasonal variation in PNSDs and number concentrations (Kanawade et al., 2014a; Hyvärinen et al., 2010; Komppula et al., 2009; Hooda et al., 2018; Laj et al., 2020) and atmospheric NPF (Sebastian et al., 2021b; Siingh et al., 2018; Neitola et al., 2011; Moorthy et al., 2011; Kanawade et al., 2014b, c; Kanawade et al., 2020a).

The Planetary Science Journal, vol. 3, issue no. 9, pp. 212, doi:10.3847/PSJ/ac6cf2

# The TRAPPIST-1 Habitable Atmosphere Intercomparison (THAI). Part II: Moist cases — The two waterworlds

Sergeev, D.E., T.J. Fauchez[1,2,3], M. Turbet, I.A. Boutle, **K. Tsigaridis[5,6]**, **M.J. Way[3,4,6]**, E.T. Wolf[3,7,8], S.D. Domagal-Goldman,[1,3,8] F. Forget, J. Haqq-Misra[8,9], R.K. Kopparapu[1,3,8], F.H. Lambert, J. Manners, and N.J. Mayne, 2022

NASA Goddard Space Flight Center, 8800 Greenbelt Road, Greenbelt, MD, USA[1]
Goddard Earth Sciences Technology and Research (GESTAR), Universities Space Research Association (USRA), Columbia, MD, USA[2]
NASA GSFC Sellers Exoplanet Environments Collaboration Greenbelt, MD, USA[3]
NASA Goddard Institute for Space Studies, New York, NY, USA[4]
Center for Climate Systems Research, Columbia University, New York, NY, USA[5]
Theoretical Astrophysics, Department of Physics and Astronomy, Uppsala University, Uppsala, Sweden[6]
Laboratory for Atmospheric and Space Physics, University of Colorado Boulder, Boulder, CO, USA[7]
NASA NExSS Virtual Planetary Laboratory, Seattle, WA, USA[8]
Blue Marble Space Institute of Science, Seattle, WA, USA[9]

**Abstract.** To identify promising exoplanets for atmospheric characterization and to make the best use of observational data, a thorough understanding of their atmospheres is needed. Three-dimensional general circulation models (GCMs) are one of the most comprehensive tools available for this task and will be used to interpret observations of temperate rocky exoplanets. Due to parameterization choices made in GCMs, they can produce different results, even for the same planet. Employing four widely used exoplanetary GCMs—ExoCAM, LMD-G, ROCKE-3D, and the UM—we continue the TRAPPIST-1 Habitable Atmosphere Intercomparison by modeling aqua-planet climates of TRAPPIST-1e with a moist atmosphere dominated by either nitrogen or carbon dioxide. Although the GCMs disagree on the details of the simulated regimes, they all predict a temperate climate with neither of the two cases pushed out of the habitable state. Nevertheless, the inter-model spread in the global mean surface temperature is nonnegligible: 14 K and 24 K in the nitrogen- and carbon dioxide-dominated case, respectively. We find substantial inter-model differences in moist variables, with the smallest amount of clouds in LMD-Generic and the largest in ROCKE-3D. ExoCAM predicts the warmest climate for both cases and thus has the highest water vapor content and the largest amount and variability of cloud condensate. The UM tends to produce colder conditions, especially in the nitrogen-dominated case due to a strong negative cloud radiative effect on the day side of TRAPPIST-1e. Our study highlights various biases of GCMs and emphasizes the importance of not relying solely on one model to understand exoplanet climates.

**Introduction.** With the advent of powerful new telescopes, such as the James Webb Space Telescope (JWST) and the Extremely Large Telescope, the characterization of a temperate rocky planet orbiting an M-dwarf star becomes highly likely (Snellen et al. **2015**; Anglada-Escudé et al. **2016**; Lovis et al. **2017**; Gillon et al. **2017**, **2020**; Fauchez et al. **2019**; Turbet et al. **2020**). In order to make the most use of the vast amount of data these telescopes will collect, a solid understanding of extraterrestrial atmospheres is needed. Three-dimensional general circulation models (or global climate models, GCMs) represent the complexity of planetary atmospheric dynamics to the best of our present knowledge. Being complex pieces of code, different GCMs typically produce different results even for the well-constrained climate of Earth (e.g., Webb et al. **2015**; Eyring et al. **2016**; Ceppi et al. **2017**). Almost all previous exoplanetary 3D GCM studies have employed only a single GCM due to the challenges of simulating exotic atmospheres on one hand and the exciting variety of possible targets on the other. It is therefore unclear how accurate predictions from a single GCM will be when used for interpreting observations of a particular exoplanet.

GeoHealth, vol. 6, issue no. 5, e2022GH000601, doi:10.1029/2022GH000601

# Premature deaths in Africa due to particulate matter under high and low warming scenarios

Shindell, D., **G.S. Faluvegi**,[1,2] L. Parsons, E. Nagamoto, and Chang J., 2022

NASA Goddard Institute for Space Studies, New York, NY, USA[1]
Center for Climate Systems Research, Columbia University, New York, NY, USA[2]

**Abstract.** Sustainable development and climate change mitigation can provide enormous public health benefits via improved air quality, especially in polluted areas. We use the latest state-of-the-art composition-climate model simulations to contrast human exposure to fine particulate matter in Africa under a "baseline" scenario with high material consumption, population growth, and warming to that projected under a sustainability scenario with lower consumption, population growth, and warming. Evaluating the mortality impacts of these exposures, we find that under the low warming scenario annual premature deaths due to $PM_{2.5}$ are reduced by roughly 515,000 by 2050 relative to the high warming scenario (100,000, 175,000, 55,000, 140,000, and 45,000 in Northern, West, Central, East, and Southern Africa, respectively). This reduction rises to ~800,000 by the 2090s, though by that time much of the difference is attributable to the projected differences in population. By contrast, during the first half of the century benefits are driven predominantly by emissions changes. Depending on the region, we find large inter-model spreads of ~25%–50% in projected future exposures owing to different physics across the ensemble of 6 global models. The spread of projected deaths attributable to exposure to fine particulate matter, including uncertainty in the exposure-response function, are reduced in every region to ~20%–35% by the non-linear exposure-response function. Differences between the scenarios have an even narrower spread of ~5%–25% and are highly statistically significant in all regions for all models. These results provide valuable information for policymakers to consider when working toward climate change mitigation and sustainable development goals.

**Introduction.** Globally, air pollution leads to a vastly larger public health burden than climate change does at present. The annual toll of premature deaths due to air pollution is estimated to be around 8–10 million (Burnett et al., **2018**; Vohra et al., **2021**) whereas the current toll from climate change is estimated in the hundreds of thousands (Romanello et al., **2021**; World Health Organization, **2014**). As many sources of the emissions that drive climate change, such as fossil fuel burning, are the same sources that cause air pollution, efforts to reduce climate change will also often benefit air quality. While climate change and sustainable development have been high on the international policy agenda and widely studied in the scientific community, there has been less effort to use the vast quantities of climate-related data to evaluate the so-called "co-benefits" for air quality of actions to mitigate climate change and achieve sustainable development.

Along with many other low- and middle-income countries, many parts of Africa suffer from both some of the world's worst air quality (Burnett et al., **2018**; Petkova et al., **2013**) and from some of the most pronounced damages due to climate change (Ranasinghe et al., **2021**). In addition, due to the relatively low income levels in much of Africa, populations tend to be more vulnerable to both the health impacts of air pollution and climate disruptions (Ranasinghe et al., **2021**; Stanaway et al., **2018**). African policymakers must face both these environmental challenges while also working toward the development goals leaders have set to improve economic and social conditions for their citizens, such as the African Union's Agenda 2063 (African Union Commission, **2015**). Fortunately, the drive toward sustainable development and climate change mitigation is likely to greatly improve Africa's air quality, leading to large public health benefits. In addition to the phasing out of fossil fuels required to meet climate goals, achievement of sustainable development goals, especially the provision of access to clean energy, would reduce use of biofuels, leading to substantial additional air quality improvements in Sub-Saharan Africa. Hence this region is one that is likely to experience some of the greatest air quality-related benefits from policies to promote sustainable development and climate change mitigation.

Geoscientific Model Development, vol. 15, issue no. 2, pp. 901-927, doi:10.5194/gmd-15-901-2022

# The Earth Model Column Collaboratory ($EMC^2$) v1.1: An open-source ground-based lidar and radar instrument simulator and subcolumn generator for large-scale models

Silber, I., R.C. Jackson, **A.M. Fridlind**[1], **A.S. Ackerman**[1], S. Collis, J. Verlinde, and J. Ding, 2022

NASA Goddard Institute for Space Studies, New York, NY, USA[1]

**Abstract.** Climate models are essential for our comprehensive understanding of Earth's atmosphere and can provide critical insights on future changes decades ahead. Because of these critical roles, today's climate models are continuously being developed and evaluated using constraining observations and measurements obtained by satellites, airborne, and ground-based instruments. Instrument simulators can provide a bridge between the measured or retrieved quantities and their sampling in models and field observations while considering instrument sensitivity limitations. Here we present the Earth Model Column Collaboratory ($EMC^2$), an open-source ground-based lidar and radar instrument simulator and sub-column generator, specifically designed for large-scale models, in particular climate models, but also applicable to high-resolution model output. $EMC^2$ provides a flexible framework enabling direct comparison of model output with ground-based observations, including generation of sub-columns that may statistically represent finer model spatial resolutions. In addition, $EMC^2$ emulates ground-based (and air- or space-borne) measurements while remaining faithful to large-scale models' physical assumptions implemented in their cloud or radiation schemes. The simulator uses either single particle or bulk particle size distribution lookup tables, depending on the selected scheme approach, to perform the forward calculations. To facilitate model evaluation, $EMC^2$ also includes three hydrometeor classification methods, namely, radar- and sounding-based cloud and precipitation detection and classification, lidar-based phase classification, and a Cloud Feedback Model Intercomparison Project Observational Simulator Package (COSP) lidar simulator emulator. The software is written in Python, is easy to use, and can be straightforwardly customized for different models, radars, and lidars.

Following the description of the logic, functionality, features, and software structure of $EMC^2$, we present a case study of highly supercooled mixed-phase cloud based on measurements from the U.S. Department of Energy Atmospheric Radiation Measurement (ARM) West Antarctic Radiation Experiment (AWARE). We compare observations with the application of $EMC^2$ to outputs from four configurations of the NASA Goddard Institute for Space Studies (GISS) climate model (ModelE3) in single-column model (SCM) mode and from a large-eddy simulation (LES) model. We show that two of the four ModelE3 configurations can form and maintain highly supercooled precipitating cloud for several hours, consistent with observations and LES. While our focus is on one of these ModelE3 configurations, which performed slightly better in this case study, both of these configurations and the LES results post-processed with $EMC^2$ generally provide reasonable agreement with observed lidar and radar variables. As briefly demonstrated here, $EMC^2$ can provide a lightweight and flexible framework for comparing the results of both large-scale and high-resolution models directly with observations, with relatively little overhead and multiple options for achieving consistency with model microphysical or radiation scheme physics.

**Introduction.** The representation of cloud processes in large-scale models is continuously advancing, conceptually, and in the level of details and complexity implemented in the micro- and macro-physical schemes (e.g., **Lin et al.**, **2019**; **Cesana et al.**, **2019**). These improvements are reflected in the accuracy of the resulting model output (e.g., **Klein et al.**, **2013**; **Lin et al.**, **2019**; **Myers et al.**, **2021**; **Wang et al.**, **2019**), yet results still show large inter-model variability (e.g., **Zelinka et al.**, **2020**).

Frontiers in Climate, vol. 4, 955414, doi:10.3389/fclim.2022.955414

# Attribution of multi-annual to decadal changes in the climate system: The Large Ensemble Single Forcing Model Intercomparison Project (LESFMIP)

Smith, D.M., N.P. Gillett, I.R. Simpson, P.J. Athanasiadis, J. Baehr, I. Bethke, T.A. Bilge, R. Bonnet, O. Boucher, K.L. Findell, G. Gastineau, S. Gualdi, L. Hermanson, L.R. Leung, J. Mignot, W.A. Müller, S. Osprey, O.H. Otterå, G.G. Persad, A.A. Scaife, **G.A. Schmidt**[1], H. Shiogama, R.T. Sutton, D. Swingedouw, S. Yang, T. Zhou, and T. Ziehn, 2022

NASA Goddard Institute for Space Studies, New York, NY, USA[1]

**Abstract.** Multi-annual to decadal changes in climate are accompanied by changes in extreme events that cause major impacts on society and severe challenges for adaptation. Early warnings of such changes are now potentially possible through operational decadal predictions. However, improved understanding of the causes of regional changes in climate on these timescales is needed both to attribute recent events and to gain further confidence in forecasts. Here we document the Large Ensemble Single Forcing Model Intercomparison Project that will address this need through coordinated model experiments enabling the impacts of different external drivers to be isolated. We highlight the need to account for model errors and propose an attribution approach that exploits differences between models to diagnose the real-world situation and overcomes potential errors in atmospheric circulation changes. The experiments and analysis proposed here will provide substantial improvements to our ability to understand near-term changes in climate and will support the World Climate Research Program Lighthouse Activity on Explaining and Predicting Earth System Change.

**Introduction.** Climate variability and change cause major impacts on human society and natural ecosystems. Of particular concern are large-scale changes in atmospheric circulation, since they can alter rainfall patterns, threatening food and water security, and increase the chances of extreme events. Prominent examples on decadal timescales include the United States "Dust Bowl" during the 1930s (**Schubert et al., 2004**), the Sahel droughts during the 1970s (**Kandji et al., 2006**), the mid-1990s increase in Atlantic hurricane activity (**Goldenberg et al., 2001**), the early twentieth century warming (**Hegerl et al., 2018**) and the early twenty-first century slowdown in global surface warming (**Medhaug et al., 2017**). Recent multi-decadal trends in atmospheric circulation also likely contributed to several extreme seasonal events including heatwaves in Europe and Russia, floods in Pakistan, and wildfires across the west coast of the United States (**Teng et al., 2022**) and Australia (**Canadell et al., 2021**), and even daily extremes such as rainfall and storms are strongly modulated by multidecadal fluctuations in large scale patterns such as the North Atlantic Oscillation (NAO; **Scaife et al., 2008**; **Dawkins et al., 2016**). Some recent extremes are also far outside the range of previously observed variability, causing severe impacts and creating serious challenges for climate adaptation (**Fischer et al., 2021**). Hence there is an urgent need to understand the causes of regional multi-annual to decadal changes in climate.

Environmental Justice, vol. 15, issue no. 3, pp. 149-159, doi:10.1089/env.2021.0059

# A new dataset integrating public socioeconomic, physical risk, and housing data for climate justice metrics: A test-case study in Miami

**Tedesco**, **M.**[1,2], C. Hultquist[2], and A. de Sherbinin, 2022

NASA Goddard Institute for Space Studies, New York, NY, USA[1]
Lamont-Doherty Earth Observatory, Department of Marine Geology and Geophysics, Palisades, NY, USA[2]

**Abstract.** Assessing the impact of climate change on vulnerable populations and the implications of such impacts is a critical step toward climate and environmental justice. In general, indices or metrics that aim at studying linkages between climatic environmental impacts and vulnerable populations lack housing information. Financially relevant real estate data (e.g., mortgages, evictions) alongside other socioeconomic and physical risk information can, however, provide a crucial lens to assess climate justice. In addition, standard socioeconomic and demographic variables aggregated at census units lack the granularity required to capture inequalities, especially in heterogeneous communities, so there is a need for publicly available, ready-to-use, digitized, and distributed datasets containing relevant inequality metrics using real estate and financial information. Also, studies focusing on damages and financial impacts of climate change often use commercial datasets, which must be acquired for hundreds of thousands of dollars, making the inclusion of such information prohibitive for advocacy groups, journalists, and other interested people. With this in mind, we integrated multiple publicly available datasets that include socioeconomic, climate risk scores, evictions, and housing variables at the census tract level over the United States to be used to investigate environmental justice themes. Our goal is that the dataset proposed here will allow for testing, assessing, and generating new analysis and metrics that can address inequalities and climate injustice. To demonstrate the potential of the new dataset, we report examples of application to the Miami area, where the recent increased risk of floods and extreme events has exposed socially vulnerable populations to the consequences of climate change.

**Introduction.** Assessing the consequences of climate change on socially vulnerable people is a critical step toward climate and environmental justice. Impacts of climate change can manifest through physical damages of infrastructures and homes, the loss of human lives, as well as rebuilding livelihoods that are damaged or destroyed. Other mechanisms that are exerted on socially vulnerable populations are not always directly observable nor can the specific impact be overtly linked to climate hazards, such as the way in which rising insurance costs associated with living in hazard prone areas disproportionately increases the financial burden on low-income populations. In Florida, for example, where the threat of climate change is manifested through increased exposure to floods and extreme events, flood insurance rates can range from around $200 to more than $2,000 a year, according to data from the Federal Reserve Survey of Consumer Finances.[1] This is in addition to already high and rising insurance rates as a result of more destructive hurricanes.[2,3] Another mechanism through which climate impacts can manifest is through losses in the real estate market. Recent work has shown that properties to be inundated with tidal flooding by 2032 can lose $3.08 each year for each square foot of living area, with properties near roads that will be inundated with tidal flooding in 2032 losing $3.71 each year on each square foot of living area.[4]

In general, indices or tools that aim at identifying such damages are composed of census-derived socioeconomic/ demographic datasets without including direct financial or real estate data (e.g., mortgages, evictions). This is driven by the abundance of standardized socioeconomic and demographic datasets, on the one hand, and to the absence of publicly available, ready-to-use datasets concerning real estate and financial information, on the other. A problem with relying on census data is that, apart from the decennial censuses, the inter-census data come from a sample of households that can have significant sampling errors, resulting in inconsistencies in results.[5]

Cities, vol. 131, 103991, doi:10.1016/j.cities.2022.103991

# Measuring, mapping, and anticipating climate gentrification in Florida: Miami and Tampa case studies

**Tedesco**, **M.**[1,2], J.M. Keenan, and C. Hultquist, 2022

NASA Goddard Institute for Space Studies, New York, NY, USA[1]
Lamont-Doherty Earth Observatory, Columbia University, New York, NY, USA[2]

**Abstract.** This article introduces an experimental methodology to identify proxy indicators that are conceptually consistent with the processes of Climate **Gentrification** ("CG"), in which a change in demand preferences among consumers and investors drives the increased consumption for real estate, in part, on lower measures of physical risk from climate change. Evaluated through case studies in the state of Florida, this article builds on the integration of multiple datasets concerning rental properties, evictions, and socioeconomic data, as well as environmental risk indices to build a Climate Gentrification Risk Index (CGRI). In the Miami case study, we find that the CGRI identifies a hotly contested neighborhood that is already known to be in a state of transition consistent with the processes of CG. In the Tampa case, the index highlights a district that exhibits strong metrics for the future accelerated occurrence of CG. Our findings suggest that transitional land uses and flexible zoning in low-exposure areas are key elements for attracting new development consistent with CG and offer insight into the challenges that local governments face understanding the types and rates of change that may be catalyzed in the broader urban processes of public and private sector climate adaptation in the built environment.

**Introduction.** Climate change is already shaping the design and planning of cities. As such, urban planning processes play an increasingly important role in both climate mitigation and adaptation. Yet, broader processes associated with the adaptation of markets—that are often outside of the agency of existing public planning models—often amplify existing resource constraints and social vulnerabilities (**Keenan et al., 2021**). This article introduces an experimental methodology to identify and evaluate proxy indicators that are conceptually consistent with the processes of Climate Gentrification ("CG"). Evaluated through case studies in the state of Florida, this methodology is based on various quantitative geospatial tools for assessing urban processes that speak to long-term land use and development trends that may catalyze residential and commercial disruption and dislocation associated with CG.

CG is a theory that has gained a foothold in practice and in popular discourse by highlighting various pathways from which a change in demand preferences among consumers and investors drives the increased consumption for housing, real estate and land based, in part, on lower measures of physical risk from climate change (**Keenan et al., 2018**; **Anguelovski et al., 2019**; **De Koning & Filatova, 2020**). This shift in valuation and consumption associated with CG has been observed to reinforce cost-burdens on existing populations leading to some anticipated measure of increased displacement over time (**Aune et al., 2020**). CG is premised, in part, by the emerging evidence that the experiences and perceptions of climate change among buyers, sellers, producers and financiers of real estate are leading to a revaluation of climate risks and asset values (**Bernstein et al., 2019**; **Keenan & Bradt, 2020**), as well as the underlying fiscal capacity of local governments who rely on these markets for taxation (**Shi & Varuzzo, 2020**). The implications of this emergent behavior in high-exposure housing markets is widespread, including everything from risk capitalization of flooding (**Hennighausen & Suter, 2020**) and insurability (**Bin et al., 2008**; **De Koning et al., 2019**) to population displacement (**Hauer, 2017**) and climate migration (**Mach et al., 2019**). Local governments have an immediate political challenge to manage the disruption of individuals or businesses subject to the cost-burdens of either being forced out, priced out, or crowded out by private investment (**Ghaffari et al., 2018**), even if such processes are incidental to their broader economic development strategies that are reliant on such dislocations (**Stein, 2019**). At the heart of this balancing act between CG-driven shifts in capital investment and in situ socioeconomic interests is the management of long-term land uses (**Bonjour, 2020**) and tax bases (**McAlpine & Porter, 2018**).

Geophysical Research Letters, vol. 49, issue no. 11, e2022GL098444, doi:10.1029/2022GL098444

# Dilution of boundary layer cloud condensation nucleus concentrations by free tropospheric entrainment during marine cold air outbreaks

**Tornow, F.[1,2], A.S. Ackerman[1], A.M. Fridlind[1], B. Cairns[1]**, E.C. Crosbie[3,4], S. Kirschler, R.H. Moore[3], D. Painemal[3,4], C.E. Robinson[3,4], C. Seethala, M.A. Shook[3], C. Voigt, E.L. Winstead[3,4], L.D. Ziemba[3], P. Zuidema, and A. Sorooshian, 2022

NASA Goddard Institute for Space Studies, New York, NY, USA[1]
Earth Institute, Columbia University, New York, NY, USA[2]
NASA Langley Research Center, Hampton, VA, USA[3]
Science, Systems, and Applications, Inc, Hampton, VA, USA[4]

**Abstract.** Recent aircraft measurements over the northwest Atlantic enable an investigation of how entrainment from the free troposphere (FT) impacts cloud condensation nucleus (CCN) concentrations in the marine boundary layer (MBL) during cold-air outbreaks (CAOs), motivated by the role of CCN in mediating transitions from closed to open-cell regimes. Observations compiled over eight flights indicate predominantly far lesser CCN concentrations in the FT than in the MBL. For one flight, a fetch-dependent MBL-mean CCN budget is compiled from estimates of sea-surface fluxes, entrainment of FT air, and hydrometeor collision-coalescence, based on in-situ and remote-sensing measurements. Results indicate a dominant role of FT entrainment in reducing MBL CCN concentrations, consistent with satellite-observed trends in droplet number concentration upwind of CAO cloud-regime transitions over the northwest Atlantic. Relatively scant CCN may widely be associated with FT dry intrusions and should accelerate cloud-regime transitions where underlying MBL air is CCN-rich, thereby reducing regional albedo.

**Introduction.** Extratropical marine boundary layer (MBL) clouds typically occupy the postfrontal sector of synoptic systems when passing over the ocean surface (e.g., Field & Wood, **2007**; Rémillard & Tselioudis, **2015**). Their presence substantially enhances regional albedo, and such clouds are challenging to faithfully represent in numerical models, whether for forecasting weather or projecting climate change (e.g., Bodas-Salcedo et al., **2016**; Forbes & Ahlgrimm, **2014**; Tselioudis et al., **2021**). Common during winter and its shoulder seasons, cold air outbreaks (CAOs) pose a particular challenge (e.g., Abel et al., **2017**; Field et al., **2017**) as they form highly reflective, nearly overcast cloud decks, typically organized in roll-like structures that contain both water and ice, which generally break up into less reflective, open-cellular cloud fields farther downwind (e.g., Brümmer, **1999**; Pithan et al., **2019**).

MBL clouds are sensitive to the number concentration of aerosol available as cloud condensation nuclei (CCN). Greater CCN concentrations can enhance cloud albedo when (a) distributing the same cloud condensate over more numerous, smaller droplets (Twomey, **1974**), (b) suppressing precipitation formation, leading to greater areal cloud cover (Albrecht, **1989**) and thicker clouds (Pincus & Baker, **1994**), and (c) affecting cloud mesoscale structure (e.g., Wang & Feingold, **2009**). On the other hand, smaller droplets fall more slowly in updrafts and can boost entrainment of overlying dry air, reducing cloud thickness and counteracting albedo-enhancing effects (Ackerman et al., **2004**; Bretherton et al., **2007**). The collisions between hydrometeors that drive precipitation formation in warm clouds also reduce CCN number concentrations and can drive a positive feedback loop in which fewer CCN promote further precipitation formation in warm stratocumulus (Yamaguchi et al., **2017**). Such a feedback loop is also implicated in mixed-phase CAO observations (e.g., Abel et al., **2017**) and simulations (Tornow et al., **2021**), and is hypothesized to explain horizontal gradients in cloud droplet number concentrations off the mid-Atlantic coast of the US (Dadashazar et al., **2021**).

Atmospheric Chemistry and Physics, vol. 22, issue no. 18, pp. 12467-12491, doi:10.5194/acp-22-12467-2022

# Highly supercooled riming and unusual triple-frequency radar signatures over McMurdo Station, Antarctica

Tridon, F., I. Silber, A. Battaglia, S. Kneifel, **A.M. Fridlind**[1], P. Kalogeras, and R. Dhillon, 2022

NASA Goddard Institute for Space Studies, New York, NY, USA[1]

**Abstract.** Riming of ice crystals by supercooled water droplets is an efficient ice growth process, but its basic properties are still poorly known. While it has been shown to contribute significantly to surface precipitation at mid-latitudes, little is known about its occurrence at high latitudes. In Antarctica, two competing effects can influence the occurrence of riming: (i) the scarcity of supercooled liquid water clouds due to the extremely low tropospheric temperatures and (ii) the low aerosol concentration, which may lead to the formation of fewer and larger supercooled drops potentially resulting in an enhanced riming efficiency.

In this work, by exploiting the deployment of an unprecedented number of multiwavelength remote sensing systems (including triple-frequency radar measurements) in West Antarctica, during the Atmospheric Radiation Measurements West Antarctic Radiation Experiment (AWARE) field campaign, we evaluate the riming incidence at McMurdo Station and find that riming occurs at much lower temperatures when compared to previous results in the mid-latitudes. This suggests the possible occurrence of a common atmospheric state over Antarctica that includes a rather stable atmosphere inhibiting turbulent mixing, and a high riming efficiency driven by large cloud droplets.

We then focus on a peculiar case study featuring a persistent layer with a particularly pronounced riming signature in triple-frequency radar data but only a relatively modest amount of supercooled liquid water. In-depth analysis of the radar observations suggests that such signatures can only be explained by the combined effects of moderately rimed aggregates or similarly shaped florid polycrystals and a narrow particle size distribution (PSD). Simulations of this case study performed with a one-dimensional bin model indicate that similar triple-frequency radar observations can be reproduced when narrow PSDs are simulated. Such narrow PSDs can in turn be explained by two key factors: (i) the presence of a shallow homogeneous droplet or humidified aerosol freezing layer aloft seeding an underlying supercooled liquid layer, and (ii) the absence of turbulent mixing throughout a stable polar atmosphere that sustains narrow PSDs, as hydrometeors grow from the nucleation region aloft to ice particles of several millimeters in size, by vapor deposition and then riming.

**Introduction.** Besides deposition and aggregation, riming is an efficient ice growth process. It contributes significantly to surface precipitation at mid-latitudes (**Grazioli et al., 2015**; **Moisseev et al., 2017**) and is pivotal for improving our understanding of the role of ice phase in the water budget. However, basic properties of riming such as its efficiency or its importance in precipitation formation are still largely unknown since it involves the collection of poorly characterized supercooled water droplets by complex ice particles. It is widely accepted, however, that at the beginning of a riming process, the mass of a rimed ice particle increases while its maximum dimension remains constant or increases only slightly (e.g., **Heymsfield, 1982; Seifert et al., 2019**); hence, the density and fall speed of rimed ice hydrometeors tend to be enhanced. Riming occurrence is strongly linked to temperature since the probability of finding supercooled liquid water decreases with temperature. By exploiting a multiyear dataset of cloud radar observations at four European sites in various environments, **Kneifel and Moisseev (2020)** showed that riming is rare below −12 °C and more frequent closer to 0 °C.

In the Arctic, supercooled liquid water clouds are frequent (e.g., **Shupe et al., 2008**; **Cesana et al., 2012**; **Morrison et al., 2012**; **Mioche et al., 2015**) and rimed precipitating particles are commonly observed (**Mioche et al., 2017**; **Fitch and Garrett, 2022**). In Antarctica, however, liquid water clouds are less frequent, in particular during winter months due to lower temperatures (e.g., **Matus and L'Ecuyer, 2017**; **Lubin et al., 2020**).

Earth System Science Data, vol. 14, issue no. 4, pp. 1795-1809, doi:10.5194/essd-14-1795-2022

# Pre- and post-production processes increasingly dominate greenhouse gas emissions from agri-food systems

Tubiello, F., K. Karl, A. Flammini, J. Gutschow, G. Obli-Laryea, G. Conchedda, X. Pan, S.Y. Qiu, H.H. Heiðarsdóttir, N. Wanner, R. Quadrelli, L. Souza, P. Benoit, M. Hayek, D. Sandalow, **E.A. Mencos Contreras[1,2]**, **C. Rosenzweig[1,2]**, J. Rosero-Moncayo, P. Conforti, and M. Torero, 2022

NASA Goddard Institute for Space Studies, New York, NY, USA[1]
Center for Climate Systems Research, Columbia University, New York, NY, USA[2]

**Abstract.** We present results from the FAOSTAT emissions shares database, covering emissions from agri-food systems and their shares to total anthropogenic emissions for 196 countries and 40 territories for the period 1990–2019. We find that in 2019, global agri-food system emissions were 16.5 (95 %; CI range: 11–22) billion metric tonnes (Gt $CO_2$ eq. $yr^{-1}$), corresponding to 31 % (range: 19 %–43 %) of total anthropogenic emissions. Of the agri-food system total, global emissions within the farm gate – from crop and livestock production processes including on-farm energy use – were 7.2 Gt $CO_2$ eq. $yr^{-1}$; emissions from land use change, due to deforestation and peatland degradation, were 3.5 Gt $CO_2$ eq. $yr^{-1}$; and emissions from pre- and post-production processes – manufacturing of fertilizers, food processing, packaging, transport, retail, household consumption and food waste disposal – were 5.8 Gt $CO_2$ eq. $yr^{-1}$. Over the study period 1990–2019, agri-food system emissions increased in total by 17 %, largely driven by a doubling of emissions from pre- and post-production processes. Conversely, the FAOSTAT data show that since 1990 land use emissions decreased by 25 %, while emissions within the farm gate increased 9 %. In 2019, in terms of individual greenhouse gases (GHGs), pre- and post-production processes emitted the most $CO_2$ (3.9 Gt $CO_2$ $yr^{-1}$), preceding land use change (3.3 Gt $CO_2$ $yr^{-1}$) and farm gate (1.2 Gt $CO_2$ $yr^{-1}$) emissions. Conversely, farm gate activities were by far the major emitter of methane (140 Mt $CH_4$ $yr^{-1}$) and of nitrous oxide (7.8 Mt $N_2O$ $yr^{-1}$). Pre- and post-production processes were also significant emitters of methane (49 Mt $CH_4$ $yr^{-1}$), mostly generated from the decay of solid food waste in landfills and open dumps. One key trend over the 30-year period since 1990 highlighted by our analysis is the increasingly important role of food-related emissions generated outside of agricultural land, in pre- and post-production processes along the agri-food system, at global, regional and national scales. In fact, our data show that by 2019, pre- and post-production processes had overtaken farm gate processes to become the largest GHG component of agri-food system emissions in Annex I parties (2.2 Gt $CO_2$ eq. $yr^{-1}$). They also more than doubled in non-Annex I parties (to 3.5 Gt $CO_2$ eq. $yr^{-1}$), becoming larger than emissions from land use change. By 2019 food supply chains had become the largest agri-food system component in China (1100 Mt $CO_2$ eq. $yr^{-1}$), the USA (700 Mt $CO_2$ eq. $yr^{-1}$) and the EU-27 (600 Mt $CO_2$ eq. $yr^{-1}$). This has important repercussions for food-relevant national mitigation strategies, considering that until recently these have focused mainly on reductions of non-$CO_2$ gases within the farm gate and on $CO_2$ mitigation from land use change. The information used in this work is available as open data with DOI **https://doi.org/10.5281/zenodo.5615082** (Tubiello et al., 2021d). It is also available to users via the FAOSTAT database (**https://www.fao.org/faostat/en/#data/EM**; FAO, 2021a), with annual updates.

**Introduction.** Agriculture is a significant contributor to climate change as well as one of the economic sectors most at risk from it. Greenhouse gas (GHG) emissions generated within the farm gate by crop and livestock production and related land use change contribute about one-fifth to one-quarter of total emissions from all human activities, when measured in $CO_2$ equivalents (Mbow et al., 2019; Smith et al., 2014; Vermeulen et al., 2012). The impacts are even starker in terms of individual GHG emissions. Agriculture contributes nearly 50 % of global anthropogenic methane ($CH_4$) and 75 % of the total nitrous oxide ($N_2O$) emissions (FAO, 2021b; Gütschow et al., 2021; Saunois et al., 2020). Once pre- and post-production activities along agri-food systems supply chains are included, food and agriculture activities generate up to one-third of all anthropogenic emissions globally (Crippa et al., 2021a, b; Rosenzweig et al., 2020; Tubiello et al., 2021a).

The Planetary Science Journal, vol. 3, issue no. 9, pp. 211, doi:10.3847/PSJ/ac6cf0

# The TRAPPIST-1 Habitable Atmosphere Intercomparison (THAI). Part I: Dry cases — The fellowship of the GCMs

Turbet, M., T.J. Fauchez[1,2,3], D.E. Sergeev, I.A. Boutle, **K. Tsigaridis[4,5]**, **M.J. Way[3,4,6]**, E.T. Wolf[3,7,8], S.D. Domagal-Goldman[1,3,8], F. Forget, J. Haqq-Misra8,9, R.K. Kopparapu[1,3,8], F.H. Lambert, J. Manners, N.J. Mayne, and **L. Sohl[4,5]**, 2022

NASA Goddard Space Flight Center, Greenbelt, MD, USA[1]
Goddard Earth Sciences Technology and Research (GESTAR), Universities Space Research Association (USRA), Columbia, MD, USA[2]
Goddard Space Flight Center Sellers Exoplanet Environments Collaboration, Greenbelt, MD, USA[3]
NASA Goddard Institute for Space Studies, New York, NY, USA[4]
Center for Climate Systems Research, Columbia University, New York, NY, USA[5]
Theoretical Astrophysics, Department of Physics and Astronomy, Uppsala University, Uppsala, Sweden[6]
Laboratory for Atmospheric and Space Physics, Department of Atmospheric and Oceanic Sciences, University of Colorado, Boulder, CO, USA[7]
NASA NExSS Virtual Planetary Laboratory, Seattle, WA, USA[8]
Blue Marble Space Institute of Science, Seattle, WA, USA[9]

**Abstract.** With the commissioning of powerful, new-generation telescopes such as the James Webb Space Telescope (JWST) and the ground-based Extremely Large Telescopes, the first characterization of a high molecular weight atmosphere around a temperate rocky exoplanet is imminent. Atmospheric simulations and synthetic observables of target exoplanets are essential to prepare and interpret these observations. Here we report the results of the first part of the TRAPPIST-1 Habitable Atmosphere Intercomparison (THAI) project, which compares 3D numerical simulations performed with four state-of-the-art global climate models (ExoCAM, LMD-Generic, ROCKE-3D, Unified Model) for the potentially habitable target TRAPPIST-1e. In this first part, we present the results of dry atmospheric simulations. These simulations serve as a benchmark to test how radiative transfer, sub-grid scale mixing (dry turbulence and convection), and large-scale dynamics impact the climate of TRAPPIST-1e and consequently the transit spectroscopy signature as seen by JWST. To first order, the four models give results in good agreement. The inter-model spread in the global mean surface temperature amounts to 7 K (6 K) for the $N_2$-dominated ($CO_2$-dominated) atmosphere. The radiative fluxes are also remarkably similar (inter-model variations less than 5%), from the surface (1 bar) up to atmospheric pressures ∼5 mbar. Moderate differences between the models appear in the atmospheric circulation pattern (winds) and the (stratospheric) thermal structure. These differences arise between the models from (1) large-scale dynamics, because TRAPPIST-1e lies at the tipping point between two different circulation regimes (fast and Rhines rotators) in which the models can be alternatively trapped, and (2) parameterizations used in the upper atmosphere such as numerical damping.

**Introduction.** With the commissioning of next-generation telescopes and instruments, the astronomical community is for the first time in the process of detecting and characterizing the chemical composition of the atmospheres of rocky exoplanets receiving a moderate instellation (Greene et al. **2016**; Morley et al. **2017**; Wunderlich et al. **2019**; Gillon et al. **2020**; Turbet et al. **2020**). Specifically, observations of the TRAPPIST-1 planets (Gillon et al. **2017**) with the James Webb Space Telescope (JWST) are likely to be our first real opportunity to characterize the surface and atmosphere of planets with a similar mass, radius, and bolometric irradiation to Earth but orbiting other stars than the Sun (Morley et al. 2017; Fauchez et al. **2019**; Lustig-Yaeger et al. **2019**; Wunderlich et al. **2019**, **2020**; Gillon et al. **2020**; Turbet et al. **2020**).

Preparing for these observations with sophisticated numerical climate models has recently become an active topic of research aimed at optimizing the scientific return from observational campaigns (see Fauchez et al. **2021** and references therein). First, model predictions guide observation proposals, and second, they are used to help in the analysis and interpretation of the data.

Atmospheric Measurement Techniques, vol. 15, issue no. 24, pp. 7411-7434, doi:10.5194/amt-15-

# Remote sensing of aerosol water fraction, dry size distribution and soluble fraction using multi-angle, multi-spectral polarimetry

Van Diedenhoven, B., O.P. Hasekamp, **B. Cairns**[1], G.L. Schuster[2], S. Stammes[2], M.A. Shook[2], and L.D. Ziemba[2], 2022

NASA Goddard Institute for Space Studies, New York, NY, USA[1]
NASA Langley Research Center, Hampton, Virginia, USA[2]

**Abstract.** A framework to infer volume water fraction, soluble fraction and dry size distributions of fine-mode aerosol from multi-angle, multi-spectral polarimetry retrievals of column-averaged ambient aerosol properties is presented. The method is applied to observations of the Research Scanning Polarimeter (RSP) obtained during two NASA aircraft campaigns, namely the Aerosol Cloud meTeorology Interactions oVer the western ATlantic Experiment (ACTIVATE) and the Cloud, Aerosol, and Monsoon Processes Philippines Experiment (CAMP$^2$Ex). All aerosol retrievals are statistically evaluated using in situ data. Volume water fraction is inferred from the retrieved ambient real part of the refractive index, assuming a dry refractive index of 1.54 and by applying a volume mixing rule to obtain the effective ambient refractive index. The uncertainties in inferred volume water fraction resulting from this simplified model are discussed and estimated to be lower than 0.2 and decreasing with increasing volume water fraction. The daily mean retrieved volume water fractions correlate well with the in-situ values with a mean absolute difference of 0.09. Polarimeter-retrieved ambient effective radius for daily data is shown to increase as a function of volume water fraction as expected. Furthermore, the effective variance of the size distributions also increases with increasing effective radius, which we show is consistent with an external mixture of soluble and insoluble aerosol. The relative variations of effective radius and variance over an observation period are then used to estimate the soluble fraction of the aerosol. Daily results of soluble fraction correlate well with in situ-observed sulfate mass fraction with a correlation coefficient of 0.79. Subsequently, inferred water and soluble fractions are used to derive dry fine-mode size distributions from their ambient counterparts. While dry effective radii obtained in situ and from RSP show similar ranges, in situ values are generally substantially smaller during the ACTIVATE deployments, which may be due to biases in RSP retrievals or in the in-situ observations, or both. Both RSP and in situ observations indicate the dominance of aerosol with low hygroscopicity during the ACTIVATE and CAMP$^2$Ex campaigns. Furthermore, RSP indicates a high degree of external mixing of particles with low and high hygroscopicity. These retrievals of fine-mode water volume fraction and soluble fraction may be used for the evaluation of water uptake in atmospheric models. Furthermore, the framework allows us to estimate the variation in the concentration of fine-mode aerosol larger than a specific dry radius limit, which can be used as a proxy for the variation in cloud condensation nucleus concentrations. This framework may be applied to multi-angle, multi-spectral satellite data expected to be available in the near future.

**Introduction.** Terrestrial aerosol is a complex mixture of liquid, solid, or mixed-phase particles emitted by natural and anthropogenic sources either directly to the atmosphere or produced in the atmosphere through complex physical and chemical pathways from precursor gases (**Riemer et al., 2019**). Aerosols affect Earth's climate as they scatter and absorb radiation and act as condensation nuclei for cloud droplets and ice crystals. Furthermore, aerosols affect air quality and health.

Substantial changes in anthropogenic aerosol emissions in the industrial age occurred (**Bauer et al., 2020**). The overall increase in aerosol emissions has led to a general cooling of Earth's atmosphere, compensating for part of the temperature increase imposed by anthropogenic greenhouse gas emissions (**Samset et al., 2018; Bauer et al., 2020**). Reductions in global aerosol emissions are expected in the next decades, improving air quality but also likely providing a net positive climate forcing.

Nature, vol. 603, pp. 450-454, doi:10.1038/s41586-021-04376-4

# New land-use change emission estimates indicate a declining $CO_2$ airborne fraction

Van Marle, M.J.E., D. van Wees, R.A. Houghton, **R.D. Field**[1,2], J. Verbesselt, and G.R. van der Werf, 2022

NASA Goddard Institute for Space Studies, New York, NY, USA[1]
Department of Physics and Applied Mathematics, Columbia University, New York, NY, USA[2]

**Abstract.** About half of the anthropogenic $CO_2$ emissions remain in the atmosphere and half are taken up by the land and ocean[1]. If the carbon uptake by land and ocean sinks becomes less efficient, for example, owing to warming oceans[2] or thawing permafrost[3], a larger fraction of anthropogenic emissions will remain in the atmosphere, accelerating climate change. Changes in the efficiency of the carbon sinks can be estimated indirectly by analysing trends in the airborne fraction, that is, the ratio between the atmospheric growth rate and anthropogenic emissions of $CO_2$ (refs. [4,5,6,7,8,9,10]). However, current studies yield conflicting results about trends in the airborne fraction, with emissions related to land use and land cover change (LULCC) contributing the largest source of uncertainty[7,11,12]. Here we construct a LULCC emissions dataset using visibility data in key deforestation zones. These visibility observations are a proxy for fire emissions[13,14], which are — in turn — related to LULCC[15,16]. Although indirect, this provides a long-term consistent dataset of LULCC emissions, showing that tropical deforestation emissions increased substantially (0.16 Pg C decade$^{-1}$) since the start of $CO_2$ concentration measurements in 1958. So far, these emissions were thought to be relatively stable, leading to an increasing airborne fraction[4,5]. Our results, however, indicate that the $CO_2$ airborne fraction has decreased by $0.014 \pm 0.010$ decade$^{-1}$ since 1959. This suggests that the combined land–ocean sink has been able to grow at least as fast as anthropogenic emissions.

**Introduction.** Carbon–climate feedbacks constitute a key uncertainty in predicting future climate change[17,18]. Over the past decades, the functioning of carbon sinks has therefore undergone increased scrutiny from the scientific community. However, partly owing to large spatio-temporal variability, direct estimates of the sink strength, its annual variability and trends remain uncertain[11]. Analysing trends in the airborne fraction (AF) provides an independent estimate of the functioning of all sinks combined. Several studies observed an increase in AF[4,5] in line with findings of a decline in $CO_2$ uptake efficiencies of parts of the land[19,20,21] and ocean sinks[2,22]. Other studies suggested that the trend is too small to be statistically significant[6], warned against misinterpreting the trend in AF[7] or argued that multiple trends are needed to describe the AF pattern over the past 60 years (refs. [8,9]). These conflicting results highlight the underlying uncertainties in this approach, partly related to uncertainties in datasets used, in particular, those of LULCC emissions.

The uncertainty in the magnitude of LULCC emissions stems, for a large part, from uncertainties in tropical forest losses, especially before satellite observations became available. Although these and other fluxes related to LULCC emissions are nowadays only about 10–20% of fossil fuel emissions, their uncertainty is larger, even in absolute terms[11]. The uncertainty in LULCC emissions has an especially large contribution to the overall uncertainty in anthropogenic emissions during the mid-twentieth century, when LULCC and fossil fuel emissions were more similar in magnitude than they are now.

One avenue that is not exploited in the context of better constraining LULCC emissions is the close link between fire and deforestation[15,16,23]. Fire is the cheapest tool to convert forest to other land uses. In moist tropical rainforests, fires thus signal human presence and deforestation[24]. Even though not all LULCC emissions are associated with fire — logging is a prime example — a better handle on trends in fire emissions in key LULCC regions could provide independent information on temporal dynamics of LULCC emissions.

Communications Earth and Environment, vol. 3, issue no. 1, pp. 222, doi:10.1038/s43247-022-00555-x

# Clean air policies are key for successfully mitigating Arctic warming

Von Salzen, K., C.H. Whaley, S.C. Anenberg, R. Van Dingenen, Z. Klimont, M.G. Flanner, R. Mahmood, S.R. Arnold, S. Beagley, R.-Y. Chien, J.H. Christensen, S. Eckhardt, A.M.L. Ekman, N. Evangeliou, **G.S. Faluvegi**[1,2], J.S. Fu, M. Gauss, W. Gong, J.L. Hjorth, U. Im, S. Krishnan, K. Kupiainen, T. Kühn, J. Langner, K.S. Law, L. Marelle, D. Olivié, T. Onishi, N. Oshima, V.-V. Paunu, Y. Peng, D. Plummer, L. Pozzoli, S. Rao, J.-C. Raut, M. Sand, J. Schmale, M. Sigmond, M.A. Thomas, **K. Tsigaridis**[1,2], S. Tsyro, S.T. Turnock, M. Wang, and B. Winter, 2022

NASA Goddard Institute for Space Studies, New York, NY, USA[1]
Center for Climate Systems Research, Columbia University, New York, NY, USA[2]

**Abstract.** A tighter integration of modeling frameworks for climate and air quality is urgently needed to assess the impacts of clean air policies on future Arctic and global climate. We combined a new model emulator and comprehensive emissions scenarios for air pollutants and greenhouse gases to assess climate and human health co-benefits of emissions reductions. Fossil fuel use is projected to rapidly decline in an increasingly sustainable world, resulting in far-reaching air quality benefits. Despite human health benefits, reductions in sulfur emissions in a more sustainable world could enhance Arctic warming by 0.8 °C in 2050 relative to the 1995–2014, thereby offsetting climate benefits of greenhouse gas reductions. Targeted and technically feasible emissions reduction opportunities exist for achieving simultaneous climate and human health co-benefits. It would be particularly beneficial to unlock a newly identified mitigation potential for carbon particulate matter, yielding Arctic climate benefits equivalent to those from carbon dioxide reductions by 2050.

**Introduction.** The Arctic annual mean surface temperature has warmed three times faster than the global average between 1971 and 2019, with consequences that reach far beyond the Arctic environment and people[1,2]. To limit Arctic warming and sea ice melt, and to mitigate risks associated with potential climate tipping points in the Arctic[3], reductions in emissions of carbon dioxide ($CO_2$) and other greenhouse gases are urgently needed. Many countries have pledged to bring emissions of greenhouse gases to "net zero" by 2050, primarily targeting $CO_2$. Despite these commitments, the world is not currently on track to meet the goals of the Paris Agreement[4].

At the same time, strong national regulations and regional agreements are in place to reduce transboundary air pollution[5,6,7], which is a major health threat in many parts of the world[8]. Air pollutants such as particulate matter and tropospheric ozone ($O_3$) act as Short-Lived Climate Forcers (SLCFs). Although SLCFs, including methane ($CH_4$), are known to contribute to both air quality degradation and climate change, these are often dealt with as separate environmental concerns, despite scientific evidence indicating strong linkages between the two[9,10,11,12,13,14,15].

Since the atmospheric lifetimes of SLCFs range from a few hours to several years, their control has substantial potential for rapidly mitigating warming, in the Arctic and globally. However, the climate change mitigation potential of SLCFs is still poorly understood. SLCF mitigation actions to limit Arctic warming over the next few decades have not yet been robustly assessed or compared with greenhouse gas (GHG) mitigation actions. Climate modeling studies have consistently failed to meaningfully constrain the competing influences of scattering and absorbing particulate matter components on future Arctic climate[16]. Unsurprisingly, detailed modelling studies disagree on the magnitude of SLCF temperature impacts in the Arctic[15,16,17,18]. Although important information about process uncertainties has become available from multiple multi-model assessments, this information is not yet widely used in studies of SLCFs. Furthermore, highly idealized SLCF scenarios have been used, which are disconnected from greenhouse gas scenarios, or do not reflect technological changes in the real world.

The Planetary Science Journal, vol. 3, issue no. 4, pp. 92, doi:10.3847/PSJ/ac6033

# Large scale volcanism and the heat-death of terrestrial worlds

**Way**, **M.J.**[1,2,3], R.E. Ernst, and J.D. Scargle[4], 2022

NASA Goddard Institute for Space Studies, New York, NY, USA[1]
Theoretical Astrophysics, Department of Physics and Astronomy, Uppsala University, Uppsala, Sweden[2]
Goddard Space Flight Center Sellers Exoplanet Environments Collaboration, Greenbelt, MD, USA [3]
NASA Ames Research Center, Moffett Field, USA[4]

**Abstract.** Large-scale volcanism has played a critical role in the long-term habitability of Earth. Contrary to widely held belief, volcanism, rather than impactors, has had the greatest influence on and bears most of the responsibility for large-scale mass extinction events throughout Earth's history. We examine the timing of large igneous provinces (LIPs) throughout Earth's history to estimate the likelihood of nearly simultaneous events that could drive a planet into an extreme moist or runaway greenhouse, leading to the end of volatile cycling and causing the heat death of formerly temperate terrestrial worlds. In one approach, we make a conservative estimate of the rate at which sets of near-simultaneous LIPs (pairs, triplets, and quartets) occur in a random history statistically the same as Earth's. We find that LIPs closer in time than 0.1–1 million yr are likely; significantly, this is less than the time over which terrestrial LIP environmental effects are known to persist. In another approach, we assess the cumulative effects with simulated time series consisting of randomly occurring LIP events with realistic time profiles. Both approaches support the conjecture that environmental impacts of LIPs, while narrowly avoiding grave effects on the climate history of Earth, could have been responsible for the heat death of our sister world Venus.

**Introduction.** Large igneous provinces (LIPs) on Earth are voluminous ($1 \times 10^5$ to $>1 \times 10^6$ km$^3$), mainly mafic (–ultramafic) magmatic events of intraplate affinity (based on tectonic setting and/or geochemistry) that occur in both continental and oceanic settings. They are typically either of short duration (<5 Myr) or consist of multiple pulses over a maximum of a few tens of megayears (Coffin & Eldholm **1994**; Ernst **2014**; Svensen et al. **2019**; Ernst **2021a**). The LIPs have been tied to dramatic climate change resulting in mass extinction events in Earth's history (Wignall **2001**; Bond & Wignall **2014**; Bond & Grasby **2017**; Ernst & Youbi **2017**; Ernst **2021a**; Ernst et al. **2021b**) due to the release of toxic (to life) gases and large $CO_2$ releases possibly heating up the climate, for example, in the end Permian (e.g., Reichow et al. **2009**; Svensen et al. **2009**; Polozov et al. **2016**; Burgess **2017**; Jurikova et al. 2020). Recent work by Schobben et al. (**2020**) and Li et al. (**2022**) indicates that enhanced weathering may have also created anoxic ocean conditions that may have played a key role in extinction events.

Crediting LIPs alone is problematic, given the poor record of large impact events we have to work with (see Figure 4 in Napier **2014**), where crater counts beyond 500 Myr old are extremely sparse. However, humans are an innovative species, and new craters have been discovered in surprising places in recent years (e.g., Kjæ et al. **2018**). Although the record of LIP events throughout Earth's history is incomplete and more dating accuracy is needed, it is possible to characterize the timing of such events on the continents to at least 2.8 Ga (Ernst **2014**; Ernst et al. **2021b**).

Germane to this study, a number of works in recent years have attempted to find periodicities and related external correlations with LIP events and mass extinction events in general (e.g., Prokoph et al. **2004**, **2013**; Melott & Bambach **2013**; Condie & Puetz **2019**; Puetz & Condie **2019**). However, such studies have found no cycles that both have high intensity and persist throughout. Section **4** presents evidence that LIPs occur independently, randomly, and at a uniform rate over time. Furthermore, any departure from this picture, including weak or intermittent periodicities of unknown statistical significance, would only increase the frequency of simultaneous LIPs, thereby enhancing our conclusions.

Environmental Research Letters, vol. 17, issue no. 11, pp. 111002, doi:10.1088/1748-9326/ac998c

# Assessing progress toward the Paris Climate Agreement from space

Weir, B.[1,2], T. Oda, L.E. Ott, and **G.A. Schmidt**[3], 2022

Morgan State University, Baltimore, MD, USA[1]
Global Modeling and Assimilation Office, NASA Goddard Space Flight Center, Greenbelt, MD, USA[2]
NASA Goddard Institute for Space Studies, New York, NY, USA[3]

**Abstract.** Since the Industrial Revolution, growing 'atmospheric stocks' of greenhouse gas (GHG) concentrations (Joos and Spahni **2008**, Dlugokencky and Tans **2022**) have led to global average temperature increases of over 1 °C with carbon dioxide ($CO_2$) the leading contributor, accounting for roughly half the total warming (IPCC **2014**). Left unchecked, continued growth in GHG concentrations due to fossil fuel combustion, deforestation, and other human activities is projected to have catastrophic impacts on the Earth's climate and habitability (IPCC **2014**). While the impact of human activity on climate may be well understood globally over several decades, the ability to trace more granular activity, e.g., annual fuel usage of individual countries, to changes in GHG concentrations remains a landmark goal needed to support climate change mitigation efforts. This commentary addresses how this goal might be achieved with a focus on transparency, verifiability, and the challenges that lie ahead.

The 2015 Paris Agreement (PA; UNFCCC **2016**), reaffirmed by the 2021 Glasgow Pact (UNFCCC **2022a**), plans to limit future global temperature increases through coordinated reduction of GHG emissions. These efforts will be evaluated every 5 years during UNFCCC Global Stocktakes (GSTs; PA Article 14) with the first ongoing. GSTs are intended to 'assess collective progress [and] have no individual Party focus' (UNFCCC **2019**). Individual Parties are instead expected to assess their own progress through the Enhanced Transparency Framework (ETF; PA Article 13), a series of biennial reports starting in 2024. Table 1 of the ETF reference manual (UNFCCC **2022b**) suggests parties detail how their effort 'contributes to the stabilization of GHG concentrations [...] at a level that would prevent dangerous interference with the climate system.' Observations of GHG concentrations and derived scientific analyses are thus expected to play a vital role in assessments of mitigation efforts (Matsunaga and Maksyutov **2018**, Buendia *et al* **2019**, Janssens-Maenhout *et al* **2020**).

Our recent study (Weir *et al* **2021b**) showed that NASA's Orbiting Carbon Observatory 2 (OCO-2; Crisp *et al* **2004**, Eldering *et al* **2017**) was able to detect the impact of human activity reductions on atmospheric $CO_2$ concentrations during the coronavirus disease 2019 (COVID-19) pandemic. This achievement marked the first time that monthly, regional changes in fossil fuel emissions were observed in the atmosphere from space. While emissions decreases due to COVID-19 were historically large, the signal in column $CO_2$ was just 0.14–0.62 ppm, about 0.1% of background values. Nevertheless, year-to-year decreases in $CO_2$ growth of similar magnitude, if not greater, will be needed to meet even the moderate goal of less than 4.5 °C warming in 2100 (Forster *et al* **2020**, Le Quéré *et al* **2020**). Current spaceborne technology is therefore at or near the threshold for detecting regional impacts of mitigation efforts on GHG levels. Future advances in coverage, resolution, quality, and co-sampled species from planned missions (Crisp *et al* **2018**, Moore *et al* **2018**, Sierk *et al* **2019**, Tsujihara *et al* **2021**), are expected to further improve the capabilities of GHG monitoring systems like our own. For example, the Geostationary Carbon Cycle Observatory (GeoCarb; Moore III *et al* **2018**) mission will observe the Americas twice daily, whereas OCO-2 soundings repeat after 16 days.

The impact of COVID-19 is just one application of our broader effort to maintain and distribute results from a quasi-operational GHG monitoring system. To support scientific and stakeholder needs, we provide 16 day, column-average $CO_2$ concentrations, anomalies, and uncertainties on a nominally 50 km global grid through the trilateral NASA/ESA/JAXA Earth observing (EO) dashboard (**https://eodashboard.org**) and other NASA assets (Weir and Ott **2022a**, **2022b**).

Environmental Modeling and Software, vol. 149, 105318, doi:10.1016/j.envsoft.2022.105318

# Increasing the uptake of ecological model results in policy decisions to improve biodiversity outcomes

Weiskopf, S.R., Z. Harmáčková, C.G. Johnson, M.C. Londoño-Murcia, B.W. Miller, B.J.E. Myers, L. Pereira, M.I. Arce-Plata, J.L. Blanchard, S. Ferrier, E.A. Fulton, M. Harfoot, F. Isbell, J.A. Johnson, A.S. Mori, **E. Weng**[1,2], and I.M.D. Rosa, 2022

NASA Goddard Institute for Space Studies, New York, NY, USA[1]
Center for Climate Systems Research, Columbia University, New York, NY, USA[2]

**Abstract.** Models help decision-makers anticipate the consequences of policies for ecosystems and people; for instance, improving our ability to represent interactions between human activities and ecological systems is essential to identify pathways to meet the 2030 **Sustainable Development Goals**. However, use of modeling outputs in decision-making remains uncommon. We share insights from a multidisciplinary National Socio-Environmental Synthesis Center working group on technical, communication, and process-related factors that facilitate or hamper uptake of model results. We emphasize that it is not simply technical model improvements, but active and iterative stakeholder involvement that can lead to more impactful outcomes. In particular, trust- and relationship-building with decision-makers are key for knowledge-based decision making. In this respect, nurturing knowledge exchange on the interpersonal (e.g., through participatory processes) and institutional level (e.g., through science-policy interfaces across scales) represents a promising approach. To this end, we offer a generalized approach for linking modeling and decision-making.

**Introduction.** Ecosystems depend on diverse biological attributes to ensure ecological functions and processes that are fundamental to life on Earth. Improved ability to represent interactions between human activities and ecological systems is essential to identify pathways to meet the 2030 **Sustainable Development Goals** (**Kim et al., 2018**). Therefore, decision-makers often want to anticipate the consequences of policies for ecosystems and human well-being (**Isbell et al., 2017**). Models - i.e., qualitative or quantitative descriptions of key components of a system and of relationships between those components - are important tools to support such endeavors and can provide a useful way to examine possible outcomes (**IPBES, 2016**). However, examples of modeling outputs that have directly influenced conservation practice and decision-making are rare (**Rapacciuolo, 2019**). While models are often created with the intention of informing decision-makers, a number of factors may hamper or facilitate the use of the models, and research more broadly, in decision-making processes (**Dilling and Lemos, 2011**; **IPBES, 2016**; **Wall et al., 2017**).

Here, we focus on the uptake of biodiversity, ecosystem function, and ecosystem services models. Integrating biodiversity and ecosystem function (BEF) models to improve projections of ecosystem services was one of the main challenges identified in the collective modeling effort that contributed to the IPBES Global Assessment (**Rosa et al., 2020**), and the insights we share in this paper are drawn from an interdisciplinary SESYNC (The National Socio-Environmental Synthesis Center) working group focused on this challenge. To draw on our collective experience, we informally interviewed working group members that have developed or work extensively with different ecological models about their model use experience.

Working group members have experience with a variety of ecological models with varying levels of uptake in policy processes at different scales, which provided a unique opportunity to compare factors hampering and facilitating model uptake. Models ranged from national fisheries management (e.g., Atlantis in Australia (**Fulton et al., 2014**) to regional water management and **land use planning** (e.g., InVEST (**Daily et al., 2009**; **Kareiva et al., 2011**; **Nelson et al., 2009**); (See list of models in appendix 1). Nearly half of the models discussed had not yet been used in a specific decision-making process.

BioScience, vol. 72, issue no. 11, pp. 1062-1073, doi:10.1093/biosci/biac074

# A conceptual framework to integrate biodiversity, ecosystem function, and ecosystem service models

Weiskopf, S.R, B.J.E Myers, M.I. Arce-Plata, J.L Blanchard, S. Ferrier, E.A Fulton, M. Harfoot, F. Isbell, J.A Johnson, A.S Mori, **E. Weng**, Z.V Harmáčková, M.C. Londoño-Murcia, B.W Miller, L.M Pereira, and I.M.D Rosa, 2022

NASA Goddard Institute for Space Studies, New York, NY, USA[1]
Center for Climate Systems Research, Columbia University, New York, NY, USA[2]

**Abstract.** Global biodiversity and ecosystem service models typically operate independently. Ecosystem service projections may therefore be overly optimistic because they do not always account for the role of biodiversity in maintaining ecological functions. We review models used in recent global model intercomparison projects and develop a novel model integration framework to more fully account for the role of biodiversity in ecosystem function, a key gap for linking biodiversity changes to ecosystem services. We propose two integration pathways. The first uses empirical data on biodiversity–ecosystem function relationships to bridge biodiversity and ecosystem function models and could currently be implemented globally for systems and taxa with sufficient data. We also propose a trait-based approach involving greater incorporation of biodiversity into ecosystem function models. Pursuing both approaches will provide greater insight into biodiversity and ecosystem services projections. Integrating biodiversity, ecosystem function, and ecosystem service modeling will enhance policy development to meet global sustainability goals.

**Introduction.** At present, global models of biodiversity and ecosystem services estimate the impacts of anthropogenic stressors (e.g., climate change, land-use change) using scenarios that operate independently (Rosa et al. **2017**). Projections of socioeconomic variables such as demography and land-use change are traditionally used to estimate impacts on biodiversity separately from those on ecosystem services (Pereira et al. **2010**). Although efforts have been made to incorporate some attributes of nature or ecosystems (e.g., total biomass or particular service-providing species), these projections are often made without explicit consideration of the role of biological diversity itself in maintaining ecological functions underpinning the provision of ecosystem services (figure **1**; Rosa et al. **2020**), even though the scientific understanding of these links has advanced significantly (Isbell et al. **2017**, van der Plas **2019**). As a result, global projections of biodiversity, ecological functions, and ecosystem services may be overly optimistic because they assume that the remaining biological components of nature will continue to provide the same flow of benefits to people, regardless of how much biodiversity is lost (Isbell et al. **2015**). For example, some carbon storage models assume constant carbon pools after land-use change (Kovacs et al. **2013**), even though biodiversity loss continues over time after the initial habitat loss (Rosenzweig **1999**). Efforts to integrate biodiversity and ecosystem function models are increasing but still fall short (Rosa et al. **2020**).

Geoscientific Model Development, vol. 15, issue no. 22, pp. 8153-8180, doi:10.5194/gmd-15-8153-2022

# Modeling demographic-driven vegetation dynamics and ecosystem biogeochemical cycling in NASA GISS's Earth system model (ModelE-BiomeE v.1.0)

**Weng, E.**[1,2], **I. Aleinov**[1,2], **R. Singh**[1,2], **M.J. Puma**[1,2], **S.S. McDermid**[1], **N.Y. Kiang**[1], **M.A Kelley**[1], K. Wilcox, R. Dybzinski, C.E. Farrior, S.W. Pacala, and **B.I. Cook**[1], 2022

NASA Goddard Institute for Space Studies, New York, NY, USA[1]
Center for Climate Systems Research, Columbia University, New York, NY, USA[2]

**Abstract.** We developed a demographic vegetation model, BiomeE, to improve the modeling of vegetation dynamics and ecosystem biogeochemical cycles in the NASA Goddard Institute of Space Studies' ModelE Earth system model. This model includes the processes of plant growth, mortality, reproduction, vegetation structural dynamics, and soil carbon and nitrogen storage and transformations. The model combines the plant physiological processes of ModelE's original vegetation model, Ent, with the plant demographic and ecosystem nitrogen processes that have been represented in the Geophysical Fluid Dynamics Laboratory's LM3-PPA. We used nine plant functional types to represent global natural vegetation functional diversity, including trees, shrubs, and grasses, and a new phenology model to simulate vegetation seasonal changes with temperature and precipitation fluctuations. Competition for light and soil resources is individual based, which makes the modeling of transient compositional dynamics and vegetation succession possible. Overall, the BiomeE model simulates, with fidelity comparable to other models, the dynamics of vegetation and soil biogeochemistry, including leaf area index, vegetation structure (e.g., height, tree density, size distribution, and crown organization), and ecosystem carbon and nitrogen storage and fluxes. This model allows ModelE to simulate transient and long-term bio-geophysical and biogeochemical feedbacks between the climate system and land ecosystems. Furthermore, BiomeE also allows for the eco-evolutionary modeling of community assemblage in response to past and future climate changes with its individual-based competition and demographic processes.

**Introduction.** Terrestrial ecosystems play a critical role in climate systems by regulating exchanges of energy, moisture, and carbon dioxide between the land surface and the atmosphere (Sellers, 1997; Pielke et al., 1998; Meir et al., 2006). In turn, climate change has significantly affected vegetation photosynthesis, water use efficiency, mortality, regeneration, and structure through gradual changes in the temperature and atmospheric $CO_2$ concentration together with shifts in climate extremes (Keenan et al., 2013; Huang et al., 2015; Brando et al., 2019; McDowell et al., 2020). These responses have triggered structural and compositional shifts in global vegetation. For example, global forest mortality has increased in recent years (Allen et al., 2010; Anderegg et al., 2012), tree sizes have decreased (Zhou et al., 2014; McDowell et al., 2020), and species composition has shifted to more opportunistic species (Clark et al., 2016; Brodribb et al., 2020). The shifts in vegetation function, composition, and structure can change the boundary conditions of the land surface and affect the climate system (Nobre et al., 1991; Avissar and Werth, 2005; Garcia et al., 2016; Green et al., 2017; Zeng et al., 2017). Realistic simulation of these processes is therefore critical for Earth system models (ESMs).

The vegetation dynamics in ESMs are usually simulated using dynamic global vegetation models (DGVMs; Prentice et al., 2007), most of which are simplified in their representation of ecological processes. The core assumptions of many vegetation models are a big-leaf canopy, vegetation represented by only a few plants functional types (PFTs), single-cohort-based vegetation dynamics (or single-cohort assumption, where the vegetation community at a land unit are simulated as a collection of identical plants), lumped-pool-based biogeochemical cycles, and first-order decay of soil organic matter.

Atmospheric Chemistry and Physics, vol. 22, issue no. 9, pp. 5775-5828, doi:10.5194/acp-22-5775-2022

# Model evaluation of short-lived climate forcers for the Arctic Monitoring and Assessment Programme: A multi-species, multi-model study

Whaley, C.H., R. Mahmood, K. von Salzen, B. Winter, S. Eckhardt, S. Arnold, S. Beagley, S. Becagli, R.-Y. Chien, J. Christensen, S.M. Damani, K. Eleftheriadis, N. Evangeliou, **G.S. Faluvegi**[1,2], M. Flanner, J.S. Fu, M. Gauss, F. Giardi, W. Gong, J.L. Hjorth, L. Huang, U. Im, Y. Kanaya, S. Krishnan, Z. Klimont, T. Kühn, J. Langner, K.S. Law, L. Marelle, A. Massling, D. Olivié, T. Onishi, N. Oshima, Y. Peng, D.A. Plummer, O. Popovicheva, L. Pozzoli, J.-C. Raut, M. Sand, L.N. Saunders, J. Schmale, S. Sharma, H. Skov, F. Taketani, M.A. Thomas, R. Traversi, **K. Tsigaridis**[1,2], S. Tsyro, S. Turnock, V. Vitale, K.A. Walker, M. Wang, D. Watson-Parris, and T. Weiss-Gibbons, 2022

NASA Goddard Institute for Space Studies, New York, NY, USA[1]
Center for Climate Systems Research, Columbia University, New York, NY, USA[2]

**Abstract.** While carbon dioxide is the main cause for global warming, modeling short-lived climate forcers (SLCFs) such as methane, ozone, and particles in the Arctic allows us to simulate near-term climate and health impacts for a sensitive, pristine region that is warming at 3 times the global rate. Atmospheric modeling is critical for understanding the long-range transport of pollutants to the Arctic, as well as the abundance and distribution of SLCFs throughout the Arctic atmosphere. Modeling is also used as a tool to determine SLCF impacts on climate and health in the present and in future emissions scenarios.

In this study, we evaluate 18 state-of-the-art atmospheric and Earth system models by assessing their representation of Arctic and Northern Hemisphere atmospheric SLCF distributions, considering a wide range of different chemical species (methane, tropospheric ozone and its precursors, black carbon, sulfate, organic aerosol, and particulate matter) and multiple observational datasets. Model simulations over 4 years (2008–2009 and 2014–2015) conducted for the 2022 Arctic Monitoring and Assessment Programme (AMAP) SLCF assessment report are thoroughly evaluated against satellite, ground, ship, and aircraft-based observations. The annual means, seasonal cycles, and 3-D distributions of SLCFs were evaluated using several metrics, such as absolute and percent model biases and correlation coefficients. The results show a large range in model performance, with no one particular model or model type performing well for all regions and all SLCF species. The multi-model mean (mmm) was able to represent the general features of SLCFs in the Arctic and had the best overall performance. For the SLCFs with the greatest radiative impact ($CH_4$, $O_3$, BC, and SO), the mmm was within ±25 % of the measurements across the Northern Hemisphere. Therefore, we recommend a multi-model ensemble be used for simulating climate and health impacts of SLCFs.

Of the SLCFs in our study, model biases were smallest for $CH_4$ and greatest for OA. For most SLCFs, model biases skewed from positive to negative with increasing latitude. Our analysis suggests that vertical mixing, long-range transport, deposition, and wildfires remain highly uncertain processes. These processes need better representation within atmospheric models to improve their simulation of SLCFs in the Arctic environment. As model development proceeds in these areas, we highly recommend that the vertical and 3-D distribution of SLCFs be evaluated, as that information is critical to improving the uncertain processes in models.

**Introduction.** The Arctic atmosphere is warming 3 times more quickly than the global average (**Bush and Lemmen, 2019**; **NOAA, 2020**; **AMAP, 2021**; **IPCC, 2021**). Arctic warming is a manifestation of global warming, and the main driver for this is the increasing carbon dioxide ($CO_2$) radiative forcing (**IPCC, 2021**). Arctic warming is amplified by sea ice and snow feedbacks and affected by local radiative forcings in the Arctic, including radiative forcings by short-lived climate forcers (SLCFs), such as methane, black carbon, and tropospheric ozone (**AMAP, 2015a, b, 2022**).

Nature Climate Change, vol. 12, issue no. 3, pp. 232-234, doi:10.1038/s41558-022-01290-z

# Rapid intensification of the emerging southwestern North American megadrought in 2020-2021

Williams, A.P.[2], **B.I. Cook**[1,2], and J.E. Smerdon[2], 2022

NASA Goddard Institute for Space Studies, New York, NY, USA[1]
Lamont-Doherty Earth Observatory of Columbia University, Palisades, NY, USA[2]

**Abstract.** A previous reconstruction back to 800 CE indicated that the 2000–2018 soil moisture deficit in southwestern North America was exceeded during one megadrought in the late-1500s. Here, we show that after exceptional drought severity in 2021, ~19% of which is attributable to anthropogenic climate trends, 2000–2021 was the driest 22-yr period since at least 800. This drought will very likely persist through 2022, matching the duration of the late-1500s megadrought.

**Introduction.** Since the year 2000, southwestern North America (SWNA, 30–45° N, 105–125° W) has been unusually dry due to low precipitation totals and heat, punctuated most recently by exceptional drought in 2021[1]. From 2000 to 2021, mean water-year (October–September) SWNA precipitation was 8.3% below the 1950–1999 average and temperature was 0.91 °C above average (Extended Data Fig. **1**). No other 22-yr period since at least 1901 was as dry or as hot. While there have been single-year breaks in these anomalous conditions, aridity has dominated the 2000s, as evidenced by declines in two of North America's largest reservoirs, Lakes Mead and Powell, both on the Colorado River. In summer 2021, these reservoirs reached their lowest levels on record, triggering unprecedented restrictions on Colorado River usage[2], in part because the 2-yr naturalized flow out of Colorado River's upper basin in water-years 2020–2021 was likely the lowest since at least 1906 (Extended Data Fig. **2**). Aridity was especially extreme and widespread from summer 2020 through summer 2021 (Extended Data Fig. **3**). Despite an active North American monsoon in 2021, the United States Drought Monitor (USDM[3]) classified >68% of the western United States as under extreme or exceptional drought for nearly all of July–October 2021 (Extended Data Fig. **4**), a record-high proportion of drought extent in the USDM's 22-yr history.

Soil moisture is a particularly important integrator of drought. Soil moisture impacts runoff ratios and therefore streamflow, agricultural productivity and irrigation demand, ecosystem productivity and health, wildfire activity and land–atmosphere feedbacks such as heatwave intensity. Summer soil moisture is particularly crucial, as summer is when water demand from ecosystems, humans and the atmosphere is generally highest, and also the season of focus in most tree-ring reconsructions of drought severity[4]. According to a bucket-type water-balance model forced by monthly climate data[5], SWNA 0–200 cm soil moisture in summer (June–August) was below average in 18 of the 22 years from 2000–2021 (Extended Data Fig. **5**). This turn-of-the-twenty-first-century drought was last investigated by Williams et al.[5] through 2018, who speculated that the extended drought event may have been terminating in 2019 due to abundant precipitation that year. Dry conditions returned in 2020 and intensified substantially in 2021, however, indicating that the turn-of-the-twenty-first-century drought is not over.

To understand the longer-term context of the turn-of-the-twenty-first-century drought in SWNA, Williams et al.[5] extended the SWNA summer soil moisture record back to 800 CE using a tree-ring reconstruction and compared the observed drought of 2000–2018 to the infamous megadroughts that occurred repeatedly from 800–1600[6]. These megadroughts were multidecade droughts that exceeded any subsequent event through the 1900s in terms of duration and severity[7]. Williams et al.[5] found that the 19-yr soil moisture anomaly from 2000 to 2018 was probably the second driest in at least 1,200 years, exceeded only by a 19-yr interval during the last of the megadroughts, in the late 1500s. The authors refrained from classifying 2000–2018 as an official megadrought because the reconstructed megadroughts lasted longer than 19 yr.

Proceedings of the National Academy of Sciences, vol. 119, issue no. 10, e2114069119,
doi:10.1073/pnas.2114069119

# Growing impact of wildfire on western US water supply.

Williams, A.P., B. Livneh, K.A. McKinnon, W.D. Hansen, J.S. Mankin[2,3], **B.I. Cook[1,2]**, J.E. Smerdon[2], A.M. Varuolo-Clarke[2,4], N.R. Bjarke, C.S. Juang[2,4], and D.P. Lettenmaier, 2022

NASA Goddard Institute for Space Studies, New York, NY, USA[1]
Lamont-Doherty Earth Observatory of Columbia University, Palisades, NY, USA[2]
Department of Geography, Dartmouth College, Hanover, NH, USA[3]
Department of Earth and Environmental Sciences, Columbia University, New York, NY, USA[4]

**Abstract.** Streamflow often increases after fire, but the persistence of this effect and its importance to present and future regional water resources are unclear. This paper addresses these knowledge gaps for the western United States (WUS), where annual forest fire area increased by more than 1,100% during 1984 to 2020. Among 72 forested basins across the WUS that burned between 1984 and 2019, the multi-basin mean streamflow was significantly elevated by 0.19 SDs ($P < 0.01$) for an average of 6 water years postfire, compared to the range of results expected from climate alone. Significance is assessed by comparing pre-fire and postfire streamflow responses to climate and also to streamflow among 107 control basins that experienced little to no wildfire during the study period. The streamflow response scales with fire extent: among the 29 basins where >20% of forest area burned in a year, streamflow over the first 6 water years postfire increased by a multi-basin average of 0.38 SDs, or 30%. Postfire streamflow increases were significant in all four seasons. Historical fire–climate relationships combined with climate model projections suggest that 2021 to 2050 will see repeated years when climate is more fire-conducive than in 2020, the year currently holding the modern record for WUS forest area burned. These findings center on relatively small, minimally managed basins, but our results suggest that burned areas will grow enough over the next 3 decades to enhance streamflow at regional scales. Wildfire is an emerging driver of runoff change that will increasingly alter climate impacts on water supplies and runoff-related risks.

**Main.** Recent declines in soil moisture, streamflow, and reservoir storage signal the precariousness of water supplies in the western United States (WUS) and the urgency of managing associated risks (**1**, **2**). Declining WUS water supplies are qualitatively consistent with modeled trends due to anthropogenic climate change (**3**, **4**), but projections are uncertain due to not only climate but also the complexity of vegetation responses to climate change and associated disturbances such as wildfire (**5**–**9**). In addition to transpiration and interception, which directly divert moisture from runoff, vegetation also affects hydrology by shaping soil depth and structure and by modulating turbulent energy fluxes that alter snowpack and evaporation (**10**). In addition to direct effects on vegetation, wildfires can further affect streamflow by promoting water repellency and soil erosion (**11**–**13**). Given that the headwater areas of major WUS rivers are generally forested, altered forest cover or ecosystem water demand could potentially affect water resources at regional scales.

In recent decades, the annual forest area burned in the WUS has risen rapidly, in step with climate trends toward warming and drying (**14**–**20**). In general, forest disturbances such as wildfire are known to temporarily enhance streamflow (**21**–**23**), although cases of post-disturbance streamflow declines, especially in arid areas, have also been documented (**21**, **24**, **25**). The likelihood that rapid increases in regional forest fire activity will continue (**26**, **27**) suggests that wildfire may increasingly impact water resources in the water-limited WUS (**6**). Yet, the duration and seasonality of post-disturbance increases in runoff are unknown, raising the question of whether increased forest fire activity will meaningfully affect water availability in the WUS.

Here we use stream gauge records from 179 river basins in the WUS to assess the strength, duration, and seasonality of postfire changes in streamflow and whether increasing forest fire activity is likely to have a detectable effect on regional streamflow.

Nature Food, vol. 3, issue no. 8, pp. 586-596, doi:10.1038/s43016-022-00573-0

# Global food insecurity and famine from reduced crop, marine fishery and livestock production due to climate disruption from nuclear war soot injection

Xia, L., A. Robock, K. Scherrer, C. Harrison, B.L. Bodirsky, I. Weindl, **J. Jägermeyr**[1,2,3], C. Bardeen, O.B. Toon, and R. Heneghan, 2022

NASA Goddard Institute for Space Studies, New York, NY, USA[1]
Center for Climate Systems Research, Columbia University, New York, NY, USA[2]
Potsdam Institute for Climate Impact Research, Potsdam, Germany[3]

**Abstract.** Atmospheric soot loadings from nuclear weapon detonation would cause disruptions to the Earth's climate, limiting terrestrial and aquatic food production. Here, we use climate, crop and fishery models to estimate the impacts arising from six scenarios of stratospheric soot injection, predicting the total food calories available in each nation post-war after stored food is consumed. In quantifying impacts away from target areas, we demonstrate that soot injections larger than 5 Tg would lead to mass food shortages, and livestock and aquatic food production would be unable to compensate for reduced crop output, in almost all countries. Adaptation measures such as food waste reduction would have limited impact on increasing available calories. We estimate more than 2 billion people could die from nuclear war between India and Pakistan, and more than 5 billion could die from a war between the United States and Russia—underlining the importance of global cooperation in preventing nuclear war.

**Introduction.** Extraordinary events such as large volcanic eruptions or nuclear war could cause sudden global climate disruptions and affect food security. Global volcanic cooling caused by sulfuric acid aerosols in the stratosphere has resulted in severe famines and political instability, for example, after the 1783 Laki eruption in Iceland[1] or the 1815 Tambora eruption in Indonesia[2,3]. For a nuclear war, the global cooling would depend on the yields of the weapons, the number of weapons and the targets, among other atmospheric and geographic factors. In a nuclear war, bombs targeted on cities and industrial areas would start firestorms, injecting large amounts of soot into the upper atmosphere, which would spread globally and rapidly cool the planet[4,5,6]. Such soot loadings would cause decadal disruptions in Earth's climate[7,8,9], which would impact food production systems on land and in the oceans. In the 1980s, there were investigations of nuclear winter impacts on global agricultural production[10] and food availability[11] for 15 nations, but new information now allows us to update those estimates. Several studies have recently analysed changes of major grain crops[12,13,14] and marine wild catch fisheries[15] for different scenarios of regional nuclear war using climate, crop and fishery models. A war between India and Pakistan, which recently are accumulating more nuclear weapons with higher yield[16], could produce a stratospheric loading of 5–47 Tg of soot. A war between the United States, its allies and Russia—who possess more than 90% of the global nuclear arsenal—could produce more than 150 Tg of soot and a nuclear winter[4,5,6,7,8,9]. While amounts of soot injection into the stratosphere from the use of fewer nuclear weapons would have smaller global impacts[17], once a nuclear war starts, it may be very difficult to limit escalation[18].

The scenarios we studied are listed in Table 1. Each scenario assumes a nuclear war lasting one week, resulting in the number and yield of nuclear weapons shown in the table and producing different amounts of soot in the stratosphere. There are many war scenarios that could result in similar amounts of smoke and thus similar climate shocks, including wars involving the other nuclear-armed nations (China, France, United Kingdom, North Korea and Israel).

Recent catastrophic forest fires in Canada in 2017[19] and Australia in 2019 and 2020[20,21] produced 0.3–1 Tg of smoke (0.006–0.02 Tg soot), which was subsequently heated by sunlight and lofted high in the stratosphere. The smoke was transported around the world and lasted for many months. This adds confidence to our simulations that predict the same process would occur after nuclear war.

Communications Earth and Environment, vol. 3, issue no. 1, pp. 328, doi:10.1038/s43247-022-00660-x

# Anthropogenic sulfate aerosol pollution in South and East Asia induces increased summer precipitation over arid Central Asia

Xie, X., G. Myhre, D. Shindell, **G.S. Faluvegi**[1,2], T. Takemura, A. Voulgarakis, Z. Shi, X. Li, X. Xie, H. Liu, X. Liu, and Y. Liu, 2022

NASA Goddard Institute for Space Studies, New York, NY, USA[1]
Center for Climate Systems Research, Columbia University, New York, NY, USA[2]

**Abstract.** Precipitation has increased across the arid Central Asia region over recent decades. However, the underlying mechanisms of this trend are poorly understood. Here, we analyze multi-model simulations from the Precipitation Driver and Response Model Intercomparison Project (PDRMIP) to investigate potential drivers of the observed precipitation trend. We find that anthropogenic sulfate aerosols over remote polluted regions in South and East Asia lead to increased summer precipitation, especially convective and extreme precipitation, in arid Central Asia. Elevated concentrations of sulfate aerosols over remote polluted Asia cause an equatorward shift of the Asian Westerly Jet Stream through a fast response to cooling of the local atmosphere at mid-latitudes. This shift favours moisture supply from low-latitudes and moisture flux convergence over arid Central Asia, which is confirmed by a moisture budget analysis. High levels of absorbing black carbon lead to opposing changes in the Asian Westerly Jet Stream and reduced local precipitation, which can mask the impact of sulfate aerosols. This teleconnection between arid Central Asia precipitation and anthropogenic aerosols in remote Asian polluted regions highlights long-range impacts of anthropogenic aerosols on atmospheric circulations and the hydrological cycle.

**Introduction.** Arid Central Asia (ACA hereafter) is located in the innermost central part of the Eurasia continent and is composed of Central Asian countries and Northwest China, where there exist several deserts with a total annual precipitation less than 200 mm (e.g., Taklamakan and Gobi deserts). Observational evidence has revealed a pronounced increase of precipitation over ACA since 1961, occurring mostly in summer and winter[1,2,3,4] (also see Fig. **1a, b**). These observational results about the ACA significant wetting challenge the paradigm of "dry gets drier, wet gets wetter" under global warming[5,6,7,8,9].

Journal of Advances in Modeling Earth Systems, vol. 14, issue no. 12, e2022MS003074,
doi:10.1029/2022MS003074

# Implementation and evaluation of irrigation techniques in the Community Land Model

Yao, Y., I. Vanderkelen, D. Lombardozzi, S. Swenson, D. Lawrence**, J. Jägermeyr**[1,2,3], L. Grant, and W. Thiery, 2022

NASA Goddard Institute for Space Studies, New York, NY, USA[1]
Potsdam Institute for Climate Impact Research, Member of the Leibniz Association, Potsdam, Germany[2]
Department of Computer Science, University of Chicago, Chicago, IL, USA[3]

**Abstract.** Several previous studies have highlighted the irrigation-induced impacts on the global and regional water cycle, energy budget, and near-surface climate. While land models are widely used to address this question, the implementations of irrigation in these models vary in complexity. Here, we expand the representation of irrigation in Community Land Model to enable six different irrigation methods. We find that using a combination of irrigation methods, including default, sprinkler, flood and paddy techniques performs best as determined by evaluating the simulated irrigation water withdrawals against observations, and therefore select this combination as the new irrigation scheme. Then, the impact of the new irrigation scheme on surface fluxes is evaluated and detected using single-point simulations. Finally, the global and regional irrigation-induced impacts on surface energy and water fluxes are compared using both the original and the new irrigation scheme. The new irrigation scheme substantially reduces the bias and root-mean-square error of simulated irrigation water withdrawal in the USA and other countries, but considerably overestimates withdrawals in Central China. Results of single-point experiments show that different irrigation methods have different effects on surface fluxes, while the magnitudes are small. At the global scale, the new scheme enlarges the irrigation-induced impacts on water and energy variables relative to the original scheme, with varying magnitudes across regions. Overall, our results suggest that this newly developed scheme is a better tool for simulating irrigation-induced impacts on climate and highlight the added value of incorporating human water management in Earth system models.

**Introduction.** Irrigation is an important aspect of agricultural management, with irrigated areas providing ~40% of global food production over only ~20% of global cropland (WWAP, **2019**). It is fundamental to the food security of less developed countries, where populations have experienced fast growth (Schultz et al., **2005**). Since the 1950s, the global irrigated land area has expanded rapidly, thereby increasing worldwide irrigation water demand. Consequently, irrigation currently accounts for ~90% (~1,200 $km^3$ by the end of 20th century) of the global total consumptive freshwater use (Döll et al., **2009**; Meier et al., **2018**; Siebert et al., **2015**; Zohaib & Choi, **2020**).

As the most dominant freshwater-use practice, irrigation plays an important role in global and regional environmental change. Irrigation practices move water from different sources into agricultural systems, altering the global and regional hydrological cycle (de Vrese et al., **2016**; Ferguson & Maxwell, **2012**; Harding & Snyder, **2012**; Leng et al., **2014**). In some regions, the extraction of water for irrigation has reduced the availability of both surface and groundwater. For example, the discharge of the Tarim River basin in northwestern China has decreased substantially since 1960s, as 70%–90% of surface water flows are used for irrigation (Hao et al., **2015**). In the High Plains in the USA, the water level of aquifers has declined substantially due to the large irrigation water withdrawal (McGuire, **2014**). A study focusing on global lakes revealed that ~11% of the lake area has been lost until 2015 mainly due to irrigation water withdrawal (Wine & Laronne, **2020**).

Geophysical Research Letters, vol. 49, issue no. 16, e2022GL098551, doi:10.1029/2022GL098551

# Use of machine learning to reduce uncertainties in particle number concentration and aerosol indirect radiative forcing predicted by climate models

Yu, F., G. Luo, A.A. Nair, **K. Tsigaridis**[1,2], and **S.E. Bauer**[1], 2022

NASA Goddard Institute for Space Studies, New York, NY, USA[1]
Center for Climate Systems Research, Columbia University, New York, NY, USA[2]

**Abstract.** The radiative forcing of anthropogenic aerosols associated with aerosol-cloud interactions ($RF_{aci}$) remains the largest source of uncertainty in climate prediction. The calculation of particle number concentration (PNC), one of the critical parameters affecting $RF_{aci}$, is generally simplified in climate models. Here we employ outputs from long-term (30-year) simulations of a global size-resolved (sectional) aerosol microphysics model and a machine-learning tool to develop a Random Forest Regression Model (RFRM) for PNC. We have implemented the PNC RFRM in GISS-ModelE2.1 with a mass-based One-Moment Aerosol module, which is one of CMIP6 models. Compared to the default setting, the GISS-ModelE2.1 simulation based on RFRM reduces the changes of cloud droplet number concentration associated with anthropogenic emissions and decreases the $RF_{aci}$ from −1.46 to −1.11 $W \cdot m^{-2}$. This work highlights a promising approach based on machine learning to reduce uncertainties of climate models in predicting PNC and $RF_{aci}$ without compromising their computing efficiency.

**Introduction.** All cloud droplets formed in the atmosphere start with tiny particles that act as cloud condensation nuclei (CCN). These aerosols can alter cloud properties and precipitation (Albrecht, **1989**; Twomey, **1977**) and thereby indirectly influence the Earth's radiation budget and climate change. The radiative forcing (RF) associated with aerosol–cloud interactions (aci) remains the largest source of uncertainty in climate prediction. According to the Intergovernmental Panel on Climate Change's Fifth Assessment Report (IPCC AR5, 2013), $RF_{aci}$ of anthropogenic aerosols was estimated to be $-0.55\ W \cdot m^{-2}$ with "low" level of confidence. A number of post-IPCC AR5 global climate modeling studies still show large discrepancy in the values of $RF_{aci}$, ranging from $\sim -0.35\ W \cdot m^{-2}$ (Nazarenko et al., **2017**), to $-0.7\ W \cdot m^{-2}$ (Rotstayn et al., **2014**) to $-1.08\ W \cdot m^{-2}$ (Bauer et al., **2020**), to $-1.28\ W \cdot m^{-2}$ (Tonttila et al., **2015**), to $-1.54\ W \cdot m^{-2}$ (Bauer et al., **2020**), and to $-2.19\ W \cdot m^{-2}$ (Zhang et al., **2016**). In order to confidently interpret past and accurately project future climate change, it is essential to reduce $RF_{aci}$ discrepancy among different models.

$RF_{aci}$ depends strongly on the response of number concentrations of particles that can act as CCN to anthropogenic emissions (Albrecht, **1989**; Twomey, **1977**). The increase in cloud drops with particle number concentration (PNC) has been confirmed by many aircraft measurements (e.g., Ramanathan et al., **2001**). PNC exhibits significant spatial and temporal variability due to the non-linear dependence of new particle formation and growth rates on atmospheric conditions and concentrations of gaseous precursors, both subject to changes resulting from climate changes and emission regulatory actions. The calculation of PNC in global climate models (GCMs), including the most recent CMIP6 models, is generally simplified which contributes to the uncertainty in $RF_{aci}$. For example, among 10 CMIP6 models compared by Zanis et al. (**2020**), 7 models employ bulk mass-based aerosol schemes not supporting PNC simulation, while 3 models use modal aerosol schemes considering particle size distribution. Large uncertainties exist in the predicted PNC in these models as PNC not only depends on mass concentrations of particles but also on their size distributions which have significant spatiotemporal variations that can only be captured by the use of an aerosol microphysics parameterization. Bellouin et al. (**2013**) showed substantial differences in the aerosol forcings simulated by the bulk and modal schemes, pointing out that the bulk approach lacked the necessary sophistication to provide realistic aerosol input for aerosol-cloud-radiation calculations.

Geoscientific Model Development, vol. 15, issue no. 5, pp. 2265-2292, doi:10.5194/gmd-15-2265-2022

# Effects of forcing differences and initial conditions on inter-model agreement in the VolMIP volc-pinatubo-full experiment

Zanchettin, D., C. Timmreck, M. Khodri, A. Schmidt, M. Toohey, M. Abe, S. Bekki, J. Cole, S.-W. Fang, W. Feng, G. Hegerl, B. Johnson, N. Lebas, **A.N. LeGrande**[1,2], G.W. Mann, L. Marshall, L. Rieger, A. Robock, S. Rubinetti, **K. Tsigaridis**[1,2], and H. Weierbach, 2022

NASA Goddard Institute for Space Studies, New York, NY, USA[1]
Center for Climate Systems Research, Columbia University, New York, NY, USA[2]

**Abstract.** This paper provides initial results from a multi-model ensemble analysis based on the volc-pinatubo-full experiment performed within the Model Intercomparison Project on the climatic response to Volcanic forcing (VolMIP) as part of the sixth phase of the Coupled Model Intercomparison Project (CMIP6). The volc-pinatubo-full experiment is based on an ensemble of volcanic forcing-only climate simulations with the same volcanic aerosol dataset across the participating models (the 1991–1993 Pinatubo period from the CMIP6-GloSSAC dataset). The simulations are conducted within an idealized experimental design where initial states are sampled consistently across models from the CMIP6-piControl simulation providing unperturbed preindustrial background conditions. The multi-model ensemble includes output from an initial set of six participating Earth system models (CanESM5, GISS-E2.1-G, IPSL-CM6A-LR, MIROC-E2SL, MPI-ESM1.2-LR and UKESM1).

The results show overall good agreement between the different models on the global and hemispheric scales concerning the surface climate responses, thus demonstrating the overall effectiveness of VolMIP's experimental design. However, small yet significant inter-model discrepancies are found in radiative fluxes, especially in the tropics, that preliminary analyses link with minor differences in forcing implementation; model physics, notably aerosol–radiation interactions; the simulation and sampling of El Niño–Southern Oscillation (ENSO); and, possibly, the simulation of climate feedbacks operating in the tropics. We discuss the volc-pinatubo-full protocol and highlight the advantages of volcanic forcing experiments defined within a carefully designed protocol with respect to emerging modelling approaches based on large ensemble transient simulations. We identify how the VolMIP strategy could be improved in future phases of the initiative to ensure a cleaner sampling protocol with greater focus on the evolving state of ENSO in the pre-eruption period.

**Introduction.** The Model Intercomparison Project on the climatic response to Volcanic forcing (VolMIP; Zanchettin et al., 2016) defined a coordinated set of idealized volcanic perturbation experiments to be carried out in alignment with the protocol of the sixth phase of the Coupled Model Intercomparison Project (CMIP6; Eyring et al., 2016). VolMIP aims to assess the diversity of simulated climate responses to large-magnitude explosive volcanic eruptions with global-scale sulfate aerosol and to identify the causes and processes that cause inter-model differences.

Accordingly, VolMIP experiments are based on multi-model ensemble simulations with coupled climate models that are designed using two pillars. First, the prescribed stratospheric volcanic aerosol optical properties (often referred to as “forcing”) used in the simulations must be the same across all participating models. Consensus volcanic forcing datasets were thus defined for each experiment and implemented in terms of zonal and monthly-mean optical properties of stratospheric volcanic aerosol. Second, climate conditions defining the initial states of individual members of the ensemble must be selected in a consistent manner across the participating models so that the diagnosed expected climate response is not biased by potential effects of a preferential phase of ongoing internal variability at the time of the eruption (see Zanchettin et al., 2013; Swingedouw et al., 2015; Lehner et al., 2016; Khodri et al., 2017; Coupe and Robock, 2021). This is achieved by defining desired states of climate variability modes to be sampled along the parent CMIP6-DECK piControl simulation representative of unperturbed preindustrial climate conditions.

Environmental Research Letters, vol 17, issue no. 2, pp. 024014, doi:10.1088/1748-9326/ac4a34

# Climate change penalty and benefit on surface ozone: A global perspective based on CMIP6 earth system models

Zanis, P., D. Akritidis, S. Turnock, V. Naik, S. Szopa, A.K. Georgoulias, **S.E. Bauer**[1], M. Deushi, L.W Horowitz, J. Keeble, P. Le Sager, F.M. O'Connor, N. Oshima, **K. Tsigaridis**[1,2], and T. van Noije, 2022

NASA Goddard Institute for Space Studies, New York, NY, USA[1]
Center for Climate Systems Research, Columbia University, New York, NY, USA[2]

**Abstract.** This work presents an analysis of the effect of climate change on surface ozone discussing the related penalties and benefits around the globe from the global modelling perspective based on simulations with five CMIP6 (Coupled Model Intercomparison Project Phase 6) Earth System Models. As part of AerChemMIP (Aerosol Chemistry Model Intercomparison Project) all models conducted simulation experiments considering future climate (ssp370SST) and present-day climate (ssp370pdSST) under the same future emissions trajectory (SSP3-7.0). A multi-model global average climate change benefit on surface ozone of $-0.96 \pm 0.07$ ppbv $°C^{-1}$ is calculated which is mainly linked to the dominating role of enhanced ozone destruction with higher water vapour abundances under a warmer climate. Over regions remote from pollution sources, there is a robust decline in mean surface ozone concentration on an annual basis as well as for boreal winter and summer varying spatially from $-0.2$ to $-2$ ppbv $°C^{-1}$, with strongest decline over tropical oceanic regions. The implication is that over regions remote from pollution sources (except over the Arctic) there is a consistent climate change benefit for baseline ozone due to global warming. However, ozone increases over regions close to anthropogenic pollution sources or close to enhanced natural biogenic volatile organic compounds emission sources with a rate ranging regionally from 0.2 to 2 ppbv $C^{-1}$, implying a regional surface ozone penalty due to global warming. Overall, the future climate change enhances the efficiency of precursor emissions to generate surface ozone in polluted regions and thus the magnitude of this effect depends on the regional emission changes considered in this study within the SSP3_7.0 scenario. The comparison of the climate change impact effect on surface ozone versus the combined effect of climate and emission changes indicates the dominant role of precursor emission changes in projecting surface ozone concentrations under future climate change scenarios.

**Introduction.** Surface ozone is widely recognized as a pollutant having an impact on human health, crops, and ecosystems while tropospheric ozone plays a key role in the oxidizing capacity of the troposphere and is an important greenhouse gas (Monks *et al* **2015**, Young *et al* **2018**). Given the multifaceted dependence of tropospheric ozone on several meteorological parameters and various gaseous precursors, and its varying lifetime (from a few hours in polluted urban regions up to several months in the upper troposphere), an estimation of the climate change impact on future tropospheric and surface ozone levels is a complicated task with a regional context.

The future tropospheric and surface ozone changes at the global scale depend on changes in chemical ozone production and loss processes, stratosphere–troposphere exchange (STE), and deposition (Young *et al* **2013**). The future changes in chemical ozone production and loss are strongly related to changes in anthropogenic and natural emissions of ozone precursors, but also to changes of meteorological parameters, such as temperature, water vapour and radiation. During the 21st century, changes in climate, ozone depleting substances (ODSs), and emissions of ozone precursor species are expected to be the major factors governing ozone concentration distribution in the stratosphere, the free troposphere, and at the surface (Fiore *et al* **2015**, Revell *et al* **2015**).

Focusing solely on the response of surface ozone to climate-driven changes (instead of the response to anthropogenic emission-driven changes of ozone precursor species), the 5th IPCC Assessment Report (Kirtman *et al* **2013**) assessed that there is high confidence that in unpolluted regions, higher water vapour abundances and temperatures in a warmer climate enhance ozone destruction leading to lower baseline ozone levels, while there is medium confidence that in polluted regions surface ozone is expected to increase.

Journal of Geophysical Research Atmospheres, vol. 127, issue no. 16, e2022JD036452, doi:10.1029/2022JD036452

# Attribution of stratospheric and tropospheric ozone changes between 1850 and 2014 in CMIP6 models

Zeng, G., N.L. Abraham, A.T. Archibald, **S.E. Bauer**[1,2], M. Deushi, L.K. Emmons, P.T. Griffiths, B. Hassler, L.W. Horowitz, J. Keeble, M.J. Mills, O. Morgenstern, L.T. Murray, V. Naik, F.M. O'Connor, N. Oshima, L.T. Sentman, S. Tilmes, **K. Tsigaridis**[1,2], J.H.T. Williams, and P.J. Young, 2022

NASA Goddard Institute for Space Studies, New York, NY, USA[1]
Center for Climate Systems Research, Columbia University, New York, NY, USA[2]

**Abstract.** We quantify the impacts of halogenated ozone-depleting substances (ODSs), greenhouse gases (GHGs), and short-lived ozone precursors on ozone changes between 1850 and 2014 using single-forcing perturbation simulations from several Earth system models with interactive chemistry participating in the Coupled Model Intercomparison Project Aerosol and Chemistry Model Intercomparison Project. We present the responses of ozone to individual forcings and an attribution of changes in ozone columns and vertically resolved stratospheric and tropospheric ozone to these forcings. We find that whilst substantial ODS-induced ozone loss dominates the stratospheric ozone changes since the 1970s, in agreement with previous studies, increases in tropospheric ozone due to increases in short-lived ozone precursors and methane since the 1950s make increasingly important contributions to total column ozone (TCO) changes. Increases in methane also lead to substantial extra-tropical stratospheric ozone increases. Impacts of nitrous oxide and carbon dioxide on stratospheric ozone are significant but their impacts on TCO are small overall due to several opposing factors and are also associated with large dynamical variability. The multi-model mean (MMM) results show a clear change in the stratospheric ozone trends after 2000 due to now declining ODSs, but the trends are generally not significantly positive, except in the extra-tropical upper stratosphere, due to relatively small changes in forcing over this period combined with large model uncertainty. Although the MMM ozone compares well with the observations, the inter-model differences are large primarily due to the large differences in the models' representation of ODS-induced ozone depletion.

**Introduction.** Anthropogenic forcing since preindustrial (PI) times has driven considerable ozone changes, in both the stratosphere and troposphere. Stratospheric ozone prevents harmful ultraviolet radiation from reaching the Earth' surface. Ozone results from photochemical production and destruction cycles in the stratosphere. Stratospheric ozone can be transported into the troposphere, constituting a natural source of tropospheric ozone that is broadly in balance with chemical destruction and deposition to the surface. However, both stratospheric and tropospheric ozone have been perturbed by anthropogenic influences. The most significant impact on stratospheric ozone is from halogenated ozone-depleting substances (i.e., the gases regulated by the Montreal Protocol, referred as "ODSs" hereafter for brevity) that have damaged the ozone layer since the 1970s (Farman et al., **1985**; Molina & Rowland, **1974**; Solomon, **1999**). In the troposphere, emissions of ozone precursors, including nitrogen oxides (NO*x* = NO + NO2), methane, and non-methane volatile organic compounds, have led to substantial ozone increases since PI times (Gaudel et al., **2018**; Volz & Kley, **1988**). These increases are concerning because tropospheric ozone is a greenhouse gas (GHG) and air pollutant harmful to human health and vegetation. These findings imply that total column ozone changes as measured for example, by ground-based instruments cannot in general be interpreted only as stratospheric ozone changes because the tropospheric contributions to such trends can be substantial (Staehelin et al., **1998**).

In addition to ODSs, increases in long-lived GHGs (especially $CO_2$, $N_2O$, and $CH_4$) also impact stratospheric ozone both chemically and dynamically (Brönnimann et al., **2013**; Butler et al., **2016**; Fleming et al., **2011**; Reader et al., **2013**; Revell et al., **2015**). Methane is an ozone precursor in the troposphere promoting ozone production in the presence of $NO_x$. In the stratosphere, methane affects ozone in several ways (Brasseur & Solomon, **1984**): (a) Increasing methane leads to water vapor production in the stratosphere which enhances the ozone loss through $HO_x$-catalytic cycles.

Frontiers in Remote Sensing, vol. 3, 840188, doi:10.3389/frsen.2022.840188

# A radiative transfer simulator for PACE: Theory and applications

Zhai, P.-W., M. Gao[1,2], B.A. Franz[1], P.J. Werdell[1], A. Ibrahim[1], Y. Hu[3], and **J. Chowdhary[4,5]**, 2022

Ocean Ecology Laboratory, NASA Goddard Space Flight Center, Greenbelt, MD, USA[1]
Science Systems and Applications, Inc., Greenbelt, MD, USA[2]
NASA Langley Research Center, Hampton, VA, USA[3]
NASA Goddard Institute for Space Studies, New York, NY, USA[4]
Department of Applied Physics and Applied Mathematics, Columbia University, New York, NY, USA[5]

**Abstract.** A radiative transfer simulator was developed to compute the synthetic data of all three instruments onboard NASA's Plankton Aerosol, Cloud, ocean Ecosystem (PACE) observatory, and at the top of the atmosphere (TOA). The instrument suite includes the ocean color instrument (OCI), the Hyper-Angular Rainbow Polarimeter 2 (HARP2), and the Spectro-Polarimeter for Planetary Exploration 1 (SPEXone). The PACE simulator is wrapped around a monochromatic radiative transfer model based on the successive order of scattering (RTSOS), which accounts for atmosphere and ocean coupling, polarization, and gas absorption. Inelastic scattering, including Raman scattering from pure ocean water, fluorescence due to chlorophyll, and colored dissolved organic matter (CDOM), is also simulated. This PACE simulator can be used to explore the sensitivity of the hyperspectral and polarized reflectance of the Earth system with tunable atmosphere and ocean parameters, which include aerosol and cloud number concentration, refractive indices, and size distribution, ocean particle microphysical parameters, and solar and sensor-viewing geometry. The PACE simulator is used to study two important case studies. One is the impact of the significant uncertainty in pure ocean water absorption coefficient to the radiance field in the ultraviolet (UV) spectral region, which can be as much as 6%. The other is the influence of different amounts of brown carbon aerosols and CDOM on the polarized radiance field at TOA. The percentage variation of the radiance field due to CDOM is mostly for wavelengths smaller than 600 nm, while brown aerosols affect the whole spectrum from 350 to 890 nm, primarily due to covaried soot aerosols. Both case studies are important for aerosol and ocean color remote sensing and have not been previously reported in the literature.

**Introduction.** NASA's Plankton, Aerosol, Cloud, and ocean Ecosystem (PACE) mission will carry the Ocean Color Instrument (OCI), which is a hyperspectral scanning radiometer with spectral coverage from the ultraviolet (340 nm) to near-infrared (890 nm) measured at 5 nm spectral resolution with 2.5-nm spectral sampling (**Werdell et al., 2019**). The 5-nm resolution will better resolve spectral features of some plankton species, as well as atmospheric gas absorption features such as the Oxygen-A band centered near 765 nm. OCI also includes seven shortwave infrared (SWIR) bands centered on 940, 1,038, 1,250, 1,378, 1,615, 2,130, and 2,260 nm, to be used for ocean color atmospheric correction and aerosol and cloud retrievals. In addition, PACE plans to carry two Multi-Angle Polarimeters (MAPs): the Hyper-Angular Rainbow Polarimeter 2 (HARP2) (**McBride et al., 2020**) and the Spectro-Polarimeter for Planetary Exploration 1 (SPEXone) (**Hasekamp et al., 2019**). HARP2 will measure the first three Stokes parameters (I, Q, and U) at four wavelengths (441, 549, 669, and 873 nm) and at multiple viewing angles (60 angles for 669 nm, and 10 angles for the other wavelengths) for each pixel. SPEXone will measure the radiance and the Degree of Linear Polarization (DoLP) from 385 to 770 nm with a variable spectral resolution of 2–5 nm for radiance and 10–40 nm for DoLP at five viewing angles, but with less swath coverage than OCI and HARP2. The combined dataset of OCI and the MAPs will provide a plethora of data that will significantly enhance our understanding of the Earth's Ocean, atmosphere, and land systems.

Journal of Climate, vol. 35, issue no. 12, pp. 3747-3765, doi:10.1175/JCLI-D-21-0387.1

# Turbulent heat flux, downward longwave radiation and large-scale atmospheric circulation associated with the wintertime Barents-Kara Sea extreme sea ice loss events

Zheng, C.[3], M. Ting[3], Y. Wu[3], N. Kurtz[1], **C. Orbe[2]**, **P.M. Alexander[2,3]**, R. Seager[3], and **M. Tedesco[2,3]**, 2022

NASA Goddard Space Flight Center, Greenbelt, MD, USA[1]
NASA Goddard Institute for Space Studies, New York, NY, USA[2]
Lamont-Doherty Earth Observatory, Columbia University, Palisades, NY, USA[3]

**Abstract.** We investigate wintertime extreme sea ice loss events on synoptic to sub-seasonal time scales over the Barents–Kara Sea, where the largest sea ice variability is located. Consistent with previous studies, extreme sea ice loss events are associated with moisture intrusions over the Barents–Kara Sea, which are driven by the large-scale atmospheric circulation. In addition to the role of downward longwave radiation associated with moisture intrusions, which is emphasized by previous studies, our analysis shows that strong turbulent heat fluxes are associated with extreme sea ice melting events, with both turbulent sensible and latent heat fluxes contributing, although turbulent sensible heat fluxes dominate. Our analysis also shows that these events are connected to tropical convective anomalies. A dipole pattern of convective anomalies with enhanced convection over the Maritime Continent and suppressed convection over the central to eastern Pacific is consistently detected about 6–10 days prior to extreme sea ice loss events. This pattern is associated with either the Madden–Julian oscillation (MJO) or El Niño–Southern Oscillation (ENSO). Composites show that extreme sea ice loss events are connected to tropical convection via Rossby wave propagation in the midlatitudes. However, tropical convective anomalies alone are not sufficient to trigger extreme sea ice loss events, suggesting that extratropical variability likely modulates the connection between tropical convection and extreme sea ice loss events.

**Introduction.** Observational studies show that Arctic warming over the past few decades is most rapid during the winter season (**Bekryaev et al. 2010**; **Screen and Simmonds 2010**). Such warming is driven by many factors including greenhouse gas increases, loss of sea ice, and energy transport by the atmosphere and the ocean (**Carmack and Melling 2011**; **Serreze and Barry 2011**; **Bintanja and van der Linden 2013**; **Pithan and Mauritsen 2014**). Recently, the role of downward longwave radiation (LWR) on both the long-term trend of Arctic sea ice decline and the fluctuations of the Arctic sea ice on shorter time scales has been addressed by many studies (**Francis and Hunter 2006**; **Graversen and Wang 2009**; **Graversen et al. 2011**; **Lee et al. 2011b**; **Woods et al. 2013**; **D. Park et al. 2015**; **H. Park et al. 2015a,b**; **Burt et al. 2016**; **Woods and Caballero 2016**; **Gong et al. 2017**; **Lee et al. 2017**; **Johansson et al. 2017**; **Kim and Kim 2017**; **Z. Wang et al. 2020**). Many of these studies also showed that fluctuations of downward LWR are often associated with moisture intrusions into the Arctic. Sea ice fluctuations can also be driven by other factors including wind-induced sea ice motion (**Fang and Wallace 1994**; **Rigor et al. 2002**; **Rigor and Wallace 2004**; **Kwok 2005**; **Sorteberg and Kvingedal 2006**; **Liptak and Strong 2014**) and local temperature anomalies (**Deser et al. 2000**). The sea ice variability on synoptic to sub-seasonal time scales has not received much attention until recently. Studies show that Ural blocking is important in modulating winter Arctic sea ice on short time scales, particularly over the Barents–Kara Sea (BKS) region (**Gong and Luo 2017**; **Luo et al. 2017**; **Chen et al. 2018**; **Cho and Kim 2021**). The primary goal of this study is to identify the primary drivers of extreme Arctic sea ice loss on these time scales during winter.

Though the role of downward LWR associated with moisture intrusions has been emphasized previously (e.g., **Woods and Caballero 2016**; **D. Park et al. 2015**; **Yang and Magnusdottir 2017**), these studies focused on the sea ice response following strong moisture intrusion events. Similar results regarding the role of downward LWR are reached with composite studies of Ural blocking events and the associated sea ice response (**Gong and Luo 2017**; **Luo et al. 2017**; **Chen et al. 2018**).

Atmospheric Chemistry and Physics, vol. 22, issue no. 17, pp. 11009-11032, doi:10.5194/acp-22-11009-2022

# Satellite-based evaluation of AeroCom model bias in biomass burning regions

Zhong, Q., N. Schutgens, G van der Werf, T. van Noije, **K. Tsigaridis**[1,2], **S.E. Bauer**[1,2], T. Mielonen, A. Kirkevåg, Ø. Seland, H. Kokkola, R. Checa-Garcia, D. Neubauer, Z. Kipling, H. Matsui, P. Ginoux, T. Takemura, P. Le Sager, S. Rémy, H. Bian[3,4], M. Chin[3], K. Zhang, J. Zhu, S.G. Tsyro, G. Curci, A. Protonotariou, B. Johnson, J.E. Penner, N. Bellouin, R.B. Skeie, and G. Myhre, 2022

NASA Goddard Institute for Space Studies, New York, NY, USA[1]
Center for Climate Systems Research, Columbia University, New York, NY, USA[2]
NASA Goddard Space Flight Center, Greenbelt, MD, USA[3]
Joint Center for Earth Systems Technology, University of Maryland, Baltimore County (UMBC), Baltimore, MD, USA[4]

**Abstract.** Global models are widely used to simulate biomass burning aerosol (BBA). Exhaustive evaluations on model representation of aerosol distributions and properties are fundamental to assess health and climate impacts of BBA. Here we conducted a comprehensive comparison of Aerosol Comparisons between Observations and Models (AeroCom) project model simulations with satellite observations. A total of 59 runs by 18 models from three AeroCom Phase-III experiments (i.e., biomass burning emissions, CTRL16, and CTRL19) and 14 satellite products of aerosols were used in the study. Aerosol optical depth (AOD) at 550 nm was investigated during the fire season over three key fire regions reflecting different fire dynamics (i.e., deforestation-dominated Amazon, Southern Hemisphere Africa where savannas are the key source of emissions, and boreal forest burning in boreal North America). The 14 satellite products were first evaluated against AErosol RObotic NETwork (AERONET) observations, with large uncertainties found. But these uncertainties had small impacts on the model evaluation that was dominated by modeling bias. Through a comparison with Polarization and Directionality of the Earth's Reflectance's measurements with the Generalized Retrieval of Aerosol and Surface Properties algorithm (POLDER-GRASP), we found that the modeled AOD values were biased by −93 % to 152 %, with most models showing significant underestimations even for the state-of-the-art aerosol modeling techniques (i.e., CTRL19). By scaling up BBA emissions, the negative biases in modeled AOD were significantly mitigated, although it yielded only negligible improvements in the correlation between models and observations, and the spatial and temporal variations in AOD biases did not change much. For models in CTRL16 and CTRL19, the large diversity in modeled AOD was in almost equal measures caused by diversity in emissions, lifetime, and the mass extinction coefficient (MEC). We found that in the AeroCom ensemble, BBA lifetime correlated significantly with particle deposition (as expected) and in turn correlated strongly with precipitation. Additional analysis based on Cloud-Aerosol LIdar with Orthogonal Polarization (CALIOP) aerosol profiles suggested that the altitude of the aerosol layer in the current models was generally too low, which also contributed to the bias in modeled lifetime. Modeled MECs exhibited significant correlations with the Ångström exponent (AE, an indicator of particle size). Comparisons with the POLDER-GRASP-observed AE suggested that the models tended to overestimate the AE (underestimated particle size), indicating a possible underestimation of MECs in models. The hygroscopic growth in most models generally agreed with observations and might not explain the overall underestimation of modeled AOD. Our results imply that current global models contain biases in important aerosol processes for BBA (e.g., emissions, removal, and optical properties) that remain to be addressed in future research.

**Introduction.** Biomass burning (BB) injects large quantities of aerosols into the atmosphere every year. It is estimated that BB is responsible for 26 % to 73 % and 27 % to 41 % of global organic carbon (OC) and black carbon (BC) emissions, respectively (Bond, 2004; Andreae and Rosenfeld, 2008; Wiedinmyer et al., 2011; Wang et al., 2014; Huang et al., 2015). As a result, BB aerosol (BBA) has a considerable impact on human health and the global climate. For example, numerous studies have shown that exposure to BBA can cause cardiovascular diseases and subsequently lead to premature death (Johnston et al., 2012; Lelieveld et al., 2015).

Nature Communications, vol. 13, issue no. 1, pp. 5914, doi:10.1038/s41467-022-33680-4

# Using modelled relationships and satellite observations to attribute modelled aerosol biases over biomass burning regions

Zhong, Q., N. Schutgens, G.R. van der Werf, T. van Noije, **S.E. Bauer**[1,2], **K. Tsigaridis**[1,2], T. Mielonen, R. Checa-Garcia, D. Neubauer, Z. Kipling, A. Kirkevåg, D.J.L. Olivié, H. Kokkola, H. Matsui, P. Ginoux, T. Takemura, P. Le Sager, S. Rémy, H. Bian[3,4], and M. Chin[3], 2022

NASA Goddard Institute for Space Studies, New York, NY, USA[1]
Center for Climate Systems Research, Columbia University, New York, NY, USA[2]
NASA Goddard Space Flight Center, Greenbelt, MD, USA[3]
University of Maryland, Baltimore County (UMBC), Baltimore, MD, USA[4]

**Abstract.** Biomass burning (BB) is a major source of aerosols that remain the most uncertain components of the global radiative forcing. Current global models have great difficulty matching observed aerosol optical depth (AOD) over BB regions. A common solution to address modelled AOD biases is scaling BB emissions. Using the relationship from an ensemble of aerosol models and satellite observations, we show that the bias in aerosol modelling results primarily from incorrect lifetimes and underestimated mass extinction coefficients. In turn, these biases seem to be related to incorrect precipitation and underestimated particle sizes. We further show that boosting BB emissions to correct AOD biases over the source region causes an overestimation of AOD in the outflow from Africa by 48%, leading to a double warming effect compared with when biases are simultaneously addressed for both aforementioned factors. Such deviations are particularly concerning in a warming future with increasing emissions from fires.

**Introduction**. Biomass burning (BB) injects large amounts of aerosols into the atmosphere, which significantly affects the Earth's climate, human health, and ecosystems[1,2,3]. Recent evidence points towards an increasing trend in fires over several forest fire-dominated BB regions, such as Siberia, North America, and Australia, resulting in substantially high BB aerosol (BBA) emissions[4,5,6,7]. With human-induced climate change in the future, such an increasing trend is likely to continue in many forested regions, suggesting even stronger BBA impacts, which could lead to BB becoming a more important source of aerosol than those with a direct anthropogenic origin[8,9].

However, our current understanding of the impacts of BBA remains weak. The net radiative effect of BBA is highly uncertain ranging from strong warming to substantial cooling effects[10,11,12,13], resulting mostly from the inaccurately represented distribution and properties of clouds and BBA[14,15]. The latter uncertainty is often linked with BBA emissions, as their estimates differ by a factor of 3.8 (for organic aerosols) on a global scale with even larger mismatches on regional scales[16]. Thus, global aerosol models driven by these emissions show large diversities in simulating aerosol optical depth (AOD) for BBAs, but with underestimations by a factor of 2−5 commonly observed[17,18,19,20]. Consequently, BBA emissions are often inflated to bring modelled AOD more in line with observations[14,17,18,19,21], while other model aspects are assumed to be reasonable. This correction may mask other potential parametric and/or structural errors in models, including (but not limited to) simplified assumptions on the aerosol mixing state[22,23], missing ageing and coating mechanisms[24,25,26], incorrect particle size distribution[27], inaccurate aerosol hygroscopicity[19,28], and misrepresented removal processes[29]. However, the relative importance of these errors for total BBA errors is still unclear. A quantitative assessment of BBA errors in terms of multiple aspects would greatly contribute to better modelling of aerosols which remain the most uncertain climate forcers[30].

Journal of Advances in Modeling Earth Systems, vol. 14, issue no. 4, e2021MS002776,
doi:10.1029/2021MS002776

# LGM paleoclimate constraints inform cloud parameterizations and equilibrium climate sensitivity in CESM2

Zhu, J., B.L. Otto-Bliesner, E.C. Brady, A. Gettelman, J.T. Bacmeister, R.B. Neale, C.J. Poulsen, J.K. Shaw, **Z.S. McGraw**[1,2], and J.E. Kay, 2022

NASA Goddard Institute for Space Studies, New York, NY, USA[1]
Department of Applied Physics and Applied Mathematics, Columbia University, New York, NY, USA[2]

**Abstract.** The Community Earth System Model version 2 (CESM2) simulates a high equilibrium climate sensitivity (ECS > 5°C) and a Last Glacial Maximum (LGM) that is substantially colder than proxy temperatures. In this study, we examine the role of cloud parameterizations in simulating the LGM cooling in CESM2. Through substituting different versions of cloud schemes in the atmosphere model, we attribute the excessive LGM cooling to the new CESM2 schemes of cloud microphysics and ice nucleation. Further exploration suggests that removing an inappropriate limiter on cloud ice number (NoNimax) and decreasing the time-step size (sub-stepping) in cloud microphysics largely eliminate the excessive LGM cooling. NoNimax produces a more physically consistent treatment of mixed-phase clouds, which leads to an increase in cloud ice content and a weaker shortwave cloud feedback over mid-to-high latitudes and the Southern Hemisphere subtropics. Microphysical sub-stepping further weakens the shortwave cloud feedback. Based on NoNimax and microphysical sub-stepping, we have developed a paleo-climate calibrated CESM2 (PaleoCalibr), which simulates well the observed twentieth century warming and spatial characteristics of key cloud and climate variables. PaleoCalibr has a lower ECS (~4°C) and a 20% weaker aerosol-cloud interaction than CESM2. PaleoCalibr represents a physically more consistent treatment of cloud microphysics than CESM2 and is a valuable tool in climate change studies, especially when a large climate forcing is involved. Our study highlights the unique value of paleoclimate constraints in informing the cloud parameterizations and ultimately the future climate projection.

**Introduction.** The Community Earth System Model version 2 (CESM2) is the newest and most comprehensive model of the CESM family and is a participant in the Coupled Model Intercomparison Projects phase 6 (CMIP6; Bacmeister et al., **2020**; Danabasoglu et al., **2020**; Meehl, Arblaster, et al., **2020**). A conspicuous difference between CESM2 and its predecessor models is its high equilibrium climate sensitivity (ECS; Bacmeister et al., **2020**; Bitz et al., **2011**; Gettelman et al., **2012**, **2019**; Kiehl et al., **2006**). In the early versions of CESM (the Climate System Model version 1, the Community Climate System Model versions 2–4, and CESM1), ECS ranges from 2.0°C to 4.0°C, increasing with the model version and spanning the likely (66%) range from multiple synthesis reports (Figure **1**; Charney et al., **1979**; IPCC, **2013**; Sherwood et al., **2020**). In CESM2, ECS has risen to 5.6°C (calculated using a 1° atmosphere coupled to a slab ocean; Zhu et al., **2021**) and well beyond the likely range in different synthesis reports including the Sixth Assessment Report of the Intergovernmental Panel on Climate Change (IPCC, **2021**). These increases of ECS with CESM model versions have been attributed to increases of model resolution and improvements of physical parameterizations, in particular clouds (Bacmeister et al., **2020**; Bitz et al., **2011**; Gettelman et al., **2012**, **2019**; Kiehl et al., **2006**). Specifically, the higher ECS in CESM2, configured with the Community Atmosphere Model version 6 (CAM6), than that in CESM1 with CAM5 (hereafter CESM1) is attributed to changes in the atmospheric parameterizations of stratiform cloud microphysics, unified turbulence, ice nucleation, and convection, as well as the adjustment of aerosol-cloud interactions (ACIs) to match the twentieth century temperature record (Gettelman et al., **2019**). A high ECS similar to that of CESM2 has been reported in other CMIP6 models and similarly attributed to the simulation of cloud processes (Zelinka et al., **2020**).

## C. Chapters, Conferences, Workshops, and other Publications

1. Bergas-Massó, E., M. Gonçalves-Ageitos, S. Myriokefalitakis, **R.L. Miller**, and C. Pérez García-Pando, 2022: How does the use of different soil mineralogical atlases impact soluble iron deposition estimates? In *Air Pollution Modeling and its Application XXVIII*. C. Mensink and O. Jorba, Eds., Springer Proceedings in Complexity, Springer International, pp. 249-254, doi:10.1007/978-3-031-12786-134……190

2. Connors, S., S. Berger, C. Péan, G. Bala, N. Caud, D. Chen, T. Edwards, S. Fuzzi, T.Y. Gan, M. Gomis, E. Hawkins, R. Jones, R. Kopp, K. Leitzell, E. Lonnoy, D. Maraun, V. Masson-Delmotte, T. Maycock, A. Pirani, R. Ranasinghe, J. Rogelj, **A.C. Ruane**, S. Szopa, and P. Zhai, 2022: Climate Change 2021: Summary for All. Intergovernmental Panel on Climate Change……...191

3. Connors, S., M. Dionne, G. Hanák, R. Musulin, N. Aellen, M. Amjad, S. Bowen, D.R. Carrascal, E. Coppola, E. Dal Moro, A. Dosio, S.H. Faria, T.Y. Gan, M. Gomis, J.M. Gutiérrez, P. Hope, R. Kopp, S. Krakovska, K. Leitzell, D. Maraun, V. Masson-Delmotte, R. Matthews, T. Maycock, S. Paddam, G.-K. Plattner, A. Pui, M. Rahimi, R. Ranasinghe, J. Rogelj, **A.C. Ruane**, S. Szopa, A. Turner, R. Vautard, Y. Velichkova, A. Weigel, and X. Zhang, 2022: Climate Science: A Summary for Actuaries: What the IPCC Climate Change Report 2021 Means for the Actuarial Profession. International Actuarial Association……192

4. **Del Genio, A.D.**, 2022: Convection as a regulator of the Earth's climate. In *Studies of Cloud, Convection and Precipitation Processes Using Satellite Observations*. Z.J. Luo and G. Tselioudis, Eds., Lectures in Climate Change, vol. 3, World Scientific, pp. 3-19, doi:10.1142/9789811256912_0001……...……193

5. **Guarin, J.R.**, and S. Asseng, 2022: Improving wheat production and breeding strategies using crop models. In *Wheat Improvement: Food Security in a Changing Climate*. M.P. Reynolds and H.-J. Braun, Eds., Springer, pp. 573-591, doi:10.1007/978-3-030-90673-3_31……...194

6. Homann-Kee Tui, S., G. Sisito, E.N. Moyo, T. Dube, R.O. Valdivia, **M. Madajewicz**, K. Descheemaeker, and **A.C. Ruane**, 2022: Developing pathways for sustainable agricultural development in Zimbabwe by 2030. In *Climate Change Adaptations in Dryland Agriculture in Semi-Arid Areas*. X. Poshiwa, G. Ravindra Chary, X. Poshiwa, and G.R. Chary, Eds., Springer Singapore, pp. 185-202, doi:10.1007/978-981-16-7861-5_13……...195

7. Luo, Z.J., **G. Tselioudis**, and W.B. Rossow (Eds.), 2022: Studies of Cloud, Convection and Precipitation Processes Using Satellite Observations. Lectures in Climate Change, Vol. 3. World Scientific, doi:10.1142/12862……196

8. McClain, S., A. Kruczkiewicz, R. Ndugwa, **C.V. Braneon**, **D. Bader**, J. Bazo, and M. Owen, 2022: Building risk-informed communities: Case studies on the applications of Earth observation data. In *Earth Observation Applications and Global Policy Frameworks*. A. Kavvada, D. Cripe, and L. Friedl, Eds., Geophysical Monograph Series, American Geophysical Union, pp. 119-132……...197

9. **Naud, C.M.**, 2022: Clouds and precipitation in extratropical cyclones: A global satellite climatology for GCM evaluation. In *Studies of Cloud, Convection and Precipitation Processes Using Satellite Observations*. Z.J. Luo and G. Tselioudis, Eds., Lectures in Climate Change, vol. 3, World Scientific, pp. 289-313, doi:10.1142/9789811256912_0015……...198

10. **Rind, D.**, 2022: The "Climate Change" in "Climate Change Impacts". In *Our Warming Planet: Climate Change Impacts and Adaptation*. C. Rosenzweig, M. Parry, and M. De Mel, Eds., Lectures in Climate Change, vol. 2, World Scientific, pp. 3-27, doi:10.1142/9789811238222_0003……...199

11. **Rosenzweig, C.**, M. Parry, and **M. De Mel** (Eds.), 2022: Our Warming Planet: Climate Change Impacts and Adaptation. Lectures in Climate Change, Vol. 2. World Scientific, doi:10.1142/12312……..…200

12. **Rosenzweig, C.**, and W.D. Solecki, 2022: Conclusions and recommendations: Prospects for action. In *Climate Change and U.S. Cities: Urban Systems, Sectors, and Prospects for Action*. W.D. Solecki and C. Rosenzweig, Eds., Island Press, pp. 305-312……..201

13. **Rosenzweig, C.**, **D. Peters**, W.D. Solecki, R. Blake, K. Jacob, and B. Holland, 2022: Sustained urban climate assessment. In *Climate Change and U.S. Cities: Urban Systems, Sectors, and Prospects for Action*. W.D. Solecki and C. Rosenzweig, Eds., Island Press, pp. 261-304……...202

14. **Rosenzweig, C.**, 2022: Cities and climate change. In *Our Warming Planet: Climate Change Impacts and Adaptation*, Lectures in Climate Change, vol. 2, World Scientific, pp. 294-317, doi:10.1142/9789811238222_0014……..203

15. **Rosenzweig, C.**, 2022: Martin Parry: Setting the course of climate change impacts and adaptation research. In *Our Warming Planet: Climate Change Impacts and Adaptation*. C. Rosenzweig, M. Parry, and M. De Mel, Eds., Lectures in Climate Change, vol. 2, World Scientific, pp. xv-xxii, doi:10.1142/9789811238222_0001……...204

16. Sillmann, J., I. Christensen, S. Hochrainer-Stigler, J. Huang-Lachmann, S. Juhola, K. Kornhuber, M. Mahecha, R. Mechler, M. Reichstein, **A.C. Ruane**, P. Schweizer, and S. Williams, 2022: ISC-UNDRR-RISK KAN Briefing Note on Systemic Risk. International Science Council, doi:10.24948/2022.01……..205

17. Solecki, W.D. and **C. Rosenzweig** (Eds.), 2022: Climate Change and U.S. Cities: Urban Systems, Sectors, and Prospects for Action. Island Press…….…..206

18. Solecki, W.D., **C. Rosenzweig**, R. Horton, and A. de Sherbinin, 2022: Introduction: Cities and climate change connections. In *Climate Change and U.S. Cities: Urban Systems, Sectors, and Prospects for Action*. W.D. Solecki and C. Rosenzweig, Eds., Island Press, pp. 1-14…….207

19. **Tselioudis, G.**, 2022: Use of satellite observations in climate model evaluation of clouds: A time history based on the NASA/GISS model. In *Studies of Cloud, Convection and Precipitation Processes Using Satellite Observations*. Z.J. Luo and G. Tselioudis, Eds., Lectures in Climate Change, vol. 3, World Scientific, pp. 247-262, doi:10.1142/9789811256912_0013……...208

20. **Zhang, Y.**, W.B. Rossow, **A.A. Lacis**, and **V. Oinas**, 2022: Calculation, evaluation and application of long-term, global radiative flux datasets at ISCCP: Past and present. In *Studies of Cloud, Convection and Precipitation Processes Using Satellite Observations*. Z.J. Luo and G. Tselioudis, Eds., Lectures in Climate Change, vol. 3, World Scientific, pp. 151-171, doi:10.1142/9789811256912_0009…….209

Springer International, pp. 249-254, doi:10.1007/978-3-031-12786-1_34

# How Does the Use of Different Soil Mineralogical Atlases Impact Soluble Iron Deposition Estimates?

Bergas-Massó, E., M. Gonçalves-Ageitos, S. Myriokefalitakis, **R.L. Miller**[1], and C. Pérez García-Pando, 2022

NASA Goddard Institute for Space Studies, New York, NY, USA[1]

**Abstract.** Atmospheric deposition is the primary input of soluble iron (Fe) in remote regions of the open ocean. Fe constitutes a fundamental micro-nutrient for marine biota, affecting biogeochemical cycles and ultimately carbon uptake. Fe is emitted to the atmosphere primarily from dust sources. Fe solubility at emission is origin-dependent, being mostly insoluble when associated with dust minerals. Earth System Models (ESMs) commonly assume that dust aerosols have a globally uniform composition, neglecting known regional variations in soil mineralogy. This work assesses the implications of soil composition uncertainties on the bio-available Fe delivery to the ocean by using a state-of-the-art ESM with a detailed atmospheric Fe cycle (EC-Earth3-Iron). We run two 1-year simulations considering two different Soil Mineralogy Atlases (SMAs). Our results reveal a non-negligible impact of soil mineralogy uncertainties on soluble Fe estimates. By only changing the source of information for the soil composition and updating the Fe content in minerals, we find differences of 31.5% in mineral Fe emissions and 26.7% in soluble Fe deposition budgets.

**Introduction**. Soluble Fe acts as an essential micronutrient for marine biota, limiting phytoplankton growth in some regions of the open ocean (i.e., High Nutrient Low-Chlorophyll regions). Ocean productivity and hence $CO_2$ uptake by the ocean relies on the availability of limiting nutrients. Therefore, quantifying soluble Fe deposition over the ocean is key to estimate ocean primary productivity and ultimately carbon uptake. Atmospheric mineral dust is the dominant source of Fe deposited over the open ocean. The interaction of airborne mineral dust with the Earth system depends on the mineralogical dust composition itself, particle size distribution (PSD), or its shape, among other characteristics. Hence, the Fe in dust and its ability to dissolve is influenced by dust mineralogy. However, Earth System Models (ESMs) usually consider dust as globally uniform, disregarding the known diversity in the sources' mineralogical composition. In particular, Fe abundance in soils is generally set to a constant ~3.5% [1], and its solubility is considered to be around 0.1% [2].

Although Fe solubility at emission is low, observations suggest that solubility is boosted downwind of the sources [3] as a result of different atmospheric chemistry processes. A primary Fe solubilization mechanism is the acidic (proton-promoted) dissolution, as at low pH values, the Fe-O bonds of iron oxides weaken, favoring its dissolution [4]. Other pathways to soluble Fe production are organic ligand (e.g., oxalate) processing [5] and photo-reductive processes. Constraining the dust mineralogical composition in models presents challenges. Soil mineralogy maps are generated by extrapolating a limited number of mineralogical analyses of soil samples, which are particularly rare in arid and semi-arid regions. Furthermore, those mineralogical analyses use the wet sieving technique, which tampers the soil size distribution by breaking coarse particles, making it hard to estimate mineral-dependent PSD at emission.

Moreover, the Fe content in some clay minerals can be highly variable depending on their origin: primary mineral characteristics and chemical weathering processes [6]. This work assesses the impacts of soil mineralogy uncertainties on soluble Fe deposition over the open ocean using a state-of-the-art ESM, EC-Earth3-Iron [7]. This model includes a detailed atmospheric Fe cycle and the ability to use two different soil mineralogy data sets [8] [9].

# Climate Change 2021: Summary for All

Connors, S., S. Berger, C. Péan, G. Bala, N. Caud, D. Chen, T. Edwards, S. Fuzzi, T.Y. Gan, M. Gomis, E. Hawkins, R. Jones, R. Kopp, K. Leitzell, E. Lonnoy, D. Maraun, V. Masson-Delmotte, T. Maycock, A. Pirani, R. Ranasinghe, J. Rogelj, **A.C. Ruane**[1,2], S. Szopa, and P. Zhai, 2022

NASA Goddard Institute for Space Studies, New York, NY, USA[1]
Center for Climate Systems Research, Columbia University, New York, NY, USA[2]

**Weather, Climate and the IPCC**. No matter where we live, we all experience weather: how the conditions of our atmosphere change over minutes, hours, days, weeks. We also all experience climate: the weather of a place averaged over several decades. Climate change is when these averaged conditions start to change, and its causes can be either natural or caused by human activities. Rising temperatures, variations in rainfall, increased extreme weather events are all examples of climate changes, but there are many others.

Back in 1990, the first report by the Intergovernmental Panel on Climate Change (IPCC) concluded that human-caused climate change would soon become apparent but could not yet confirm that it was already happening. Now, some 30 years later, the evidence is overwhelming that human activities have changed the climate.

Hundreds of scientists from all over the world come together to produce IPCC reports. They base their conclusions on several kinds of scientific evidence, including:

• Measurements or observations, sometimes spanning more than a century back in time
• Paleo (very old) climate evidence from thousands or millions of years ago (for example: tree rings, rock or ice cores)
• Computer models that look at past, current and future changes (see box *What are climate models?* on page 9)
• Understanding of how the climate works (physical, chemical and biological processes)

Since the IPCC first started, we now have much more data and better climate models. We understand more now about how the atmosphere interacts with the ocean, ice, snow, ecosystems and land of the Earth. Computer climate simulations have considerably improved and now provide past change and future projections that are much more detailed. Plus, we have now had decades more greenhouse gas emissions, making the effects of climate change more apparent (see box *What are greenhouse gases?* on page 6). As a result, the latest IPCC report is able to confirm and strengthen the conclusions from previous reports.

### What's covered in this summary?

• Climate Change Today: what changes have already occurred and how we know humans are responsible.
• Our Future Climate: what changes could happen in the future depending on the actions we take.
• Limiting Future Climate Change: what is required to stop global temperature from continuing to rise.

International Actuarial Association (IAA) and the Working Group I Technical Support Unit of the Intergovernmental Panel on Climate Change (IPCC)

# Climate Science: A Summary for Actuaries: What the IPCC Climate Change Report 2021 Means for the Actuarial Profession

Connors, S., M. Dionne, G. Hanák, R. Musulin, N. Aellen, M. Amjad, S. Bowen, D.R. Carrascal, E. Coppola, E. Dal Moro, A. Dosio, S.H. Faria, T.Y. Gan, M. Gomis, J.M. Gutiérrez, P. Hope, R. Kopp, S. Krakovska, K. Leitzell, D. Maraun, V. Masson-Delmotte, R. Matthews, T. Maycock, S. Paddam, G.-K. Plattner, A. Pui, M. Rahimi, R. Ranasinghe, J. Rogelj, **A.C. Ruane**[1,2], S. Szopa, A. Turner, R. Vautard, Y. Velichkova, A. Weigel, and X. Zhang, 2022

NASA Goddard Institute for Space Studies, New York, NY, USA[1]
Center for Climate Systems Research, Columbia University, New York, NY, USA[2]

**Introduction.** This Summary, based on the IPCC Sixth Assessment Report, is tailored to the actuarial community. It has been co-developed by the authors of the IPCC report and a team of actuaries and catastrophe experts from the IAA. The scientific data and conclusions are attributed alone to the IPCC, while the need for emphasis on some risks, and the comments about actuarial practices have been provided by the IAA team.

The Intergovernmental Panel on Climate Change (IPCC) is the United Nations body for assessing the science related to climate change. Now in its sixth assessment cycle, the IPCC comprises three Working Groups. The Working Group I (WGI) contribution to the Sixth Assessment Report (AR6) addresses the physical understanding of the climate system and climate change. It brings together the latest advances in climate science and combines multiple lines of evidence from observations, paleoclimate, process understanding and global and regional climate simulations to get the clearest picture of past, present and possible future climate. Released in August 2021, the report is based on the research of thousands of scientists worldwide from more than 14,000 scientific studies. A team of more than 234 scientists from 65 countries worked together for over three years to deliver the report. The WGI Sixth Assessment Report key findings include:

• For decades, we have known that the world is warming. Recent changes in the climate are widespread, rapid, and intensifying. They are unprecedented in thousands of years.

• It is indisputable that human activities are causing climate change. Human influence is making extreme climate events, including heatwaves, heavy rainfall, and droughts,
more frequent and severe.

• Climate change is already affecting every region on Earth, in multiple ways. Its effects will increase with further warming.

• There is no going back from some changes in the climate system. However, some of these changes could be slowed and others could be stopped by limiting future warming.

• Unless there are immediate, rapid, and large-scale reductions in greenhouse gas emissions, limiting global warming to 1.5°C or even 2°C relative to 1850–1900 (pre- industrial levels) will not be possible.

• To limit global warming, strong, rapid, and sustained reductions in emissions of carbon dioxide, methane, and other greenhouse gases are necessary. This would not only reduce the consequences of climate change but also improve air quality.

Studies of Cloud, Convection and Precipitation Processes Using Satellite Observations. Z.J. Luo and G. Tselioudis, Eds., Lectures in Climate Change, vol. 3, World Scientific, pp. 3-19, doi:10.1142/9789811256912_0001

# Convection as a regulator of the Earth's climate

**Del Genio, A.**[1], 2022

NASA Goddard Institute for Space Studies, New York, NY, USA[1]

**Introduction.** Bill began his career as a planetary scientist, creating one of the first general circulation models (GCMs) to represent the strong greenhouse effect and circulation of the thick CO2 atmosphere of Venus. Bill's seminal paper on the time scales of cloud microphysical source and sink processes and how they can be used to understand clouds on a variety of Solar System planets (Rossow, 1978) introduced that community to the physics in clouds and it is still used today by scientists trying to characterize the atmospheres of planets outside our Solar System.

Bill then shifted his focus to climate science, a field that was just beginning to struggle with the idea that clouds play an important role in climate change. Bill entered the field fairly early in the history of satellite remote sensing, a time when satellite data consisted almost exclusively of images or global maps. As the leader of the International Satellite Cloud Climatology Project (ISCCP), Bill revolutionized the field of remote sensing by retrieving systematic, quantitative information about clouds from operational weather satellite datasets that were not designed with that purpose in mind (Rossow and Schiffer, 1991). This was the first comprehensive estimate of the fraction of the Earth covered by clouds, using different approaches that helped quantify uncertainties and gave users data options to make their own decisions on what to include or exclude. In retrospect, one of the more important contributions of ISCCP was its retrievals of cloud optical thickness and top pressure. In the ISCCP dataset, these are available in compact form in mesoscale joint-histograms of frequencies of occurrence of different ranges of optical thickness and top pressure. These histograms are of considerable utility in objectively identifying the cloud morphological types long used by surface weather observers (Hahn et al., 2001).

An objective analysis of the ISCCP histograms defines a set of six tropical "weather states" (WSs) (Rossow et al., 2005) and 11 global WSs (Tselioudis et al., 2013). Three of these states identify convective clouds in their various realizations — shallow fair-weather cumulus that is most prevalent over the subtropical oceans but also in the equatorial regions when they are unusually dry; isolated convective cells with tops from mid-levels to the deep troposphere that occur in warm humid regions of the tropics when the atmosphere is beginning to moisten from previously dry conditions; and organized heavily precipitating mesoscale convective systems that occur under the wettest atmospheric conditions. These clouds are essential to many aspects of the Earth's climate and projected future climate change. We describe some of these below.

Clouds are integral to the Earth's global energy budget at the top of the atmosphere, at the surface, and within the atmosphere (Slide 2). At the top of the atmosphere, approximately 2/3 of the Earth's ~0.3 planetary albedo is due to the reflection of sunlight by clouds, and outgoing thermal (heat) radiation to space is reduced by ~10% due to the greenhouse effect of clouds. A significant fraction of both these effects is due to convective clouds. Convective clouds are central to the Earth's global water cycle as well (Slide 3). Water evaporated from the oceans is carried upward into the free troposphere by shallow cumulus clouds. This allows the general circulation to transport it to other parts of the globe, including continental regions where some of it is delivered to the land surface as precipitation, often by convective storms. In heavily precipitating parts of the world, deep convective storms deliver more precipitation to the ocean than is evaporated by the ocean, freshening (i.e., reducing the salinity of) the ocean and affecting its density, helping to drive its circulation. These regional variations in ocean salinity driven by convection are clearly detectable in satellite data.

Wheat Improvement: Food Security in a Changing Climate. M.P. Reynolds and H.-J. Braun, Eds., Springer, pp. 573-591, doi:10.1007/978-3-030-90673-3_31

# Improving wheat production and breeding strategies using crop models

**Guarin, J.R.**[1,2,3], and S. Asseng, 2022

NASA Goddard Institute for Space Studies, New York, NY, USA[1]
Center for Climate Systems Research, Columbia University, New York, NY, USA[2]
Department of Agricultural and Biological Engineering, University of Florida, Gainesville, FL, USA[3]

**Abstract.** Crop simulation models are robust tools that enable users to better understand crop growth and development in various agronomic systems for improved decision making regarding agricultural productivity, environmental sustainability, and breeding. Crop models can simulate many agronomic treatments across a wide range of spatial and temporal scales, allowing for improved agricultural management practices, climate change impact assessment, and development of breeding strategies. This chapter examines current applications of wheat crop models and explores the benefits from model improvement and future trends, such as integration of G × E × M and genotype-to-phenotype interactions into modeling processes, to improve wheat (Triticum spp.) production and adaptation strategies for agronomists, breeders, farmers, and policymakers.

**Introduction.** The global demand for food is continuously increasing due to the growing population and agricultural production strategies must continue to improve to ensure future global food security (see Chap. 4). Wheat (*Triticum* spp.) is the most important food crop in the world due to its high nutrition content contributing to approximately 20% of calories and protein in the human diet [1]. This chapter discusses potential agricultural strategies for improving wheat production by using crop simulation models as instruments for adaptation. Crop simulation models are computational tools used to determine crop growth and development using quantitative knowledge and input data from agronomic systems. Crop models produce dynamic simulations of crop phenology and growth based on the combined principles of crop physiology, soil science, and agrometeorology. Most crop models use daily maximum and minimum temperature, rainfall, solar radiation, atmospheric $CO_2$ concentration, soil attributes, cultivar characteristics, and crop management as inputs to simulate crop phenological development, biomass and yield accumulation, water use, and nutrient uptake.

Wheat crop modeling emerged in the 1980s based on the computational integration of mathematical relationships between environmental interactions and wheat growth developed in the 1960s and 1970s. In the 1990s, models began merging into crop modeling platforms, i.e., software that combines multiple models of various crops to facilitate evaluation and application for users [2]. Over the past decades, individual crop models and crop modeling platforms have received many technological and functional improvements which has promoted the development of new modeling approaches and new models. Currently, there are more than 30 wheat crop models used by modeling groups across the world [3]. These present-day crop models have progressed to become helpful tools in understanding how crops develop, grow, and yield in various agricultural scenarios which makes them advantageous for projecting how internal (e.g., genes, traits) and external (e.g., climate, crop management) factors impact crop production [4]. Thus, crop models are often integrated into new agricultural research activities, such as the improvement of breeding strategies. However, as knowledge and understanding of agricultural systems increases, model improvement is necessary to address the new challenges that arise when simulating complex agricultural systems interactions.

This chapter outlines the benefits and limitations of current wheat crop models for applications of wheat production regarding environmental sustainability, climate change, and breeding.

Climate Change Adaptations in Dryland Agriculture in Semi-Arid Areas. X. Poshiwa, G. Ravindra Chary, X. Poshiwa, and G.R. Chary, Eds., Springer Singapore, pp. 185-202, doi:10.1007/978-981-16-7861-5_13

# Developing pathways for sustainable agricultural development in Zimbabwe by 2030

Homann-Kee Tui, S., G. Sisito, E.N. Moyo, T. Dube, R.O. Valdivia, M. Madajewicz, K. Descheemaeker, and **A.C. Ruane**[1], 2022

NASA Goddard Institute for Space Studies, New York, NY, USA[1]

**Abstract.** Agricultural production systems in Zimbabwe are facing high intensity of climate change impacts. Stakeholders require actionable information to direct investments towards a climate resilient future. The Agricultural Model Inter-comparison and Improvement Project, Climate Change Adaptation and Resilience (AgMIP CLARE) uses an integrated multi-modeling approach to support policy-level decision making and priority setting for sustainable development and climate adaptation with the goal of improving farmers' livelihoods, food and nutrition security and gender equity. The Zimbabwe Vision 2030 was used to co-develop, with stakeholders' and experts, plausible future scenarios of the agricultural sector in Zimbabwe. For systems like in Nkayi district, the simulation results illustrate that investing in a sustainable future, yields more favourable outcomes than investing in 'high emission' economic growth: pro-active diversification and intensification of small (traditional) grains and legumes and integration with livestock, supported by inclusive, functional value chains and access to information leads to higher returns per unit land on farm. Policies and interventions that promote a switch to more legumes in the farming system and make the uptake of productivity enhancing technologies more attractive, achieve greater food and nutrition security and increase social and economic equity, offset the impacts of climate change and improve farmers livelihoods. Importantly, to make effective investments there is need to create incentives for all farmers to invest; under a sustainable future, vulnerability is less and the poorest benefit more. Deciding for one future helps prioritizing what it would take in terms of policies and investments to achieve the vision 2030. Testing technologies and adaptations under different possible futures, integrating socio-economic and agroecological dimensions across different scales, simulation experiments help stakeholders and experts to design and evaluate policies aimed at meeting sustainable development, climate and food security goals.

It is well known that drylands represent more than a third of the world’s land mass, 90% of which are in developing countries and rely mainly on degrading agricultural lands for their livelihoods. In fact, there are pronounced differences within drylands, particularly in terms of water availability, poverty, stage of development and sustainable intensification options.

Sadly, dryland farmers face multiple constraints due to poor soil, short growing seasons, low and uncertain rainfall, desertification and recurrent droughts along with poorer infrastructure and market access that affect their abilities to overcome chronic poverty and food insecurity.

Climate change and agriculture are interrelated processes that take place at a global scale. Climate change-related phenomena, such as changes in average temperatures, rainfall and climate extremes (like heat waves), and changes in atmospheric carbon dioxide-level and ground-level ozone concentrations, affect farming in several ways. Climate change is already affecting “dryland agriculture” with effects unevenly distributed across the globe. Higher temperatures eventually reduce the length of growing seasons and force large regions of marginal agriculture out of production, while encouraging weeds and pest proliferation. Also, heat waves cause lower yields of the crop and wilted growth in plants. In simple words, the overall impacts of climate change are expected to be significantly negative as it threatens the global food security.

Lectures in Climate Change, Vol. 3. World Scientific, doi:10.1142/12862

# Studies of Cloud, Convection and Precipitation Processes Using Satellite Observations

Luo, Z.J., **G. Tselioudis**[1], and W.B. Rossow (Eds.), 2022

NASA Goddard Institute for Space Studies, New York, NY, USA[1]

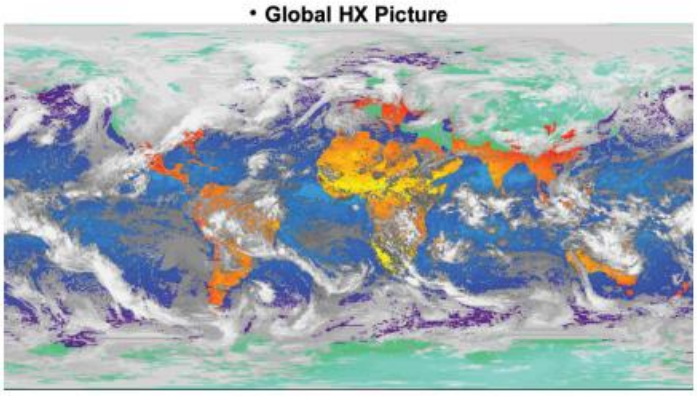
**Abstract.** Clouds, convection and precipitation processes are central components of Earth's weather and climate. They are produced by atmospheric motions across a very wide range of space-time scales from local weather to long-term global climate variation. They feedback on these motions by perturbing the heating/cooling that drive the atmospheric circulation. These processes also perturb the oceanic circulation and land surface properties that affect the atmospheric circulation.

Because of the coupling of the atmosphere-ocean-land system across all scales by cloud, convection and precipitation processes, studying their behaviors requires measurements in space-time variations across all these scales simultaneously. Satellite constellations with global coverage and high time resolution offer the ideal platforms for such observations. This book summarizes some of the latest research using combinations of various satellite observations to study these processes and to evaluate their representations in global weather and climate models.

Included with this publication are downloadable electronic slides and accompanying notes of each lecture for students, teachers, and public speakers around the world to be better able to understand cloud, convection and precipitation processes.

**Introduction.** The ceaseless circulations of the Earth's atmosphere are comprised of motions on all space time scales ranging from three-dimensional dissipating turbulence (meters, minutes) up to global, multi-decadal scales, where the larger and most energetic scales of the general circulations are recognizable in the form of prevailing winds and currents, distinct streams and waves, and storm systems and eddies. The atmospheric and oceanic circulations are driven by and coupled by imbalances in heating-cooling by solar and thermal radiation and by water phase changes (as well as direct sensible heat exchanges at the surface), but they also transport energy and water, forming a complex system of feedbacks that is the central component of the Earth's climate system.

The presence of heating-cooling imbalances over the whole range of scales means that circulation-induced processes are transient, not static — the time derivative is of significant magnitude and cannot be neglected in an analysis of processes. The most important circulation-induced processes are cloud and precipitation formation because they significantly perturb the radiation and latent heating-cooling of the atmosphere and ocean. These perturbations are, in turn, major feedbacks on the atmospheric and oceanic circulations that produce the clouds and precipitation.



Earth Observation Applications and Global Policy Frameworks. A. Kavvada, D. Cripe, and L. Friedl, Eds., Geophysical Monograph Series, American Geophysical Union, pp. 119-132

# Building risk-informed communities: Case studies on the applications of Earth observation data

McClain, S.[1,2], A. Kruczkiewicz, R. Ndugwa, **C. Braneon**[2,3], **D. Bader**[1,5], J. Bazo, and M. Owen, 2022

NASA Headquarters, Washington, D.C., USA[1]
American Association for the Advancement of Science, Washington, D.C., USA[2]
NASA Goddard Institute for Space Studies, New York, NY, USA[3]
SciSpace, LLC., New York, NY, USA[4]
Center for Climate Systems Research, Columbia University, New York, USA[5]

**Abstract.** Disaster risk is configured over time through complex climate interactions and development processes that generate conditions of hazard, vulnerability, and exposure. Unplanned urban expansion places communities at increased risk of human and economic loss from disasters. Limited examples exist of communities that have procedures for urban growth that incorporate disaster risk management into planning and development. Though global frameworks exist to provide guidance on how to mainstream disaster risk into urban settings, gaps remain in how to visualize and understand risk systemically and in transboundary and changing contexts. One method for addressing these gaps is through the use of Earth observation data products and tools, which can enhance knowledge of changing environments and the fundamental forces that drive vulnerability and exposure. This chapter considers two case studies on climate and disaster risk reduction in growing urban settings, where the applications of Earth observation data offer opportunities for building risk-informed systems. Integrating new methodologies such as these can improve the landscape of future urbanization toward more inclusive approaches for climate and disaster risk management.

**Introduction.** Building resilience through disaster risk reduction is often a key priority of governments, businesses, and the international community. This is attributable not only to the acceleration in the number and intensity of disasters, but also to the increasing exposure and vulnerability of communities, particularly those living in growing informal settlements and urban areas (Peel & Fisher, 2017). While public attention is often focused on the large or extreme events, many disasters remain less visible, including extreme temperatures and droughts, flash and coastal floods, and landslides and subsidence, but have extensive impacts on urban growth and development, and on lives and livelihoods. Notably, the European heat wave in the summer of 2003 led to approximately 70,000 excess deaths across Europe (Robine et al., 2008). Slightly more than half of the world's population is currently living in urban areas, a number that is expected to rise to 60% by 2030 (Brenner & Schmidt, 2014; UN DESA, 2014). Around 90% of growth in urban areas will occur in low-income countries (UN DESA, 2014).

The primary factor contributing to these trends is neither fertility nor age structure, but migration (UN Habitat,2016a). Unplanned urban expansion influenced by the quality of urban management practices places communities at increased risk of human and economic loss from disasters. Urban poor that live in peri-urban areas and in informal settlements are particularly vulnerable to disasters due to the development of insecure shelters in high-risk areas. (Peri-urban areas are transition spaces with some degree of intermingling of both urban and rural uses and are located on the fringe of heavily developed cities, often comprising a scattered pattern of low-density concentrations near transportation hubs (Wandl & Magoni, 2016). This is exacerbated by limited access to basic and emergency services, and an overall lack of resilience (Dickson et al., 2012).

Disaster risk is configured over time through complex climate interactions between development processes that generate conditions of hazard, vulnerability, and exposure. City governments are constrained by a lack of up-to-date, comprehensive information about hazard and exposure in urban areas, and there exist limited examples of cities that have standardized procedures for incorporating disaster risk management into city planning (Dickson et al., **2012**).

Studies of Cloud, Convection and Precipitation Processes Using Satellite Observations. Z.J. Luo and G. Tselioudis, Eds., Lectures in Climate Change, vol. 3, World Scientific, pp. 289-313, doi:10.1142/9789811256912_0015

# Clouds and precipitation in extratropical cyclones: A global satellite climatology for GCM evaluation

**Naud, C.**[1,2], 2022

NASA Goddard Institute for Space Studies, New York, NY, USA[1]
Center for Climate Systems Research, Columbia University, New York, NY, USA[2]

**Introduction.** The space race of the 1960s brought a new tool to meteorologists and climatologists: satellite-based observations of the Earth. With the advent of the Nimbus missions, the Earth could be observed globally and regularly. A new vantage point became available to observe clouds and other atmospheric components. Meteorologists could now follow weather systems, thanks to the strong contrast between bright clouds and the dark ocean surface in visible imagery and the strong link between the atmosphere dynamics and the condensation of water. Rapidly, methods emerged on how best to exploit the satellite imagery to obtain more detailed information on the clouds and continuously improve weather predictions. In parallel, climatological questions such as the impact of clouds on the global climate could be tackled finally, given the globally uniform view satellites offer. With this in mind, the International Satellite Cloud Climatology Project (ISCCP) was born; using multiple platforms that at any given time observe a significant portion of the planet, and by applying the same set of rules on similar measurements these platforms make, a global, 3-hourly, gridded dataset of cloud top pressure and optical depth was created by Robert Schiffer and William Rossow (Schiffer and Rossow, 1983). This was to be the first comprehensive, coherent (i.e., calibrated and normalized) and publicly accessible dataset specifically targeting cloud properties. It now spans four decades and has been used by thousands of researchers around the world. In its wake, more global climatologies have emerged, either based on different types of measurements or other atmospheric components, such as global datasets of precipitation, water vapor amounts, or aerosols.

The impact this influential dataset has had on current research is tremendous, but here we focus specifically on what this has implied for the interrelation between clouds and atmospheric dynamics. The choice of cloud top pressure and optical depth in the ISCCP was deliberate because these two parameters can uniquely inform on the atmospheric state. Inversely, specific weather phenomena have their own signature in the cloud fields, and such have extratropical cyclones in the mid-latitudes (Tselioudis et al., 2000).

**So Why Focus on Extratropical Cyclones?** Precipitation in the mid-latitudes depends strongly on the occurrence of extratropical cyclones. In the northern hemisphere, about 80% of the winter precipitation occurs in extra- tropical cyclones (Hawcroft et al., 2012). Furthermore, in the United States, between 41% and 99% of the extreme precipitation events in the southeastern and northwestern states, respectively, are caused by either extratropical cyclones or their associated fronts (Kunkel et al., 2012). Therefore, it is paramount to understand the dynamics of these systems and also the processes that lead to precipitation and its potentially devastating effects.
From a climatological standpoint, extratropical cyclones have a major regulating role, in terms of transferring energy and heat from the Equator to the pole and also through their radiative impact (Tselioudis et al., 2000). Overall, they have a cooling effect (Polly and Rossow, 2016) of a magnitude that depends on their strength (Tselioudis and Rossow, 2006).

In a warming climate, the Equator-to-pole gradient is expected to decrease, lowering baroclinicity and the formation of cyclones. Therefore, a warming should entail a smaller number of cyclones. Coincidently, a warmer climate means a moister climate, which would imply greater precipitation in cyclones, resulting in greater latent heat release that would enhance the cyclones' intensity. However, past studies of the changes in extratropical cyclones give conflicting results — some studies find increases and other decreases in the number of cyclones, depending on the period considered (Feser et al., 2015).

Our Warming Planet: Climate Change Impacts and Adaptation. C. Rosenzweig, M. Parry, and M. De Mel, Eds., Lectures in Climate Change, vol. 2, World Scientific, pp. 3-27, doi:10.1142/9789811238222_0003

# The "Climate Change" in "Climate Change Impacts"

**Rind**, **D.**[1], 2022

NASA Goddard Institute for Space Studies, New York, NY, USA[1]

**Abstract.** This book is concerned with the impacts of climate change and the mitigation and adaptation measures that can be undertaken to ameliorate them. The purpose of this Introduction is to discuss what "climate change" we are really talking about, how well we know what climate change will be like, and when we will know more about how climate will progress in the future.

**Aim and Scope**. Climate change is a portending issue not only for our time, but indeed for generations to come. Informing current and future leaders regarding this issue is a vital task, so that they harbor the knowledge to devise and implement the actions that are required to forestall its consequences. Those actions must be directed towards curtailing the emissions of greenhouse gases to the greatest extent possible, and towards adapting to unavoidable changes of climate.

In recent decades, leading scientists have made significant progress developing and communicating the science of climate change to the scientific community at large and to students in particular, thus motivating many to confront the challenges ahead. The present series, entitled Lectures in Climate Change, is aimed to contribute to that vital endeavor. Each installment in this series will be compiled by colleagues and students of one of several leading scientists who have made particularly significant contributions.

The goal of this series is to provide resources that can be used by scholars and students worldwide concerning topics related to climate change. Released in both print and online versions, the lectures in this series are targeted at university-level educators and their students across the globe to aid in teaching these particular topics. The series would provide the materials necessary for online learning by individuals seeking to gain a deeper understanding of relevant topics. The lecture presentations with their accompanying written introductions and notes are peer reviewed.

The first installment in this series is entitled Our Warming Planet: Topics in Climate Change, highlighting the significant contributions that Dr. David Rind had made to climate change science throughout his career. Colleagues of Dr. Rind are each providing an introduction, a lecture in the form of slides, and accompanying lecture notes to the volume. Further volumes in the series will honor other outstanding scientists by enlisting their colleagues and students in similar endeavors.

The second installment in this series is entitled Our Warming Planet: Climate Change Impacts and Adaptation, highlighting the significant contributions that Dr. Martin Parry has made to climate change impacts and adaptation research throughout his career. Colleagues of Dr. Parry, all world-recognised leading scientists, provided a unique set of authoritative lectures on climate change impacts and adaptation.

Lectures in Climate Change, Vol. 2. World Scientific, doi:10.1142/12312

# Our Warming Planet: Climate Change Impacts and Adaptation

**Rosenzweig**, **C.**[1,2]**,** M. Parry, **and M. De Mel**[1,2], 2022

NASA Goddard Institute for Space Studies, New York, NY, USA[1]
Center for Climate Systems Research, Columbia University, New York, NY, USA[2]

**Abstract.** This volume, the second in the Lectures in Climate Change series, covers the full array of climate impacts and adaptation measures. It has been brought together by friends and colleagues of Dr Martin Parry, Co-Chair of the Intergovernmental Panel on Climate Change (IPCC) 2007 assessment on impacts and adaptation. The writers are experts in this field and have been lead authors in many of the IPCC assessments and other major publications.

Lectures in Climate Change is a unique combination of written text plus electronic slides that together comprise an informative and up-to-date set of presentations. This second volume, entitled "Our Warming Planet: Climate Change Impacts and Adaptation", covers areas of climate impacts related to climate science, methods and approaches, sectors, regional and national studies, and policy and practice.

The volume comprises topics such as current and future challenges of climate change, global assessments, downscaling, community-based adaptation, impacts on biodiversity, food systems, water resources, and cities. Research from across the world is presented on making science actionable through assessments, early warning and early action, communicating climate risk, documenting the uptake of adaptation on the global front, and transformation towards systemic resilience.

Included with this publication are downloadable electronic slides and accompanying notes of each lecture for students, teachers, and public speakers around the world to be better able to understand and present climate change impacts and adaptation.

**Climate Lecture 1**. Explaining Climate. It all begins with the Sun. The global-mean solar illumination of the Earth has been determined to be about 340 W/m2 of which about 100 W/m2 is reflected back to space. Hence, the Earth absorbs a global annual-mean 240 W/m2 of solar energy. This amount of energy is just sufficient to support a global-mean temperature of 255 K. However, the global-mean surface temperature of the Earth is known to be about 288 K, which implies that the Planck emission from the ground surface must be about 390 W/m2. It is this 'missing energy' circumstance that led Joseph Fourier to conclude back in 1824 that there must be an atmospheric greenhouse effect causing thermal heat energy to be radiated downward from the atmosphere in order to supply the additional heat energy needed at the ground surface. This is because in the absence of the greenhouse effect, 240 W/m2 of absorbed solar energy is not sufficient to sustain a surface temperature of 288 K.

Climate Change and U.S. Cities: Urban Systems, Sectors, and Prospects for Action. W.D. Solecki and C. Rosenzweig, Eds., Island Press, pp. 305-312

# Conclusions and recommendations: Prospects for action

**Rosenzweig**, **C.**[1], and W.D. Solecki, 2022

NASA Goddard Institute for Space Studies, New York, NY, USA[1]

**Abstract.** The objective of this book is to provide a state-of-the-art assessment of how climate change is impacting U.S. cities and will become even more impactful in the future. The focus is assessing recent literature on infrastructure and population vulnerability, and ongoing and emerging adaptation planning strategies. Urban climate risk assessment embedded in this book is made up of several critical aspects including how (1) fundamental connections between urban systems and the climate system and the associated climate risks and hazards are defined; (2) these interactions manifest as impacts, vulnerabilities, and adaptations a1nong the key urban sectors and services which enable cities and their residents to thrive; (3) socio-political factors mediate the ability of cities to manage and respond to the opportunities and challenges of climate change in the context of adaptation planning; and (4) a sustained urban climate change assessment process can be undertaken for cities in the United States. Several specific conclusions and recommendations are drawn from the assessment.

**6.1. Urban Systems and Climate System Interactions.** U.S. cities are both significant drivers of climate change and sites where climate change already is having an impact. Evidence exists that the urban areas of the United States are currently being affected by climate change, but the nature and magnitude of these impacts vary. The amount of future impact will differ, depending on location and time. Urban systems and sectors currently under stress are likely to become more stressed due to climate change. For example, water supply for urban areas in the west, currently under stress, will become even more stressed, causing chronic water shortages. Coastal cities of the eastern seaboard already exposed to extreme coastal storms will become more exposed to coastal flooding due to sea level rise and potentially more frequent intense storms.

Urbanization in the United States is an ongoing and dynamic process. Increasing settlement in risk-exposed sites, spatial income inequalities, and aging infrastructure present additional challenges to urban climate change response and adaptation. The overall level of climate change impact and vulnerability vary due to a range of factors. Patterns of urbanization and local climate risk can interact. The variability in size, density, configuration and environmental context of cities sets in motion a broad range of potential impacts and vulnerabilities. Even modest global-scale changes cause local extremes resulting from non-linear impacts. For example, even relatively modest climate change shifts, such as accelerated rates of sea level rise, can result in large scale increased coastal flooding from a storm event.

**6.2. Urban Sectors and Services – Impacts, Vulnerability, and Adaptation**. Climate change is not an isolated phenomenon; its impacts are embedded in other ongoing stresses present within urban sectors and basic services. It is also clear that the impacts of climate change affect groups of people differently. Some groups face a disproportionate amount of effects because of a lack of access to public services that are fragile or could be easily disrupted by climate stresses.

The Assessment reveals that climate change provides some opportunities and benefits within many urban sectors and services, such as reduced loss and damage from cold waves and extreme cold. It is clear however that the challenges and negative implications predominate. Some short-term positive outcomes also have long-term negative consequences-as example, warmer winter temperatures might seem pleasant and beneficial in many aspects. Persistent warm winter weather also might reveal system level design vulnerabilities (e.g., from accelerated rates of evapotranspiration from surface water supplies and resulting summertime supply shortages). Given this, it is important to consider timescales when evaluating climate impacts and vulnerability. Overall, it is clear that given the evidence of current and existing service and sector infrastructure vulnerability, adaptation opportunities and challenges should be considered public safety and national security issues.

Climate Change and U.S. Cities: Urban Systems, Sectors, and Prospects for Action. W.D. Solecki and C. Rosenzweig, Eds., Island Press, pp. 261-304

# Sustained urban climate assessment

**Rosenzweig**, **C.**[1], **D. Peters**[1], W.D. Solecki, R. Blake, K. Jacob, and B. Holland, 2022

NASA Goddard Institute for Space Studies, New York, NY, USA[1]

**Abstract.** The reliable and continuous monitoring of a set of key urban climate change indicators is essential for the development of sustained climate assessment in metropolitan regions. Indicators are empirically based measurements of climate variables (e.g., number of heat waves per year, daily rainfall totals, or annual sea level rise) which reveal a signal of the occurrence and pace of climate change to scientists and decision-makers.

A sustained assessment is the persistent monitoring or those indicators, which shares information about how changes to those climate indicators are progressing in real time. Such continuous monitoring is critically important because it guides adaptation actions based on how those changes are occurring over time.

The goal of this chapter is, therefore, two-fold. Firstly, this chapter will set forth a vision for a nested, multi-level indicators and a monitoring framework. This framework underpins and supports urban climate adaptation assessment and the implementation or 'flexible pathways' for policies at both regional and national scales. Flexible pathways allow room for adaptation plans to be malleable given new climate information that is given to decision-makers at regular intervals. Secondly, the goal is to highlight examples of extant networks and organizations that conduct urban climate assessments for adaptation purposes. "Top-down" and "bottom-up" approaches to indicators and monitoring are combined in a regional and national framework for sustained urban climate assessment.

To this end, U.S. cities like Boston, Seattle, and New York and international cities like Toronto and London have taken bold and novel approaches to establish and support climate change adaptation partnerships among agencies, research institutions, universities, private entities, and local communities. These partnerships have proven to be fruitful in enhancing and fostering sound, dynamic adaptation planning, initiatives, and pathways. Throughout this chapter, lessons learned from these existing information sharing networks are presented and discussed that can be used as a model for replication in other cities across the United States.

Our Warming Planet: Climate Change Impacts and Adaptation, Lectures in Climate Change, vol. 2, World Scientific, pp. 294-317, doi:10.1142/9789811238222_0014

# Cities and climate change

**Rosenzweig**, **C.**[1], 2022

NASA Goddard Institute for Space Studies, New York, NY, USA[1]

**Abstract.** Cities and urban areas are now recognized as globally significant in regard to climate change because they are responsible for a significant portion of global greenhouse gas emissions as well as being highly vulnerable to extreme weather events. Because cities are at the nexus of both the causes and effects of climate change, they have emerged as leaders in climate change response actions via low-carbon and adaptation innovation. However, for cities to achieve their potential as climate change leaders, they require joined-up timescale's transformation in a number of spheres: integration of mitigation and adaptation responses, timescales of environmental challenges, expansion of decision-making discourse, and enhanced capacity in governance and finance.

**Urbanization and Sustainable Development.** We now live on an urban-dominated planet, with more than half of the world's 7.3 billion people living in cities. Almost two-thirds of the world's projected population growth through the year 2050 is expected to take place in cities (UN Population Fund, 2019). The trends towards urbanization will be especially dramatic in Asia and Africa and in smaller cities.

Massive urban population growth is driven by a key attribute of cities: They are centers of economic activity and weatlth-generating capacity (likely 90% or more) (Seto *et al.*, 2012). Thus, the prospects for global sustainability will be determined primarily by what happens in cities. Recognizing the importance of these trends, the United Nations included, for the first time, a Sustainable Development Goal (SDG) related to cities. SDG 11 to "Make cities inclusive, safe, resilient and sustainable" was adopted in 2015.

Cities as Urban Social-Ecological Systems. Cities are complex social eco-logical systems (SES), with attributes and functions that unable them to be leading responders to climate change challenges (Redman *et al*., 2004). Social and ecological components of cities have their internal processes, which in turn interact across the urban system to produce overall forms and dynamics. Drivers external to the urban systems are dynamically interactive at multiple spatial and temporal scales.

Equity and Environmental Justice. Social categories – such as stratification based on class, caste, gender, profession, race, ethnicity, age, and ability – affect the ability of individuals and groups to endure climate stresses and minimize climate risks (Reckien et al., 2018). Such differences often lead to discrimination based on group membership. Poor people and ethnic and racial minorities tend to live in more hazard-prone, and crowded parts of cities. These circumstances increase their susceptibility to the impacts of climate change and reduce their capacity to adapt and withstand extreme events.

Developing countries and communities that have historically contributed the least to global climate change are projected in many instances to be impacted the most. The distribution of recent natural disasters highlights the disproportionate impact of massive flooding in Bangkok in 2011, Typhoon Haiyan in the Philippines in 2013, the Chicago heat wave in 1995, and Hurricane Katrina in New Orleans in 2005. Hurricanes Harvey and Maria caused great damage in Houston and San Juan (Puerto Rico), respectively, in 2017.

Highly vulnerable people often share a set of similar and often interacting characteristics, including minority status, race, ethnicity, gender, education, income, age, and health. Theses characteristics determine where people live, how sensitive they are, their assets, and how adaptive they are after one r several hazard occurrences.

Our Warming Planet: Climate Change Impacts and Adaptation. C. Rosenzweig, M. Parry, and M. De Mel, Eds., Lectures in Climate Change, vol. 2, World Scientific, pp. xv-xxii, doi:10.1142/9789811238222_0001

# Martin Parry: Setting the course of climate change impacts and adaptation research

**Rosenzweig**, **C.**[1], 2022

NASA Goddard Institute for Space Studies, New York, NY, USA[1]

**Abstract.** Martin Parry has always reminded me a bit of Jack Aubrey — the courageous British naval sea captain of the early 1800s created by the author Patrick O'Brian. Perhaps this is because sailing is one of Martin's passions, but also because he is a natural leader and a keen scholar, which were Jack Aubrey's signature traits (O'Brian, 1970). As Co-Chair of IPCC Working Group II on Climate Change Impacts, Adaptation, and Vulnerability for the Fourth Assessment Report (AR4), Martin marshaled over 60 authors, led us through a bruising approval fight with dozens of national delegates, and then defended the Report in the face of vicious attacks during "ClimateGate". Throughout his career, he has guided our field to a series of important "victories", by which I mean significant advances in the science of climate change impacts and adaptation, deepening understanding of the planetary crisis of our time.

**Early Exploration of Climate Risk Frontiers**. How did Martin Parry become one of the main creators of the field of climate change impacts?1 I believe a key factor is his academic training as a geographer. The discipline of Geography has produced many key scholars of climate change impacts because it is the only discipline to combine rigorous analysis of physical, biological, and social sciences. Its students and practitioners are trained in all three. To navigate the complex conundrum of climate change, scholars who could rigorously work in all three disciplines emerged early and often as leaders. As Bill Travis reminds us in his contribution to this volume, Martin Parry started testing hypotheses about and mapping the role of climate change in landscapes in the late 1960s and 1970s, with a first publication in 1975 (Parry, 1975). In his 1978 book on climate and early agricultural settlement in Britain and his contribution to the 1979 conference on Climate and History at the University of East Anglia, Martin introduced a now increasingly important concept to climate and society research: the climate risk frontier (Parry, 1978; 1979a; 1979b; 1981). As shown in Fig. 1, Parry used the probability of crop failure, mapped on the Scottish uplands, to show the effect of historical climate swings during the medieval period (Parry, 1976; 1985).

Before attention turned to the threat of anthropogenic global warming, researchers began to pin down societal impacts of climate that varied in any direction: colder, warmer, wetter, drier. Martin Parry argued that the best places to look for these signals were at the margins of human activity, for example, farms in upland or semi-arid areas. In line with his focus on margins, Parry published a paper in 1979 that explored “tipping points”, a concept explain-ing that once critical levels of climatic change occur, consequences will compound and subsequently be very difficult to reverse (Parry, 1979a).

Martin also believed that good science required statements of hypotheses that would posit effects that would support the researcher’s a priori expectation of impacts, or what impacts and adaptations to examine in a changing climate. This rigorous attention to science is still important today as media reports of “climate catastrophe” abound.

**Precursors to the IPCC and the Blue and Orange Books**. Expanding his focus to marginal agriculture worldwide, Martin chaired a workshop at the Conference on The Sensitivity of Natural Ecosystems and Agriculture to Climate Change at Villach, 1983 (Parry, 1984). This was one of the influential series of Villach conferences that led eventually to the establishment of the Intergovernmental Panel on Climate Change (IPCC). Bert Bolin, the founding Chair of the IPCC, led the conference and Martin headed the Working Group on cold margins, while Micky Glantz chaired another on dry margins.

International Science Council, doi:10.24948/2022.01

# ISC-UNDRR-RISK KAN Briefing Note on Systemic Risk

Sillmann, J., I. Christensen, S. Hochrainer-Stigler, J. Huang-Lachmann, S. Juhola, K. Kornhuber, M. Mahecha, R. Mechler, M. Reichstein, **A.C. Ruane**[1], P. Schweizer, and S. Williams, 2022

NASA Goddard Institute for Space Studies, New York, NY, USA[1]

**Introduction.** Systemic risk is the name given to impacts that spread within and across systems and sectors (e.g., ecosystems, health, infrastructure and the food sector) via the movements of people, goods, capital and information within and across boundaries (e.g. regions, countries and continents). The spread of these impacts can lead to potentially existential consequences and system collapse across a range of time horizons. Globalization contributes to systemic risk affecting people worldwide. The impacts of climate change or COVID-19 show how the challenges of addressing systemic risk go beyond conventional risk management and governance. Critical system interdependencies, amplified by underlying vulnerabilities, highlight that there is a growing need to better understand cascading impacts, systemic risks and the possible political (governance) and societal responses. This includes improving our understanding of the root causes of systemic risk, both biophysical and socio-economic, and related information needs. Addressing contemporary challenges in terms of systemic risk requires integrating different systems perspectives and fostering system thinking, while implementing key intergovernmental agendas, such as the Paris Agreement, the Sendai Framework for Disaster Risk Reduction and the Sustainable Development Goals.

This Briefing Note represents an integrated perspective of climate, environmental and disaster risk science and practice regarding systemic risk. It provides an overview of the concepts of systemic risk that have evolved over time and identifies commonalities across terminologies and perspectives associated with systemic risk used in different contexts. Key attributes of systemic risk are outlined without prescribing a single definition, and information and data requirements that are essential for a better and more actionable understanding of the systemic nature of risk are discussed. Finally, the opportunities to connect research and policy for addressing systemic risk are highlighted, followed by recommendations for future work in science, policy and practice on systemic risk. The Briefing Note is based on insights and knowledge gained from an expert workshop, literature review and expert elicitation.

**Systemic Risk: Why Do We Need to Care**. Understanding and managing systemic risk is more important than ever due to our immense global connectivity, whether between sectors, such as food–health–water– energy, countries and continents, or even between individuals (Gaupp, 2020). Although the notion of systemic risk is several decades old (Faulhaber et al., 1990), the term is used in diverse ways across different disciplines (e.g., financial systems, medicine, Earth system sciences, disaster risk research and climate science). Triggered by the repercussions of the global financial crisis of the late 2000s, and more recently the COVID-19 pandemic, which are clear realizations of systemic risk, the perception of systemic risk has often focused on global and catastrophic or even existential risks (e.g., Helbing, 2013; World Economic Forum, 2021). Systemic risk, however, can be seen as a feature of systems at all possible scales – global, national, regional and local – with system boundaries varying depending on the context.

The systemic nature of risk (or systemic risk) is based on the notion that risk, for instance arising from a policy, response action or a hazard event (for definitions see Murray et al., 2021), depends on how the elements of the affected systems interact with each other. These interactions either aggravate or contain the overall effect of the constituent parts, creating the potential for cascading impacts on system elements far from the first impact. Interactions occur through positive or negative feedback processes that can lead to system malfunction or even collapse. Systemic risk is different from conventional risk and thus challenges well-established approaches to risk analysis and risk governance that seek to analyse and manage by addressing individual elements of a system or sub-systems as though they are or act in isolation (Cutter *et al.*, 2015). Systems can be affected by critical events or shocks (see examples in Figure 1) that occur outside or within the system.

Island Press, 2022

# Climate Change and U.S. Cities: Urban Systems, Sectors, and Prospects for Action

Solecki, W.D. and **C. Rosenzweig**[1], 2022

NASA Goddard Institute for Space Studies, New York, NY, USA[1]

**Abstract**. Approximately 80% of the U.S. population now lives in urban metropolitan areas, and this number is expected to grow significantly in the coming years. At the same time, the built infrastructure sustaining these populations has become increasingly vulnerable to climate change. Stresses to existing systems, such as buildings, energy, transportation, water, and sanitation are growing. If the status quo continues, these systems will be unable to support a high quality of life for urban residents over the next decades, a vulnerability exacerbated by climate change impacts. Understanding this dilemma and identifying a path forward is particularly important as cities are becoming leading agents of climate action.

Prepared as a follow-up to the Fourth National Climate Assessment (NCA), Climate Change and U.S. Cities documents the current understanding of existing and future climate risk for U.S. cities, urban systems, and the residents that depend on them. Beginning with an examination of the existing science since 2012, chapters develop connections between existing and emerging climate risk, adaptation planning, and the role of networks and organizations in facilitating climate action in cities. From studies revealing disaster vulnerability among low-income populations to the development of key indicators for tracking climate change, this is an essential, foundational analysis. Importantly, the assessment puts a critical emphasis on the cross-cutting factors of economics, equity, and governance.

Urban stakeholders and decision makers will come away with a full picture of existing climate risks and a set of conclusions and recommendations for action. Many cities in the United States still have not yet planned for climate change and the costs of inaction are great. With bold analysis, Climate Change and U.S. Cities reveals the need for action and the tools that cities must harness to effect decisive, meaningful change.

Climate Change and U.S. Cities: Urban Systems, Sectors, and Prospects for Action. W.D. Solecki and C. Rosenzweig, Eds., Island Press, pp. 1-14

# Introduction: Cities and climate change connections

Solecki, W.D., **C. Rosenzweig**[1], R. Horton, and A. de Sherbinin, 2022

NASA Goddard Institute for Space Studies, New York, NY, USA[1]

**Abstract**. The goal of this book is to assess the new knowledge and information about climate change and U.S. cities. lt is now known that climate change is already being experienced by U.S. cities through gradual shifts in climate variables and through extreme events. This book attempts to document the state-of-the-art understanding of current and future climate risk for U.S. cities, urban systems and the residents that depend on them. Contemporary climate change represents an era of increasing climate variability that is driving urban managers and residents to be more flexible and adaptive in response to these dynamic risks. Urban systems such as water, energy, and transportation infrastructure are designed and managed to operate within an expected range of environmental conditions. Climate change is associated with gradual and punctuated shifts in the environmental baseline of cities and in turn is placing increased stress on city life.

This book is an expansion and extension of the urban focused assessment research presented in the 2014 U.S. National Climate Assessment and a follow-up to the work being done as part of the Fourth National Climate Assessment due to be released at the end of 2018. Urban issues have played an important role in large scale climate assessn1ent activities since the late 1990s. For example, as part of the initial National Climate Assessment in 2000, Rosenzweig and Solecki (2001) led the development of the first major assessment of how a large city and its surrounding metropolitan region could be impacted by climate variability and change. The work focused on the New York Metropolitan Region. For the 2009 Assessment, climate change and cities issues were presented within several sections of 1he report. The results of 2009 assessment provided some updates of the findings from the 2000 assessment effort with a focus on new climate models and associated in1pacts and vulnerabilities. The 2014 National Climate Assessment for this first time includes a chapter with urban in its title (i.e., Chapter 11 — Vulnerability, Urban, and Infrastructure). The NCA4 also will include an urban related chapter.

The research team assembled for this book focused on an assessment of the scholarly literature of climate change and U.S. cities, with an emphasis on research findings generated in the past five years (since early 2012). The scope of the book is to create a foundational document on climate change and U.S. cities that assesses state-of-the-art knowledge and information across a broad set of topics. The assessment is designed to be policy relevant that is particularly important as cities have become agents of climate action moving forward after the COP21 meeting in December of 2015 and the resulting Paris Agreement. The audience for this current assessment book includes a wide variety of interested parties, including policymakers, academics, and science and technical experts, as well as the general public.

**Urban Issues – Results from Previous U.S. National Climate Assessments**. As part of 200 U.S. National *Climate Assessment the Climate Change and a Global City Report* was published (Rosenzweig and Solecki 2001). The most significant conclusions from that assessment illustrated the key potentials impacts, vulnerabilities and challenges across a set of urban sectors including water, energy, transportation, public health, and decision-making. The assessment documented that climate change already was having an impact on the region and that significant populations and assets were at risk. Because of the tightly coupled character of urban systems, integrative or cascading impacts from extreme climate events could occur in urban areas.

Studies of Cloud, Convection and Precipitation Processes Using Satellite Observations. Z.J. Luo and G. Tselioudis, Eds., Lectures in Climate Change, vol. 3, World Scientific, pp. 247-262, doi:10.1142/9789811256912_0013

# Use of satellite observations in climate model evaluation of clouds: A time history based on the NASA/GISS model

**Tselioudis, G.**[1], 2022

NASA Goddard Institute for Space Studies, New York, NY, USA[1]

**Abstract**. The importance of clouds in determining the Earth's radiative budget was well known to the Earth and planetary scientists who, back in the late 1960s and early 1970s, built the first climate models. Cloud cover was simulated in early climate models as a simple function of the grid box relative humidity, while cloud properties like optical depth were assigned as a function of cloud height. Convective clouds were simulated using the convective instability theory. Right from the start of climate modeling efforts, the need to evaluate the clouds simulated by the models was urgent, as cloud amount and property variability played a large role in determining the models' simulated climate. In this lesson, we will follow the efforts of the NASA Goddard Institute for Space Studies (GISS) climate modeling group to evaluate the clouds simulated by the GISS climate model against the available observations of each different time period, and thus improve the representation of clouds in the model.

The first version of the GISS climate model was documented in a paper by Somerville et al. (1974), which was published in the Journal of the Atmospheric Sciences. The model included a stratiform cloud parameterization that produced clouds whenever supersaturation occurred in a grid box, which at the time was 4 by 5 degrees wide, and the mixing ratio was reduced until the relative humidity reached 100%. The excess condensation was moved to the lower layer where it evaporated if it was unsaturated or precipitated if it was saturated, and a cloud was formed that was assumed to be black in the infrared and had a visible optical depth that depended on the cloud height and layer thickness. There was also a moist convection parameterization that produced shallow or deep convective clouds depending on the vertical gradients of static energy and saturation static energy. An instantaneous array of total (convective plus supersaturation) clouds is shown in Slide 2. Note that due to the lack of graphing capabilities in the mainframe computers of the time, cloud occurrence is indicated by a printed "0" sign. The pattern shows the expected cloud-free areas over major dessert regions and clouds occurring in major storm tracks, but the authors needed observational validation of their cloud simulations. At the time, available observations came either from surface observations that were collected by the national meteorological services (but covered only a small portion of the Earth's continents) or by the very first satellite retrievals coming from the series of Television InfraRed Observation Satellites (TIROS) launched by NASA in the 1960s. As GISS is a NASA organization, the authors appropriately compared their model output with TIROS nephanalysis data. The bottom-right panel in Slide 2 shows a comparison of zonal mean cloud cover between the model output and the TIROS retrievals. It can be seen that the model is doing well in the tropical convective zones and mid-latitude storm tracks but severely lacks cloud cover in the subtropical zones. Keep this feature in mind as we will return to it in the next few figures. The authors also compared their global mean cloud cover number of 52% to that derived from surface observer data (53% at the time) and noted the good agreement between the two. Later satellite figures, however, showed that this number was closer to 70%. In this first version of the climate model, the evaluation of the cloud field is restricted to the zonal mean cloud distribution and global mean cloud amount, which was for the first time calculated from the TIROS satellite retrievals.

The next incarnations of the GISS climate model, named Models I and II, were described in a paper by Hansen et al. (1983). The cloud scheme was again based on the saturation mixing ratio of the grid box, but this time, a subgrid-scale variability of temperature was introduced, which allowed for varying relative humidity and, therefore, cloud cover. The simulated cloud cover in the model is compared to observations from surface observer cloud climatology, in a sense a step backward since the original model was compared to satellite retrievals. This time around, global maps of cloud cover are produced, and the cloud distribution patterns around the globe are used for the evaluation (Slide 3).

Studies of Cloud, Convection and Precipitation Processes Using Satellite Observations. Z.J. Luo and G. Tselioudis, Eds., Lectures in Climate Change, vol. 3, World Scientific, pp. 151-171, doi:10.1142/9789811256912_0009

# Calculation, evaluation, and application of long-term, global radiative flux datasets at ISCCP: Past and present

**Zhang, Y.**[1], W.B. Rossow, **A.A. Lacis**[1], and **V. Oinas**[1], 2022

NASA Goddard Institute for Space Studies, New York, NY, USA[1]

**Introduction.** It should never be overemphasized that the tempo-spatial variations of all the forms of energy in the atmosphere and at the surface are vitally important to any branch of earth sciences as well as human lives. Among all the forms of energy exchanges, radiative fluxes play a fundamental role as this is virtually the only way for energy exchange between the earth-atmosphere system and outer space, and it is the primary driving force in the general circulation of the whole atmosphere-ocean system.

There are three main inference methods for estimating global radiative fluxes at the top of atmosphere (TOA), surface and in the atmosphere, namely, (1) regression methods based on satellite observations (see, e.g., [Cess and Vulis, 1989]), often with the assistance of some radiation model, (2) so-called "look-up table (LUT) approaches" or "matching" methods that match radiative transfer computations and satellite observations to infer the desired radiative fluxes at TOA and surface under various scenarios (see, e.g., [Ma and Pinker, 2012]) and (3) detailed flux calculation methods that use observation-based physical parameters as realistic as possible for all the associated atmospheric and surface properties as inputs to a detailed, relatively accurate and efficient radiative transfer model to calculate fluxes. This third method is probably the most comprehensive and more physically meaningful method that we have employed since the beginning of the ISCCP flux-calculation project. This project was pioneered by Rossow and Lacis (1990), but the production of an actual global flux product had to wait for a global, comprehensive cloud data product to appear, which is the first generation of the International Satellite Cloud Climatology Project (ISCCP) datasets, the C-series product, or ISCCP-C (Schiffer and Rossow, 1983; Rossow and Schiffer, 1991). This is because all of the global cloud climatologies prior to the ISCCP-C usually report on cloud amount only and do not contain sufficient information on cloud-top temperature (or altitude) and/or on the optical properties of clouds required by climate modelers to calculate the first-order effects of clouds on the Earth's radiation budget or the climate feedbacks produced by cloud variations (WMO, 1975). The ISCCP-C product for the first time made it possible for us to use the detailed radiation model of the NASA Goddard Institute for Space Studies (GISS) GCM Model II (Hansen et al., 1983) to calculate global, satellite-observation-based radiative fluxes at TOA and surface, which is our first-generation global flux product, the ISCCP-FC (Zhang et al., 1995), where the acronym FC means Flux calculated (mainly) using C data (ISCCP-C, or C-series, and similarly for FD and FH for the second and third-generation flux products as described below).

In the following years, ISCCP has developed two more generations of its products, D-series (Rossow and Schiffer, 1999) and the current H-series products (Young et al., 2018). The ISCCP-D product reported separate cloud properties for liquid and ice forms of low and middle-level clouds along with other many important improvements (Rossow and Schiffer, 1999) and, as the third-generation product, the ISCCP-H has been more advanced. Instead of using every-30-km-sampled B3 for ISCCP-D, ISCCP-H uses 10-km-sampled B1. There are also other refinements in radiance quality control (QC), calibration, cloud detection (especially high, thin and polar clouds), cloud and surface property retrievals with more modern and more homogeneous ancillary datasets, e.g., more accurate surface type and topography, snow/ice datasets, reprocessed ozone data, etc. The cloud and surface retrievals are now b4684 Studies of Cloud, Convection and Precipitation Processes Through Satellite Observations11"x8.5" Calculation, Evaluation and Application of Long-term, Global Radiative Flux Datasets at ISCCP 153based on more realistic atmospheric properties, with MACv1 aerosols (Kinne et al., 2013) included so that the uncertainties are reduced as all the ancillary datasets have been improved. The temperature and humidity profiles with increased vertical resolution have been statistically adjusted to have diurnal variation wherever suitable. The new ISCCP H-series has also increased sub-data product categories (e.g., five for L3) with new globally gridded pixel-level (L2) data.

## D. Theses

1. **Lenssen, N.**, 2022: Uncertainty and Predictability of Seasonal-to-Centennial Climate Variability. Ph.D. thesis. Columbia University, doi:10.7916/4j9y-yv29……..211

Ph.D. thesis. Columbia University, doi:10.7916/4j9y-yv29

# Uncertainty and Predictability of Seasonal-to-Centennial Climate Variability.

**Lenssen, N.**[1,2], 2022

NASA Goddard Institute for Space Studies, New York, NY, USA[1]
Center for Climate Systems Research, Columbia University, New York, NY, USA[2]

The work presented in this dissertation is driven by three fundamental questions in climate science: (1) What is the natural variability of our climate system? (2) What components of this variability are predictable? (3) How does climate change affect variability and predictability? Determining the variability and predictability of the chaotic and nonlinear climate system is an inherently challenging problem. Climate scientists face the additional complications from limited and error-filled observational data of the true climate system and imperfect dynamical climate models used to simulate the climate system. This dissertation contains four chapters, each of which explores at least one of the three fundamental questions by providing novel approaches to address the complications.

Chapter 1 examines the uncertainty in the observational record. As surface temperature data is among the highest quality historical records of the Earth's climate, it is a critical source of information about the natural variability and forced response of the climate system. However, there is still uncertainty in global and regional mean temperature series due to limited and inaccurate measurements. This chapter provides an assessment of the global and regional uncertainty in temperature from 1880-present in the NASA Goddard Institute for Space Studies (GISS) Surface Temperature Analysis (GISTEMP).

Chapter 2 extends the work of Chapter 1 to the regional spatial scale and monthly time scale. An observational uncertainty ensemble of historical global surface temperature is provided for easy use in future studies. Two applications of this uncertainty ensemble are discussed. First, an analysis of recent global and Arctic warming shows that the Arctic is warming four times faster than the rest of the global, updating the oft-provided statistic that Arctic warming is double that of the global rate. Second, the regional uncertainty product is used to provide uncertainty on country-level temperature change estimates from 1950-present.

Chapter 3 investigates the impacts of the El Niño-Southern Oscillation (ENSO) on seasonal precipitation globally. In this study, novel methodology is developed to detect ENSO-precipitation teleconnections while accounting for missing data in the CRU TS historical precipitation dataset. In addition, the predictability of seasonal precipitation is assessed through simple empirical forecasts derived from the historical impacts. These simple forecasts provide significant skill over climatological forecasts for much of the globe, suggesting accurate predictions of ENSO immediately provide skillful forecasts of precipitation for many regions.

Chapter 4 explores the role of initialization shock in long-lead ENSO forecasts. Initialized predictions from the CMIP6 decadal prediction project and uninitialized predictions using an analogue prediction method are compared to assess the role of model biases in climatology and variability on long-lead ENSO predictability. Comparable probabilistic skill is found in the first year between the model-analogs and the initialized dynamical forecasts, but the initialized dynamical forecasts generally show higher skill. The presence of skill in the initialized dynamical forecasts in spite of large initialization shocks suggest that initialization of the subsurface ocean may be a key component of multi-year ENSO skill.

Chapter 5 brings together ideas from the previous chapters through an attribution of historical temperature variability to various anthropogenic and natural sources of variability. The radiative forcing due to greenhouse gas emissions is necessary to explain the observed variability in temperature nearly everywhere on the land surface. Regional fingerprints of anthropogenic aerosols are detected as well as the impact of major sources of natural variability such as ENSO and Atlantic Multidecadal Variability (AMV).

## Author Index


**A**

Ackerman A.S. 50, 79, 135, 156, 160
Aleinov I. 111, 129, 135, 151, 171
Alexander P.M. 51, 183
Alexandrov M.D. 50, 88

**B**

Bader D.A. 197
Bauer M. 135
Bauer S.E. 54, 58, 60, 111, 135, 178, 180, 181, 184, 185
Braneon C.V. 13, 14, 59, 127, 197

**C**

Cairns B. 50, 88, 90, 108, 119, 120, 150, 160, 164
Canuto V.M. 135
Carlson B.E. 63, 115, 117
Cesana G. 64, 135
Chandler M.A. 139
Chiang F. 66
Cheng Y. 135
Chowdhary J. 120, 182
Clifton O.E. 70
Cook B.I. 66, 72, 73, 77, 126, 129, 135, 171, 173, 174

**D**

DallaSanta K.J. 28, 76, 83
Del Genio A.D. 82, 135, 148, 193
De Mel J.M. 200

**E**

Elsaesser G.S. 82, 96, 128, 135, 142, 148, 149

**F**

Faluvegi G.S. 54, 111, 134, 135, 155, 166, 172, 176
Field R.D. 86, 94, 100, 146, 165
Fridlind A.M. 79, 101, 156, 160, 161

**G**

Glaser D.M. 93
Glenn E. 127
Gloege L. 55
Guarin J.R. 80, 95, 194

**H**

Huang Y. 118, 130

**J**

Jägermeyr J. 56, 68, 69, 87, 98, 99, 102, 116, 131, 136, 175, 177
Jonas J.A. 28

**K**

Kelley M. 54, 66, 135, 148, 171
Kiang N.Y. 110, 111, 135, 171

**L**

Lacis A.A. 63, 115, 117, 135, 209
Leboissetier A. 135
LeGrande A.N. 53, 61, 135, 142, 179
Lenssen N. 152, 211
Liddy H.M. 113, 124
Litchmore D.T. 142
Lo K.K. 135

**M**

Ma Q. 57
Madajewicz M. 195
Marshall J. 135
Marvel K.D. 27, 66, 72, 73, 97, 126
Matthews E.E. 135
McDermid S.S. 66, 78, 116, 129, 135, 171
McGraw Z.S. 186
Mencos Contreras E.A. 162
Mezuman K. 135
Miller R.L. 54, 135, 190
Mishchenko M.I. 125
Mitevski I. 132
Mutter C.Z. 89

**N**

Naud C.M. 198
Nazarenko L.S. 28, 54, 66, 135
Nielsen M. 123

**O**

Oinas V. 135, 209
Orbe C. 9, 24, 28, 65, 105, 132, 135, 183
Ottaviani M. 138

**P**

Perlwitz J.P. 135
Peteet D.M. 75, 91, 109
Peters D. 202
Puma M.J. 78, 129, 135, 171

**R**

Rind D.H. 28, 135, 199
Roach L.A. 74, 103, 133, 143, 144, 145
Romanou A. 135
Rosenzweig C. 15, 16, 52, 104, 127, 162, 200, 201, 202, 203, 204, 206, 207
Ruane A.C. 62, 87, 89, 112, 122, 147, 191, 192, 195, 205
Ruedy R.A. 135

## Author Index


| | | |
|---|---|---|
| Russell | G.L. | 63, 115, 135 |
| **S** | | |
| Schmidt | G.A. | 16, 23, 27, 54, 66, 88, 97, 135, 157, 168 |
| Singh | R. | 171 |
| Sohl | L.E. | 67, 139, 163 |
| **T** | | |
| Tausnev | N.L. | 135 |
| Tedesco | M. | 51, 71, 81, 140, 158, 159, 183 |
| Tornow | T. | 119, 160 |
| Tselioudis | G. | 135, 196, 208 |
| Tsigaridis | K. | 54, 58, 60, 85, 111, 135, 154, 163, 166, 172, 178, 179, 180, 181, 184, 185 |
| **V** | | |
| van Diedenhoven | B. | 88, 137, 150, 164 |
| van Lier-Walqui | M. | 105, 114 |
| **W** | | |
| Way | M.J. | 17, 18, 19, 20, 85, 92, 151, 154, 163, 167 |
| Westervelt | D.M. | 107, 141, 153 |
| Weng | E. | 129, 135, 169, 170, 171 |
| Wu | J. | 82, 135 |
| **Y** | | |
| Yao | M.S. | 135 |
| Yang | M. | 84, 106, 121 |
| **Z** | | |
| Zhang | Y. | 209 |